Biosynthesis of the allelopathic inhibitor 7-deoxysedoheptulose in *Synechococcus elongatus* PCC 7942 and its mode of inhibition in the shikimate pathway

Dissertation

der Mathematisch-Naturwissenschaftlichen Fakultät

der Eberhard Karls Universität Tübingen

zur Erlangung des Grades eines Doktors

der Naturwissenschaften

(Dr. rer. nat.)

vorgelegt von

Johanna Rapp

aus Stuttgart

Tübingen

2021

Gedruckt mit Genehmigung der Mathematisch-Naturwissenschaftlichen Fakultät der Eberhard Karls Universität Tübingen.

Tag der mündlichen Qualifikation: 08.09.2021

Dekan: Prof. Dr. Thilo Stehle

1. Berichterstatter: Prof. Dr. Karl Forchhammer

2. Berichterstatter: Apl. Prof. Dr. Evi Stegmann

Erklärung

Ich erkläre hiermit, dass ich die zur Promotion eingereichte Arbeit selbständig verfasst, nur die angegebenen Quellen und Hilfsmittel benutzt und Stellen, die wörtlich oder inhaltlich nach den Werken anderer Autoren entnommen sind, als solche gekennzeichnet habe. Eine detaillierte Abgrenzung meiner eigenen Leistungen von den Beiträgen meiner Kooperationspartner habe ich in „Declaration of author contribution“ vorgenommen.

Tübingen, den 08.09.2021 _____

Johanna Rapp

Für Opa Norbert

Table of contents

Abbreviations

5dAdo	5-Deoxyadenosine
5dR	5-Deoxyribose (5-deoxy-D-ribose)
5dR-1P	5-Deoxyribose 1-phosphate
5dRu-1P	5-Deoxyribulose 1-phosphate
7dGh	7-Deoxy-L-*gluco*-2-heptulose
7dSh	7-Deoxysedoheptulose (7-deoxy-D-*altro*-2-heptulose)
A. thaliana	*Arabidopsis thaliana*
A. variabilis	*Anabaena variabilis* ATCC 29413
AMPA	Aminomethylphosphonic acid
ANOVA	Analysis of variance
ATCC	American Type Culture collection
*At*DHQS	3-Dehydroquinate synthase from *Arabidopsis thaliana*
*Av*DHQS	3-Dehydroquinate synthase from *Anabaena variabilis*
B. subtilis	*Bacillus subtilis*
B. thuringiensis	*Bacillus thuringiensis*
BG11	Cyanobacterial cultivation medium
BG11–N	BG11 without combined nitrogen
bld	Below detection limit
bp	Base pairs
DAHP	3-Deoxy-D-*arabino*-heptulosonate 7-phosphate
DEPC	Diethyl pyrocarbonate
DHAP	Dihydroxyacetone phosphate
DHQS	3-Dehydroquinate synthase
E. coli	*Escherichia coli*
EPSPS	5-Enolpyruvylshikimate 3-phosphate-synthase
ESI	Electrospray ionization
ExPEC	Extraintestinal pathogenic *E. coli*
GC-MS	Gas chromatography-mass spectrometry
HAD	Haloacid dehalogenase
HPLC	High pressure liquid chromatography
HR-LC-MS	High resolution liquid chromatography mass spectrometry
IC_{50}	Half maximal inhibitory concentration
KDO	3-Deoxy-D-*manno*-octulosonic acid, 2-keto-deoxyoctonate
k_i	Inhibition constant
k_M	Michaelis constant
m/z	Mass to charge ratio
MPLC	Medium pressure liquid chromatography
MSP	Methionine salvage pathway
MTA	5-Methylthioadenosine
MTR	Methylthioribose
MTR-1P	Methylthioribose 1-phosphate

MTRu-1P	Methylthioribulose 1-phosphate
N. benthamiana	*Nicotiana benthamiana*
NMR	Nuclear magnetic resonance
NRPS	Non-ribosomal peptide synthetase
NRPS-PKS	NRPS-PKS hybrid gene cluster
OD_{750}	Optical density at 750 nm
PCC	Pasteur Culture Collection
PKS	Polyketide synthase
R. rubrum	*Rhodospirillum rubrum*
R_f	Retardation factor (TLC)
RT-PCR	Reverse transcriptase polymerase chain reaction
S. elongatus	*Synechococcus elongatus* PCC 7942
S. setonensis	*Streptomyces setonensis* SF666
SAM	*S*-Adenosyl-L-methionine
Synechocystis sp.	*Synechocystis* sp. PCC 6803
TAE	TRIS-acetate-EDTA
TLC	Thin layer chromatography
U	Enzyme unit (1 U=1 µmol*min^{-1})
v_{max}	Maximum reaction velocity

Summary

Cyanobacteria are known as producers of a wide range of secondary metabolites with various functions. This includes the synthesis of allelopathic inhibitors, which suppress the growth of other organisms within the same ecological niche. These compounds are usually produced by filamentous cyanobacteria via huge gene clusters. Nevertheless, a bioactive deoxy-sugar, namely 7-deoxysedoheptulose (7dSh), was recently isolated from the culture supernatant of the unicellular cyanobacterium *Synechococcus elongatus* PCC 7942 (*S. elongatus*). In this work the biosynthetic pathway of 7dSh formation was elucidated by means of supernatant analysis via gas chromatography-mass spectrometry, feeding experiments and knockout mutants. 7dSh derives from 5-deoxyadenosine (5dAdo), an inhibitory by-product of radical SAM enzymes, which are present in all domains of life. 5dAdo is metabolized by solely promiscuous activity of enzymes of the primary metabolism, resulting in the excretion first of 5-deoxyribose and subsequently of 7dSh into the culture supernatant. This strategy enables *S. elongatus*, which has a small, stream-lined genome lacking canonical gene clusters for the synthesis of secondary metabolites, to produce an allelopathic inhibitor from a "waste" product of primary metabolism by enzymatic promiscuity, without involving a specific gene cluster. This discovery challenges the view on the biosynthesis of bioactive molecules as sole products of biosynthetic gene clusters and expands the range of bioactive compounds which can be synthesized. Additionally, with the elucidation of the biosynthesis of 7dSh, an alternative pathway for 5dAdo salvage was discovered, which had previously not been described.

In the second part of this work, the intracellular target of 7dSh, the dehydroquinate synthase, which is the second enzyme of the shikimate pathway, was confirmed. By the development of an *in vitro* inhibition assay using purified enzyme, it was shown that 7dSh inhibits the enzyme in a competitive manner, with an inhibition constant as well as an IC_{50}-value in the lower µM range.

Besides the inhibition of other cyanobacteria, 7dSh also inhibits the growth of germinating plant seedlings on soil, indicating that it might be used as an herbicide. Furthermore, it was shown that in *Anabaena variabilis* ATCC 29413 and *Synechocystis* sp. PCC 6803, the inhibitory effect of this molecule is correlated with an effective uptake via structurally different, promiscuous sugar transporters – a fructose ABC-transporter or a glucose permease. Spontaneous mutations in these transport proteins can result in the loss of 7dSh sensitivity, however the capability of heterotrophic growth is disabled at the same time. 7dSh can therefore be assumed to represent the first allelopathic inhibitor targeting the shikimate pathway, supporting *S. elongatus* in its niche competition.

Zusammenfassung

Cyanobakterien sind Produzenten einer Vielzahl von Sekundärmetaboliten mit verschiedenen Funktionen. Dazu zählt beispielsweise auch die Synthese allelopathischer Inhibitoren, die in der gleichen ökologischen Nische lebende Organismen hemmen. Üblicherweise werden solche Metaboliten von filamentösen Cyanobakterien mittels großer Gencluster hergestellt. Überraschenderweise wurde kürzlich ein bioaktiver Desoxy-Zucker, genauer 7-Desoxysedoheptulose (7dSh), aus dem Kulturüberstand des einzelligen Cyanobakteriums *Synechococcus elongatus* PCC 7942 (*S. elongatus*) isoliert. In der vorliegenden Arbeit wurde durch die Analyse des Kulturüberstandes mittels Gaschromatographie-gekoppelter Massenspektrometrie, Fütterungsexperimenten, sowie Knockout Mutanten der Biosyntheseweg von 7dSh aufgeklärt. Dieses leitet sich von 5-Desoxyadenosin (5dAdo) ab, einem inhibitorischen Nebenprodukt radikalischer SAM Enzyme, die in allen drei Domänen des Lebens vorkommen. 5dAdo wird dabei lediglich durch promiskuitive Aktivität von Enzymen des Primärstoffwechsels metabolisiert. Dies führt zunächst zu einer Ausscheidung und Akkumulation von 5-Desoxyribose, gefolgt von einer Anreicherung von 7dSh. Da *S. elongatus* ein kleines Genom ohne kanonische Gencluster für die Sekundärmetabolitsynthese besitzt, erlaubt diese Strategie die Synthese eines bioaktiven Moleküls direkt aus einem „Abfall"-Produkt des Primärstoffwechsels. Dies findet vollständig durch promiskuitive Enzymaktivitäten statt, ohne dass daran ein spezifisches Gencluster involviert wäre. Diese Entdeckung stellt die klassische Sicht auf die Synthese von Sekundärmetaboliten als Produkte spezifischer Gencluster in Frage und erweitert damit die Bandbreite an bioaktiven Molekülen. Neben der Aufklärung des Biosyntheseweges von 7dSh wurde hiermit auch ein alternativer Recyclingweg für 5dAdo, der bisher noch nicht bekannt war, beschrieben.

Im zweiten Teil dieser Arbeit wurde außerdem das Zielenzym von 7dSh in der Zelle, die Dehydrochinat-Synthase, das zweite Enzym des Shikimatwegs, bestätigt. Durch die Entwicklung eines *in vitro* Inhibitionsassays mit aufgereinigtem Enzym konnte gezeigt werden, dass dieses Molekül die DHQS kompetitiv hemmt. Dabei liegen die Inhibitionskonstante wie auch der IC_{50}-Wert im niedrigeren µM Bereich.

7dSh inhibiert das Wachstum verschiedener Cyanobakterien. Es kann aber auch das Wachstum auskeimender Pflanzen auf Erde hemmen, was für eine potenzielle Verwendung als Herbizid sprechen könnte. Außerdem konnte gezeigt werden, dass die hemmende Wirkung von 7dSh auf *Anabaena variabilis* ATCC 29413 und *Synechocystis* sp. PCC 6803 über eine effektive und rasche Aufnahme mittels strukturell verschiedener, promiskuitiver

Zuckertransporter zustande kommt. Beteiligt daran sind ein Fructose ABC-Transporter bzw. eine Glucose-Permease. Spontane Mutationen im jeweiligen Kohlenhydrattransporter führen zu einem Verlust der 7dSh-Sensitivität, gehen aber auch mit einem Verlust der Fähigkeit des heterotrophen Wachstums einher. Aufgrund dieser Ergebnisse wird angenommen, dass 7dSh der erste allelopathische Inhibitor des Shikimatwegs ist, welcher *S. elongatus* in der Verteidigung seiner ökologischen Nische unterstützt.

1 Publications and Personal Contributions

1.1. Accepted Publications

1.1.1. Publication 1 - Research Article

Brilisauer, Klaus; **Rapp, Johanna**; Rath, Pascal; Schöllhorn, Anna; Bleul, Lisa; Weiß, Elisabeth; Stahl, Mark; Grond, Stephanie; Forchhammer, Karl (2019): Cyanobacterial antimetabolite 7-deoxy-sedoheptulose blocks the shikimate pathway to inhibit the growth of prototrophic organisms. *Nature Communications*, 10 (545), https://doi.org/10.1038/s41467-019-08476-8.

Personal Contribution: I designed and performed the germination assays of *Arabidopsis thaliana* seedlings on soil. I performed the statistical analysis of all data in the manuscript.

1.1.2. Publication 2 - Research Article

Rapp, Johanna; Rath, Pascal; Kilian, Joachim; Brilisauer, Klaus; Grond, Stephanie; Forchhammer, Karl (2021): A bioactive molecule made by unusual salvage of radical SAM enzyme by-product 5-deoxyadenosine blurs the boundary of primary and secondary metabolism. *Journal of Biological Chemistry*, 296 (100621), https://doi.org/10.1016/j.jbc.2021.100621.

Personal Contribution: I conceived, conducted, and interpreted all experiments shown in this publication, except for the chemical synthesis of 5-deoxyribose and the synthesis of ^{13}C-labeled compounds. I prepared all figures in the publication. Method development and the quantification of polar compounds in cyanobacterial supernatants was performed by me with the support of Joachim Kilian. The manuscript was written by me with the support of Karl Forchhammer. I was responsible for the submission and revision process, including answering the reviewer's comments. During the whole study I was under the supervision of Karl Forchhammer and Stephanie Grond.

1.1.3. Publication 3 - Research Article

Rapp, Johanna; Wagner, Berenike; Brilisauer, Klaus; Forchhammer, Karl (2021): *In vivo* inhibition of the 3-dehydroquinate synthase by 7-deoxysedoheptulose depends on promiscuous uptake by sugar transporters in cyanobacteria. *Frontiers in Microbiology*, 12 (692986), https://doi.org/10.3389/fmicb.2021.692986.

Personal Contribution: I planned, performed, and interpreted most experiments in this study. Analysis of spontaneous 7dSh-resistant mutants was supported by Berenike Wagner

(bioactivity assays, PCR of selected genes, construction of *Anabaena* sp. PCC7120+*frtRABC*). Klaus Brilisauer performed pre-experiments with another spontaneous 7dSh-resistant *A. variabilis* mutant and performed experiments shown in figure S3 and figure S4. The manuscript was written by me with the input from all authors. All figures in the manuscript were prepared by me. I was responsible for the submission and revision process, including answering the reviewer's comments. During the whole study I was under the supervision of Karl Forchhammer.

1.1.4. Publication 4 - Review Article

Rapp, Johanna; Forchhammer, Karl: 5-Deoxyadenosine metabolism – more than "waste disposal" (2021). *Microbial Physiology*, https://doi.org/10.1159/000516105.

Personal Contribution: The manuscript and the figures were prepared by me. The manuscript was proof-read by Karl Forchhammer. I was responsible for the submission and revision process, including answering the reviewer's comments.

1.2. Submitted Manuscripts

1.2.1. Publication 5 – Research Article

Rammler, Tim; Wackenhut, Frank; Zur Oven-Krockhaus, Sven; **Rapp, Johanna**; Forchhammer, Karl; Harter, Klaus; Meixner, Alfred J. (2019). Quantum coherence in the photosynthesis apparatus of living cyanobacteria. *bioRxiv*, https://doi.org/10.1101/2019.12.13.875344.

Personal Contribution: I performed the cultivation of the cyanobacterial cultures and wrote the respective part of the method section.

2 Introduction

2.1. Cyanobacteria

The phylum Cyanobacteria, also known as Cyanophyta, comprises one of the largest sub-groups of Gram-negative bacteria. Most of them have the capability to perform oxygenic photosynthesis (Soo et al., 2017). The name derives from their bluish-green color (Greek word *κυανός* (*kyanós*); English: blue), which also leads to the trivial name blue-green algae (Whitton and Potts, 2012). Cyanobacteria are very ancient organisms: the earliest assured microfossils of cyanobacteria emanate from 2.7–2.5 billion years ago (Altermann and Kazmierczak, 2003; Bosak et al., 2009).

Cyanobacteria played an outstanding role in the development of today's earth atmosphere by evolving the ability to perform oxygenic photosynthesis, thus coupling the consumption of carbon dioxide with the release of oxygen (Schirrmeister et al., 2015). The resulting deposition and accumulation of the photosynthetic waste product oxygen into the – until then – anoxic environment about 2.5–2.3 billion years ago led to the Great Oxidation Event, which set the foundation of today's life (Bekker et al., 2004; Anbar et al., 2007). As they were the only organisms evolving oxygenic photosynthesis, they additionally set the basement for the development of eukaryotic algae and plants. Cyanobacteria are believed to be the ancestors of the chloroplasts, the photosynthetically active organelles in eukaryotic (photosynthetic) organisms presumably obtained by means of endosymbiosis (Giovannoni et al., 1988; McFadden, 2001). Besides performing oxygenic photosynthesis, some cyanobacteria gained the capability to use carbohydrates as an additional carbon source or even grow heterotrophically (*e.g.*, *Anabaena variabilis* (*A. variabilis*), *Synechocystis* sp. PCC 6803 (*Synechocystis* sp.); Rippka et al., 1979).

During evolution, cyanobacteria developed a striking diversity, leading to the presence of simple, unicellular cyanobacteria, but also complex, multicellular organisms. Because of their traditional assignment to algae, their classification was first carried out by phycologists under the provisions of the Botanical Code (Stafleu et al., 1972), in which structural or ecological properties in field-material were responsible for determination. For cyanobacteria, this classification turned out to be difficult or even impractical. Additionally, type cultures were not allowed. Therefore, Rippka et al. (1979) suggested a categorization of cyanobacteria in five different subsections, distinguishable by structure, reproduction and degree of differentiation. Subsections I and II consist of unicellular cyanobacteria, either single cells or colonial aggregates which reproduce by binary fission, budding or multiple fission. Subsections III–IV

are filamentous cyanobacteria. Cyanobacteria of section III only comprise of vegetative cells, whereas species in sections IV and V are able to form differentiated cells. They can form heterocysts for the fixation of atmospheric nitrogen. Sometimes they form akinetes, spore-like cells, as well as hormogonia, which are motile filaments. Section V differs from the others because the division takes place in more than one plane. Due to intensive molecular analyses the taxonomic classification of cyanobacteria (species, genera, families, orders) is nowadays again under intensive discussion and restructuring is in progress (Komárek et al., 2014).

2.1.1. *Synechococcus elongatus* PCC 7942

Synechococcus elongatus PCC 7942 (*S. elongatus*, former name: *Anacystis nidulans* R2) is a unicellular, freshwater cyanobacterium belonging to subsection I (Rippka et al., 1979). It was first isolated from the San Francisco Bay area and was deposited in the Pasteur Culture Collection (PCC) in 1979 as the 42nd strain in this year (hence PCC 7942) (Golden, 2019). Shortly afterwards, it was shown that the strain is highly transformable as it possesses natural competence (Shestakov and Khyen, 1970). This led to the development of tools for the genetic modification of this strain (van den Hondel et al., 1980; Golden and Sherman, 1984; Golden et al., 1987), resulting in its use as a common model organism for photosynthesis research (Selim et al., 2018), circadian clock mechanisms (Kondo et al., 1994) and nitrogen metabolism (Sauer et al., 2001).

S. elongatus holds a small, stream-lined genome (Copeland et al., 2014), containing a single circular chromosome (≈ 2.7 Mb, GenBank accession number: CP000100.1) as well as two endogenous plasmids, pANS (accession number: S89470.1) and pANL (accession number: F441790.2). Although *S. elongatus* was originally isolated from freshwater and is usually cultivated in its planktonic lifestyle in the laboratory, it can also exhibit a terrestrial lifestyle, occurring in microbial mats or biofilms on soil, rocks, humid stone walls and even in caves (Schlösser, 1994; Czerwik-Marcinkowska and Mrozińska, 2011; Mattern and Mareš, 2018; Yang et al., 2018; Conradi et al., 2020). A closely related strain of *S. elongatus* PCC 7942, *Synechococcus elongatus* PCC 6301 (also known as *Synechococcus* sp. PCC 6301) has an almost identical genome, with the exception of a large inversion of 189 kb (Sugita et al., 2007). The genus *Synechococcus* is a diverse and polyphyletic group of organisms living in salt, fresh and brackish water (Waterbury et al., 1979). Together with *Prochlorococcus*, organisms of this genus are the most abundant members of the picophytoplankton, dominating global marine primary production and carbon fixation (Scanlan and West, 2002; Richardson and Jackson, 2007) and contributing to at least 25 % of global primary productivity (Flombaum et al., 2013).

2.2. Secondary metabolism

With minor variations, primary metabolic pathways are almost identical in all living organisms. They are involved in the synthesis and degradation of essential carbohydrates, fatty acids as well as amino acids for growth, development, and reproduction. In contrast, secondary metabolites are not essentially necessary but provide selective advantages (Yunes, 2019). They are only produced under certain conditions and solely by certain genera or species (Cavalier-Smith, 2007; Dewick, 2009). Secondary metabolites possess a large variety of (complex) chemical structures (Figure 1; overview for cyanobacteria in: Leão et al., 2012; Dittmann et al., 2015), sometimes with unusual modifications like halogenations (Jones et al., 2010). They however mainly derive from only a few common building blocks provided by primary metabolism (Dewick, 2009; Gomes et al., 2017): coenzyme A (acetyl-CoA)-derivatives are used in the acetate-malonate pathway, resulting in the formation of fatty acids and polyketides (*e.g.*, nosperin; Kampa et al., 2013). Shikimic acid is an intermediate deriving from the shikimate pathway. It is a precursor molecule for the synthesis of phenolic or alkaloid compounds (*e.g.*, scytonemin; Soule et al., 2007). Methylerythritol phosphate or mevalonic acid are involved in the synthesis of terpenoids (*e.g.*, noscomin; Jaki et al., 1999) via the methylerythritol phosphate pathway or, alternatively, the mevalonate pathway (not present in cyanobacteria; Pattanaik and Lindberg, 2015). Besides these building blocks, canonical amino acids but also non-proteinogenic amino acids (*e.g.*, ornithine) also play important roles in the synthesis of secondary metabolites, for example in the synthesis of post-translationally modified ribosomal peptides (*e.g.*, cyanobactins; Gu et al., 2018 or bacteriocins/microcins; Wang et al., 2011) or non-ribosomal peptides (*e.g.*, lyngbyatoxin; Edwards and Gerwick, 2004). Secondary metabolites are synthesized by specific enzymes, which are probably derive from duplication and divergence of genes originally participating in primary metabolism (Cavalier-Smith, 2007).

1.100 different secondary metabolites are described for cyanobacteria, 737 of these show inhibitory effects on prokaryotes, eukaryotes or inhibit a wide range of different enzymes (Dittmann et al., 2015). 39 different genera are described to be producers of secondary metabolites but the vast majority is isolated from the filamentous genera *Hapalosiphon*, *Lyngbya*, *Nostoc*, *Planktothrix* or the colonial *Microcystis*, whereas unicellular cyanobacteria belonging to the genera *Synechococcus* and *Prochlorococcus* usually do not produce any secondary metabolites (Méjean and Ploux, 2013; Dittmann et al., 2015). Unicellular cyanobacteria host smaller genomes (about 5–6 Mb smaller than those of filamentous ones) which solely exhibit space for genes of the primary metabolism (Méjean and Ploux, 2013).

In bacteria and fungi, the synthesis of secondary metabolites is usually organized in biosynthetic gene clusters (Blin et al., 2019). A majority of cyanobacterial secondary metabolites are products of non-ribosomal peptide synthetases (NRPS), polyketide synthases (PKS) and mixed NRPS-PKS systems, which are encoded in huge 8–64 kb gene clusters (Wase and Wright, 2008; Dittmann et al., 2015). NRPS and PKS are large multifunctional enzyme complexes (200–2.000 kDa) with a modular organization, assembling either amino acids or acyl-CoA in an assembly line manner (Ehrenreich et al., 2005). Although cyanobacterial secondary metabolites can exhibit antibacterial, antiviral, antifungal, herbicidal, antiprotozoal, antitumoral, anti-inflammatory, neurotoxic or cytotoxic activities (Maurya et al., 2019), the ecological role or function of secondary metabolites is not yet always clear. It is reported that they can used for photoprotection purposes (*e.g.*, shinorine; Balskus and Walsh, 2010), for chemical communication (*e.g.*, acylated homoserine lactones; Sharif et al., 2008), to scavenge iron (siderophores; Årstøl and Hohmann-Marriott, 2019) or for the inhibition of organisms living in the same ecological niche (allelochemicals, see chapter 2.2.2).

Secondary metabolic gene clusters can be predicted by genome mining, *e.g.*, by using bioinformatical tools like anti-SMASH (Weber et al., 2015) which are however based on the currently known pathways.

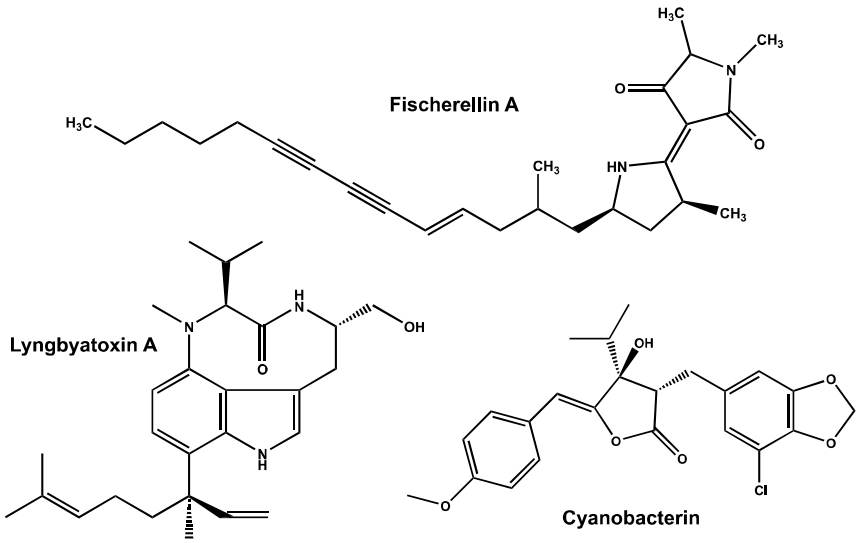

Figure 1: Selected secondary metabolites from cyanobacteria. Fischerellin A, an inhibitor of photosystem II, was isolated from the freshwater cyanobacterium *Fischerella muscicola* (Gross et al., 1991; Hagmann and Jüttner, 1996). The non-ribosomal peptide Lyngbyatoxin A was isolated from the marine cyanobacterium *Lyngbya majuscula* (Cardellina et al., 1979) and inhibits the proteinkinase C (Basu et al., 1992). Cyanobacterin, a chlorine-containing γ-lactone, was isolated from the freshwater cyanobacterium *Scytonema hofmanii* and inhibits photosystem II (Mason et al., 1982; Gleason and Paulson, 1984).

2.2.1. Secondary metabolites from *S. elongatus*

For a long time, it was assumed that unicellular cyanobacteria with a small genome, like *S. elongatus*, are not able to produce secondary metabolites. Accordingly, the genome of *S. elongatus* is free from known NRPS, PKS or hybrid NRPS/PKS gene clusters (Shih et al., 2013), but two putative bacteriocin gene clusters were eventually located by genome mining (Wang et al., 2011). Bacteriocins or microcins (small bacteriocins) are ribosomally synthesized, commonly post-translationally modified short peptides, which are, due to a double glycine excretion motif, secreted into the environment (Håvarstein et al., 1995). Indeed, Parnasa et al. (2016) identified four small secreted microcins (EbfG1–4), encoded by one of the above mentioned gene clusters. They are essential for the induction of biofilm formation in *S. elongatus*. In the wildtype, the expression of these biofilm promoting compounds is usually autoinhibited by a constitutively excreted protein (EbsA), which does not exhibit any sequence similarity to proteins of known functions (Schatz et al., 2013; Yegorov et al., 2021). Additionally, Cohen et al. (2014) reported that collapsing, aged cultures excrete a not yet identified hydrophobic compound that inhibits various photosynthetic organisms.

Only recently, a rare and bioactive deoxy-sugar, 7-deoxy-D-*altro*-2-heptulose (7-deoxysedoheptulose, 7dSh), was isolated from the supernatant of *S. elongatus* cultures (Brilisauer et al., 2019). This compound inhibits the growth of other cyanobacteria, *e.g.*, *A. variabilis*, but also fungi and plants (Brilisauer et al., 2019). Initial experiments indicated that 7dSh is an antimetabolite of the shikimate pathway as 7dSh treated cells strongly accumulated an intermediate: 3-deoxy-D-*arabino*-heptulosonate 7-phosphate (DAHP) (Brilisauer et al., 2019). DAHP is the substrate of the dehydroquinate synthase (DHQS), which is the second enzyme of this pathway, which is responsible, *e.g.*, for the synthesis of aromatic amino acids (Figure 3). Additionally, 7dSh treated *A. variabilis* cells showed a decreased pool of aromatic amino acids, whereas the concentrations of certain non-aromatic amino acids were significantly increased (Brilisauer et al., 2019). 7dSh was also isolated from the culture supernatant of the non-sequenced strain *Streptomyces setonensis* SF666 (*S. setonensis*, NBRC No. 13797) (Ito et al., 1971; Brilisauer et al., 2019), indicating that the formation of 7dSh is a common mechanism in nature. The biosynthesis and the ecological role of this rare deoxy-sugar remained enigmatic, but a putative precursor molecule, 5-deoxy-D-ribose (5dR), was isolated from the supernatant of *S. elongatus* cultures (Brilisauer et al., 2019). *In vitro*, 5dR can serve as a precursor molecule for 7dSh formation in a promiscuous transketolase reaction (Brilisauer et al., 2019).

2.2.2. Allelopathy in cyanobacteria

Cyanobacteria produce a wide range of secondary metabolites, including various bioactive compounds; a minor proportion of these is regarded as allelochemicals (Leflaive and Ten-Hage, 2007). In general, allelopathy is a phenomenon, by which an organism (plant or microbe) influences another organism of the same ecological community, either in a positive or a negative way by excreting a chemical compound (Rice, 1984). Initially, allelopathic interactions were observed in plants (Molisch, 1937). But already in the 1970s, allelopathy was observed in field studies of freshwater cyanobacteria. There it was shown that allelopathic interactions play a crucial role in the formation and succession of cyanobacterial and diatom blooms (Keating, 1977, 1978). Besides this, allelochemicals are excreted to outcompete predators or competitors. This can happen during direct source competition (*e.g.*, light; De Nobel et al., 1998), during interference competition (*e.g.*, varying temperature; van der Grinten et al., 2005), during competition under unfavorable conditions (*e.g.*, P-/N-limitation; Elert and Jüttner, 1997; Ray and Bagchi, 2001), or even to invade a habitat (Figueredo et al., 2007; Rzymski et al., 2014).

Target organisms of cyanobacterial allelochemicals are other cyanobacteria, micro- and macroalgae as well as angiosperms (Leão et al., 2009). Cyanobacterin from *Scytonema hoffmanni*, a chlorine-containing γ-lactone (Figure 1) targeting photosystem II, was the first allelochemical described from cyanobacteria (Mason et al., 1982; Gleason and Paulson, 1984). Another allelochemical, fischerellin A (Figure 1) from *Fischerella muscicola*, synthesized by a hybrid NRPS-PKS gene cluster, also targets photosystem II (Gross et al., 1991; Etchegaray et al., 2004). Inhibition of photosynthesis is a common mode of action of cyanobacterial allelochemicals (Gross, 2003), but inhibition of RNA synthesis and DNA replication has also been described (Doan et al., 2000). It is additionally reported that allelochemicals affect secondary targets or cause effects besides their primary mode of action (Doan et al., 2001; Gomes et al., 2017). Although allelopathic interactions were described for unicellular cyanobacteria, also from the genus *Synechococcus* (Paz-Yepes et al., 2013), no allelopathic compound had so far been described for *S. elongatus*.

2.3. 5-Deoxyadenosine metabolism[1]

S-Adenosyl-L-methionine (SAM or AdoMet) is used as an essential co-substrate and cofactor in various biological reactions in all domains of life (Fontecave et al., 2004). Besides

[1] A deeper insight into 5-deoxyadenosine metabolism can be found in publication 4: Rapp and Forchhammer (2021): 5-Deoxyadenosine metabolism – more than “waste” disposal, *Microbial Physiology*.

its function as the major methyl-group donor for the methylation of nucleic acids, proteins, lipids and carbohydrates and as an aminoalkyl group donor in the synthesis of polyamines, the quorum sensing signal *N*-acylhomoserine lactone as well as the plant hormone ethylene, it plays an important role in reactions catalyzed by the radical SAM enzyme superfamily (*e.g.*, biotin synthase; Sofia et al., 2001). By the reductive cleavage of SAM by an unusual iron-sulfur cluster, radical SAM enzymes are generating the 5-deoxyadenosyl radical, which abstracts a hydrogen atom from diverse substrates while 5-deoxyadenosine (5dAdo) is released as a by-product (Figure 2 B; Sofia et al., 2001; Wang and Frey, 2007). As 5dAdo is a product inhibitor of the radical SAM enzyme reaction, it has to be removed from the cells (Challand et al., 2009; Parveen and Cornell, 2011). For a long time, metabolic pathways for 5dAdo recycling or salvage received little attention, whereas the salvage of methylthioadenosine (MTA), a similar molecule, via the canonical methionine salvage pathway (MSP) was characterized in depth (publication 4, figure 2d; Wray and Abeles, 1995; Sekowska and Danchin, 2002; Sekowska et al., 2004). Because of the structural similarity of both molecules, salvage of 5dAdo was either suggested to occur by promiscuous enzyme activity of the MSP or by a paralogous pathway (Parveen and Cornell, 2011; Sekowska et al., 2018). Only recently, different pathways for 5dAdo salvage were reported in the literature (Figure 2 B; Beaudoin et al., 2018; Miller et al., 2018b; North et al., 2020). In the so-called dihydroxyacetone phosphate (DHAP) shunt, 5dAdo is metabolized by promiscuous enzymes of the MSP into DHAP and acetaldehyde, which can both processed in the primary metabolism (Figure 2 B; Beaudoin et al., 2018; North et al., 2020). There, 5dAdo is either cleaved by the promiscuous MTA phosphorylase (MtnP), where the adenine residue is replaced with a phosphate, resulting in the formation of 5-deoxyribose 1-phosphate (5dR-1P), or by the promiscuous methylthioribose (MTR) nucleosidase (MtnN), where 5dR and adenine are released (Figure 2 B). Before metabolization, 5dR has to be essentially phosphorylated by the promiscuous MTR kinase (MtnK) (Beaudoin et al., 2018; Sekowska et al., 2018; North et al., 2020). 5dR-1P is then isomerized by promiscuous methylthioribose 1-phosphate (MTR-1P) isomerase (MtnA), leading to the formation of 5-deoxyribulose 1-phosphate (5dRu-1P). Cleavage of 5dRu-1P into dihdroxyacetone phosphate and acetaldehyde, is either conducted by a specialized class II aldolase (*e.g.*, DrdA in *Bacillus thuringiensis* (*B. thuringiensis*); Beaudoin et al., 2018) or by promiscuous activity of the methylthioribulose-1P (MTRu-1P) dehydratase (MtnB; *e.g.*, DEP1 of *Arabidopsis thaliana* (*A. thaliana*); Beaudoin et al., 2018) of the MSP pathway. 5dAdo salvage via the DHAP shunt can be either conducted by promiscuous enzyme activity of enzymes of the MSP (*e.g.*, *Rhodospirillum rubrum* (*R. rubrum*); North et al., 2020), or by a paralogous gene cluster (*e.g.*,

B. thuringiensis or extraintestinal pathogenic *Escherichia coli* (ExPEC *E. coli*) strains; Beaudoin et al., 2018; North et al., 2020). Further details on 5dAdo metabolism are provided in publication 4 (Rapp and Forchhammer, 2021).

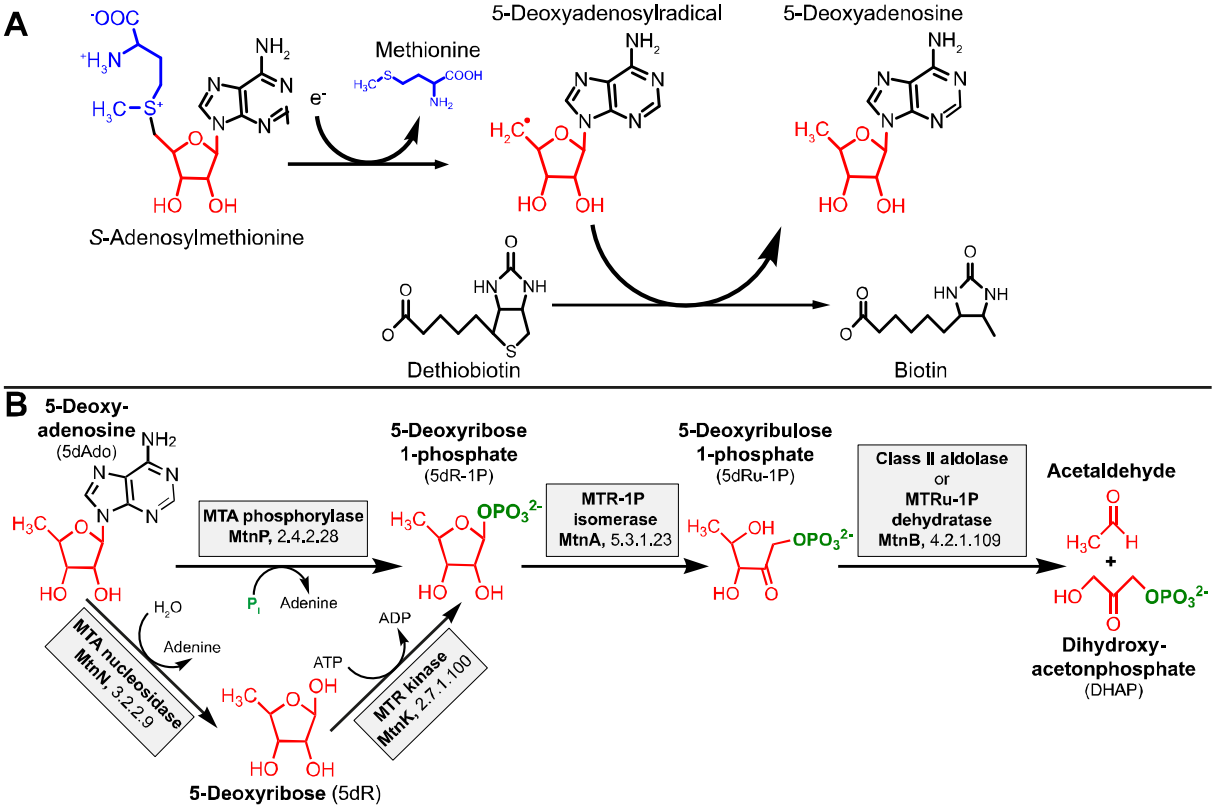

Figure 2: Mechanism of radical SAM enzymes and the salvage of the inhibitory 5dAdo by-product. A: Simplified mechanism of the biotin synthase, a radical SAM enzyme (modified from Berkovitch et al., 2004). *S*-Adenosylmethionine is reductively cleaved by an unusual iron sulfur cluster, generating the 5-deoxyadenosylradical. This radical intermediate is responsible for the conversion of dethiobiotin into biotin and 5dAdo is released as a by-product. B: 5dAdo salvage pathway described in the literature (Beaudoin et al., 2018; North et al., 2020).

2.4. Enzyme promiscuity

In general, enzymes are considered to be highly specific for their substrates and the reactions they catalyze. Nevertheless, most enzymes can catalyze fortuitous reactions, which is in general regarded as enzyme promiscuity. The term can be subdivided into substrate, catalytic and condition(al) promiscuity (Hult and Berglund, 2007). The first, which is also called broad-/ multispecificity, describes the phenomenon that an enzyme can act on a wide range of substrates, often with similar efficiencies (Khersonsky and Tawfik, 2010), *e.g.*, phosphatases from the haloacid dehalogenase (HAD) superfamily (Huang et al., 2015; Copley, 2017). Catalytic promiscuity is used to describe the ability of an enzyme to catalyze different chemical transformations (Copley, 2003; Hult and Berglund, 2007), *e.g.*, widely distributed in the metallo-β-lactamase superfamily (Baier and Tokuriki, 2014). Condition(al) promiscuity, in

contrast, describes enzymatic activity, besides its native activity under altered reaction conditions, which can either be exploited for industrial biocatalysis by using different solvents or high temperature (Schmid et al., 2001; Hult and Berglund, 2007) or can occur *in vivo*, due to environmental changes or stresses, *e.g.*, due to enhanced concentrations of low-affinity substrates, post-translational modifications or stress-induced conformational changes (Piedrafita et al., 2015). In contrast, the term "moonlighting" refers to events where parts of the protein outside of the active side are used for other functions, especially of regulatory and structural nature (Copley, 2003). Reactions, where enzymes are using alternative, endogenous metabolites, are also called underground metabolism (D'Ari and Casadesús, 1998). During normal growth, underground metabolism plays a minor role, but it was shown that *E. coli* mainly uses an alternative, promiscuous pathway for isoleucine biosynthesis under anaerobic conditions, when propionate was present in the medium (Cotton et al., 2020). The capability of organism to use their underground metabolism confers them metabolic plasticity (D'Ari and Casadesús, 1998). It was reported that in *E. coli* 37 % of the enzymes can act on several substrates, thereby catalyzing 65 % of the known metabolic reactions (Nam et al., 2012). Besides playing a role *in vivo*, enzyme promiscuity is also exploited for biotechnological applications, either during the development of new metabolic pathways (Rosenberg and Commichau, 2019) or for biocatalysis purposes, *e.g.*, in the synthesis of rare carbohydrates like 7dSh (Brilisauer et al., 2019).

Early on, enzyme promiscuity was connected to protein evolution. Ancient cells must have held a small genome with a comparatively small number of proteins. Jensen (1976) suggested that ancient, primordial enzymes possessed very broad specificities and undeveloped regulatory mechanisms. Thereby, few enzymes were capable to offer a wider range of metabolites, thereby generating a greater flexibility for primordial cells. Gene duplication provided the basis for increased gene content as well as the divergence of the new gene copies by mutational events. This, in turn, may have altered the specificities, and selection led to the expansion of metabolic capacities and the evolution of new metabolic pathways.

2.5. The shikimate pathway

The shikimate pathway, shown in Figure 3, consists of seven sequential enzymatic steps. It converts phosphoenolpyruvate and erythrose 4-phosphate into chorismate, the precursor molecule for the synthesis of aromatic amino acids, isoprenoid quinones, folate cofactors and various secondary metabolites (Srinivasan et al., 1955; Herrmann, 1995; Herrmann and Weaver, 1999). This pathway is only present in microorganisms (bacteria, fungi,

apicomplexans, …) as well as in plants but it is absent in animals and humans (Roberts et al., 1998; Herrmann and Weaver, 1999). Therefore, the latter need to take up aromatic amino acids through their daily diet (Herrmann, 1995).

The shikimate pathway connects carbohydrate and aromatic amino acid synthesis. Therefore, it has to be tightly regulated. In microorganisms, regulation occurs on the level of the first enzyme, DAHP synthase (EC 2.5.1.54), by allosteric feedback inhibition via different aromatic amino acids (Byng et al., 1983; Knaggs, 2001). In plants, the regulation occurs at the level of gene expression (Tzin and Galili, 2010). Although the metabolites of the shikimate pathway are identical in all organisms, the primary structure and properties of the prokaryotic and eukaryotic enzymes exhibits big differences in several cases (Herrmann and Weaver, 1999). In fungi (*e.g., Neurospora crassa*), the first five enzymes are encoded on a single multifunctional polypeptide called AROM complex (Case and Giles, 1971). Plant enzymes are usually about 150 amino acids longer and possess an amino-terminal signal sequence for plastid import as the shikimate pathway occurs solely there (Bickel et al., 1978; Herrmann and Weaver, 1999). Interestingly, methanogenic archaea, which do not house the enzymatic equipment for the oxidative pentose phosphate pathway and are thereby unable to provide erythrose 4-phosphate, are devoid of the first two enzymes of the shikimate pathway (Grochowski et al., 2005). In these organisms, the pathway starts with 3-dehydroquinate, which is synthesized by the condensation of 6-deoxy-5-ketofructose 1-phosphate and L-aspartate (see publication 4; White, 2004; Gulko et al., 2014).

Since the shikimate pathway is absent in animals and humans, inhibitors of the pathway are considered to be harmless for those when handled in reasonable concentrations. These can therefore be used as herbicides, fungicides and antibiotics (Herrmann and Weaver, 1999). The most common and industrially applied inhibitor is the broad-spectrum herbicide glyphosate (*N*-(phosphonomethyl)glycine), which targets the penultimate step – the 5-enolpyruvyl-shikimate 3-phosphate synthase (EPSPS; Figure 3) – where it forms a transition state analogue of phosphoenolpyruvate (Boocock and Coggins, 1983; Steinrücken and Amrhein, 1984; Duke and Powles, 2008). Regarding phosphoenolpyruvate glyphosate is a competitive inhibitor, whereas regarding the second substrate of this reaction shikimate 3-phosphate, glyphosate showed an uncompetitive inhibition (Steinrücken and Amrhein, 1984). The enormous success and distribution of glyphosate – or its commercially available formulation “Roundup” – as the major herbicide for weed control was a result of the introduction of transgenic, glyphosate-resistant crops in 1996 (Duke and Powles, 2008). The major problem is the occurrence of

glyphosate resistant weed (Powles, 2008) but also the detrimental effects of the compound, *e.g.*, on honey bees by disturbing their gut microbiota (Motta et al., 2018).

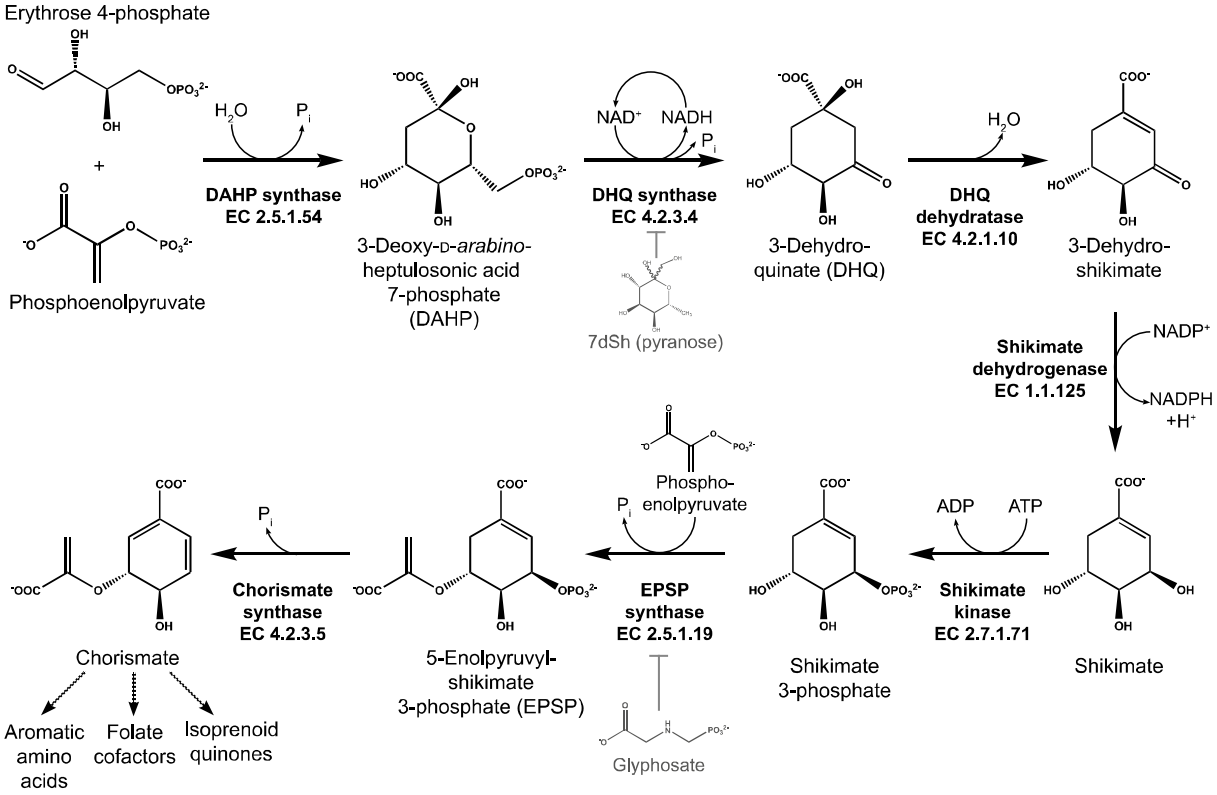

Figure 3: Shikimate pathway and selected inhibitors (shown in grey). Erythrose 4-phosphate and phosphoenolpyruvate are converted into chorismate by seven enzymatic steps. Chorismate is a precursor molecule for various molecules, *e.g.*, aromatic amino acids, folate cofactors and isoprenoid quinones.

2.5.1. The dehydroquinate synthase and its inhibitors

The DHQS is the second enzyme of the shikimate pathway, converting DAHP into 3-dehydroquinate by the release of phosphate (Figure 3). The activity of this enzyme is dependent on divalent cations, whereas Co^{2+} is the most active but Zn^{2+} is presumably used *in vivo* (Bender et al., 1989a). Additionally, the reaction needs catalytic amounts of NAD^+, although the enzyme reaction is redox neutral.

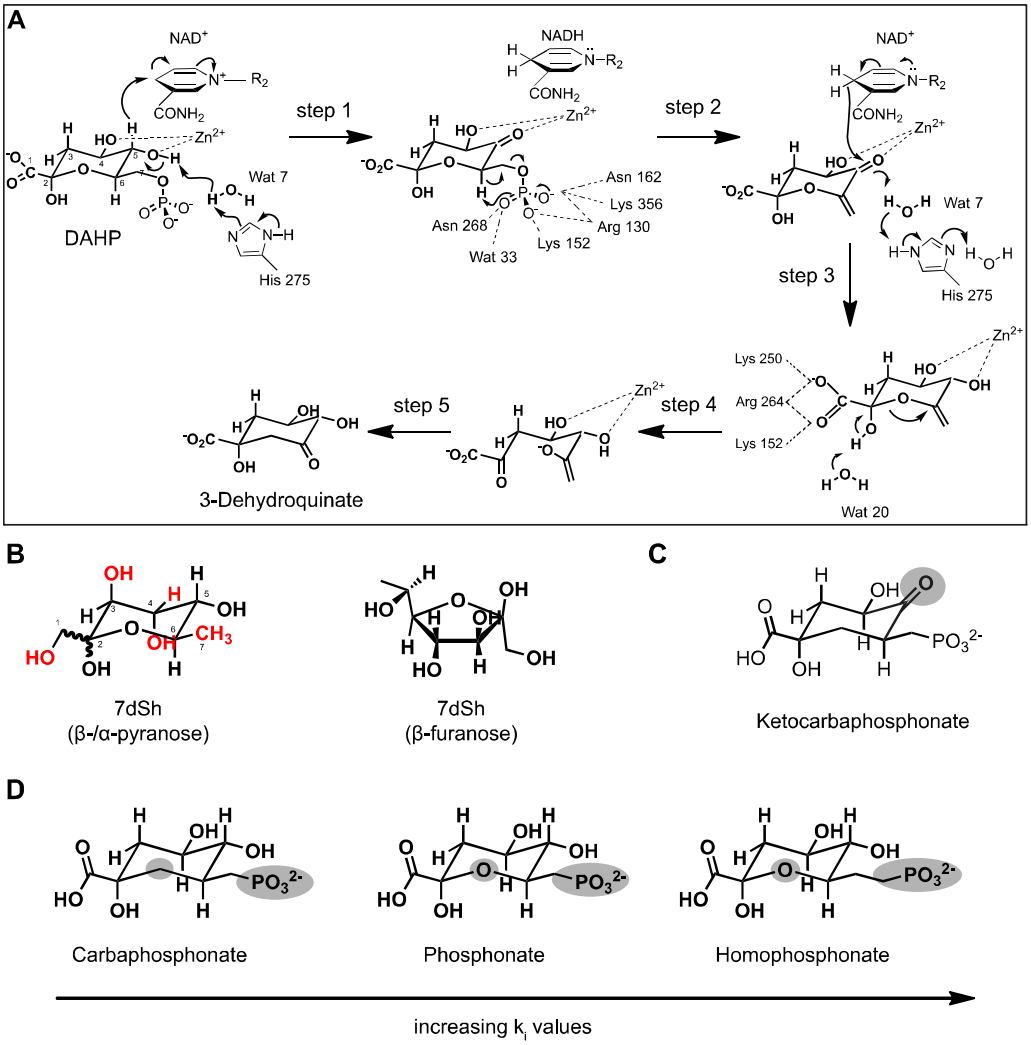

Figure 4: The DHQS mediates the conversion of DAHP into 3-dehydroquinate. A: Proposed mechanism of the DHQS mediated reaction (modified from Carpenter et al., 1998). B: 7dSh in its different conformations. Differences of the pyranose – when compared to DAHP – are labeled in red. C: Irreversible inhibitor of the DHQS (Montchamp and Frost, 1991). Important features are labeled in grey. D: Competitive inhibitors of the DHQS (Bender et al., 1989b). Important features are labeled in grey.

DAHP is converted into 3-dehydroquinate by a complex five-step mechanism involving alcohol oxidation, phosphate β-elimination, carbonyl reduction, ring opening and intramolecular aldol condensation (Figure 4 A; Srinivasan et al., 1963; Carpenter et al., 1998). When the substrate has entered the active site, the hydroxyl group at C_5 is oxidized in a NAD^+ and Zn^{2+} dependent manner (Figure 4 A, step 1). In the second step, the phosphate group is removed by β-elimination. Most known DHQS inhibitors (*e.g.*, (carba-) phosphonates; see Figure 4 D) inhibit this step as they possess an "unbreakable" phosphonate group instead of a phosphate group, thereby being competitive inhibitors of the reaction (Bender et al., 1989b). The binding of the inhibitors to the enzyme strongly depends on the composition of the ring: carbacyclic inhibitors (*e.g.*, carbaphosphonate, Figure 4 D) exhibit inhibition constants (k_i) in the low nM range, whereas oxacyclic inhibitors (*e.g.*, phosphonate, Figure 4 D) only act in the low µM range (Bender et al., 1989b). Nevertheless, none of the wide variety of (homo-)

phosphonate inhibitors was reported to be a good inhibitor *in vivo* (Pompliano et al., 1989; Montchamp et al., 1992; Tian et al., 1996). In the third reaction step, the ketone at C_5 is reduced by NADH. The only known irreversible inhibitor, ketocarbaphosphonate (Montchamp and Frost, 1991), mimics this step as it has a keto-group at C_5. The carbonic acid group at C_1 further stabilizes the binding of the substrate, but also the binding of the carba-/homo- or phosphonate inhibitors in the enzyme. In step 4, deprotonation occurs at C_2 leading to ring-opening. In the last step, intramolecular aldol condensation leads to the reformation of the ring and release of 3-dehydroquinate.

3 Research Aims

Recently, the bioactive deoxy-sugar 7-deoxysedoheptulose (7dSh) was isolated from the culture supernatant of the unicellular cyanobacterium *Synechococcus elongatus* PCC 7942 (*S. elongatus*). As the strain holds a small, stream-lined genome, which is free from known NRPS-/PKS-gene clusters for the synthesis of secondary metabolites, the isolation of a bioactive compound was surprising. 7dSh can inhibit the growth of other cyanobacteria, presumably by inhibiting the second enzyme of the shikimate pathway. In the work presented here, the biosynthetic pathway of 7dSh in *S. elongatus* should be investigated in detail. For this purpose, a method for the absolute quantification of polar compounds in cyanobacterial supernatants had to be developed. With the help of feeding experiments (*e.g.*, with ^{13}C-labeled compounds) and knockout mutants, the biosynthetic pathway, including all of the involved genes, as well as the precursor molecules should be elucidated. Furthermore, the specificity of 7dSh formation should be investigated by screening culture supernatants of other cyanobacteria regarding the presence of 7dSh.

In the second part of this work, the effect of 7dSh on the shikimate pathway should be further investigated. Therefore, an *in vitro* inhibition assay with purified dehydroquinate synthase should be developed and the kinetic parameters of the inhibition should be determined. By the synthesis of a 7dSh derivative, the influence of the terminal deoxy-group and the configuration of the hydroxyl-groups should be analyzed. Additionally, the effect of 7dSh on various other cyanobacteria should be investigated – including the question if 7dSh plays a role in niche protection of *S. elongatus* by being an allelopathic inhibitor. This also led to the question how 7dSh uptake is mediated in sensitive organisms. Finally, the potential of 7dSh as an herbicide should be considered.

4 Results

The main results of the following publications are summarized in this chapter:

Publication 1 – Research Article:

Brilisauer, Klaus; **Rapp, Johanna**; Rath, Pascal; Schöllhorn, Anna; Bleul, Lisa; Weiß, Elisabeth; Stahl, Mark; Grond, Stephanie; Forchhammer, Karl (2019): Cyanobacterial antimetabolite 7-deoxy-sedoheptulose blocks the shikimate pathway to inhibit the growth of prototrophic organisms. *Nature Communications*, 10 (545), https://doi.org/10.1038/s41467-019-08476-8.

Own results of this publications are referred in the following as "publication 1", whereas the other results are referred as " Brilisauer et al. (2019)".

Publication 2 – Research Article:

Rapp, Johanna; Rath, Pascal; Kilian, Joachim; Brilisauer, Klaus; Grond, Stephanie; Forchhammer, Karl (2021): A bioactive molecule made by unusual salvage of radical SAM enzyme by-product 5-deoxyadenosine blurs the boundary of primary and secondary metabolism. *Journal of Biological Chemistry*, 296 (100621), https://doi.org/10.1016/j.jbc.2021.100621.

Publication 3 – Research Article:

Rapp, Johanna; Wagner, Berenike; Brilisauer, Klaus; Forchhammer, Karl (2021): *In vivo* inhibition of the 3-dehydroquinate synthase by 7-deoxysedoheptulose depends on promiscuous uptake by sugar transporters in cyanobacteria. *Frontiers in Microbiology*, 12 (692986), https://doi.org/10.3389/fmicb.2021.692986.

Publication 4 - Review Article:

Rapp, Johanna; Forchhammer, Karl: 5-Deoxyadenosine metabolism – more than "waste disposal" (2021). *Microbial Physiology*, https://doi.org/10.1159/000516105.

This chapter also includes additional non-published results, which are related to the topic of the thesis.

4.1. Biosynthesis of 7dSh

7dSh is a bioactive deoxy-sugar excreted by the unicellular cyanobacterium *S. elongatus*, but also from the streptomycete *S. setonensis* (Ito et al., 1971; Brilisauer et al., 2019). Additionally, another unusual carbohydrate, 5dR, is also excreted by *S. elongatus* and was assumed to be a precursor molecule for 7dSh (Brilisauer et al., 2019). *In vitro*, 5dR can serve as a precursor molecule for 7dSh in a promiscuous transketolase-based reaction (Brilisauer et al., 2019).

4.1.1. 5dR and 7dSh formation is dependent on the cultivation condition

To elucidate the biosynthesis of 5dR and 7dSh in *S. elongatus*, a gas chromatography-mass spectrometry (GC-MS) based method for the absolute quantification of these metabolites in cyanobacterial supernatants was developed (publication 2). With this, it was possible to monitor the formation of 5dR and 7dSh in the culture supernatant of *S. elongatus* (publication 2, figure 2). The accumulation of both carbohydrates is strongly dependent on the cultivation condition. 5dR and 7dSh solely accumulate when cultures are aerated with air supplemented with 2 % CO_2, whereas in cultures aerated with ambient air, only minor amounts of 5dR and no 7dSh at all are formed (publication 2, figure 2). In CO_2-supplemented cultures, 5dR accumulation in the supernatant correlates with growth, whereas 7dSh accumulation only occurs during later growth phases (publication 2, figure 2). Hardly any 5dR and 7dSh accumulate intracellularly, thereby showing that the molecules are immediately excreted after formation (publication 2, figure S1). This is necessary because both compounds (in high concentrations) inhibit the growth of the producer strain (publication 2, figure 3). Supernatant analysis of various cyanobacterial strains showed that only a few strains are excreting 5dR and 7dSh (*S. elongatus*, *Synechococcus* sp. PCC 6301, *Synechococcus* sp. PCC 7002). In contrast, in the supernatant of *S. setonensis* only 7dSh, but no 5dR is detected (publication 2).

4.1.2. 5dR is a precursor molecule for 7dSh in vivo

By feeding experiments with $^{13}C_5$-labeled 5dR, it was shown that 5dR is a direct precursor molecule for 7dSh *in vivo* (publication 2, figure 4). *S. elongatus* cultures supplemented with uniformly labeled $^{13}C_5$-labeled 5dR accumulate $^{13}C_5$-7dSh. However, only a minor portion of $^{13}C_5$-5dR is converted into $^{13}C_5$-7dSh. Since the concentration of exogenously added $^{13}C_5$-5dR continuously decreased in the supernatant, but endogenously formed unlabeled 5dR is excreted at the same time, it is obvious that 5dR is continuously im- and exported.

4.1.3. 5dAdo, a by-product of radical SAM enzymes, is the precursor molecule for 5dR and 7dSh in *S. elongatus*

5dAdo, a by-product of radical SAM enzymes (Wang and Frey, 2007), can be cleaved into 5dR by a promiscuous MTA nucleosidase or into 5dR-1P by a promiscuous MTA phosphorylase (Figure 2 B; Beaudoin et al., 2018; North et al., 2020). Since *S. elongatus* only possesses an annotated gene for the latter, an insertion mutant was created by replacing the gene (*Synpcc7942_0923*) with an antibiotic resistance cassette (publication 2). The mutant no longer excretes 5dR as well as 7dSh. Instead of this, the mutant excretes 5dAdo, in contrast to the wildtype (publication 2, figure 6). This indicates that 5dAdo is a precursor molecule for 5dR and 7dSh *in vivo*, but 5dR-1P is formed as an intermediate before (publication 2, figure 7, figure S3).

4.1.4. 5dR-1P is dephosphorylated by a promiscuous phosphatase

In the literature it was suggested that 5dR or the 5dR moiety of 5dAdo has to be phosphorylated before further metabolization (Savarese et al., 1981; Beaudoin et al., 2018; North et al., 2020). As dephosphorylation of 5dR-1P was not yet described, a specific phosphatase was assumed to be present in *S. elongatus*, which is responsible for the dephosphorylation of 5dR-1P. By analyzing the genome of *S. elongatus* regarding the presence of phosphoric monoester hydrolases, gene *Synpcc7942_1005*, which is annotated as glucose-1-phosphatase (EC: 3.1.3.10), belonging to the HAD-like hydrolase superfamily subfamily IA, seemed a promising candidate (publication 2, table S3). The gene was replaced by an antibiotic resistance cassette and a culture supernatant analysis via GC-MS was performed. The mutant only excretes minor amounts of 5dR and no 7dSh at all. Instead, the mutant strongly accumulates 5dAdo in the supernatant (publication 2, figure 8), indicating that 5dR-1P is mainly dephosphorylated by the phosphatase encoded by gene *Synpcc7942_1005*. As the gene is annotated as a glucose-1-phosphatase, it was assumed that this enzyme also acts promiscuously.

Figure 5 shows the biosynthetic pathway for 7dSh in *S. elongatus* which was elucidated in this work. 5dAdo is solely metabolized by promiscuous enzyme activity. Besides the elucidation of the biosynthetic pathway for the bioactive molecule 7dSh, a new pathway for 5dAdo salvage was identified.

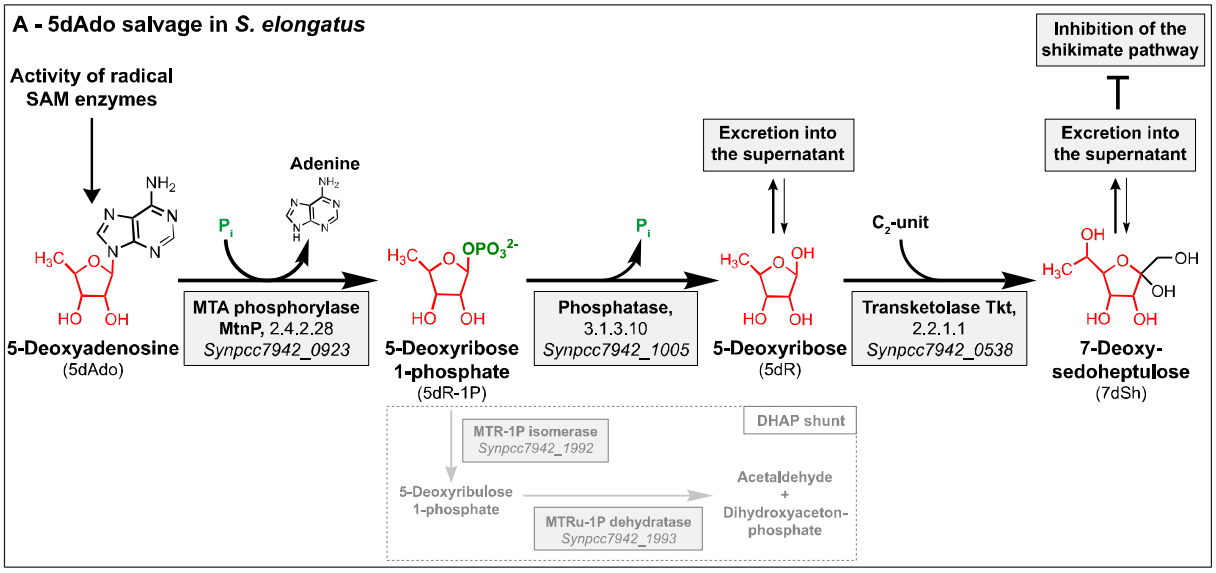

Figure 5: Biosynthesis of 7dSh in *S. elongatus*. 5dAdo is metabolized into 7dSh by promiscuous enzyme activity (marked in black). Under certain conditions 5dAdo is metabolized via another pathway, presumably the DHAP shunt (marked in grey). Figure obtained from publication 2 (Rapp et al., 2021).

4.1.5. Alternative salvage pathway for 5dAdo under ambient CO_2 conditions

5dAdo salvage in *S. elongatus* via 5dR and 7dSh excretion is dependent on the environmental conditions (publication 2, figure 2 B, C). 5dAdo is partially metabolized into 5dR and 7dSh when cultures were aerated with air supplemented with 2 % CO_2. Under ambient air, the amount of 5dAdo per cell is unaltered (publication 2, figure 6 E), but only a very small portion is metabolized into 5dR. Additionally, no 7dSh is formed. This indicates that 5dAdo can also be metabolized via another pathway and that there is a trigger or regulatory mechanism for 5dAdo salvage via 5dR/7dSh formation. It is very likely that 5dAdo can be metabolized via the DHAP shunt (Beaudoin et al., 2018; North et al., 2020), because the respective genes, involved in this pathway, are present in *S. elongatus* (Figure 5, pathway in grey).

4.1.6. Additional results: biosynthesis of 7dSh

4.1.6.1. Regulation of 7dSh biosynthesis

To analyze the regulation of 7dSh biosynthesis, semi-quantitative reverse transcriptase (RT)-PCR was used to monitor the expression of genes, which are involved in 5dR/7dSh biosynthesis under the above-mentioned environmental conditions. The gene expression of all genes involved in the biosynthesis of 7dSh (*Synpcc7942_0923* – MTA phosphorylase; *Synpcc7942_1005* – glucose-1-phosphatase; *Synpcc7942_0538* – transketolase) were unaltered, when compared with cultures aerated with ambient air (Figure 6, **2**) or cultures aerated with air supplemented with 2 % CO_2 (Figure 6, **1**). Additionally, the expression of the

genes involved in the MSP (*Synpcc7942_0923* – MTA phosphorylase; *Synpcc7942_1992* – MTR 1-P isomerase, *Synpcc7942_1992* – MTRu 1-P dehydratase) were examined, because the DHAP shunt takes advantage of the promiscuous activity of enzymes of this pathway. However, the expression of these genes remained unaltered, too. The knockout of the glucose-1-phosphatase (Figure 6, **3**), encoded on gene *Synpcc7942_1005*, does also not lead to an enhanced expression of the genes of the MSP.

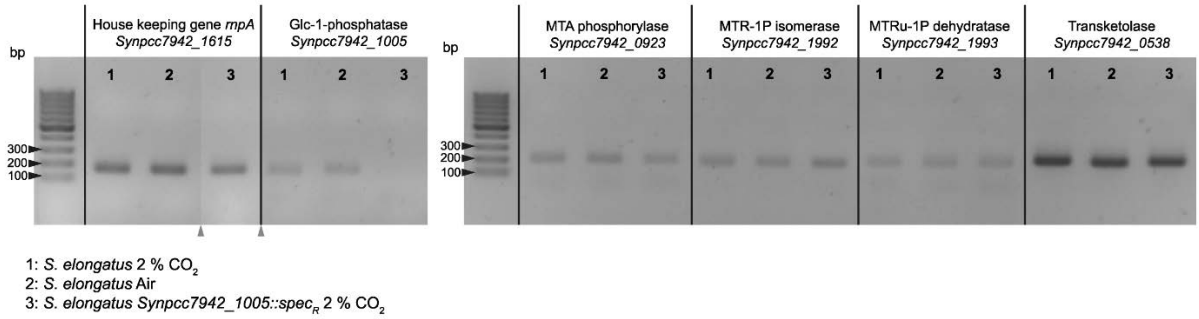

Figure 6: Expression of genes involved in the biosynthesis of 5dR/7dSh and the MSP under different conditions. Gene expression of the indicated genes in *S. elongatus* cultures aerated with 2 % CO_2 (**1**), in *S. elongatus* cultures aerated with ambient air (**2**) or in *S. elongatus Synpcc7942_1005*::*spec*$_R$ cultures aerated with 2 % CO_2 (**3**) after 21 days of cultivation determined by semi-quantitative RT-PCR. RNA was extracted from cell pellets of the respective cultures, transcribed into cDNA by using reverse transcriptase. Gene expression was determined by amplifying the gene of interest by using gene specific primers resulting in fragments of 100–200 bp in size and the analysis of these via agarose gel-electrophoresis. Splice borders in the image of the agarose gel are labeled with grey triangles, but marker and samples were run on the same gel. The expression of the house-keeping gene *rnpA* served as a control.

4.1.6.2. Heterogeneity of 7dSh production

5dR and 7dSh formation of *S. elongatus* cultures were reproducibly measured several times (publication 2, figure 2, 4, 6, 8). The total amount of 5dR and 7dSh slightly differed from batch to batch, but the timely formation, in which 5dR accumulates in a growth dependent manner and 7dSh accumulation starts during later growth phases, remained constant. In a few cases, single cultures excreted 5dR during growth, just as the other cultures (Figure 7 A, B), but no 7dSh formation was observed (Figure 7 C, three biological replicates are shown). This phenomenon was also observed once for *Synechococcus* sp. PCC 6301. This showed that in some cases subpopulations produce 5dR, which is then not used for 7dSh biosynthesis. But the mechanism behind this phenomenon is not yet known.

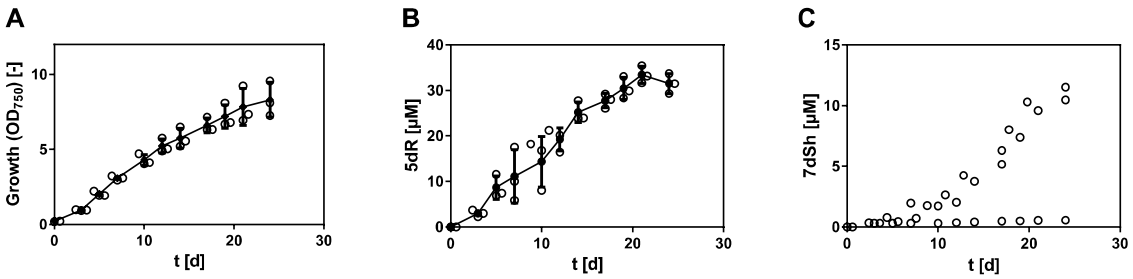

Figure 7: Heterogeneity of 7dSh production was observed infrequently. Growth (A), 5dR (B) and 7dSh excretion (C) of *S. elongatus* aerated with air supplemented with 2 % CO_2. Graphs show mean and standard deviation of three biological replicates (A, B). In graph C, data points of each replicate are shown independently.

4.1.6.3. External pH of *S. elongatus* cultures

Strong 5dR and 7dSh formation was only observed when cultures were aerated with air supplemented with 2 % CO_2 (publication 2, figure 2). Cultures aerated with ambient air only accumulate minor amounts of 5dR and no 7dSh at all. Besides an enhanced carbon supply in cultures aerated with air supplemented with 2 % CO_2, which leads to enhanced growth of the cultures (Figure 8 A, black dots), the pH of the medium was significantly influenced compared with cultures, which were aerated only with ambient air. The external pH of cultures aerated with ambient air is at around 10.5 (Figure 8 B, grey squares), whereas the external pH during the cultivation under high carbon conditions is significantly decreased to around 8.0 (Figure 8 B, black dots) during the full cultivation process, presumably due to the buffering capacity of CO_2/HCO_3^-. Interestingly, the supernatant of CO_2 supplemented cultures was more yellowish than the supernatant of cultures aerated with ambient air. The yellow color of the supernatant of CO_2 supplemented cultures further increased with the duration of the cultivation process.

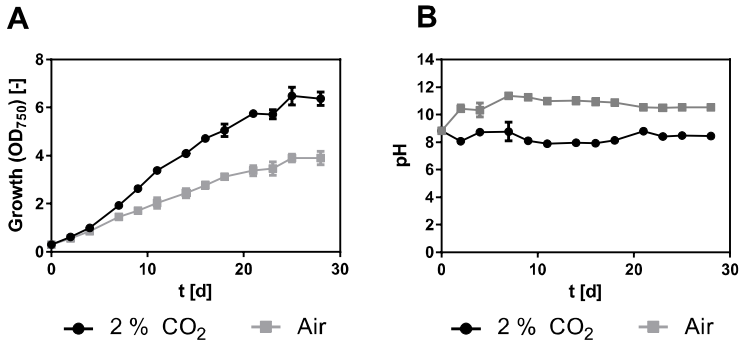

Figure 8: Effect of CO_2 content during aeration on the external pH of *S. elongatus* cultures. Growth (A) and external pH (B) of *S. elongatus* cultures aerated either with air supplemented with 2 % CO_2 (black dots) or aerated with ambient air (grey squares). Values shown in the graphs represent mean and standard deviation of three biological replicates.

4.1.6.4. Stability of 5dAdo in BG11 medium

Before performing 5dAdo feeding experiments (publication 2, figure 5), the stability of 5dAdo in BG11 medium as well as the uptake of 5dAdo by *S. elongatus* were examined. Therefore, a final concentration of 20 µM 5dAdo (total volume: 1.5 mL) was either added to BG11 medium or to *S. elongatus* cultures (inoculated at an optical density of 750 nm (OD_{750}) of 0.05) in a 24-well plate and incubated for 6 days (29 °C, shaking, continuous illumination). *S. elongatus* cultures without 5dAdo served as a control. After 6 days, the medium or the supernatant of the cultures were analyzed via high resolution liquid chromatography mass spectrometry (HR-LC-MS) (Figure 9). As a control, 20 µM 5dAdo in water were analyzed (Figure 9, green peaks). 5dAdo is stable in BG11 (Figure 9, blue peaks) over 6 days, as the peaks showed the same size as the control (5dAdo in water, not incubated, green peaks). 5dAdo is completely taken up by *S. elongatus*, as there is no accumulation in the supernatant (black peaks). In the supernatant of the control cultures, no accumulation was observed, too (grey peaks).

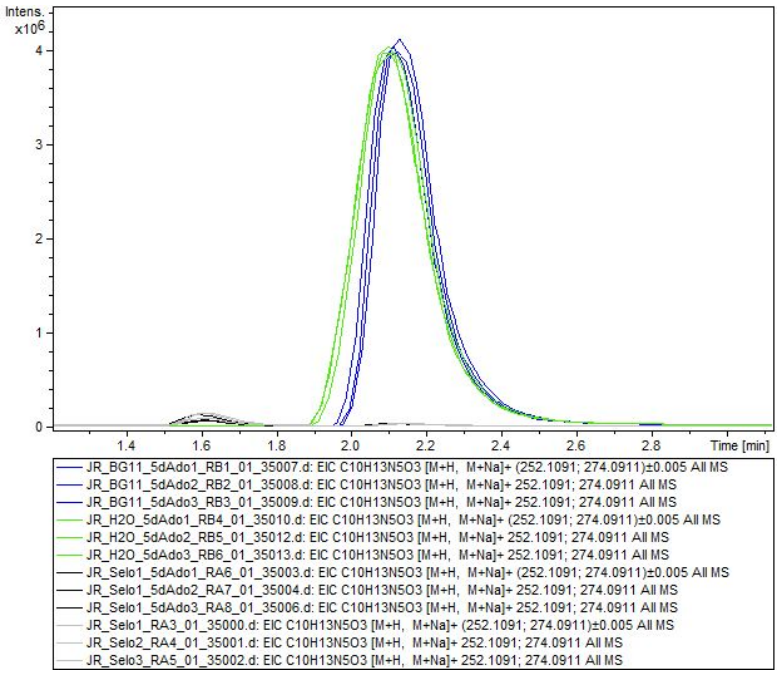

Figure 9: 5dAdo stability in BG11 and 5dAdo uptake by *S. elongatus*. Extracted ion chromatograms of 5dAdo ($C_{10}H_{13}N_5O_3$ $[M+H, M+Na]^+$) obtained by HR-LC-MS analysis of 20 µM 5dAdo incubated in BG11 (blue peaks), 20 µM 5dAdo in water (green peaks), supernatant of *S. elongatus* cultures cultivated in the presence of 20 µM 5dAdo (black peaks) or *S. elongatus* cultures (grey peaks). Each condition is shown in three replicates.

4.1.6.5. Influence of different cultivation conditions on 5dR/7dSh formation

During the elucidation of the biosynthesis of 5dR/7dSh different cultivation conditions of *S. elongatus* and their influence on 5dR/7dSh production were investigated. *S. elongatus* was cultivated for 17 days under continuous light and aeration with air supplemented with 2 % CO_2.

The cultures were harvested, washed, inoculated with fresh media, and split into two cultures. One of these was then cultivated in the light and the other was cultivated in the dark for 48 h (both were further aerated with 2 % CO_2). Figure 10 A shows that only cultures which were maintained in the light were able to produce 5dR. Cultures incubated in the dark do not excrete 5dR. 7dSh formation after 48 h was neither observed in light or dark grown cultures.

In another experiment, *S. elongatus* cultures were cultivated for 8 days under continuous light and aeration with air supplemented with 2 % CO_2. After that, each culture was harvested, washed, split into two and inoculated either with fresh BG11 or BG11 –N (without combined nitrogen) and then cultivated for 5 days (both were further aerated with air supplemented with 2 % CO_2). Figure 10 B shows that 5dR and 7dSh formation were almost unaltered under both treatments.

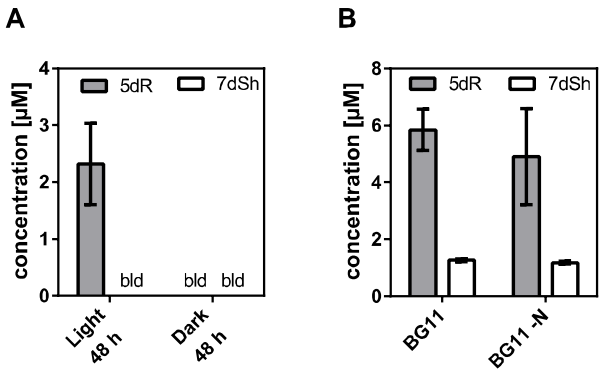

Figure 10: Influence of different cultivation conditions on 5dR/7dSh formation. A: 5dR and 7dSh concentration in the culture supernatant of *S. elongatus* cultures shifted to light or dark for 48 h. *S. elongatus* was cultivated for 17 days (continuous light, aeration with air supplemented with 2 % CO_2). Each culture was harvested, washed, inoculated with fresh media, and split into two. One culture was then cultivated in the light and the other was cultivated in the dark for 48 h. B: 5dR and 7dSh concentrations in the supernatant of *S. elongatus* shifted to BG11 medium without combined nitrogen (BG11 –N) compared to cultures shifted to BG11 medium. Before shifting, cultures were cultivated under normal conditions. Graphs show mean and standard deviation of three biological replicates. bld: below detection limit.

4.1.6.6. 5dR/7dSh formation in a spontaneous 7dSh-resistant mutant

In publication 3, a spontaneous 7dSh-resistant *S. elongatus* mutant was isolated during the cultivation of the strain at sublethal 7dSh concentrations. To examine, if the mutant is able to form and excrete 5dR and 7dSh, the strain was cultivated (aeration with air supplemented with 2 % CO_2) and the supernatant was analyzed via GC-MS (as described in publication 2) and compared with the wildtype. The growth of the mutant was not affected (Figure 11 A). 5dR and 7dSh accumulation in the supernatant of both strains was similar, whereas the resistant mutant excretes slightly less 5dR, but slightly more 7dSh (Figure 11 B, C).

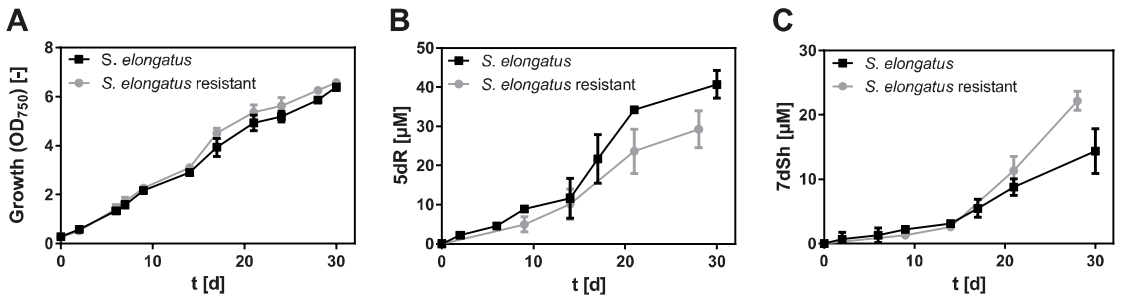

Figure 11: Supernatant analysis of a spontaneous 7dSh-resistant *S. elongatus* mutant compared to the wildtype. A: Growth of a spontaneous 7dSh-resistant *S. elongatus* mutant (grey circles) and *S. elongatus* wildtype (black squares) aerated with air supplemented with 2 % CO_2. B: 5dR and C: 7dSh accumulation in the supernatant of both strains. Graphs show mean and standard deviation of three biological replicates.

4.2. 7dSh and its inhibitory effect on the shikimate pathway

A. variabilis cells treated with 7dSh strongly accumulate DAHP (Brilisauer et al., 2019). As DAHP is an intermediate of the shikimate pathway by acting as a substrate for the DHQS, it was assumed that 7dSh is an antimetabolite of the DHQS (Brilisauer et al., 2019). This was underlined by the fact that 7dSh treated cells accumulated increased levels of non-aromatic amino acids but reduced levels of aromatic amino acids (Brilisauer et al., 2019). To elucidate this inhibition in detail, the inhibitory effects were further investigated (see publication 3).

4.2.1. 7dSh is a competitive inhibitor of the DHQS

To investigate the inhibitory effect of 7dSh on the DHQS, the enzyme from *A. variabilis* was heterologously expressed and purified (publication 3). In the DHQS-mediated reaction, DAHP is converted to 3-dehydroquinate by the release of phosphate (Figure 3). To monitor the reaction, the phosphate release was detected by means of malachite green. The kinetic parameters of the reaction were calculated (k_M=1.8 ±0.3 µM for DAHP; v_{max}=149.3 ±6.1 U*µmol$_{enzyme}^{-1}$). If increasing concentrations of 7dSh were applied, the k_M-value of DAHP increased but v_{max} remained nearly constant, which indicates a competitive inhibition of the DHQS by 7dSh (publication 3, figure 1 C). Additionally, an inhibition constant (k_i) of 17.6 µM was calculated. In its pyranose form, 7dSh seems to be a structural analogue of DAHP, as it exhibits a similar structure (Figure 4 B).

4.2.2. Bactericidal effect of 7dSh is correlated with an effective uptake

Although 7dSh is a competitive inhibitor of the DHQS enzyme and should therefore be replaced by increasing concentrations of its native substrate DAHP, which indeed strongly

accumulates in 7dSh treated cells over time, 7dSh exhibits bactericidal effects on the cells of *A. variabilis* (Brilisauer et al., 2019). This effect is strongly dependent on the cell density. In cultures inoculated at a low optical density, even low concentrations of 7dSh exhibit a bactericidal effect (Brilisauer et al., 2019).

By the isolation of a spontaneous 7dSh-resistant *A. variabilis* mutant, which was no longer able to use fructose as additional carbon source, the fructose ABC-transporter was identified to be responsible for 7dSh uptake (publication 3, figure 2). 7dSh uptake via the fructose ABC-transporter seemed quite effective as the 40-fold amount of fructose only partially alleviates its toxic effect. Additionally, in *Synechocystis* sp. a structurally different transporter, the glucose permease, belonging to the major facilitator superfamily, was identified to be responsible for 7dSh uptake (publication 3, figure 4). In *S. elongatus*, a putative ribokinase (*Synpcc7942_0116*) plays an essential role in 7dSh-sensitivity, indicating that phosphorylated 7dSh might play a role in the inhibition of the producer strain (publication 3, figure 5).

4.2.3. 7dSh and its inhibitory effect on plants and other cyanobacteria

As described in publication 1, a growth assay for *A. thaliana* seedlings on soil was established. With this the effect of 7dSh was examined in a more physiological system as before on agar plates. After 18 days of cultivation, *A. thaliana* seedlings that had germinated on soil in the presence of 260 µM 7dSh showed a significantly reduced fresh weight when compared to untreated seedlings and even to seedlings that had been treated with the same amount of the commercially available herbicide glyphosate.

Additionally, the effect of 7dSh on 19 strains from all subsections of cyanobacteria was examined (publication 3). Two strains, *A. variabilis* and *Oscillatoria acuminata*, were completely inhibited in their growth by low concentrations (10 µM) of 7dSh, whereas others (*e.g.*, *Synechocystis* sp., *Nostoc muscorum*) were only inhibited by higher concentrations. Some of the examined cyanobacteria were not affected by 7dSh, even if it was applied in a concentration of 250 µM, which is distinctly higher than physiologically occurring concentrations (around 10 µM in *S. elongatus* cultures).

4.2.4. Additional results: 7dSh and its inhibitory role in the shikimate pathway

4.2.4.1. Enzymatic synthesis of a 7dSh derivative: 7-Deoxy-L-*gluco*-heptulose

7dSh can be synthesized in a promiscuous transketolase-based reaction with the substrates 5dR and hydroxypyruvate (Brilisauer et al., 2019). To synthesize a derivative of 7dSh, the commercially available 5-deoxy-L-arabinose was used as substrate in the above mentioned

transketolase-based reaction. The product 7-deoxy-L-*gluco*-heptulose (7dGh; Figure 12 I) was purified via medium pressure liquid chromatography (MPLC) and high pressure liquid chromatography (HPLC) as described by Brilisauer et al. (2019). Educt and product containing fractions were analyzed via thin layer chromatography (TLC) (retardation factor $R_{f\ (5\text{-deoxy-L-arabinose})}$=0.8, $R_{f\ (7dGh)}$=0.53, mobile phase $CHCl_3$:MeOH (8:5, *v/v*)). 370 µmol 5-deoxy-L-arabinose were converted to 93 µmol 7dGh, and thus a yield of 25 % was reached. The product was confirmed by HR-(+)ESI-MS (Mass to charge ratio (*m/z*) calculated for $C_7H_{14}O_6$ $[M+H]^+$: 175.0965, found: 175.0967; *m/z* calculated for $C_7H_{14}O_6$ $[M+Na]^+$: 197.0784, found: 197.0786) and nuclear magnetic resonance (NMR): ^{1}H-NMR (600 MHz, D_2O) α-pyranose: δ(ppm)=3.86 (dq, $J_{6,5}$=9.7 Hz, $J_{6,7}$=6.3 Hz, 1H, H-6), 3.69 (dd, $J_{4,3}$=9.6 Hz, $J_{4,5}$=9.4 Hz, 1H, H-4), 3.69 (d, $J_{1a,1b}$=11.7 Hz, 1H, H-1a), 3.52 (d, $J_{1b,1a}$=11.7 Hz, 1H, H-1b), 3.53 (d, $J_{3,4}$=9.6 Hz, 1H, H-3), 3.15 (dd, $J_{5,6}$=9.7 Hz, $J_{5,4}$=9.4 Hz, 1H, H-5), 1.27 (d, $J_{7,6}$=6.3 Hz, 3H, H-7); ^{13}C-NMR (150 MHz, D_2O): α-pyranose δ(ppm)=97.3 (C-2), 75.1 (C-5), 73.4 (C-4), 70.6 (C-3), 68.2 (C-6), 63.6 (C-1), 16.7 (C-7)). NMR measurement and analysis was conducted by Pascal Rath (University of Tübingen, Organic Chemistry).

4.2.4.2. Characterization of the 7dSh-mediated inhibition of the DHQS from *A. variabilis* and *A. thaliana*

In publication 3 (figure 1), it was shown that 7dSh inhibits the DHQS-mediated conversion of DAHP into 3-dehydroquinate in a competitive manner by using purified enzyme from *A. variabilis* (*Av*DHQS). Additionally, an inhibition constant of k_i=17.6 µM was determined. To further characterize this inhibition, an IC_{50}-value (half maximal inhibition) of 23.3 µM for 7dSh for *Av*DHQS was determined (Figure 12 A). As it was also shown that 7dSh strongly inhibits the germination of *A. thaliana* seedlings, the DHQS enzyme from this organism (*At*DHQS) was heterologously expressed, purified and used during an *in vitro* inhibition assay as already described for the *Av*DHQS.

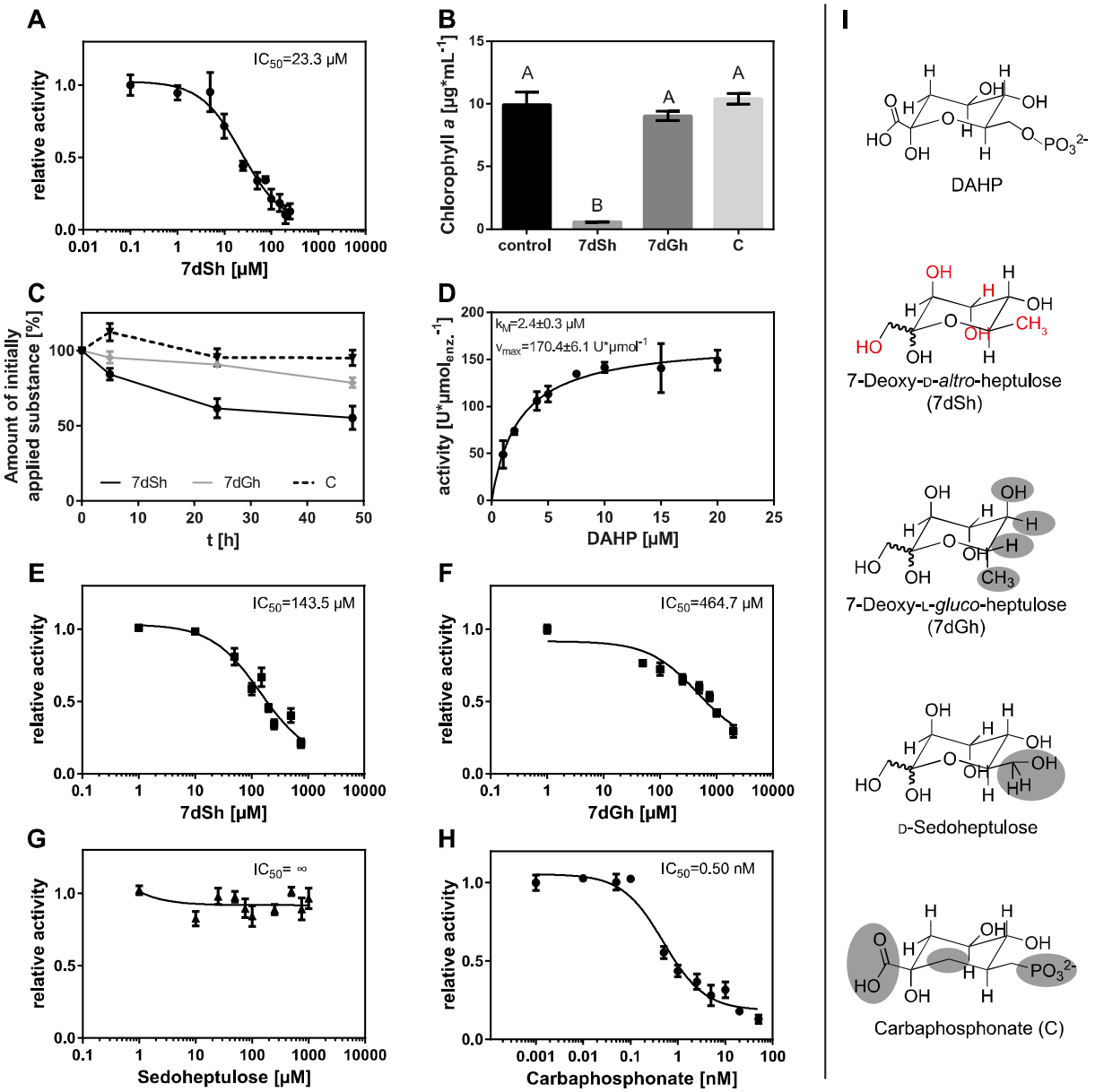

Figure 12: Analysis of inhibitory effects of 7dSh and 7dSh-like compounds on the DHQS from *A. variabilis* (*Av*DHQS) and *A. thaliana* (*At*DHQS). A: Determination of the IC_{50}-value for 7dSh for *Av*DHQS. B: Uptake of the respective compounds into *A. variabilis*, shown as the decrease of the compounds in the supernatant. C: Effect of different compounds on the growth of *A. variabilis* shown as cell density after four days of cultivation. 250 µM of the respective compound were applied to *A. variabilis* cultures inoculated at a cell density of 0.2 $\mu g*mL^{-1}$ chlorophyll *a* and cultivated for four days. Statistical analysis was performed by using a one-way ANOVA, followed by Tukey's multiple comparison test. Means that were significantly different (*p*-value <0.05) are labeled with different capital letters. D: Michaelis-Menten kinetic of the DHQS from *A. thaliana* with the native substrate DAHP. E–H: Determination of IC_{50}-values for different compounds for *At*DHQS. I: Compounds, shown in chair confirmation, examined regarding their inhibitory potential towards the DHQS mediated reaction. Differences of 7dSh and DAHP are labeled in red. Differences compared to 7dSh are labeled in grey. All graphs show mean and standard deviation of 3–4 replicates.

Initially, the kinetic parameters for DAHP using *At*DHQS were determined (k_M=2.4 ±0.3 µM; v_{max}=170.4 ±8.1 $U*\mu mol_{enzyme}^{-1}$; Figure 12 D), which were slightly higher than the parameters for DAHP using *Av*DHQS (k_M=1.8 ±0.3 µM; v_{max}=149.3 ±6.1 $U*\mu mol_{enzyme}^{-1}$; publication 3, table 1). With 143.3 µM, 7dSh showed a considerably higher IC_{50}-value for *At*DHQS (Figure 12 E) than for *Av*DHQS (Figure 12 A).

D-Sedoheptulose, a structurally very similar molecule (Figure 12 G), does not inhibit the *At*DHQS-mediated reaction, whereas carbaphosphonate, a known DHQS inhibitor (which also served as a positive control), exhibited an IC_{50}-value of 0.5 nM for *At*DHQS (Figure 12 H), which lies in the same range as the k_i-value described in literature (k_i=0.8 nM; Tian et al., 1996).

Additionally, 7dGh inhibits the *At*DHQS with an IC_{50}-value of 464.7 µM (Figure 12 F), which is much higher than that for 7dSh. To examine the effect of 7dSh, 7dGh and carbaphosphonate (C) on *A. variabilis*, a bioactivity assay was performed (Figure 12 B). After 4 days of cultivation in the presence of 250 µM of the respective compound, the optical density of 7dSh treated cells was significantly reduced, whereas 7dGh and carbaphosphonate treated cultures were not growth inhibited (Figure 12 B). Additionally, the uptake of the compounds by the cells was examined (Figure 12 C). After 48 h, around 50 % of the initially applied 7dSh was taken up by *A. variabilis* (black), whereas only a small fraction of 7dGh (grey) was taken up. Carbaphosphonate was not imported by *A. variabilis* (dashed).

4.2.4.3. Pre-incubation of *At*DHQS with 7dSh

In publication 3 (figure 1), it was shown that 7dSh is a competitive inhibitor of the DHQS enzyme. But, it can cause bactericidal effects on *A. variabilis* (Brilisauer et al., 2019). To analyze whether 7dSh has an irreversible influence on the enzyme, the enzyme was preincubated with 7dSh and the activity after different incubation times was analyzed (Figure 13). The activity of the enzyme in the presence of 200 µM 7dSh was normalized to the activity of the enzyme without inhibitor, incubated for the same time. Figure 13 clearly shows that the duration of 7dSh pre-incubation does not alter the activity of the enzyme, as the relative activity remains unaltered (grey bars).

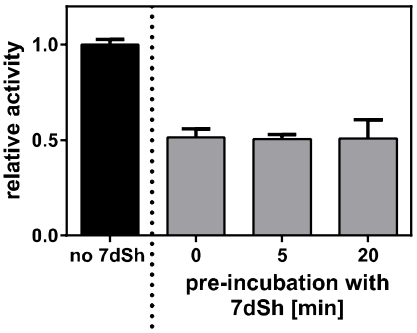

Figure 13: Influence of the pre-incubation of *At*DHQS with 7dSh on the activity of the enzyme. *At*DHQS was incubated in buffer with 200 µM 7dSh for 5 or 20 min. The reaction was started by the addition of DAHP. The approach without pre-incubation (0 min) was started by the addition of 7dSh and DAHP at the same time. Activity was normalized to activity without inhibitor. The graph shows mean and standard deviation of 3–4 biological replicates.

4.2.4.4. 7dSh accumulation in *A. variabilis*

In publication 3 (figure 2), we showed that an effective uptake of 7dSh, which results in an intracellular enrichment, is responsible for its strong inhibitory effect in *A. variabilis*. To estimate the maximum possible intracellular concentration, a rough calculation was performed. Brilisauer et al. (2019) showed that 13 µM 7dSh exhibit a bactericidal effect on *A. variabilis* when inoculated at OD_{750}=0.05. To estimate the cellular volume, a microscopical analysis was performed. Cell length and diameter were determined. *A. variabilis* possesses an average length of 4.4 ±0.7 µm and an average width of 2.8 ±0.4 µm (n=21). Assuming that the cell exhibits a cylindrical shape, the average cell volume is 28 μm^3, which corresponds to 2.8 $*10^{-8}$ µL. With the help of a "Fuchs-Rosenthal-Zählkammer", the number of cells at OD_{750}=0.05 was determined. 750 cells were present in 1 µL of culture (750 cells*μL^{-1}), which corresponds to a total cell volume of 0.021 nL in 1 µL of culture. Assuming that the entire extracellular 7dSh is taken up (13 µM=13 pmol*μL^{-1}), this leads to an intracellular concentration of 619 pmol*nL^{-1} (=0.6 M) 7dSh, which corresponds to an enrichment of around 48.000-fold and is dramatically higher than the IC_{50}/k_i-value which is around 20 µM (publication 3).

4.2.4.5. Effect of 7dSh on germinating *Nicotiana benthamiana* seedlings on soil

Brilisauer et al. (2019) showed that 7dSh as well as the commercially available herbicide glyphosate strongly reduce the germination of *A. thaliana* seedlings on agar plates (from a concentration of more than 25 µM). When applied in higher concentrations (260 µM), 7dSh showed a significantly stronger inhibition on germinating seedings than glyphosate.

To examine this effect in a physiological system, an inhibition assay for germinating seedlings on soil was developed, which can be performed in a 24-well plate. It was shown that the effect of 7dSh on soil is comparable to the effect on agar plates (publication 1, figure 6 c). To examine the effect on a further model organism, *Nicotiana benthamiana* (*N. benthamiana*) seedlings were also cultivated on soil during the presence of 260 µM 7dSh (50 µg per seedling) or 260 µM glyphosate for 14 days (38 µg per seedling) (Figure 14 C). The fresh weight of 7dSh and glyphosate treated seedlings was significantly lower when compared to the untreated control. A significant difference in the fresh weight was not observed between the two treatments (Figure 14 A). Furthermore, the number of germinated seedlings and the number of leaves were determined (Figure 14 B). Interestingly, 7dSh treated seedlings were less often germinated when compared to glyphosate treatment.

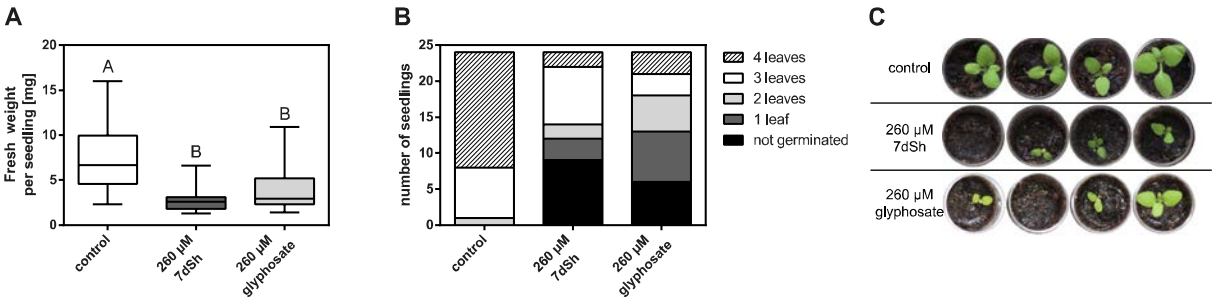

Figure 14: Effect of 7dSh and glyphosate (260 µM each) on the germination of *N. benthamiana* seedlings on soil after cultivation for 14 days in long day regime (16 h light, 8 h dark). A: Fresh weight of the seedlings. Statistical analysis was performed by means of a one-way ANOVA, followed by Tukey's multiple comparison test. Means that were significantly different (p-value <0.05) are labeled with different capital letters. Box-and-whisker plots represent the values of 15–24 germinated seedlings. B: Number of non-germinated seedlings and number of leaves per seedling after 14 days of cultivation. C: Photograph of selected seedlings after 14 days of cultivation to visualize the experimental setup.

5 Additional Material and Methods

5.1. RNA extraction, semi-quantitative RT-PCR

For RNA extraction, 2 mL cyanobacterial culture (OD_{750}≈4) was harvested by centrifugation (10 min, 16.000 x *g*, 4 °C). The supernatant was discarded, and the cell pellet was immediately frozen in liquid nitrogen. RNA extraction was performed with the RNeasy Mini Kit (Qiagen, Hilden, Germany) according to the protocol with slight modifications. Pellets were resuspended with 100 µL TE-buffer and 350 µL RLT buffer (containing β-mercaptoethanol) and then transferred into screw cap vials containing around 150 µL glass beads (⌀=0.10–0.11 mm). Cell disruption was performed with a FastPrep-24 instrument (MP Biomedicals, 5 $m*s^{-1}$, 20 sec, 3x 5 min break on ice in between). Elution of RNA was performed with 30 µL diethyl pyrocarbonate (DEPC)-H_2O. Remaining DNA was removed by digestion with DNase I (Sigma Aldrich, St. Louis, USA). The total RNA was transcribed into DNA by using High-Capacity cDNA Reverse Transcription kit (Applied Biosystems, Waltham, USA). To monitor the transcription of selected genes, semi-quantitative PCR was performed by designing gene-specific primers (Table 1), resulting in fragments of 100–200 bp in length. The PCR was performed with Red Master-Mix Taq-Polymerase (Genaxxon bioscience, Ulm, Germany) and analyzed via agarose gel electrophoresis (1.5 % agarose in TRIS-acetate-EDTA (TAE)-buffer).

Table 1: Primers used for semi-quantitative qPCR. Primers were designed with a melting temperature of 60–61 °C. Primer pairs were selected to form fragments with a size of 100–200 bp.

Amplified gene	Name	Sequence (5' → 3')
Synpcc7942_1615, *rnpA* (House keeping gene)	77_rnpA_fw	GAGTCCGTCAACGAAAGTC
	78_rnpA_rev	GTGAGCAGGCCATCAAAG
Synpcc7942_1005, Glucose-1-phosphatase	79_1005_fw	GACTGGCACGCTCTTTAC
	80_1005_rev	GGCATTCCAAGCCGTATC
Synpcc7942_1992, MTR-1P isomerase	83_1992_fw	AGCCAACTCCGACTACTC
	84_1992_rev	GGCTGGTCAGAACCAAAC
Synpcc7942_1993, MTRu-1P dehydratase	89_1993_fw	GGTGGTAACAGGCAATGG
	90_1993_rev	TTTCGTAGCCGGAGAAGG
Synpcc7942_0923, MTA phosphorylase	91_0923_fw	TTCTTTCGGCCTCAGCAG
	92_0923_rev	TCGGCCAGTAGTTGACTC
Synpcc7942_0538, Transketolase	93_0538_fw	AACAAACCCGATGCCAAG
	94_0538_rev	GTGAAGGCAACGTCAGTC

5.2. pH measurement of culture supernatants

To measure the pH of the medium during the cultivation of *S. elongatus* under different conditions, 1.5 mL of the culture were harvested by centrifugation (16.000 x *g*, 10 min, 4 °C)

and the supernatant was transferred into a new 1.5 mL reaction tube. The pH was measured with a pH meter (SevenEasy, Mettler Toledo, Columbus, USA), equipped with a micro electrode (InLab Ultra-Micro-ISM) for small volumes.

5.3. Stability of 5dAdo in BG11 and 5dAdo uptake by *S. elongatus*

After 6 days of incubation (20 µM 5dAdo in BG11, H_2O, or in *S. elongatus* cultures), 20 µL of the solution/supernatant were mixed with 80 µL MeOH and then analyzed via electrospray ionization (ESI)-HR-LC-MS as described in publication 2.

5.4. Enzymatic synthesis of 7-deoxy-L-*gluco*-2-heptulose

50 mg of 5-deoxy-L-arabinose (Carbosynth, Berkshire, UK), 1 mg thiamine pyrophosphate, 1 mg $MgCl_2x6H_2O$, 50 mg hydroxypyruvate were dissolved in 1.5 mL ultrapure water and the pH was adjusted to 7.5. After that 20 µL transketolase were added and the reaction was incubated at 30 °C and 400 rpm shaking for 7 days. The reaction was stopped by evaporation to dryness. After that the enzyme was precipitated by the addition of 25 mL MeOH and a following centrifugation step. The supernatant was evaporated to dryness in the presence of silica gel and then separated via MPLC (Chromabond Flash, RS 4 SiOH, Macherey-Nagel, Düren; flow rate: 10 $mL*min^{-1}$; 100 % $CHCl_3$, 0 % MeOH to 60 % $CHCl_3$, 40 % MeOH within 25 min). MPLC fractions were analyzed via TLC (Alugram Xtra SIL G UV_{254} Macherey-Nagel, Düren; solvent: $CHCl_3$:MeOH (8:5, *v/v*); detection with orcinol staining (Brilisauer et al., 2019)). Product containing fractions were pooled and further purified using HPLC as described by Brilisauer et al. (2019) for 7dSh.

5.5. Cultivation of *S. elongatus* (different environmental conditions; cultivation of resistant mutant)

S. elongatus was cultivated as described in publication 2. The whole culture was split in halves and then harvested by centrifugation (10 min, 4000 x *g*, room temperature), the supernatant was discarded. To remove previously formed 5dR/7dSh or combined nitrogen, the pellet was resuspended in BG11 medium or BG11 –N medium (without combined nitrogen) and centrifugation was repeated. After that, the cultures were again inoculated with fresh medium (BG11 or BG11 –N) and cultivated either in continuous light or in the dark aerated by air supplemented with 2 % CO_2. Supernatant analysis was performed via GC-MS as described in publication 2.

A spontaneous 7dSh-resistant *S. elongatus* (see publication 3 for characterization of the mutant) was cultivated as described in publication 2. Supernatant analysis was performed via GC-MS as described in publication 2.

5.6. Expression and purification of the dehydroquinate synthase from *A. thaliana*

The DHQS (EC 4.2.3.4) of *A. thaliana* (AT5G66120, thereafter: *At*DHQS) was amplified with primers 1 and 2 (Table 2). This comprises the whole protein including its N-terminal transit signal sequence for import in the chloroplasts (predicted with ChloroP; Emanuelsson et al., 1999). Cloning, expression, and purification of the DHQS was performed as described for the *Av*DHQS (see publication 3).

Table 2: Primers for the amplification of the DHQS from *A. thaliana* (AT5G66120).

Name	Sequence (5' → 3')
1_At AroB fw	GAGAGACATATGGCAGCCAACACCATTTC
2_At AroB rev His	GAGAGACTCGAGGGATTTGGAGAATGCACG

5.7. Determination of kinetic parameters (k_M, v_{max}, IC_{50})

The *in vitro* inhibition assay of the *At*DHQS-mediated reaction was performed as described for *Av*DHQS (see publication 3) with a slightly modified buffer (25 mM Tris-HCl pH 7.5). The kinetic parameters v_{max} and k_M were determined as described for *Av*DHQS (see publication 3). For IC_{50} determination, the respective, prewarmed buffer (29 °C) was mixed with 10 µM NAD^+, 2 nM of the enzyme (*Av*DHQS or *At*DHQS) and varying concentrations of 7dSh, 7dGh, carbaphosphonate (kindly provided by BASF, Ludwigshafen, Germany), D-sedoheptulose (Sigma-Aldrich, St. Louis, USA) (at least 9 different concentrations) and then preincubated for 5 min at 29 °C. For IC_{50} determination, substrate concentrations in the range of the k_M-value were chosen (2 µM DAHP for *Av*DHQS, 2.5 µM DAHP for *At*DHQS) (Brooks et al., 2012). To start the reaction, DAHP was added, and the samples were again incubated at 29 °C. Phosphate release was monitored after 5 min as described in publication 3. The measurement was performed in 3–4 replicates. For time point zero, a blank without enzyme was used. For IC_{50} determination the relative activity (activity at a specific inhibitor concentration divided by activity without inhibitor) was plotted versus the inhibitory concentration. IC_{50}-values were calculated with GraphPad Prism 6 by fitting the data to the formula: $Y = Bottom + \frac{(Top-Bottom)}{(1+\frac{X}{IC_{50}})}$ assuming a standard Hill Slope of –1.0.

Pre-incubation experiments were performed by incubating *At*DHQS (2 nM) with 200 µM 7dSh in the above-mentioned buffer for 5 or 20 min at 29 °C. The reaction was started by the addition of 2.5 µM DAHP, stopped after 5 min by the addition of malachite green as described in publication 3. The activity without pre-incubation (0 min pre-incubation) was performed by adding 7dSh as well as DAHP. The activity in the presence of the inhibitor was normalized to the activity without 7dSh (same time of pre-incubation).

5.8. Bioactivity assay with *A. variabilis*

To examine the inhibitory potential of 7dGh *in vivo*, a bioactivity assay with *A. variabilis* was performed. *A. variabilis* was inoculated in BG11 medium (Rippka et al., 1979) with an OD_{750}=0.05 (corresponding to a chlorophyll *a* content of ≈0.2 µg*mL^{-1}) and 250 µM 7dSh, 7dGh or carbaphosphonate. The assay was performed in a 24-well plate and a total volume of 1.5 mL. Cultivation was performed under constant light, continuous shaking (125 rpm) and at a temperature of 29 °C. Cell density expressed as chlorophyll *a* content was determined after 4 days. Therefore, 1 mL of culture was centrifuged, the supernatant was discarded, and the cell pellet was extracted with 1 mL 90 % MeOH (*v/v*) and incubated for 30 min in the dark. The cell debris was removed by centrifugation. Chlorophyll *a* was measured by the absorbance at 665 nm and the amount was calculated as described by Mackinney (1941).

5.9. Uptake assays with *A. variabilis*

For the examination of the uptake of 7dSh and derivatives into *A. variabilis*, 10 mL BG11 medium was inoculated with *A. variabilis* at an OD_{750}=0.5. 250 µM of 7dSh, 7dGh or carbaphosphonate were applied in water. At different time points (0, 5, 24, 48 h) 1 mL of the culture was harvested by centrifugation (25.000 x *g*, 1 min, 4 °C). 50 µL of the supernatant were mixed with 50 µL MeOH and analyzed via HR-MS (maXis 4 G ESI QTOF mass spectrometer (Bruker Daltonics, Billerica, USA) in flow injection mode. The peak areas of the extracted ion chromatograms of the respective substance ([M+H], $[M+Na]^+$) were used for a relative quantification of the derivatives in the supernatant. Therefore, the peak areas at the different time points were divided by the peak area at time point zero.

5.10. Germination assays of *N. benthamiana* on soil

To examine the germination of *N. benthamiana* on soil in the presence of 7dSh and glyphosate (Sigma-Aldrich, St. Louis, USA), each well of a 24-well plate was half-filled with autoclaved and dried soil (GS90 standard soil with vermiculite). The wells were then filled with

either 750 µL water (control), 7dSh or glyphosate (both in aqueous solutions with a concentration of 260 µM; the glyphosate solution was adjusted to pH 7.0 with NaOH; final amount: 195 nmol or 38 µg per well). *N. benthamiana* seedlings were sprayed with 70 % EtOH, incubated for 10 min for sterilization and then plated into the 24-well plate, one seed per well. To ensure simultaneous germination, the plate was sealed with parafilm and incubated for 24 h at 4 °C in the dark. After that, the seedlings were transferred to a growth chamber (air humidity 40 %) with a long day light regime (16 h light, 20 °C, light intensity of 85 µE; 8 h dark, 18 °C). Seedlings were harvested after 14 days. Number of leaves were determined by eye; fresh weight was determined by carefully removing the soil from the seedlings.

6 Discussion

Although 7dSh was already isolated from *S. setonensis* (Ito et al., 1971) in the 1970's, the discovery that the common laboratory strain *S. elongatus* also excretes this compound took place significantly later (Brilisauer et al., 2019). In the work presented here, the biosynthetic pathway for 7dSh in *S. elongatus* was elucidated. 7dSh derives from 5dAdo, an inhibitory by-product of radical SAM enzymes, which is converted into 7dSh solely by promiscuous enzyme activity, without the involvement of a specific gene cluster (Figure 5; publication 2). Moreover, it was shown that 7dSh is a competitive inhibitor of the DHQS, the second enzyme of the shikimate pathway.

7dSh can inhibit the growth of other cyanobacteria but also the growth of germinating plants (publications 1+3). Furthermore, it could be shown that the inhibitory effect on cyanobacteria is in some cases correlated with an effective uptake via promiscuous sugar transporters (publication 3). Additionally, as different cyanobacteria are sensitive towards 7dSh treatment, its role as an allelopathic inhibitor of the shikimate pathway was suggested (publication 3).

6.1. 7dSh biosynthesis blurs the line between primary and secondary metabolism

7dSh biosynthesis challenges the "classical" view on the synthesis of bioactive, secondary metabolites in two aspects: secondary metabolites in bacteria are usually products of specific metabolic pathways organized in biosynthetic gene clusters (Blin et al., 2019). In contrast, 7dSh biosynthesis is merely performed by promiscuous activity of primary metabolism enzymes, which are not even clustered (Figure 5; publication 2). As organisms with a small genome only possess the enzymatic equipment for the synthesis of essential metabolites ("primary metabolism"), the herein described strategy presents a remarkable example of how this deficiency can be circumvented by using promiscuous enzymes. In contrast to other secondary metabolites, which are basically synthetized from simple building blocks of the primary carbon metabolism, 7dSh derives from 5dAdo, an inhibitory by-product of radical SAM enzymes, which has anyway to be removed (publication 2). One could even say that the formation of "classical" secondary metabolites is an anabolic process, whereas the biosynthesis of 7dSh is rather a catabolic process, in which 5dAdo is degraded. It is very likely that the production of "secondary metabolites" from waste-products by promiscuous enzyme activity is a more common, but widely overlooked strategy. Such metabolites cannot be predicted by classical bioinformatical tools, as they rely on known, conserved biosynthetic gene clusters (Blin et al.,

2019). This is underlined by the high abundance of unexplained peaks in metabolomic datasets (Scalbert et al., 2009).

It is suggested that pathways for the synthesis of secondary metabolites are results of gene duplication events as well as the divergence of genes encoding for primary metabolism (Cavalier-Smith, 2007) and that ancient primordial enzymes were promiscuous, thereby providing the required metabolic flexibility for organisms with a small genome (Jensen, 1976). 7dSh formation via promiscuous enzyme activity in *S. elongatus*, which has a small, streamlined genome, might be an example for such an "ancient" pathway of secondary metabolite biosynthesis. It would be very interesting to see, if other 7dSh-producing organisms with large genomes, like *S. setonensis*, incorporate a specialized, non-promiscuous biosynthetic gene cluster for this purpose as this strain only excretes 7dSh but not 5dR. Unfortunately, only a 16 S rRNA sequence (Gene bank: AB184488.1), but not the full genome sequence of the strain is currently known.

Deoxy-sugars are widely distributed in nature, especially in prokaryotes, that use them as building blocks for cell wall synthesis (*e.g.*, 3,6-dideoxysugars in lipopolysaccharides of Gram-negative bacteria), as elements of extracellular polysaccharides, and as secondary metabolites with antibiotic properties (Trefzer et al., 1999; Nedal and Zotchev, 2004; Christopher et al., 2007). In contrast to 5dR/7dSh biosynthesis, where the deoxy-group derives from a radical intermediate (Figure 2 A), other deoxy-sugars are synthesized via the deoxygenation of hydroxyl groups of common carbohydrates like glucose, which have initially to be activated by a nucleoside monophosphate or diphosphate (Christopher et al., 2007). This is for example conducted by dehydratases belonging to the short-chain dehydrogenase/reductase family (Christopher et al., 2007).

6.2. Regulation of 7dSh biosynthesis

5dAdo salvage in *S. elongatus* via 5dR/7dSh excretion is dependent on the environmental conditions, although the amount of 5dAdo formed per cell is unaltered under the different conditions (publication 2, figure 2+6), suggesting that another pathway for 5dAdo salvage exists. 5dAdo degradation via the DHAP shunt is described in the literature and the enzymatic equipment is available in the strain (Figure 5, pathway marked in grey). However, the regulatory mechanism how 5dAdo or its subsequent intermediate 5dR-1P are directed either towards 5dR/7dSh formation and excretion or towards another pathway (*e.g.*, DHAP shunt; Figure 2 B) is currently unknown.

The expression of the genes involved in 5dR/7dSh biosynthesis as well as the DHAP shunt were unaltered under both conditions (Figure 6), indicating that the regulation does not take place on a transcriptional level. The apparent trigger of 5dAdo salvage via 5dR/7dSh formation is the supplementation of the cultures with 2 % CO_2. As a side-effect, the external pH of the cultures is lowered from 10.5 to around 8.0 (Figure 8 B). It should therefore be further investigated whether the external pH has a direct influence on the fate of 5dAdo in *S. elongatus*.

Different other environmental conditions were examined regarding their influence on 5dR/7dSh formation. By shifting 5dR/7dSh producing cultures into the dark, the formation of both substances was interrupted (Figure 10 A). It would be interesting to find out if this observation is due to absent 5dAdo formation or due to 5dAdo salvage via another pathway. In contrast, temporary nitrogen starvation does not have any influence on the formation of 5dR/7dSh (Figure 10 B). Due to the long cultivation periods of *S. elongatus* (around 30 days), in which cell densities of around OD_{750}=6 were reached, it might be possible that other macronutrients like phosphate or even light become limiting; this in turn might be the trigger for 5dR/7dSh formation. For the cultivation medium BG11 according to Rippka et al. (1979), it is suggested that phosphorous might be the limiting nutrient because it is supplied in amounts that does not fit to the Redfield ratio (van Alphen et al., 2018).

By supernatant analysis of knockout mutants of the involved genes, it was clearly shown that MTA phosphorylase as well as glucose-1-phosphatase are involved in 7dSh biosynthesis. The promiscuity or bifunctionality of the MTA phosphorylase to use both MTA and 5dAdo with similar efficiencies is described in different organisms (Savarese et al., 1981; Plagemann and Wohlhueter, 1983; North et al., 2020). The glucose-1-phosphatase, belonging to the HAD-like hydrolase superfamily, is in general characterized as a promiscuous enzyme which is able to dephosphorylate various sugars (Turner and Turner, 1960; Pradel and Boquet, 1988). As it can also exhibit phytase activity (Herter et al., 2006; Suleimanova et al., 2015), it might be regulated by phosphate limitation, which could be the case in *S. elongatus* cultures producing 5dR/7dSh (see paragraph above). *In vitro*, the transketolase of *S. elongatus* has a 100-fold lower affinity for 5dR than for its native substrate ribose 5-phosphate (Brilisauer et al., 2019), indicating that conditional promiscuity (altered reaction conditions: *e.g.*, pH, substrate concentrations; Piedrafita et al., 2015) might play a role in 7dSh formation.

6.3. Origin of 5dAdo

5dAdo, the precursor molecule for 7dSh biosynthesis, is an inhibitory by-product of radical SAM enzymes (Figure 2 A; Sofia et al., 2001; Wang and Frey, 2007). Due to the unique, oxygen

labile [4Fe-4S] cluster, it was assumed that these enzymes only occur in anaerobic organisms and it was speculated that they had already evolved before the advent of oxygenic photosynthesis (Marsh et al., 2010; Broderick et al., 2014). Besides occurring in obligate anaerobic organisms like *Methanocaldococcus jannaschii*, in which 2 % of the genome encodes for them, various radical SAM enzymes were also identified in aerobic organisms during the last years (*e.g.*, *R. rubrum*, *S. elongatus*, humans; Beaudoin et al., 2018; North et al., 2020), but with a lower frequency (publication 2; publication 4). In *R. rubrum*, radical SAM enzymes are active, both under anaerobic and aerobic conditions, however 5dAdo formation was 75-fold lower under the latter (North et al., 2020).

For *S. elongatus* in was also clearly shown that at least some of the 18 radical SAM enzymes (publication 2, supporting information) are active under aerobic conditions, because a mutant impaired in 5dAdo salvage excretes significant amounts of this substance (publication 2, figure 6). As several radical SAM enzymes are involved in the synthesis of essential cofactors – like biotin and lipoic acid, which are essential for the activities of the acetyl-CoA-carboxylase and the pyruvate dehydrogenase complex – it is assumed that they are mainly responsible for 5dAdo formation in *S. elongatus*. It is certainly worth to further investigate which of the radical SAM enzymes are exactly responsible for its synthesis, *e.g*., by monitoring the gene expression of all radical SAM enzymes (publication 2, table S3) by semi-quantitative RT-PCR.

6.4. 7dSh biosynthesis – an alternative pathway for 5dAdo salvage[2]

Along with the elucidation of the biosynthetic pathway of 7dSh in *S. elongatus*, a new 5dAdo salvage pathway was discovered (publication 2). 5dR was reported in the literature as an intermediate of 5dAdo salvage (Beaudoin et al., 2018; North et al., 2020), but the excretion and accumulation in the supernatant as a consequence of 5dAdo salvage had not been previously described. By the formation of 7dSh, it is clearly shown that 5dAdo salvage can be more than the removal of an inhibitory "waste" product. This pathway provides *S. elongatus* with an advantage regarding its growth and helps to colonize its own niche. A similar phenomenon is described for pathogenic strains of several organisms (*e.g*., *Clostridium tetani*, *Clostridium botulinum*, *Bacillus cereus*, *Bacillus anthracis*, various *E. coli* ExPEC strains), which possess putative DHAP shunt gene clusters, whereas the non-pathogenic genera of this strain do not (Beaudoin et al., 2018; North et al., 2020; Rapp and Forchhammer, 2021). The presence of this gene cluster enables *E. coli* strains, colonizing nutrient-limited extraintestinal

[2] Parts of this chapter are adopted from publication 4: Rapp and Forchhammer (2021), 5-Deoxyadenosine metabolism – more than "waste" disposal. *Microbial Physiology*.

environments (urine, blood, and cerebrospinal fluid), to use 5dAdo and its intermediates, which are common metabolites in this environment (Lee et al., 2004), as an exclusive carbon source (North et al., 2020). Commensal *E. coli* were not able to utilize these metabolites, indicating that the presence of a DHAP shunt gene cluster leads to a growth advantage (North et al., 2020). These examples clearly show that 5dAdo is more than an inhibitory by-product, and its salvage is more than simply a kind of "waste disposal".

As during the last years, various non-canonical MSP pathways were discovered, some of them connected to 5dAdo salvage, it is likely that further salvage pathways might exist (Erb et al., 2012; North et al., 2017; Miller et al., 2018b; Miller et al., 2018a; North et al., 2020).

6.5. The cyanobacterial exometabolome

Metabolomic analyses of cell extracts, including cyanobacteria, are commonly applied (Schwarz et al., 2013), but the composition of the exometabolome, or the metabolic footprint, which contains the full set of extracellular metabolites (Kell et al., 2005), is usually not profoundly analyzed. In addition to bioactive compounds, which are usually isolated by a bioactivity guided purification protocol (*e.g.*, Brilisauer et al., 2019; Atanasov et al., 2021), a huge variety of other compounds is known to be excreted by bacteria (*e.g.*, organic acids; Dörries and Lalk, 2013; Ueda et al., 2016). Due to the high salt content of cyanobacterial media (Rippka et al., 1979), the analysis via ion exchange chromatography is impossible without prior desalting. In this work, a GC-MS based method for the analysis of polar compounds in cyanobacterial supernatants was developed, which can be further used to study the exometabolome of cyanobacteria. The occurrence of a multitude of unidentified peaks in the GC-MS measurements conducted in the study shows that there are much more substances to unravel. This is underlined by the finding that *Synechococcus* sp. PCC 7002 excretes at least 55 metabolites (Baran et al., 2010).

6.6. Ecological role of 7dSh

Following its synthesis, 7dSh is immediately excreted by *S. elongatus* to avoid autotoxicity (publication 2). A yet unidentified excretion system helps the strain to overcome the inhibitory effect of the endogenously formed 7dSh. Additionally, the precursor molecule 5dR, which also inhibits the producer strain when present in high concentrations, is instantaneously exported, but also (re-) imported (publication 2, figure 4). The import- and export system, however, has not yet been identified.

Some other cyanobacteria, but also dicotyledonous plants, are highly affected by 7dSh, whereas only minor/no activity was shown towards heterotrophic bacteria like *E. coli* or *Gluconobacter oxidans* (publications 1+3; Brilisauer et al., 2019). Therefore, it can be suggested that 7dSh is an allelochemical, targeting organisms residing within the same ecological niche (publication 3).

7dSh is the first allelopathic inhibitor from cyanobacteria targeting the shikimate pathway (publication 3); others rather inhibit photosystem II (*e.g.*, cyanobacterin, fischerellin A; Mason et al., 1982; Gross et al., 1991). For *A. variabilis* and *Synechocystis* sp., it was shown that 7dSh sensitivity is correlated with an effective uptake via structurally different, but promiscuous sugar transporters (publication 3). Spontaneous mutations lead to a loss in 7dSh sensitivity, but more important also in the capability to use fructose/glucose as a(n) (additional) carbon source (publication 3). This suggests that *S. elongatus* might compensate its inability to grow heterotrophically by the excretion of 7dSh, which either inhibits its competitors or results in the loss of their capability of heterotrophic growth (publication 3). Nevertheless, other cyanobacterial strains are not affected by 7dSh, indicating that other resistance mechanisms, like export systems, might exist, too (publication 3). The different sensitivities of cyanobacteria support the common phenomenon, that in complex communities, some species remain sensitive towards an allelopathic inhibitor, whereas others develop strategies to tolerate it (Bubak et al., 2020).

6.7. 7dSh and its potential application as an herbicide

In this work, the herbicidal potential of 7dSh was further examined. Therefore, a germinating assay on soil was developed (see Figure 14 C for a visualization of the assay). The growth of *A. thaliana* seedlings in the presence of 7dSh was significantly reduced compared to the untreated control, but also compared to the treatment with glyphosate (publication 1, figure 6 c). The effect on the fresh weight of germinating *N. benthamiana* seedlings was comparable (Figure 14 A). However, no difference was observed compared with glyphosate treatment. Interestingly, the total number of non-germinated seedlings treated with 7dSh was higher than during glyphosate treatment (Figure 14 B). This suggests that in this state of development, 7dSh is a more potent herbicide.

The breakthrough of glyphosate as the dominant herbicide was strongly supported by the development of transgenic, resistant crops, which were obtained by the introduction of glyphosate insensitive EPSP synthases (Della-Cioppa et al., 1987; Funke et al., 2006; Duke and Powles, 2008). In this work, an alternative mechanism for the development of resistance is

shown: it can be obtained by the disruption of the uptake, which was observed for *A. variabilis* and *Synechocystis* sp., in which the respective transporters were affected (publication 3, figure 2, figure 4). Interestingly, *Bacillus subtilis* (*B. subtilis*) also gained glyphosate resistance by the disruption of the respective transporter, whereas *E. coli* elevated the production of the target gene EPSPS or obtained a target with decreased sensitivity (Wicke et al., 2019).

A potential herbicide must be taken up, but the compound must subsequently be distributed quickly and evenly within the whole plant in order to exhibit systemic toxicity. In plants, carbohydrates are distributed via monosaccharide transporters belonging to the major facilitator superfamily (Williams et al., 2000). Since it was shown that 7dSh can be transported via the glucose permease in *Synechocystis* sp. (publication 3, figure 4), which belongs to the same superfamily (Schmetterer, 1990), it is very likely that 7dSh can also be distributed within plants. This could be monitored by means of $^{13}C_5$-labeled 7dSh in the future, whose synthesis is described in publication 2.

The necessity of a proper uptake of an inhibitory substance is underlined by the fact that carbaphosphonate, a very strong inhibitor of the DHQS (IC_{50} is 287.000-times lower than for 7dSh; Figure 12 E, H), has no influence on the growth of *A. variabilis* (Figure 12 B), but also of plants (Pompliano et al., 1989; Montchamp et al., 1992; Tian et al., 1996), as is not taken up (Figure 12 C). A rapid uptake, leading to strong intracellular accumulation is essential for the strong inhibitory effect of 7dSh in *A. variabilis*, but also in *Synechocystis* sp. (publication 3; additional results, chapter 4.2.4.4). It is very likely that the missing uptake of carbaphosphonate is due to the highly negative charge of the phosphonate group. Uncharged 7dSh mimics useful carbohydrates and can sneak into the cells of different cyanobacteria like a Trojan horse (publication 3). Interestingly, glyphosate is also charged, but it can nevertheless taken up, *e.g.*, by an amino acid transporter in *B. subtilis*, whereas the uptake mechanism in plants is not known (Wicke et al., 2019).

The *in vitro* data clearly showed that *At*DHQS is inhibited by 7dSh, although the sensitivity is 6-times lower that for *Av*DHQS. The influence of the presence of the N-terminal transit signal sequence should be further investigated. 7dSh, as an antimetabolite of DAHP (k_i=17.6 µM for *Av*DHQS), as well as glyphosate as an antimetabolite of phosphoenolpyruvate (k_i=1 µM for EPSPS of *Klebsiella pneumoniae*), are competitive inhibitors of the shikimate pathway by either inhibiting the DHQS or the EPSPS (publication 3; Steinrücken and Amrhein, 1984). The competitive way of the 7dSh-mediated DHQS inhibition is further underlined by the fact that pre-incubation of the enzyme with 7dSh does not diminish the activity (Figure 13).

Glyphosate can be degraded by the soil microbiota, but the main degradation product aminomethylphosphonic acid (AMPA) accumulates in the soil and the degradation of this product is very slow (Rueppel et al., 1977; Kolpin et al., 2006). In contrast, due to the elucidation of the biosynthetic pathway of 7dSh, which is performed by promiscuous enzymes of the primary metabolism, it is most likely that 7dSh can be completely degraded by the soil microbial community. This might be a useful property when developing a sustainable herbicide. All this data, together with the results that 7dSh has no detrimental effect on eukaryotic cell lines and the development of zebra fish (Brilisauer et al., 2019; Schweizer et al., 2019), suggest that 7dSh might be used as a sustainable and safe herbicide.

6.8. The terminal deoxy-group of 7dSh is essential for the inhibition of the DHQS

To further analyze the 7dSh-mediated inhibition of the DHQS enzyme, D-sedoheptulose was used as a control in the *in vitro* inhibition assay. 7dSh (7-deoxy-D-sedoheptulose) and D-sedoheptulose (sedoheptulose) have the same constitution and configuration, except for the hydroxyl-group at C_7 which is replaced by a hydrogen in 7dSh (see Figure 12 I). Despite the high similarity of both molecules, D-sedoheptulose did not show an inhibitory effect towards *At*DHQS, whereas an IC_{50}-value of 143.5 µM could be determined for 7dSh. This clearly showed that the deoxy-group (or – in other words – the missing hydroxyl-group) is essential for its inhibitory effect. This might be explained by the observation that synthetic inhibitors with shortened side chains (phosphonate compared to homophosphonate; see Figure 4 D) can also bind more tightly to the enzyme (Bender et al., 1989b).

The importance of the terminal deoxy-group is further underlined by the fact that the 7dGh derivative which is structurally more different than 7dSh as well as the native substrate DAHP, inhibits *At*DHQS with an IC_{50}-value of 465 µM, whereas D-sedoheptulose does not. At first glance, this is surprising as the configuration of the hydroxyl-group of 7dGh at C_5, which is essential for the first step of the DHQS mediated reaction (see Figure 4 A; Widlanski et al., 1989; Carpenter et al., 1998), is altered (Figure 12 I). The inhibitory potential might be explained with the following hypothesis: 7dGh, just like DAHP, is predominantly present as α-pyranose (chapter 4.2.4.1; Garner and Herrmann, 1984), whereas 7dSh and D-sedoheptulose are mainly present as furanoses (β-/α-furanose; 64 %/16 % for D-sedoheptulose). Only a minor fraction exhibits α-pyranose constitution (20 % for D-sedoheptulose; Ceusters et al., 2013; Brilisauer et al., 2019; Rapp et al., 2021). DHQS can solely bind pyranoses (Widlanski et al., 1989), therefore only the small pyranose fraction of 7dSh can act as inhibitor. Although 7dGh

fits into the active site less well than 7dSh, its (small) inhibitory potential can be explained by its exclusive occurrence in pyranose constitution.

The insertion of a carboxylic acid group at C_1, which is present in carbaphosphonate and DAHP, might improve the inhibitory effect of 7dSh, as its negative charge is involved in the coordination of the substrate or the inhibitor in the active site (see Figure 4 A; Carpenter et al., 1998). Additionally, the synthesis of 7-deoxy-D-*manno*-2-heptulose might be interesting, as the configuration of its hydroxyl-groups (to be more precise: the hydroxyl-group on C_4), is even more similar to the native substrate DAHP than in 7dSh. It is however, impossible to synthesize this carbohydrate by means of the transketolase as described for 7dSh and 7dGh because the transketolase reaction leads to the formation of 3*S*/4*R*-configured ketoses (Turner, 2000).

6.9. Additional target for 7dSh?

It was clearly shown by *in vitro* inhibition assays (publication 3; Figure 12 A, E) as well as metabolome analysis (Brilisauer et al., 2019), that 7dSh inhibits DHQS. It can nevertheless not be excluded that secondary targets of 7dSh might exist: 7dSh-treated *A. variabilis* cells showed a morphologically aberrant phenotype (Brilisauer, 2017). The cells looked swollen and exhibited a lower autofluorescence. The filaments showed a strong fragmentation: after 48 h nearly all of them only consisted of 1–5 cells per filament, whereas in untreated cultures more than 50 % of the filaments were built up of more than 25 cells (Brilisauer, 2017). It was speculated that 7dSh might also influence cell division or cell wall synthesis (Brilisauer, 2017). Indeed, the initial steps of 3-deoxy-D-*manno*-octulosonic acid (KDO, 2-keto-deoxyoctonate) synthesis, an essential component of the lipopolysaccharide layer of Gram-negative bacteria as well as the plant cell wall (Doong et al., 1991; Radaev et al., 2000), are similar to the first reactions of the shikimate pathway (Figure 15). Besides the structural similarities of the intermediates, KDO 8-P synthase and DAH 7-P synthase are catalytically similar and are probably a product of a divergent evolutionary process from a common ancestor (Radaev et al., 2000).

7dSh – as an antimetabolite of DAHP – could also be an antimetabolite of KDO 8-phosphate. This hypothesis is underlined by unpublished metabolome data from 7dSh treated *Lemna paucicostata*. Besides the known effects on amino acid metabolism, these data showed a dramatically increased pool size of ribulose 5-phosphate, the precursor molecule for KDO biosynthesis (Figure 15 B). Additionally, significant changes within the metabolic class of "complex lipids, fatty acids and related" were observed, indicating that the inhibition of the synthesis of cell wall components will disturb the composition of the membranes. Additionally,

5dR (the precursor molecule of 7dSh) inhibits the growth of bacteria, *e.g.*, *S. elongatus* (publication 2) and *B. subtilis* (Beaudoin et al., 2018). It can therefore speculated that it might be an antimetabolite of arabinose 5-phosphate. The influence of 7dSh or 5dR on the KDO biosynthetic pathway should be further investigated in the future.

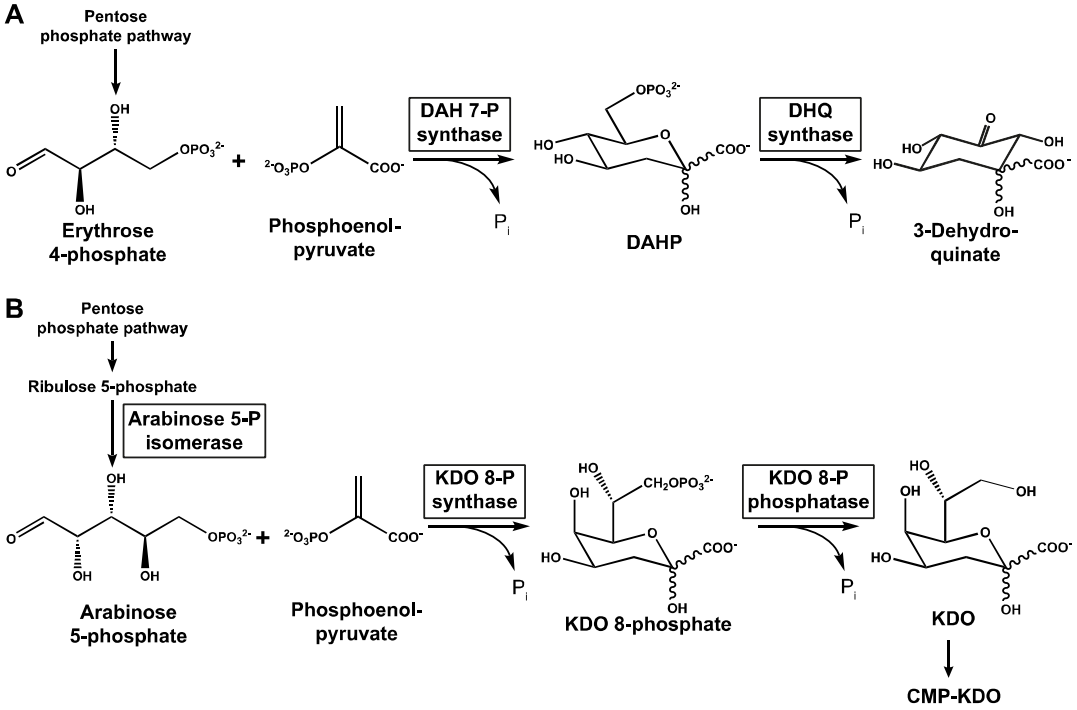

Figure 15: Comparison of the first steps of the shikimate pathway and the biosynthetic pathway for KDO biosynthesis. A: First steps of the shikimate pathway. The precursor molecule erythrose 4-phosphate derives from the pentose phosphate pathway. B: First steps of the biosynthetic pathway for KDO biosynthesis. Ribulose 5-phosphate, the precursor molecule for arabinose 5-phosphate, derives from the pentose phosphate pathway.

7 References

Altermann, W. and Kazmierczak, J. (2003). Archean microfossils: a reappraisal of early life on Earth. *Research in Microbiology*, 154 (9), https://doi.org/10.1016/j.resmic.2003.08.006.

Anbar, A. D., Duan, Y., Lyons, T. W., Arnold, G. L., Kendall, B., Creaser, R. A., Kaufman, A. J., Gordon, G. W., Scott, C., Garvin, J. and Buick, R. (2007). A whiff of oxygen before the Great Oxidation Event? *Science*, 317 (5846), https://doi.org/10.1126/science.1140325.

Årstøl, E. and Hohmann-Marriott, M. F. (2019). Cyanobacterial siderophores-physiology, structure, biosynthesis, and applications. *Marine Drugs*, 17 (5), https://doi.org/10.3390/md17050281.

Atanasov, A. G., Zotchev, S. B., Dirsch, V. M. and Supuran, C. T. (2021). Natural products in drug discovery: advances and opportunities. *Nature Reviews Drug Discovery*, 20 (3), https://doi.org/10.1038/s41573-020-00114-z.

Baier, F. and Tokuriki, N. (2014). Connectivity between catalytic landscapes of the metallo-β-lactamase superfamily. *Journal of Molecular Biology*, 426 (13), https://doi.org/10.1016/j.jmb.2014.04.013.

Balskus, E. P. and Walsh, C. T. (2010). The genetic and molecular basis for sunscreen biosynthesis in cyanobacteria. *Science*, 329 (5999), https://doi.org/10.1126/science.1193637.

Baran, R., Bowen, B. P., Bouskill, N. J., Brodie, E. L., Yannone, S. M. and Northen, T. R. (2010). Metabolite identification in *Synechococcus* sp. PCC 7002 using untargeted stable isotope assisted metabolite profiling. *Analytical Chemistry*, 82 (21), https://doi.org/10.1021/ac1020112.

Basu, A., Kozikowski, A. P. and Lazo, J. S. (1992). Structural requirements of lyngbyatoxin A for activation and downregulation of protein kinase C. *Biochemistry*, 31 (15), https://doi.org/10.1021/bi00130a013.

Beaudoin, G. A. W., Li, Q., Folz, J., Fiehn, O., Goodsell, J. L., Angerhofer, A., Bruner, S. D. and Hanson, A. D. (2018). Salvage of the 5-deoxyribose byproduct of radical SAM enzymes. *Nature Communications*, 9 (1), https://doi.org/10.1038/s41467-018-05589-4.

Bekker, A., Holland, H. D., Wang, P.-L., Rumble, D., Stein, H. J., Hannah, J. L., Coetzee, L. L. and Beukes, N. J. (2004). Dating the rise of atmospheric oxygen. *Nature*, 427 (6970), https://doi.org/10.1038/nature02260.

Bender, S. L., Mehdi, S. and Knowles, J. R. (1989a). Dehydroquinate synthase: The role of divalent metal cations and of nicotinamide adenine dinucleotide in catalysis. *Biochemistry*, 28 (19), https://doi.org/10.1021/bi00445a009.

Bender, S. L., Widlanski, T. and Knowles, J. R. (1989b). Dehydroquinate synthase: The use of substrate analogues to probe the early steps of the catalyzed reaction. *Biochemistry*, 28 (19), https://doi.org/10.1021/bi00445a010.

Berkovitch, F., Nicolet, Y., Wan, J. T., Jarrett, J. T. and Drennan, C. L. (2004). Crystal structure of biotin synthase, an *S*-adenosylmethionine-dependent radical enzyme. *Science*, 303 (5654), https://doi.org/10.1126/science.1088493.

Bickel, H., Palme, L. and Schultz, G. (1978). Incorporation of shikimate and other precursors into aromatic amino acids and prenylquinones of isolated spinach chloroplasts. *Phytochemistry*, 17 (1), https://doi.org/10.1016/S0031-9422(00)89691-0.

Blin, K., Kim, H. U., Medema, M. H. and Weber, T. (2019). Recent development of antiSMASH and other computational approaches to mine secondary metabolite biosynthetic gene clusters. *Briefings in Bioinformatics*, 20 (4), https://doi.org/10.1093/bib/bbx146.

Boocock, M. R. and Coggins, J. R. (1983). Kinetics of 5-enolpyruvylshikimate-3-phosphate synthase inhibition by glyphosate. *FEBS Letters*, 154 (1), https://doi.org/10.1016/0014-5793(83)80888-6.

Bosak, T., Liang, B., Sim, M. S. and Petroff, A. P. (2009). Morphological record of oxygenic photosynthesis in conical stromatolites. *Proceedings of the National Academy of Sciences*, 106 (27), https://doi.org/10.1073/pnas.0900885106.

Brilisauer, K. (2017). A novel antimetabolite from *Synechococcus elongatus* PCC 7942 as an inhibitor of photoautotrophic organisms. *Dissertation. Eberhard Karls Universität Tübingen.*

Brilisauer, K., Rapp, J., Rath, P., Schöllhorn, A., Bleul, L., Weiß, E., Stahl, M., Grond, S. and Forchhammer, K. (2019). Cyanobacterial antimetabolite 7-deoxy-sedoheptulose blocks the shikimate pathway to inhibit the growth of prototrophic organisms. *Nature Communications*, 10 (545), https://doi.org/10.1038/s41467-019-08476-8.

Broderick, J. B., Duffus, B. R., Duschene, K. S. and Shepard, E. M. (2014). Radical *S*-adenosylmethionine enzymes. *Chemical Reviews*, 114 (8), https://doi.org/10.1021/cr4004709.

Brooks, H. B., Geeganage, S., Kahl, S. D., Montrose, C., Sittampalam, S., Smith, M. C. and Weidner, J. R. (2012). "Basics of enzymatic assays for HTS," in *Assay Guidance Manual*, eds. H. B. Brooks, S. Geeganage, S. D. Kahl, C. Montrose, S. Sittampalam, M. C. Smith, et al. (Eli Lilly & Company and the National Center for Advancing Translational Sciences).

Bubak, I., Śliwińska-Wilczewska, S., Głowacka, P., Szczerba, A. and Możdżeń, K. (2020). The importance of allelopathic picocyanobacterium *Synechococcus* sp. on the abundance, biomass formation, and structure of phytoplankton assemblages in three freshwater lakes. *Toxins*, 12 (4), https://doi.org/10.3390/toxins12040259.

Byng, G. S., Johnson, J. L., Whitaker, R. J., Gherna, R. L. and Jensen, R. A. (1983). The evolutionary pattern of aromatic amino acid biosynthesis and the emerging phylogeny of pseudomonad bacteria. *Journal of Molecular Evolution*, 19 (3), https://doi.org/10.1007/BF02099974.

Cardellina, J. H., Marner, F. J. and Moore, R. E. (1979). Seaweed dermatitis: structure of lyngbyatoxin A. *Science*, 204 (4389), https://doi.org/10.1126/science.107586.

Carpenter, E. P., Hawkins, A. R., Frost, J. W. and Brown, K. A. (1998). Structure of dehydroquinate synthase reveals an active site capable of multistep catalysis. *Nature*, 394 (6690), https://doi.org/10.1038/28431.

Case, M. E. and Giles, N. H. (1971). Partial enzyme aggregates formed by pleiotropic mutants in the *arom* gene cluster of *Neurospora crassa*. *Proceedings of the National Academy of Sciences of the United States of America*, 68 (1), https://doi.org/10.1073/pnas.68.1.58.

Cavalier-Smith, T. (2007). "Origins of secondary metabolism," in *Ciba Foundation Symposium 171 - Secondary Metabolites: their Function and Evolution* (John Wiley & Sons, Ltd), p. 64–87.

Ceusters, J., Godts, C., Peshev, D., Vergauwen, R., Dyubankova, N., Lescrinier, E., Proft, M. P. de and van den Ende, W. (2013). Sedoheptulose accumulation under CO_2 enrichment in leaves of *Kalanchoë pinnata*: A novel mechanism to enhance C and P homeostasis? *Journal of Experimental Botany*, 64 (6), https://doi.org/10.1093/jxb/ert010.

Challand, M. R., Ziegert, T., Douglas, P., Wood, R. J., Kriek, M., Shaw, N. M. and Roach, P. L. (2009). Product inhibition in the radical *S*-adenosylmethionine family. *FEBS Letters*, 583 (8), https://doi.org/10.1016/j.febslet.2009.03.044.

Christopher, J. T., Charles, E. M. and Liu, H. (2007). Unusual sugar biosynthesis and natural product glycodiversification. *Nature*, 446 (7139), https://doi.org/10.1038/nature05814.

Cohen, A., Sendersky, E., Carmeli, S. and Schwarz, R. (2014). Collapsing aged culture of the cyanobacterium *Synechococcus elongatus* produces compound(s) toxic to photosynthetic organisms. *PLOS ONE*, 9 (6), https://doi.org/10.1371/journal.pone.0100747.

Conradi, F. D., Mullineaux, C. W. and Wilde, A. (2020). The role of the cyanobacterial type IV pilus machinery in finding and maintaining a favourable environment. *Life*, 10 (11), https://doi.org/10.3390/life10110252.

Copeland, A., Lucas, S., Lapidus, A., Barry, K., Detter, J. C., Glavina, T., Hammon, N., Israni, S., Pitluck, S., Schmutz, J., Larimer, F., Land, M. M., Kyrpides, N., Lykidis, A., Golden, S. and Richardson, P. (2014). Complete sequence of chromosome 1 of *Synechococcus elongatus* PCC 7942.

Copley, S. (2003). Enzymes with extra talents: moonlighting functions and catalytic promiscuity. *Current Opinion in Chemical Biology*, 7 (2), https://doi.org/10.1016/S1367-5931(03)00032-2.

Copley, S. D. (2017). Shining a light on enzyme promiscuity. *Current Opinion in Structural Biology*, 47, https://doi.org/10.1016/j.sbi.2017.11.001.

Cotton, C. A. R., Bernhardsgrütter, I., He, H., Burgener, S., Schulz, L., Paczia, N., Dronsella, B., Erban, A., Toman, S., Dempfle, M., Maria, A. de, Kopka, J., Lindner, S. N., Erb, T. J. and Bar-even, A. (2020). Underground isoleucine biosynthesis pathways in *E. coli*. *eLife*, 9, https://doi.org/10.7554/eLife.54207.

Czerwik-Marcinkowska, J. and Mrozińska, T. (2011). Algae and cyanobacteria in caves of the polish Jura. *Polish Botanical Journal*, 56 (2).

D'Ari, R. and Casadesús, J. (1998). Underground metabolism. *BioEssays*, 20 (2), https://doi.org/10.1002/(SICI)1521-1878(199802)20:2<181:AID-BIES10>3.0.CO;2-0.

De Nobel, W. T., Matthijs, H. C. P., von Elert, E. and Mur, L. R. (1998). Comparison of the light-limited growth of the nitrogen-fixing cyanobacteria *Anabaena* and *Aphanizomenon*. *The New Phytologist*, 138 (4), https://doi.org/10.1046/j.1469-8137.1998.00155.x.

Della-Cioppa, G., Bauer, S. C., Taylor, M. L., Rochester, D. E., Klein, B. K., Shah, D. M., Fraley, R. T. and Kishore, G. M. (1987). Targeting a herbicide–resistant enzyme from *Escherichia coli* to chloroplasts of higher plants. *Nature Biotechnology*, 5 (6), https://doi.org/10.1038/nbt0687-579.

Dewick, P. M. (2009). *Medicinal natural products: A biosynthetic approach*. Chichester: Wiley a John Wiley and Sons Ltd.

Dittmann, E., Gugger, M., Sivonen, K. and Fewer, D. P. (2015). Natural product biosynthetic diversity and comparative genomics of the cyanobacteria. *Trends in Microbiology*, 23 (10), https://doi.org/10.1016/j.tim.2015.07.008.

Doan, N. T., Rickards, R. W., Rothschild, J. M. and Smith, G. D. (2000). Allelopathic actions of the alkaloid 12-*epi*- hapalindole E isonitrile and calothrixin A from cyanobacteria of the genera *Fischerella* and *Calothrix*. *Journal of Applied Phycology*, 12 (3), https://doi.org/10.1023/A:1008170007044.

Doan, N. T., Stewart, P. R. and Smith, G. D. (2001). Inhibition of bacterial RNA polymerase by the cyanobacterial metabolites 12-epi-hapalindole E isonitrile and calothrixin A. *FEMS Microbiology Letters*, 196 (2), https://doi.org/10.1111/j.1574-6968.2001.tb10554.x.

Doong, R. L., Ahmad, S. and Jensen, R. A. (1991). Higher plants express 3-deoxy-D-*manno*-octulosonate 8-phosphate synthase. *Plant, Cell & Environment*, 14 (1), https://doi.org/10.1111/j.1365-3040.1991.tb01377.x.

Dörries, K. and Lalk, M. (2013). Metabolic footprint analysis uncovers strain specific overflow metabolism and D-isoleucine production of *Staphylococcus Aureus* COL and HG001. *PLOS ONE*, 8 (12), https://doi.org/10.1371/journal.pone.0081500.

Duke, S. O. and Powles, S. B. (2008). Glyphosate: a once-in-a-century herbicide. *Pest Management Science*, 64 (4), https://doi.org/10.1002/ps.1518.

Edwards, D. J. and Gerwick, W. H. (2004). Lyngbyatoxin biosynthesis: sequence of biosynthetic gene cluster and identification of a novel aromatic prenyltransferase. *Journal of the American Chemical Society*, 126 (37), https://doi.org/10.1021/ja047876g.

Ehrenreich, I. M., Waterbury, J. B. and Webb, E. A. (2005). Distribution and diversity of natural product genes in marine and freshwater cyanobacterial cultures and genomes. *Applied and Environmental Microbiology*, 71 (11), https://doi.org/10.1128/AEM.71.11.7401-7413.2005.

Elert, E. von and Jüttner, F. (1997). Phosphorus limitation and not light controls the extracellular release of allelopathic compounds by *Trichormus doliolum* (cyanobacteria). *Limnology and Oceanography*, 42 (8), https://doi.org/10.4319/lo.1997.42.8.1796.

Emanuelsson, O., Nielsen, H. and Heijne, G. von (1999). ChloroP, a neural network-based method for predicting chloroplast transit peptides and their cleavage sites. *Protein Science*, 8 (5), https://doi.org/10.1110/ps.8.5.978.

Erb, T. J., Evans, B. S., Cho, K., Warlick, B. P., Sriram, J., Wood, B. M., Imker, H. J., Sweedler, J. V., Tabita, F. R. and Gerlt, J. A. (2012). A RubisCO-like protein links SAM metabolism with isoprenoid biosynthesis. *Nature Chemical Biology*, 8 (11), https://doi.org/10.1038/nchembio.1087.

Etchegaray, A., Rabello, E., Dieckmann, R., Moon, D. H., Fiore, M. F., Döhren, H. von, Tsai, S. M. and Neilan, B. A. (2004). Algicide production by the filamentous cyanobacterium *Fischerella* sp. CENA 19. *Journal of Applied Phycology*, 16 (3), https://doi.org/10.1023/B:JAPH.0000048509.77816.5e.

Figueredo, C. C., Giani, A. and Bird, D. F. (2007). Does allelopathy contributes to *Cylindrospermopsis raciborskii* (cyanobacteria) bloom occurence and geographic expansion? *Journal of Phycology*, 43 (2), https://doi.org/10.1111/j.1529-8817.2007.00333.x.

Flombaum, P., Gallegos, J. L., Gordillo, R. A., Rincón, J., Zabala, L. L., Jiao, N., Karl, D. M., Li, W. K. W., Lomas, M. W., Veneziano, D., Vera, C. S., Vrugt, J. A. and Martiny, A. C. (2013). Present and future global distributions of the marine cyanobacteria *Prochlorococcus* and *Synechococcus*. *Proceedings of the National Academy of Sciences*, 110 (24), https://doi.org/10.1073/pnas.1307701110.

Fontecave, M., Atta, M. and Mulliez, E. (2004). *S*-adenosylmethionine: nothing goes to waste. *Trends in Biochemical Sciences*, 29 (5), https://doi.org/10.1016/j.tibs.2004.03.007.

Funke, T., Han, H., Healy-Fried, M. L., Fischer, M. and Schönbrunn, E. (2006). Molecular basis for the herbicide resistance of Roundup Ready crops. *Proceedings of the National Academy of Sciences*, 103 (35), https://doi.org/10.1073/pnas.0603638103.

Garner, C. C. and Herrmann, K. M. (1984). Structural analysis of 3-deoxy-D-*arabino*-heptulosonate 7-phosphate by ^{1}H-and natural-abundance ^{13}C-n.m.r. spectroscopy. *Carbohydrate Research*, 132 (2), https://doi.org/10.1016/0008-6215(84)85228-3.

Giovannoni, S. J., Turner, S., Olsen, G. J., Barns, S., Lane, D. J. and Pace, N. R. (1988). Evolutionary relationships among cyanobacteria and green chloroplasts. *Journal of Bacteriology*, 170 (8), https://doi.org/10.1128/jb.170.8.3584-3592.1988.

Gleason, F. K. and Paulson, J. L. (1984). Site of action of the natural algicide, cyanobacterin, in the blue-green alga, *Synechococcus* sp. *Archives of Microbiology*, 138 (3), https://doi.org/10.1007/BF00402134.

Golden, S. S. (2019). The international journeys and aliases of *Synechococcus elongatus*. *New Zealand Journal of Botany*, 57 (2), https://doi.org/10.1080/0028825X.2018.1551805.

Golden, S. S., Brusslan, J. and Haselkorn, R. (1987). Genetic engineering of the cyanobacterial chromosome. *Methods in Enzymology*, 153, https://doi.org/10.1016/0076-6879(87)53055-5.

Golden, S. S. and Sherman, L. A. (1984). Optimal conditions for genetic transformation of the cyanobacterium *Anacystis nidulans* R2. *Journal of Bacteriology*, 158 (1), https://doi.org/10.1128/jb.158.1.36-42.1984.

Gomes, M. P., Garcia, Q. S., Barreto, L. C., Pimenta, L. P. S., Matheus, M. T. and Figueredo, C. C. (2017). Allelopathy: An overview from micro- to macroscopic organisms, from cells to environments, and the perspectives in a climate-changing world. *Biologia*, 72 (2), https://doi.org/10.1515/biolog-2017-0019.

Grochowski, L. L., Xu, H. and White, R. H. (2005). Ribose-5-phosphate biosynthesis in *Methanocaldococcus jannaschii* occurs in the absence of a pentose-phosphate pathway. *Journal of Bacteriology*, 187 (21), https://doi.org/10.1128/JB.187.21.7382-7389.2005.

Gross, E. M. (2003). Allelopathy of aquatic autotrophs. *Critical Reviews in Plant Sciences*, 22 (3&4), https://doi.org/10.1080/713610859.

Gross, E. M., Wolk, C. P. and Juttner, F. (1991). Fischerellin, a new allelochemical from the freshwater cyanobacterium *Fischerella muscicola*. *Journal of Phycology*, 27 (6), https://doi.org/10.1111/j.0022-3646.1991.00686.x.

Gu, W., Dong, S.-H., Sarkar, S., Nair, S. K. and Schmidt, E. W. (2018). The biochemistry and structural biology of cyanobactin pathways: enabling combinatorial biosynthesis. *Methods in Enzymology*, 604, https://doi.org/10.1016/bs.mie.2018.03.002.

Gulko, M. K., Dyall-Smith, M., Gonzalez, O. and Oesterhelt, D. (2014). How do haloarchaea synthesize aromatic amino acids? *PLOS ONE*, 9 (9), https://doi.org/10.1371/journal.pone.0107475.

Hagmann, L. and Jüttner, F. (1996). Fischerellin A, a novel photosystem-II-inhibiting allelochemical of the cyanobacterium *Fischerella muscicola* with antifungal and herbicidal activity. *Tetrahedron Letters*, 37 (36), https://doi.org/10.1016/0040-4039(96)01445-1.

Håvarstein, L. S., Diep, D. B. and Nes, I. F. (1995). A family of bacteriocin ABC transporters carry out proteolytic processing of their substrates concomitant with export. *Molecular Microbiology*, 16 (2), https://doi.org/10.1111/j.1365-2958.1995.tb02295.x.

Herrmann, K. M. (1995). The shikimate pathway: early steps in the biosynthesis of aromatic compounds. *The Plant Cell*, 7 (7), https://doi.org/10.1105/tpc.7.7.907.

Herrmann, K. M. and Weaver, L. M. (1999). The shikimate pathway. *Annual Review of Plant Physiology and Plant Molecular Biology*, 50, https://doi.org/10.1146/annurev.arplant.50.1.473.

Herter, T., Berezina, O. V., Zinin, N. V., Velikodvorskaya, G. A., Greiner, R. and Borriss, R. (2006). Glucose-1-phosphatase (AgpE) from *Enterobacter cloacae* displays enhanced phytase activity. *Applied Microbiology and Biotechnology*, 70 (1), https://doi.org/10.1007/s00253-005-0024-8.

Huang, H., Pandya, C., Liu, C., Al-Obaidi, N. F., Wang, M., Zheng, L., Keating, S. T., Aono, M., Love, J. D., Evans, B., Seidel, R. D., Hillerich, B. S., Garforth, S. J., Almo, S. C., Mariano, P. S., Dunaway-Mariano, D., Allen, K. N. and Farelli, J. D. (2015). Panoramic view of a superfamily of

phosphatases through substrate profiling. *Proceedings of the National Academy of Sciences of the United States of America*, 112 (16), https://doi.org/10.1073/pnas.1423570112.

Hult, K. and Berglund, P. (2007). Enzyme promiscuity: mechanism and applications. *Trends in Biotechnology*, 25 (5), https://doi.org/10.1016/j.tibtech.2007.03.002.

Ito, T., Ezaki, N., Tsuruoka, T. and Niida, T. (1971). Structure of SF-666 A and SF-666 B, new monosaccharides. *Carbohydrate Research*, 17 (2), https://doi.org/10.1016/S0008-6215(00)82545-8.

Jaki, B., Orjala, J. and Sticher, O. (1999). A novel extracellular diterpenoid with antibacterial activity from the cyanobacterium *Nostoc commune*. *Journal of Natural Products*, 62 (3), https://doi.org/10.1021/np980444x.

Jensen, R. A. (1976). Enzyme recruitment in evolution of new function. *Annual Review of Microbiology*, 30, https://doi.org/10.1146/annurev.mi.30.100176.002205.

Jones, A. C., Monroe, E. A., Eisman, E. B., Gerwick, L., Sherman, D. H. and Gerwick, W. H. (2010). The unique mechanistic transformations involved in the biosynthesis of modular natural products from marine cyanobacteria. *Natural Product Reports*, 27 (7), https://doi.org/10.1039/C000535E.

Kampa, A., Gagunashvili, A. N., Gulder, T. A. M., Morinaka, B. I., Daolio, C., Godejohann, M., Miao, V. P. W., Piel, J. and Andrésson, Ó. S. (2013). Metagenomic natural product discovery in lichen provides evidence for a family of biosynthetic pathways in diverse symbioses. *Proceedings of the National Academy of Sciences of the United States of America*, 110 (33), https://doi.org/10.1073/pnas.1305867110.

Keating, K. I. (1977). Allelopathic influence on blue-green bloom sequence in a eutrophic lake. *Science*, 196 (4292), https://doi.org/10.1126/science.196.4292.885.

Keating, K. I. (1978). Blue-green algal inhibition of diatom growth: transition from mesotrophic to eutrophic community structure. *Science*, 199 (4332), https://doi.org/10.1126/science.199.4332.971.

Kell, D. B., Brown, M., Davey, H. M., Dunn, W. B., Spasic, I. and Oliver, S. G. (2005). Metabolic footprinting and systems biology: the medium is the message. *Nature Reviews Microbiology*, 3 (7), https://doi.org/10.1038/nrmicro1177.

Khersonsky, O. and Tawfik, D. S. (2010). Enzyme promiscuity: a mechanistic and evolutionary perspective. *Annual Review of Biochemistry*, 79, https://doi.org/10.1146/annurev-biochem-030409-143718.

Knaggs, A. R. (2001). The biosynthesis of shikimate metabolites. *Natural Product Reports*, 18 (3), https://doi.org/10.1039/B001717P.

Kolpin, D. W., Thurman, E. M., Lee, E. A., Meyer, M. T., Furlong, E. T. and Glassmeyer, S. T. (2006). Urban contributions of glyphosate and its degradate AMPA to streams in the United States. *Science of The Total Environment*, 354 (2), https://doi.org/10.1016/j.scitotenv.2005.01.028.

Komárek, J., Kaštovský, J., Mareš, J. and Johansen, J. R. (2014). Taxonomic classification of cyanoprokaryotes (cyanobacterial genera) 2014, using a polyphasic approach. *Preslia*, 86.

Kondo, T., Tsinoremas, N. F., Golden, S. S., Johnson, C. H., Kutsuna, S. and Ishiura, M. (1994). Circadian clock mutants of cyanobacteria. *Science*, 266 (5188), https://doi.org/10.1126/science.7973706.

Leão, P. N., Engene, N., Antunes, A., Gerwick, W. H. and Vasconcelos, V. (2012). The chemical ecology of Cyanobacteria. *Natural Product Reports*, 29 (3), https://doi.org/10.1039/C2NP00075J.

Leão, P. N., Vasconcelos, M. T. S. D. and Vasconcelos, V. M. (2009). Allelopathy in freshwater cyanobacteria. *Critical Reviews in Microbiology*, 35 (4), https://doi.org/10.3109/10408410902823705.

Lee, S. H., Jung, B. H., Kim, S. Y. and Chung, B. C. (2004). A rapid and sensitive method for quantitation of nucleosides in human urine using liquid chromatography/mass spectrometry with direct urine injection. *Rapid Communications in Mass Spectrometry*, 18 (9), https://doi.org/10.1002/rcm.1400.

Leflaive, J. and Ten-Hage, L. (2007). Algal and cyanobacterial secondary metabolites in freshwaters: a comparison of allelopathic compounds and toxins. *Freshwater Biology*, 52 (2), https://doi.org/10.1111/j.1365-2427.2006.01689.x.

Mackinney, G. (1941). Absorption of light by chlorophyll solutions. *Journal of Biological Chemistry*, 140, https://doi.org/10.1016/S0021-9258(18)51320-X.

Marsh, E. N. G., Patterson, D. P. and Li, L. (2010). Adenosyl radical: reagent and catalyst in enzyme reactions. *ChemBioChem*, 11 (5), https://doi.org/10.1002/cbic.200900777.

Mason, C. P., Edwards, K. R., Carlson, R. E., Pignatello, J., Gleason, F. K. and Wood, J. M. (1982). Isolation of chlorine-containing antibiotic from the freshwater cyanobacterium *Scytonema hofmanni*. *Science*, 215 (4531), https://doi.org/10.1126/science.6800032.

Mattern, H. and Mareš, J. (2018). "Cyanobacteria," in *Beiträge zu den Algen Baden-Württembergs. Band 1. Allgemeiner Teil & Cyanobacteria, Glaucobionta, Rhodobionta und Chlorobionta*, eds. S. Stutz and H. Mattern (Verlag Manfred Hennecke).

Maurya, S. K., Niveshika and **Mishra, R.** (2019). "Chapter 24 - Importance of bioinformatics in genome mining of cyanobacteria for production of bioactive compounds," in *Cyanobacteria: From Basic Science to Applications*, eds. A. K. Mishra, A. N. Rai and D. N. Tiwari (London: Academic Press).

McFadden, G. I. (2001). Primary and secondary endosymbiosis and the origin of plastids. *Journal of Phycology*, 37 (6), https://doi.org/10.1046/j.1529-8817.2001.01126.x.

Méjean, A. and Ploux, O. (2013). "A genomic view of secondary metabolite production in cyanobacteria," in *Genomics of Cyanobacteria* (Elsevier), p. 189–234.

Miller, A. R., North, J. A., Wildenthal, J. A. and Tabita, R. F. (2018a). Two distinct aerobic methionine salvage pathways generate volatile methanethiol in *Rhodopseudomonas palustris*. *mBio*, 9 (2), https://doi.org/10.1128/mBio.00407-18.

Miller, D. V., Rauch, B. J., Harich, K., Xu, H., Perona, J. J. and White, R. H. (2018b). Promiscuity of methionine salvage pathway enzymes in *Methanocaldococcus jannaschii*. *Microbiology*, 164 (7), https://doi.org/10.1099/mic.0.000670.

Molisch, H. (1937). *Der Einfluss einer Pflanze auf die andere Allelopathie*. Jena: Gustav Fischer.

Montchamp, J. L. and Frost, J. W. (1991). Irreversible inhibition of 3-dehydroquinate synthase. *Journal of the American Chemical Society*, 113 (16), https://doi.org/10.1021/ja00016a070.

Montchamp, J. L., Piehler, L. T. and Frost, J. W. (1992). Diastereoselection and *in vivo* inhibition of 3-dehydroquinate synthase. *Journal of the American Chemical Society*, 114 (12), https://doi.org/10.1021/ja00038a002.

Motta, E. V. S., Raymann, K. and Moran, N. A. (2018). Glyphosate perturbs the gut microbiota of honey bees. *Proceedings of the National Academy of Sciences*, https://doi.org/10.1073/pnas.1803880115.

Nam, H., Lewis, N. E., Lerman, J. A., Lee, D.-H., Chang, R. L., Kim, D. and Palsson, B. O. (2012). Network context and selection in the evolution to enzyme specificity. *Science*, 337 (6098), https://doi.org/10.1126/science.1216861.

Nedal, A. and Zotchev, S. B. (2004). Biosynthesis of deoxyaminosugars in antibiotic-producing bacteria. *Applied Microbiology and Biotechnology*, 64 (1), https://doi.org/10.1007/s00253-003-1535-9.

North, J. A., Miller, A. R., Wildenthal, J. A., Young, S. J. and Tabita, F. R. (2017). Microbial pathway for anaerobic 5'-methylthioadenosine metabolism coupled to ethylene formation. *Proceedings of the National Academy of Sciences*, 114 (48), https://doi.org/10.1073/pnas.1711625114.

North, J. A., Wildenthal, J. A., Erb, T. J., Evans, B. S., Byerly, K. M., Gerlt, J. A. and Tabita, F. R. (2020). A bifunctional salvage pathway for two distinct *S*-adenosylmethionine by-products that is widespread in bacteria, including pathogenic *Escherichia coli*. *Molecular Microbiology*, 113 (5), https://doi.org/10.1111/mmi.14459.

Parnasa, R., Nagar, E., Sendersky, E., Reich, Z., Simkovsky, R., Golden, S. and Schwarz, R. (2016). Small secreted proteins enable biofilm development in the cyanobacterium *Synechococcus elongatus*. *Scientific Reports*, 6, https://doi.org/10.1038/srep32209.

Parveen, N. and Cornell, K. A. (2011). Methylthioadenosine/*S*-adenosylhomocysteine nucleosidase, a critical enzyme for bacterial metabolism. *Molecular Microbiology*, 79 (1), https://doi.org/10.1111/j.1365-2958.2010.07455.x.

Pattanaik, B. and Lindberg, P. (2015). Terpenoids and their biosynthesis in cyanobacteria. *Life*, 5 (1), https://doi.org/10.3390/life5010269.

Paz-Yepes, J., Brahamsha, B. and Palenik, B. (2013). Role of a microcin-C-like biosynthetic gene cluster in allelopathic interactions in marine *Synechococcus*. *Proceedings of the National Academy of Sciences*, 110 (29), https://doi.org/10.1073/pnas.1306260110.

Piedrafita, G., Keller, M. A. and Ralser, M. (2015). The impact of non-enzymatic reactions and enzyme promiscuity on cellular metabolism during (oxidative) stress conditions. *Biomolecules*, 5 (3), https://doi.org/10.3390/biom5032101.

Plagemann, P. G. and Wohlhueter, R. M. (1983). 5′-Deoxyadenosine metabolism in various mammalian cell lines. *Biochemical Pharmacology*, 32 (8), https://doi.org/10.1016/0006-2952(83)90458-6.

Pompliano, D. L., Reimer, L. M., Myrvold, S. and Frost, J. W. (1989). Probing lethal metabolic perturbations in plants with chemical inhibition of dehydroquinate synthase. *Journal of the American Chemical Society*, 111 (5), https://doi.org/10.1021/ja00187a049.

Powles, S. B. (2008). Evolved glyphosate-resistant weeds around the world: lessons to be learnt. *Pest Management Science*, 64 (4), https://doi.org/10.1002/ps.1525.

Pradel, E. and Boquet, P. L. (1988). Acid phosphatases of *Escherichia coli*: molecular cloning and analysis of *agp*, the structural gene for a periplasmic acid glucose phosphatase. *Journal of Bacteriology*, 170 (10), https://doi.org/10.1128/jb.170.10.4916-4923.1988.

Radaev, S., Dastidar, P., Patel, M., Woodard, R. W. and Gatti, D. L. (2000). Structure and mechanism of 3-deoxy-D-*manno*-octulosonate 8-phosphate synthase. *Journal of Biological Chemistry*, 275 (13), https://doi.org/10.1074/jbc.275.13.9476.

Rapp, J. and Forchhammer, K. (2021). 5-Deoxyadenosine Metabolism: More than "Waste Disposal". *Microbial Physiology*, https://doi.org/10.1159/000516105.

Rapp, J., Rath, P., Kilian, J., Brilisauer, K., Grond, S. and Forchhammer, K. (2021). A bioactive molecule made by unusual salvage of radical SAM enzyme by-product 5-deoxyadenosine blurs the boundary of primary and secondary metabolism. *Journal of Biological Chemistry*, 296 (100621), https://doi.org/10.1016/j.jbc.2021.100621.

Ray, S. and Bagchi, S. N. (2001). Nutrients and pH regulate algicide accumulation in cultures of the cyanobacterium *Oscillatoria laetevirens*. *New Phytologist*, 149 (3), https://doi.org/10.1046/j.1469-8137.2001.00061.x.

Rice, E. L. (1984). *Allelopathy*. Orlando .a. Academic Press.

Richardson, T. L. and Jackson, G. A. (2007). Small phytoplankton and carbon export from the surface ocean. *Science*, 315 (5813), https://doi.org/10.1126/science.1133471.

Rippka, R., Deruelles, J., Waterbury, J. B., Herdman, M. and Stanier, R. Y. (1979). Generic assignments, strain histories and properties of pure cultures of cyanobacteria. *Journal of General Microbiology*, 111 (1), https://doi.org/10.1099/00221287-111-1-1.

Roberts, F., Roberts, C. W., Johnson, J. J., Kyle, D. E., Krell, T., Coggins, J. R., Coombs, G. H., Milhous, W. K., Tzipori, S., Ferguson, D. J., Chakrabarti, D. and McLeod, R. (1998). Evidence for the shikimate pathway in apicomplexan parasites. *Nature*, 393 (6687), https://doi.org/10.1038/31723.

Rosenberg, J. and Commichau, F. M. (2019). Harnessing underground metabolism for pathway development. *Trends in Biotechnology*, 37 (1), https://doi.org/10.1016/j.tibtech.2018.08.001.

Rueppel, M. L., Brightwell, B. B., Schaefer, J. and Marvel, J. T. (1977). Metabolism and degradation of glyphosate in soil and water. *Journal of Agricultural and Food Chemistry*, 25 (3), https://doi.org/10.1021/jf60211a018.

Rzymski, P., Poniedziałek, B., Kokociński, M., Jurczak, T., Lipski, D. and Wiktorowicz, K. (2014). Interspecific allelopathy in cyanobacteria: Cylindrospermopsin and *Cylindrospermopsis raciborskii* effect on the growth and metabolism of *Microcystis aeruginosa*. *Harmful Algae*, 35, https://doi.org/10.1016/j.hal.2014.03.002.

Sauer, J., Schreiber, U., Schmid, R., Völker, U. and Forchhammer, K. (2001). Nitrogen starvation-induced chlorosis in *Synechococcus* PCC 7942. Low-level photosynthesis as a mechanism of long-term survival. *Plant Physiology*, 126 (1), https://doi.org/10.1104/pp.126.1.233.

Savarese, T. M., Crabtree, G. W. and Parks, R. E. (1981). 5′-methylthioadenosine phosphorylase—I: Substrate activity of 5′-deoxyadenosine with the enzyme from Sarcoma 180 cells. *Biochemical Pharmacology*, 30 (3), https://doi.org/10.1016/0006-2952(81)90077-0.

Scalbert, A., Brennan, L., Fiehn, O., Hankemeier, T., Kristal, B. S., van Ommen, B., Pujos-Guillot, E., Verheij, E., Wishart, D. and Wopereis, S. (2009). Mass-spectrometry-based metabolomics: limitations and recommendations for future progress with particular focus on nutrition research. *Metabolomics*, 5 (4), https://doi.org/10.1007/s11306-009-0168-0.

Scanlan, D. J. and West, N. J. (2002). Molecular ecology of the marine cyanobacterial genera *Prochlorococcus* and *Synechococcus*. *FEMS Microbiology Ecology*, 40 (1), https://doi.org/10.1111/j.1574-6941.2002.tb00930.x.

Schatz, D., Nagar, E., Sendersky, E., Parnasa, R., Zilberman, S., Carmeli, S., Mastai, Y., Shimoni, E., Klein, E., Yeger, O., Reich, Z. and Schwarz, R. (2013). Self-suppression of biofilm formation in the cyanobacterium *Synechococcus elongatus*. *Environmental Microbiology*, 15 (6), https://doi.org/10.1111/1462-2920.12070.

Schirrmeister, B. E., Gugger, M. and Donoghue, P. C. J. (2015). Cyanobacteria and the Great Oxidation Event: evidence from genes and fossils. *Palaeontology*, 58 (5), https://doi.org/10.1111/pala.12178.

Schlösser, U. G. (1994). SAG - Sammlung von Algenkulturen at the University of Göttingen Catalogue of Strains 1994. *Botanica Acta*, 107 (3), https://doi.org/10.1111/j.1438-8677.1994.tb00784.x.

Schmetterer, G. R. (1990). Sequence conservation among the glucose transporter from the cyanobacterium *Synechocystis* sp. PCC 6803 and mammalian glucose transporters. *Plant Molecular Biology*, 14 (5), https://doi.org/10.1007/BF00016502.

Schmid, A., Dordick, J. S., Hauer, B., Kiener, A., Wubbolts, M. and Witholt, B. (2001). Industrial biocatalysis today and tomorrow. *Nature*, 409 (6817), https://doi.org/10.1038/35051736.

Schwarz, D., Orf, I., Kopka, J. and Hagemann, M. (2013). Recent applications of metabolomics toward cyanobacteria. *Metabolites*, 3 (1), https://doi.org/10.3390/metabo3010072.

Schweizer, M., Brilisauer, K., Triebskorn, R., Forchhammer, K. and Köhler, H.-R. (2019). How glyphosate and its associated acidity affect early development in zebrafish (*Danio rerio*). *PeerJ*, 7, https://doi.org/10.7717/peerj.7094.

Sekowska, A., Ashida, H. and Danchin, A. (2018). Revisiting the methionine salvage pathway and its paralogues. *Microbial Biotechnology*, 12 (1), https://doi.org/10.1111/1751-7915.13324.

Sekowska, A. and Danchin, A. (2002). The methionine salvage pathway in *Bacillus subtilis*. *BMC Microbiology*, 2 (1), https://doi.org/10.1186/1471-2180-2-8.

Sekowska, A., Denervaud, V., Ashida, H., Michoud, K., Haas, D., Yokota, A. and Danchin, A. (2004). Bacterial variations on the methionine salvage pathway. *BMC Microbiology*, 4 (9), https://doi.org/10.1186/1471-2180-4-9.

Selim, K. A., Haase, F., Hartmann, M. D., Hagemann, M. and Forchhammer, K. (2018). P_{II}-like signaling protein SbtB links cAMP sensing with cyanobacterial inorganic carbon response. *Proceedings of the National Academy of Sciences*, 115 (21), https://doi.org/10.1073/pnas.1803790115.

Sharif, D. I., Gallon, J., Smith, C. J. and Dudley, E. (2008). Quorum sensing in cyanobacteria: *N*-octanoyl-homoserine lactone release and response, by the epilithic colonial cyanobacterium *Gloeothece* PCC6909. *The ISME Journal*, 2 (12), https://doi.org/10.1038/ismej.2008.68.

Shestakov, S. V. and Khyen, N. T. (1970). Evidence for genetic transformation in blue-green alga *Anacystis nidulans*. *Molecular and General Genetics*, 107 (4), https://doi.org/10.1007/BF00441199.

Shih, P. M., Wu, D., Latifi, A., Axen, S. D., Fewer, D. P., Talla, E., Calteau, A., Cai, F., Tandeau de Marsac, N., Rippka, R., Herdman, M., Sivonen, K., Coursin, T., Laurent, T., Goodwin, L., Nolan, M., Davenport, K. W., Han, C. S., Rubin, E. M., Eisen, J. A., Woyke, T., Gugger, M. and Kerfeld, C. A. (2013). Improving the coverage of the cyanobacterial phylum using diversity-driven genome sequencing. *Proceedings of the National Academy of Sciences*, 110 (3), https://doi.org/10.1073/pnas.1217107110.

Sofia, H. J., Chen, G., Hetzler, B. G., Reyes-Spindola, J. F. and Miller, N. E. (2001). Radical SAM, a novel protein superfamily linking unresolved steps in familiar biosynthetic pathways with radical mechanisms: Functional characterization using new analysis and information visualization methods. *Nucleic Acids Research*, 29 (5), https://doi.org/10.1093/nar/29.5.1097.

Soo, R. M., Hemp, J., Parks, D. H., Fischer, W. W. and Hugenholtz, P. (2017). On the origins of oxygenic photosynthesis and aerobic respiration in Cyanobacteria. *Science*, 355 (6332), https://doi.org/10.1126/science.aal3794.

Soule, T., Stout, V., Swingley, W. D., Meeks, J. C. and Garcia-Pichel, F. (2007). Molecular genetics and genomic analysis of scytonemin biosynthesis in *Nostoc punctiforme* ATCC 29133. *Journal of Bacteriology*, 189 (12), https://doi.org/10.1128/JB.01816-06.

Srinivasan, P. R., Katagiri, M. and Sprinson, D. B. (1955). The enzymatic synthesis of shikimic acid from D-erythrose and phosphoenolpyruvate. *Journal of the American Chemical Society*, 77 (18), https://doi.org/10.1021/ja01623a089.

Srinivasan, P. R., Rothschild, J. and Sprinson, D. B. (1963). The enzymic conversion of 3-deoxy-D-*arabino*-heptulosonic acid 7-phosphate to 5-dehydroquinate. *Journal of Biological Chemistry*, 238 (10), https://doi.org/10.1016/S0021-9258(18)48643-7.

Stafleu, F. A., Bonner, C. E., McVaugh, R., Meikle, R. D., Rollins, R. C., Ross, R., Schopf, J. M., Schulze, G. M., Vilmorin, R. d. and Voss, E. G., eds (1972). *International code of botanical nomenclature: Adopted by the Eleventh International Botanical Congress, Seattle, August 1969*. Utrecht, The Netherlands: A. Oosthoek.

Steinrücken, H. C. and Amrhein, N. (1984). 5-Enolpyruvylshikimate-3-phosphate synthase of *Klebsiella pneumoniae*. *European Journal of Biochemistry*, 143 (2), https://doi.org/10.1111/j.1432-1033.1984.tb08379.x.

Sugita, C., Ogata, K., Shikata, M., Jikuya, H., Takano, J., Furumichi, M., Kanehisa, M., Omata, T., Sugiura, M. and Sugita, M. (2007). Complete nucleotide sequence of the freshwater unicellular cyanobacterium *Synechococcus elongatus* PCC 6301 chromosome: gene content and organization. *Photosynthesis Research*, 93 (1-3), https://doi.org/10.1007/s11120-006-9122-4.

Suleimanova, A. D., Beinhauer, A., Valeeva, L. R., Chastukhina, I. B., Balaban, N. P., Shakirov, E. V., Greiner, R. and Sharipova, M. R. (2015). Novel glucose-1-phosphatase with high phytase activity and unusual metal ion activation from soil bacterium *Pantoea* sp. strain 3.5.1. *Applied and Environmental Microbiology*, 81 (19), https://doi.org/10.1128/AEM.01384-15.

Tian, F., Montchamp, J.-L. and Frost, J. W. (1996). Inhibitor ionization as a determinant of binding to 3-dehydroquinate synthase. *The Journal of Organic Chemistry*, 61 (21), https://doi.org/10.1021/jo960709h.

Trefzer, A., Bechthold, A. and Salas, J. A. (1999). Genes and enzymes involved in deoxysugar biosynthesis in bacteria. *Natural Product Reports*, 16 (3), https://doi.org/10.1039/A804431G.

Turner, D. H. and Turner, J. F. (1960). The hydrolysis of glucose monophosphates by a phosphatase preparation from pea seeds. *Biochemical Journal*, 74 (3), https://doi.org/10.1042/bj0740486.

Turner, N. J. (2000). Applications of transketolases in organic synthesis. *Current Opinion in Biotechnology*, 11 (6).

Tzin, V. and Galili, G. (2010). New insights into the shikimate and aromatic amino acids biosynthesis pathways in plants. *Molecular Plant*, 3 (6), https://doi.org/10.1093/mp/ssq048.

Ueda, S., Kawamura, Y., Iijima, H., Nakajima, M., Shirai, T., Okamoto, M., Kondo, A., Hirai, M. Y. and Osanai, T. (2016). Anionic metabolite biosynthesis enhanced by potassium under dark, anaerobic conditions in cyanobacteria. *Scientific Reports*, 6 (1), https://doi.org/10.1038/srep32354.

van Alphen, P., Najafabadi, H. A., Santos, F. B. d. and Hellingwerf, K. J. (2018). Increasing the photoautotrophic growth rate of *Synechocystis* sp. PCC 6803 by identifying the limitations of its cultivation. *Biotechnology Journal*, 13.

van den Hondel, C. A., Verbeek, S., van der Ende, A., Weisbeek, P. J., Borrias, W. E. and van Arkel, G. A. (1980). Introduction of transposon Tn901 into a plasmid of *Anacystis nidulans*: Preparation for cloning in cyanobacteria. *Proceedings of the National Academy of Sciences of the United States of America*, 77 (3), https://doi.org/10.1073/pnas.77.3.1570.

van der Grinten, E., Janssen, A. P., de Mutsert, K., Barranguet, C. and Admiraal, W. (2005). Temperature- and light-dependent performance of the cyanobacterium *Leptolyngbya foveolarum* and the diatom *Nitzschia perminuta* in mixed biofilms. *Hydrobiologia*, 548 (1), https://doi.org/10.1007/s10750-005-5324-6.

Wang, H., Fewer, D. P. and Sivonen, K. (2011). Genome mining demonstrates the widespread occurrence of gene clusters encoding bacteriocins in cyanobacteria. *PLOS ONE*, 6 (7), https://doi.org/10.1371/journal.pone.0022384.

Wang, S. C. and Frey, P. A. (2007). *S*-adenosylmethionine as an oxidant: the radical SAM superfamily. *Trends in Biochemical Sciences*, 32 (3), https://doi.org/10.1016/j.tibs.2007.01.002.

Wase, N. V. and Wright, P. C. (2008). Systems biology of cyanobacterial secondary metabolite production and its role in drug discovery. *Expert Opinion on Drug Discovery*, 3 (8), https://doi.org/10.1517/17460441.3.8.903.

Waterbury, J. B., Watson, S. W., Guillard, R. R. L. and Brand, L. E. (1979). Widespread occurrence of a unicellular, marine, planktonic, cyanobacterium. *Nature*, 277 (5694), https://doi.org/10.1038/277293a0.

Weber, T., Blin, K., Duddela, S., Krug, D., Kim, H. U., Bruccoleri, R., Lee, S. Y., Fischbach, M. A., Müller, R., Wohlleben, W., Breitling, R., Takano, E. and Medema, M. H. (2015). antiSMASH 3.0-a comprehensive resource for the genome mining of biosynthetic gene clusters. *Nucleic Acids Research*, 43 (W1), https://doi.org/10.1093/nar/gkv437.

White, R. H. (2004). L-Aspartate semialdehyde and a 6-deoxy-5-ketohexose 1-phosphate are the precursors to the aromatic amino acids in *Methanocaldococcus jannaschii*. *Biochemistry*, 43 (23), https://doi.org/10.1021/bi0495127.

Whitton, B. A. and Potts, M. (2012). "Introduction to the Cyanobacteria," in *Ecology of Cyanobacteria II: Their Diversity in Space and Time*, ed. B. A. Whitton (Dordrecht: Springer Netherlands).

Wicke, D., Schulz, L. M., Lentes, S., Scholz, P., Poehlein, A., Gibhardt, J., Daniel, R., Ischebeck, T. and Commichau, F. M. (2019). Identification of the first glyphosate transporter by genomic adaptation. *Environmental Microbiology*, https://doi.org/10.1111/1462-2920.14534.

Widlanski, T., Bender, S. L. and Knowles, J. R. (1989). Dehydroquinate synthase: The use of substrate analogues to probe the late steps of the catalyzed reaction. *Biochemistry*, 28 (19), https://doi.org/10.1021/bi00445a011.

Williams, L. E., Lemoine, R. and Sauer, N. (2000). Sugar transporters in higher plants – a diversity of roles and complex regulation. *Trends in Plant Science*, 5 (7), https://doi.org/10.1016/S1360-1385(00)01681-2.

Wray, J. W. and Abeles, R. H. (1995). The methionine salvage pathway in *Klebsiella pneumoniae* and rat liver. Identification and characterization of two novel dioxygenases. *The Journal of Biological Chemistry*, 270 (7), https://doi.org/10.1074/jbc.270.7.3147.

Yang, Y., Lam, V., Adomako, M., Simkovsky, R., Jakob, A., Rockwell, N. C., Cohen, S. E., Taton, A., Wang, J., Lagarias, J. C., Wilde, A., Nobles, D. R., Brand, J. J. and Golden, S. S. (2018). Phototaxis in a wild isolate of the cyanobacterium *Synechococcus elongatus*. *Proceedings of the National Academy of Sciences*, 115 (52), https://doi.org/10.1073/pnas.1812871115.

Yegorov, Y., Sendersky, E., Zilberman, S., Nagar, E., Waldman Ben-Asher, H., Shimoni, E., Simkovsky, R., Golden, S. S., LiWang, A. and Schwarz, R. (2021). A cyanobacterial component required for pilus biogenesis affects the exoproteome. *mBio*, 12 (2), https://doi.org/10.1128/mBio.03674-20.

Yunes, J. S. (2019). "Cyanobacterial Toxins," in *Cyanobacteria: From Basic Science to Applications*, eds. A. K. Mishra, A. N. Rai and D. N. Tiwari (London: Academic Press).

8 Dank

Ich bedanke mich herzlich bei meinem Doktorvater, Prof. Dr. Karl Forchhammer, für die Möglichkeit, meine Doktorarbeit an seinem Lehrstuhl für Mikrobiologie/Organismische Interaktionen durchzuführen, für die Bereitstellung des spannenden Themas, sowie für die großen Freiräume, die er mir bei der Entwicklung eigener Ideen gegeben hat.

Prof. Dr. Stephanie Grond möchte ich für die Einwerbung meiner Finanzierung im Rahmen des Glykobiologie-Projektes, sowie die Möglichkeit, die Labore und Geräte in der Organischen Chemie zu nutzen, danken.

Für die gute Einarbeitung, die nette Gesellschaft im Labor, sowie für die vorangegangen Arbeiten zur 7dSh und dafür, dass er immer ein offenes Ohr für mich hatte, möchte ich besonders Dr. Klaus Brilisauer danken.

Dr. Joachim Kilian und Dr. Mark Stahl möchte ich für die Möglichkeit danken, an der Analytik Einheit des ZMBPs meine Messungen durchzuführen. Vielen Dank für die tolle Unterstützung und die (spontane) Bereitstellung von Messzeit.

Berenike Wagner möchte ich für die Unterstützung während ihrer Masterarbeit, sowie das nette Miteinander im Labor danken.

Pascal Rath danke ich für die gute Kooperation im 7dSh-Projekt.

Danken möchte ich auch Frau Dr. Libera Lo Presti für die prompte Unterstützung durch das Korrekturlesen meiner Manuskripte und die ausführlichen Diskussionen über Titel und Abstracts.

Bedanken möchte ich mich bei apl. Prof. Dr. Evi Stegmann für die Begutachtung meiner Arbeit.

Dem GRK 1708 „Bacterial Survival Strategies” danke ich für die Anschlussfinanzierung.

Mein Dank geht auch an alle jetzigen und ehemaligen Mitglieder der AGs Forchhammer/Maldener/Grond für gute Diskussionen, aber auch für schöne Ausflüge und nette Kaffeepausen.

Des Weiteren möchte ich meinen den Betreuern meiner Bachelor- und Masterarbeit danken, die die Grundlagen meines wissenschaftlichen Arbeitens gelegt haben.

Zuletzt möchte ich meiner Familie, meinen Freunden und besonders Simon für die großartige Unterstützung während der gesamten Zeit danken.

9 Appendix

9.1. Accepted Publications

Publication 1:

Brilisauer, Klaus; Rapp, Johanna; Rath, Pascal; Schöllhorn, Anna; Bleul, Lisa; Weiß, Elisabeth; Stahl, Mark; Grond, Stephanie; Forchhammer, Karl (2019): Cyanobacterial antimetabolite 7-deoxy-sedoheptulose blocks the shikimate pathway to inhibit the growth of prototrophic organisms. *Nature Communications*, 10 (545), https://doi.org/10.1038/s41467-019-08476-8,

nature COMMUNICATIONS

ARTICLE

https://doi.org/10.1038/s41467-019-08476-8 OPEN

Cyanobacterial antimetabolite 7-deoxy-sedoheptulose blocks the shikimate pathway to inhibit the growth of prototrophic organisms

Klaus Brilisauer[1,2], Johanna Rapp[2], Pascal Rath[1], Anna Schöllhorn[2], Lisa Bleul[3], Elisabeth Weiß[3], Mark Stahl[4], Stephanie Grond[1] & Karl Forchhammer[2]

Antimetabolites are small molecules that inhibit enzymes by mimicking physiological substrates. We report the discovery and structural elucidation of the antimetabolite 7-deoxy-sedoheptulose (7dSh). This unusual sugar inhibits the growth of various prototrophic organisms, including species of cyanobacteria, *Saccharomyces*, and *Arabidopsis*. We isolate bioactive 7dSh from culture supernatants of the cyanobacterium *Synechococcus elongatus*. A chemoenzymatic synthesis of 7dSh using *S. elongatus* transketolase as catalyst and 5-deoxy-D-ribose as substrate allows antimicrobial and herbicidal bioprofiling. Organisms treated with 7dSh accumulate 3-deoxy-D-*arabino*-heptulosonate 7-phosphate, which indicates that the molecular target is 3-dehydroquinate synthase, a key enzyme of the shikimate pathway, which is absent in humans and animals. The herbicidal activity of 7dSh is in the low micromolar range. No cytotoxic effects on mammalian cells have been observed. We propose that the in vivo inhibition of the shikimate pathway makes 7dSh a natural antimicrobial and herbicidal agent.

[1] Institute of Organic Chemistry, Eberhard Karls Universität Tübingen, Auf der Morgenstelle 18, 72076 Tübingen, Germany. [2] Microbiology, Organismic Interactions, Eberhard Karls Universität Tübingen, Auf der Morgenstelle 28, 72076 Tübingen, Germany. [3] Interfaculty Institute of Microbiology and Infection Medicine Tübingen (IMIT), Eberhard Karls Universität Tübingen, Eugenstraße 6, 72076 Tübingen, Germany. [4] Center for Plant Molecular Biology, Eberhard Karls Universität Tübingen, Auf der Morgenstelle 32, 72076 Tübingen, Germany. Correspondence and requests for materials should be addressed to S.G. (email: biomolchemie@orgchem.uni-tuebingen.de) or to K.F. (email: biomolchemie@orgchem.uni-tuebingen.de)

Cyanobacteria—the dominating photoautotrophic, oxygen-producing microbes on earth—have gained increasing attention in natural product research in recent years. Their omnipresence in the light-exposed biosphere is based on a large repertoire of survival strategies for withstanding challenging environmental conditions and protecting their niches against competitors. To this end, cyanobacteria produce a wide range of secondary metabolites, often with a unique composition and specialized functions, which mediate manifold processes, such as chemical defense[1], preservation[2], and quorum sensing[3]. Some of the known cyanobacterial metabolites exhibit antiviral[4], antibacterial[5], antifungal[6], or herbicidal[7] activities, with promising possible applications in human health, agriculture, or industry[8].

Although cyanobacteria produce a broad range of bioactive compounds in terms of structure and targets, only few are described as classical antimetabolites. Antimetabolites are chemical analogs of the natural substrates of enzymes, where they bind to the active site but are not converted to the functional product. In this way, antimetabolites block a biological process, such as a biosynthetic pathway. One of the best-studied cyanobacterial antimetabolites is the non-proteinogenic amino acid β-methylamino-L-alanine (BMAA), which was initially isolated from cultures of species of *Nostoc*[9]. BMAA can be mistakenly incorporated into nascent proteins in place of L-serine, which possibly causes protein misfolding and aggregation[10].

Antimetabolites are useful for controlling the growth of microorganisms, fungi, and plants. To avoid harmful side effects, these compounds should target biological processes that do not occur in animals, especially mammals. One such process involves the enzymes of the shikimate pathway, in which seven enzymes catalyze the sequential conversion of erythrose 4-phosphate and phosphoenolpyruvate (PEP) via shikimate to chorismate[11], the essential precursor of the aromatic amino acids phenylalanine, tyrosine, and tryptophan. Each enzyme of the shikimate pathway catalyzes an essential reaction in chorismate biosynthesis that cannot be bypassed by an alternative enzyme. The inhibition of any enzyme of this pathway, therefore, leads to impairment of the entire cell metabolism and results in arrested growth or even cell death[12]. Chemical compounds that interfere specifically with any enzyme activity in this pathway are considered harmless for humans and other mammals when handled at reasonable concentrations[13]. Therefore, the enzymes of the shikimate pathway are attractive potential targets for the development of novel antimetabolites.

One of the most prominent antimetabolites that targets the shikimate pathway is the synthetic herbicide glyphosate [*N*-(phosphonomethyl)glycine][14], whose use is intensely discussed, most recently due to its perturbation of the gut microbiota of honey bees[15]. Since its initial commercialization in 1974, glyphosate has become the main component of various total herbicides applied in agriculture, industry and private households, today in amounts of >800,000 tons per year[16]. Glyphosate is a potent inhibitor of the 5-enolpyruvylshikimate 3-phosphate (EPSP) synthase, which converts PEP and shikimate 3-phosphate to EPSP. As a transition state analog of PEP, glyphosate leads to the accumulation of shikimate 3-phosphate[17]. This blocking of the synthesis of the end products of the aromatic pathway results in perturbation of metabolic homeostasis and eventually leads to cell death. To our knowledge, glyphosate is the only bioactive compound with a potent in vivo inhibitory effect on the shikimate pathway that has been described to date. Another target of antimetabolites is the first enzyme in branched-chain amino acid synthesis, acetohydroxyacid synthase (AHAS, E.C. 2.2.1.6). Like the shikimate pathway, the branched-chain amino acid synthesis pathway is only found in plants, bacteria and fungi and therefore, compounds inhibiting the AHAS are highly successful commercial herbicides[18,19].

Allelochemicals, bioactive compounds for the inhibition of rival organisms, play a major role in cyanobacterial niche competition. Both filamentous and colonial cyanobacteria are known to be potent producers of a wide variety of allelochemicals and other secondary metabolites[20,21]. By contrast, little is known about the synthesis of such metabolites by simple unicellular cyanobacteria like *Synechococcus* and *Prochlorococcus* species. Indeed, for a long time it was not even anticipated that these cyanobacteria produce bioactive metabolites because of their small, stream-lined genomes and lack of non-ribosomal peptide synthase gene clusters[22]. However, newer findings suggest an extensive ability of simple unicellular cyanobacteria for the production of secondary metabolites, which is mainly based on catalytic promiscuity[23].

Synechococcus elongatus PCC 7942 is one of the most commonly used model organisms for molecular genetic studies in cyanobacteria[24]. Its circular chromosome (ca. 2.7 Mb, GenBank accession no. CP000100) and plasmids (GenBank accession nos. AF441790 and S89470) lack apparent gene clusters for the synthesis of complex secondary metabolites[25]. However, it has been reported that collapsing aged cultures of *S. elongatus* secrete a non-identified hydrophobic metabolite that inhibits the growth of a large variety of photosynthetic organisms[26].

In this work, we identify an anti-cyanobacterial bioactivity in supernatants of stationary *S. elongatus* cultures. We assign this bioactivity to a hydrophilic compound that therefore differs from the metabolite cited above. Subsequent bioactivity-guided isolation, structural elucidation, and characterization of the mode of action reveal the first identified natural antimetabolite that targets the shikimate pathway in vivo.

Results

Isolation of the bioactive metabolite. Supernatants of stationary cultures of *S. elongatus* inhibited the growth of *Anabaena variabilis*. The inhibitory activity could be extracted from lyophilized culture supernatants with the polar solvent methanol, but not with chloroform, acetone, or ethyl acetate as visualized by agar-diffusion plate assays (Fig. 1a). The producer strain was not affected by these extracts. Significant production of the inhibitor required CO_2 supplementation of liquid cultures and was dependent on the cell density of the producer strain. Inhibitor content apparently peaked after about 2 weeks of growth of *S. elongatus* cultivated in batch cultures in BG11 medium (Fig. 1b).

The chemical characterization of the bioactive compound indicated high polarity and absence of UV absorption. The low levels produced demanded an optimized bioactivity-guided isolation protocol with several enrichment and purification steps. A chromatographically pure compound was obtained via successive size-exclusion chromatography, medium-pressure liquid chromatography (MPLC) on normal phase, and ligand/ion-exchange high-performance liquid chromatography (HPLC) coupled to evaporative light-scattering detection (ELSD) (Supplementary Fig. 1). The molecular formula of the bioactive molecule was determined by electrospray ionization high-resolution mass spectrometry (ESI-HRMS) to be $C_7H_{14}O_6$ ($M_R = 194.18$ Da from $m/z = 217.0675$ $[M+Na]^+$) (Supplementary Fig. 2).

We elucidated the structure of the chromatographically pure compound using nuclear magnetic resonance (^{1}H-NMR, ^{13}C-NMR, and two-dimensional spectra; Supplementary Table 1, Supplementary Figs. 12–16). The signals were assigned to the constitution of a 7-deoxyheptulose and indicated the relative

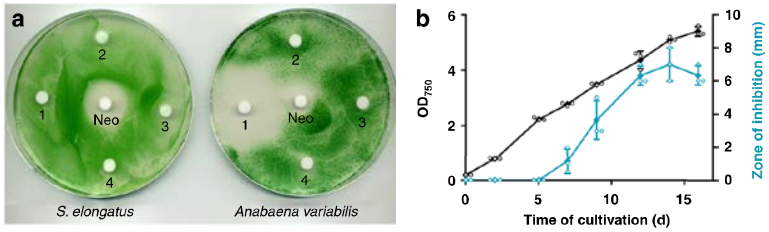

Fig. 1 Extracts of supernatant of *Synechococcus elongatus* inhibits growth of *Anabaena variabilis*. **a** Agar-diffusion plate assay with the effect of organic extracts (1, methanol; 2, chloroform; 3, acetone, and 4, ethyl acetate) of lyophilized supernatant of stationary-phase *S. elongatus* cultures on the growth of the producer strain and *A. variabilis*. Neomycin (Neo, 20 µg) served as positive control. **b** Optical density of producer strain *S. elongatus* (black) and zone of *A. variabilis* growth inhibition (diameter) of methanol extracts of *S. elongatus* supernatant on agar diffusion plates (turquoise). Values represent the mean values of three biological replicates; standard deviations are indicated. Dots indicate data distribution. Source data are provided as a Source Data file

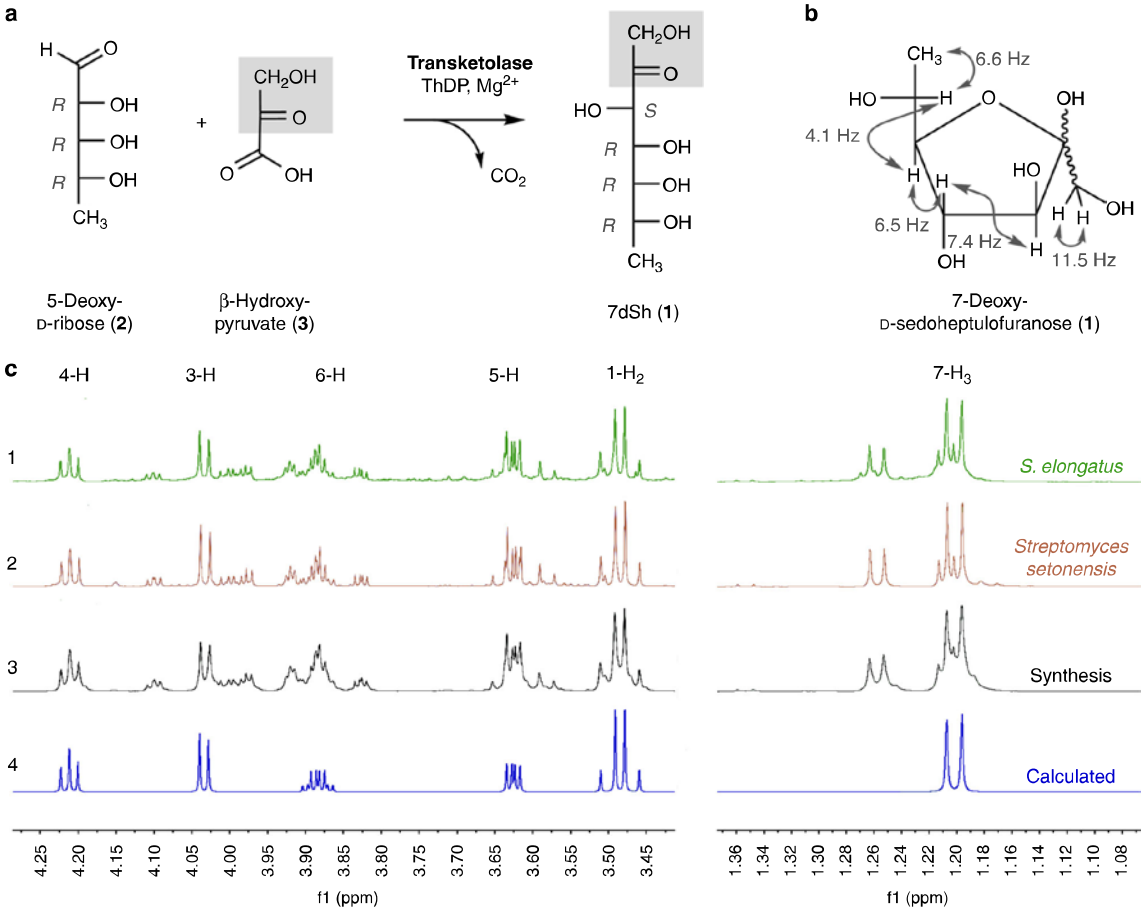

Fig. 2 Structure and chemoenzymatic synthesis of 7-deoxy-sedoheptulose (7dSh, **1**). **a** Chemoenzymatic synthesis of 7-deoxy-sedoheptulose (7dSh). Absolute configurations of stereo-centers are indicated. **b** Chemical structure of 7dSh in the furanose form with given assignments of coupling constants (gray). **c** (1–4) ^{1}H NMR spectra of 7dSh (CD_3OD, 600 MHz) chromatographically purified from supernatants of stationary phase cultures of *S. elongatus* (1, green), of the purified 7dSh from the supernatants of *Streptomyces setonensis* as control (2, red), and of enzymatically synthesized 7dSh (3, black). Predicted from assigned NMR-data (4, blue) of 7dSh in the 7-deoxy-D-*altro*-heptulofuranose form (Bruker, TopSpin software). Additional proton NMR signals in 1–3 give evidence for the dynamic forms of 7dSh in solution (open chain tautomers, ring conformers)

configuration mainly present in the furanose form (Fig. 2b, c). In marked contrast to six-membered sugar rings (pyranoses), the five-membered furanoses exhibit complex multiple ring conformations, and the coupling pattern only allows a suggested relative configuration[27]. The occurrence of pyranose and furanose forms of D-2-heptuloses are known for D-*altro*-2-heptulose, D-*manno*-2-heptulose, D-*galacto*-2-heptulose, and D-*gluco*-2-heptulose[28]. The only D-2-heptulose existing mainly in furanose form

corresponds to the *altro* configuration, which rendered this configuration most probable for the inhibitor isolated from culture supernatants of *S. elongatus*.

Chemoenzymatic synthesis of 7-deoxy-sedoheptulose. To unambiguously prove the chemical structure of the 7-deoxyheptulose from *S. elongatus* culture supernatants, we established the chemoenzymatic synthesis of 7-deoxy-D-*altro*-2-heptulose (**1**) (7-deoxy-sedoheptulose, 7dSh). C_7-carbohydrate intermediates occur in the pentose phosphate pathway and can be biosynthesized by the transfer of a C_2-unit onto a C_5-precursor using the enzyme transketolase. Transketolase (EC 2.2.1.1) stereospecifically adds the nucleophile to the *re*-face of the D-enantiomers of 2-hydroxyaldehydes (aldoses) and controls the stereochemistry of the reaction to result in (3*S*, 4*R*)-configured ketoses[29]. We cloned the gene encoding the *S. elongatus* transketolase (Synpcc7942_0538) in an *Escherichia coli* His-tag (pET15b) overexpression vector and purified the recombinant protein by affinity chromatography (see Methods). In the enzymatic synthesis of 7dSh, recombinant *S. elongatus* transketolase transfers the C1–C2 ketol unit of β-hydroxypyruvate (**3**) to 5-deoxy-D-ribose (**2**) in the presence of thiamine diphosphate and divalent cations (Mg^{2+})[30] (Fig. 2a). Release of CO_2 from β-hydroxypyruvate during the transketolase reaction prevents the back-reaction and enables a one-way synthesis of 7-deoxy-D-*altro*-2-heptulose (**1**), which is the only product according to NMR and MS data.

Transketolases efficiently react with phosphorylated sugars, but reactions with dephosphorylated sugars result in low yields[31]. In agreement, the chemoenzymatic synthesis of 7dSh from 5-deoxy-D-ribose gave yields of about 20%. We purified chemoenzymatically synthesized 7dSh following the same protocol used for purifying 7dSh from culture supernatants (Supplementary Fig. 1), except that size-exclusion chromatography on Sephadex LH20 could be omitted.

The ^{1}H-NMR spectrum of chemoenzymatically synthesized 7dSh (**1**) was identical to that of the compound isolated from *S. elongatus* culture supernatant. The chemical structure of 7dSh was reported in 1970 as the metabolite SF-666B from *Streptomyces setonensis* nav. sp. by Ezaki, Tsuruoka[32]. SF-666B was described to show exclusive activity against *Gluconobacter oxydans* subsp. *suboxydans* at low micromolar concentrations (0.8 μg mL^{-1})[33]. Therefore, we isolated SF-666B from culture supernatants of the *Streptomyces setonensis* production strain following our purification protocol (Supplementary Fig. 1). NMR spectroscopy revealed that SF-666B is indeed identical to 7dSh isolated from *S. elongatus* culture supernatants and to chemoenzymatically synthesized 7dSh (Fig. 2c).

Activity of 7dSh against cyanobacterial strains. With the assigned structure of 7dSh (**1**) and milligram amounts of pure compound at hand, we aimed for detailed biological profiling of the compound. In contrast to the previously reported activity of SF-666B, none of the 7dSh preparations (chemoenzymatically synthesized, purified from culture supernatants of *S. elongatus* or *Streptomyces setonensis*) showed any activity against *Gluconobacter oxydans* under the previously described assay conditions[33] and under various other tested conditions (not shown). By contrast, all 7dSh preparations inhibited the growth of the filamentous cyanobacterium *A. variabilis*. To clarify the biological activity of 7dSh and its biological mode of action, we first analyzed the effects of 7dSh on cyanobacteria in more detail (Fig. 3).

The effect of 7dSh (**1**) on *A. variabilis* depended on the ratio between the 7dSh concentration and the cell density of the cultures (determined as optical density at 750 nm, OD_{750}; Fig. 3a). Cultures with an initial OD_{750} of 0.5 were hardly affected by 7dSh concentrations up to 5 μg mL^{-1} (ca. 25 μM). When the cell density of *A. variabilis* was lowered to an OD_{750} of 0.2, 7dSh had a dose-dependent effect. At a concentration of 2.5 μg mL^{-1} (ca. 13 μM), 7dSh showed a cytostatic effect. A further increase of 7dSh to 5 μg mL^{-1} resulted in lysis of the cells. With even lower initial cell densities (initial $OD_{750} < 0.05$), the effect of 7dSh was even more pronounced; already 2.5 μg mL^{-1} 7dSh had a bactericidal effect. Therefore, the effect of 7dSh on *A. variabilis* can be either bacteriostatic or bactericidal, depending on the amount of 7dSh available per cell. This result indicated a cellular binding site for 7dSh that reduces the titer of the compound in solution or a metabolic alteration of 7dSh.

We subsequently used bactericidal concentrations of 7dSh (**1**) for bioprofiling to obtain unambiguous results. Since 7dSh was active against a cyanobacterium but not against *Gluconobacter oxydans*, we speculated that 7dSh might target the photosynthetic apparatus. Treatment of *A. variabilis* with 7dSh (ca. 50 μM) led to a slow decrease in photosynthetic oxygen formation over a period of 24 h (Fig. 3b). This effect is in contrast to that of specific inhibitors of photosynthesis, such as 3-(3,4-dichlorophenyl)-1,1-dimethylurea, which act almost immediately. The slow decrease resembled the effect of the protein synthesis inhibitor

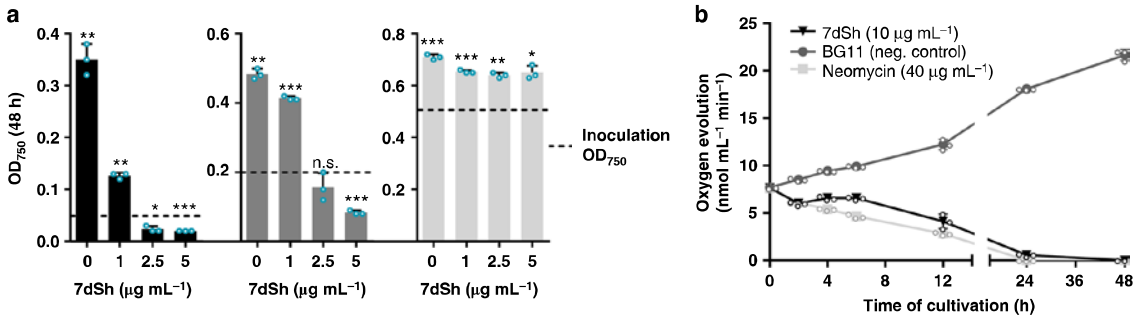

Fig. 3 Effect of 7dSh (**1**) on the growth and photosynthetic oxygen evolution of *A. variabilis* cultures. **a** Growth of *A. variabilis* (OD_{750}) at different concentrations of 7dSh after 48 h of incubation. Cultures were inoculated to an OD_{750} of 0.05, 0.2, or 0.5 (marked by dashed lines). 7dSh in aqueous solution was added at time 0. Significant differences between adjusted initial OD_{750} and OD_{750} after 48 h were analyzed in a one sample *t*-test (*p-value < 0.05; **p-value < 0.01; ***p-value < 0.001; n.s., not significant). **b** Photosynthetic oxygen evolution by *A. variabilis* (initial $OD_{750} = 0.3$) in the presence of 7dSh or neomycin (positive control) or without supplementation (BG11, negative control). 7dSh (ca. 50 μM) and neomycin (ca. 65 μM) were added as aqueous solution. Values in both graphs represent the mean values of three biological replicates; standard deviations are indicated. Dots indicate data distribution. Source data are provided as a Source Data file

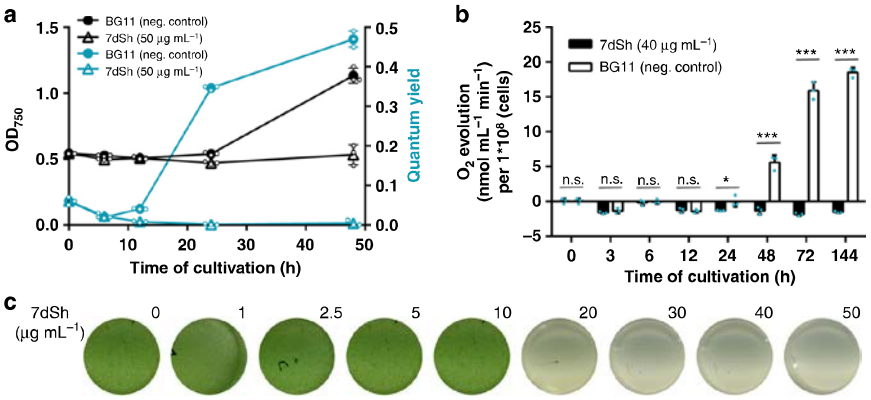

Fig. 4 7dSh (**1**) prevents regeneration of resuscitating *Synechocystis*. **a** Optical density (black) and PSII quantum yield (turquoise) of chlorotic *Synechocystis* cultures (initial OD_{750} = 0.5) regenerating in the absence or presence of 7dSh. $NaNO_3$ (17.3 mM) and 7dSh (ca. 260 µM) were added in aqueous solution at 0 h. Values represent the mean values of three biological replicates; standard deviations are indicated. Dots indicate data distribution. **b** Oxygen evolution of resuscitating *Synechocystis* cultures (initial OD_{750} = 0.5) upon addition of nitrate ($NaNO_3$, 17.3 mM) in the presence or absence of 7dSh (ca. 206 µM). Significant differences between 7dSh treatment and untreated control for each timepoint were analyzed in an unpaired *t*-test (*p-value < 0.05; **p-value < 0.01; *** p-value < 0.001; n.s., not significant). Values represent the mean values of three biological replicates; standard deviations are indicated. Dots indicate data distribution. **c** Cultures of chlorotic *Synechocystis* (initial OD_{750} = 0.5) 48 h after addition of nitrate ($NaNO_3$, 17.3 mM) and 7dSh. Numbers indicate concentration (µg mL^{-1}) of 7dSh added to the culture. Source data are provided as a Source Data file

neomycin, which slowly decreases photosynthetic oxygen evolution by inhibiting the PSII repair cycle. This similarity suggested an indirect effect of 7dSh on photosynthesis, ultimately mediated by the inability to maintain the PSII repair cycle.

To narrow down the cellular processes targeted by 7dSh (**1**), we made use of the unique properties of the recovery of nitrogen-starved chlorotic cells as an experimental system, where different metabolic activities are activated in a sequential order[34]. Here, long-term nitrogen-starved *Synechocystis* sp. cells were allowed to resuscitate from chlorosis by adding nitrate. In a typical experiment, the cells return to vegetative growth within 48 h in a highly coordinated process. Almost immediately after nitrate addition, dormant cells switch on metabolism and re-establish the basic enzymatic machinery. After approximately 16 h, photosynthesis and CO_2 fixation are turned on, and at the end of recovery, cells divide again. To reveal whether and at which stage resuscitation is blocked by 7dSh, chlorotic *Synechocystis* sp. cells were treated with 7dSh immediately before nitrate was added to initiate resuscitation. Following the addition of nitrate, control cultures showed the expected re-greening and return of photosynthetic activity[34]. The presence of 7dSh prevented resuscitation and re-greening in a dose-dependent manner (Fig. 4c). Measurement of oxygen exchange (Fig. 4b) and of PSII activity through pulse amplitude modulation (PAM) fluorometry[35] (Fig. 4a) showed that 7dSh-treated cells initially started respiratory glycogen consumption but then were unable to proceed further in the recovery and to restore their photosynthetic machinery. This clearly indicated that 7dSh affected metabolism at an early stage of resuscitation that is mainly characterized by anabolic reactions such as de novo amino acid synthesis[34].

Inhibition of 3-dehydroquinate synthase by 7dSh. To elucidate the mechanism of action, the effect of 7dSh (**1**) on the metabolic pattern of resuscitating *Synechocystis* sp. and exponentially growing *A. variabilis* was analyzed. Liquid cultures of the respective cyanobacteria were incubated in the absence or presence of 7dSh. At different time points, cells were collected and extracted with an acidic methanol/water solution (see Methods) for molecular analysis by LC-HRMS. Software-based subtraction (MetaboliteDetect 2.1, Bruker Daltonics) of the standardized MS chromatograms facilitated the detection of metabolic differences between cell samples of untreated and 7dSh-treated cultures. This analysis revealed a fast and massive accumulation of a metabolite with the sum formula of $C_7H_{13}O_{10}P$ (M_R = 288.14 Da from m/z = 289.0325 $[M+H]^+$ and 287.0171 $[M-H]^-$) in 7dSh-treated cells. Within 1 h after 7dSh (**1**) addition to *A. variabilis* cultures, the concentration of the respective compound increased more than fifteen fold as compared to initial concentration of untreated control cultures (t = 0 h) (Supplementary Fig. 3a, b). The accumulation of the respective compound further increased over time, reaching the 72-fold concentration (about 1.1 µM) as compared to untreated control cultures (about 16 nM) after 4 h. The sum formula ($C_7H_{13}O_{10}P$) and comparison of the MS/MS fragmentation pattern (Supplementary Fig. 3c) with MetFrag insilico fragmentation[36] and data in the literature[37] revealed that the accumulated compound was 3-deoxy-D-*arabino*-heptulosonate 7-phosphate (DAHP) (**4**, Supplementary Fig. 4). DAHP is the substrate of 3-dehydroquinate (DHQ) synthase, one of the first enzymes in the shikimate pathway, which converts DAHP to DHQ. This essential reaction in shikimate biosynthesis cannot be bypassed by alternative enzymes. The accumulation of DAHP is in accordance with DHQ synthase being the biological target of 7dSh[38]. Within the five-step reaction mechanism for conversion of DAHP to DHQ by DHQ synthase[39], the second step represents the β-elimination of the phosphate group of DAHP (Supplementary Fig. 4). We propose that 7dSh (**1**) mimics DAHP (**4**), the natural substrate of DHQ synthase. The C-7-methyl group of 7dSh, which is absent in DAHP, would impede the β-elimination in step 2, thereby leading to an inhibition of DHQ synthase and consequently the accumulation of DAHP.

Inhibition of the shikimate pathway triggers a metabolic perturbation that leads to decreased pools of aromatic amino acids, and, as a result of perturbed protein synthesis, also to the accumulation of non-aromatic amino acids such as leucine, valine, and arginine[40]. Thus, to confirm our hypothesis, we analyzed the levels of aromatic and selected non-aromatic amino

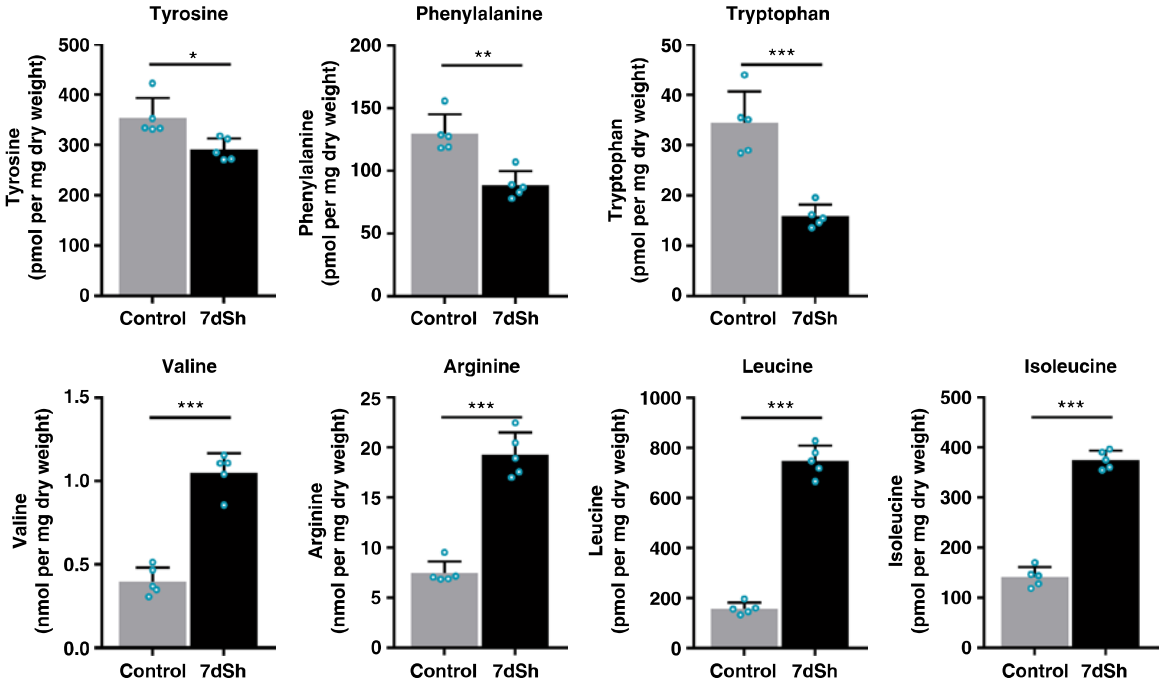

Fig. 5 Effects of 7dSh (**1**) on amino acid levels in *A. variabilis* cells. Levels of selected amino acids in *A. variabilis* (initial $OD_{750} = 0.5$) treated with 7dSh (260 µM) for 4 h and respective untreated control cultures. Significant differences between 7dSh treatment and untreated control were analyzed in an unpaired *t*-test (**p*-value < 0.05; ***p*-value < 0.01; ****p*-value < 0.001; n.s., not significant). Values represent the mean values of five biological replicates; standard deviations are indicated. Dots indicate data distribution. Source data are provided as a Source Data file

acids in 7dSh-treated and untreated *A. variabilis* cultures by LC-HRMS (Fig. 5). 7dSh (**1**) induced a significant accumulation of the non-aromatic amino acids leucine, isoleucine, valine and arginine. Within 4 h, the levels of isoleucine, arginine and valine increased almost threefold, and that of leucine about fivefold. By contrast, the levels of all aromatic amino acids significantly decreased in comparison to untreated control cultures (about 55% for tryptophan, 30% for phenylalanine and 20% for tyrosine).

The significant accumulation of DAHP (**4**) and changes in amino acid levels were also detected in cultures of nitrogen-starved *Synechocystis* sp. that were resuscitating from chlorosis in the presence of 7dSh (**1**) (Supplementary Fig. 5). Because of the lower metabolic activity of chlorotic cultures, DAHP accumulation was delayed but comparable to 7dSh-treated *A. variabilis* cultures.

We obtained further evidence that 7dSh (**1**) is an inhibitor of the shikimate pathway in an amino acid feeding experiment. The uptake of aromatic metabolites should mitigate the effects induced by 7dSh. PAM fluorometry of *A. variabilis* cultures revealed a 7dSh-induced decrease in the PSII quantum yield to about 10% of that of untreated control cultures (Supplementary Fig. 6). This effect was alleviated by supplementation with a mixture of aromatic amino acids. By contrast, supplementation of untreated control cultures with the aromatic amino acid mixture did not affect their PSII quantum yield. Supplementation with aromatic amino acids similarly alleviates the effects of glyphosate on other cyanobacteria[41].

Antifungal and herbicidal effects of 7dSh. As the shikimate pathway occurs in other bacteria and in fungi and plants, we decided to investigate the effects of 7dSh (**1**) on organisms other than cyanobacteria. We chose the yeast model organism *Saccharomyces cerevisiae* as the fungal representative. When *S. cerevisiae* was cultivated in YPD complex medium, 7dSh did not affect growth. By contrast, when the yeast was grown in YNB minimal medium with defined carbon and nitrogen sources, 7dSh (10 µg mL^{-1}, ca. 50 µM) inhibited growth (Supplementary Fig. 7), with a lower growth rate and a significantly lowered final optical density (OD_{600} of about 0.5) compared to growth in the absence of 7dSh (final OD_{600} of about 0.95). Glyphosate (100 µg mL^{-1}, ca. 590 µM) had to be applied at more than tenfold higher concentration to achieve a similar effect. A similar decreased growth rate instead of complete growth inhibition of microbes has earlier been described for glyphosate[42]. If an anti-metabolite binds reversibly to the targeted enzyme, it will be replaced by the accumulating natural substrate. Therefore, a high intracellular concentration of the antimetabolite and low abundance of target enzyme favor inhibition of the targeted reaction. The observed residual growth of *S. cerevisiae* is consistent with a putative reversible binding of 7dSh.

As the representative for testing the effects of 7dSh (**1**) on plants, we chose the model organism *Arabidopsis thaliana*. Seedlings of *A. thaliana* germinated in mineral salt medium were significantly affected by micromolar concentrations of 7dSh. After 7 days, seedlings of the untreated control formed distinct roots with numerous root hairs and green cotyledons (Fig. 6a). The control seedlings showed gravitropism, and the distance between the shoot and root apical meristem was about 6 mm (Fig. 6b). Even a low concentration of 7dSh (5 µg mL^{-1}, ca. 25 µM) significantly affected the size of the seedlings. At concentrations of 25 or 50 µM, the growth inhibition effects of 7dSh were similar to those of glyphosate at the same concentrations.

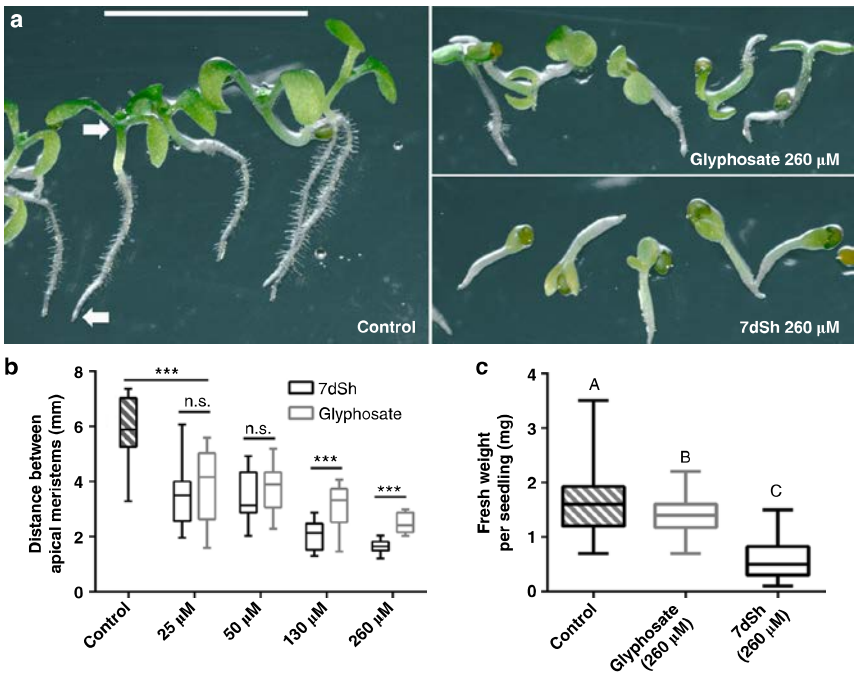

Fig. 6 7dSh (**1**) reduces the growth of *A. thaliana* seedlings. **a** Morphological appearance of autotrophically grown *Arabidopsis thaliana* seedlings 7 days after induction of germination. Seedlings were grown in constant light on agar plates without an antimetabolite (control) or in the presence of 7dSh or glyphosate. Plates were mounted vertically and illuminated from above. White arrows mark the root and shoot apical meristem. Scale bar (5 mm) applies to all images. **b** Measurement of the distance between root and shoot apical meristem. Significant differences between seedling sizes were analyzed in an unpaired *t*-test (*p-value < 0.05; ** p-value < 0.01; *** p-value < 0.001; n.s., not significant). Box-and-whisker plots represent the values of at least 16 seedlings. **c** Effect of 7dSh and glyphosate (each 260 µM) on the growth of *A. thaliana* on soil after 18 days in a day/night cycle. Statistical analysis was performed by using a one-way ANOVA. Tukey's multiple comparison test was used as the post-hoc test. Means that were significantly different (p-value < 0.05) are marked with different capital letters in the diagram. Box-and-whisker plots represent the values of at least 58 *A. thaliana* seedlings. For **b, c**: Error bars indicate range, box bounds indicate second and third quartiles, center lines indicate median. Source data are provided as a Source Data file

At concentrations of 130 and 260 µM, the inhibitory effect of 7dSh significantly surpassed that of glyphosate at the same concentrations, both in terms of seedling size (Fig. 6b) and morphological appearance (Fig. 6a). Impaired growth and aberrant morphology of the seedlings were particularly evident at higher concentrations of 7dSh (260 µM). In this case, the seedling growth was arrested within the first days. Only minor root and cotyledon formation was observed, and gravitropism was impaired (Fig. 6a and b). In comparison, *A. thaliana* seedlings that had been treated with higher concentration of glyphosate (260 µM) were less affected. They developed further, formed roots with small root hairs and bigger cotyledons. In the following days (day 7 to 14), no further plant growth or morphological change was observed in the presence of the inhibitors.

LC-HRMS analysis of whole plant extracts of the *A. thaliana* seedlings revealed a 7dSh-induced accumulation of DAHP, which was not detectable for the control or glyphosate-treated seedlings (Supplementary Fig. 8). As a proof of principle the accumulation of shikimate 3-phosphate was detectable in glyphosate-treated seedlings but not detectable in control or 7dSh-treated plants.

In order to evaluate the herbicidal activity of 7dSh (**1**) in more natural conditions, growth of *A. thaliana* in presence of the inhibitor was investigated in soil in a day/night cycle (Fig. 6c). After 18 days, seedlings were harvested and weighted. The weight of the seedlings was significantly reduced in 7dSh and glyphosate treatment as compared to untreated control. Furthermore, the inhibitory effect of 7dSh significantly surpassed that of glyphosate as the weight of the 7dSh-treated seedlings was less than half as much as that of the glyphosate-treated seedlings.

Early germination events are characterized by the efficient reactivation of metabolic pathways[43]. Metabolites required for the induction of germination are stored in the seeds. Once these reserve materials are depleted, the proliferation of the seedlings relies on de novo synthesis of intermediates and growth factors. Glyphosate- or 7dSh-induced inhibition of the shikimate pathway therefore leads to an effective arrest of the seedling growth.

Cytotoxicity of 7dSh on mammalian cells. To determine whether 7dSh (**1**) affects mammalian metabolism, we tested various human cell lines (THP-1 macrophages, A549 human lung epithelial cells, HepG2 human liver epithelial-like cells, 293 human embryonal kidney cells) and primary human neutrophils in cytotoxicity assays. 7dSh did not show any cytotoxic effects on tested human cell lines and primary cells (Supplementary Fig. 9a), even at 5 mM, a concentration that is two orders of magnitude higher than that required for its herbicidal effect. Neither 7dSh nor glyphosate at 5 mM lysed cells, as measured by the release of lactate dehydrogenase. Further, the morphological appearance

of 7dSh-treated macrophages did not differ from that of the untreated control (Supplementary Fig. 9b,c).

The biology of 7dSh for the producer strain. It is surprising to us that 7dSh (**1**), which has never before been described in cyanobacteria, was isolated from the unicellular cyanobacterium *S. elongatus*. *S. elongatus* is a common laboratory strain but has never been described as a producer of hydrophilic secondary metabolites. The role of 7dSh in metabolism and for the physiology of the producer strain yet remains enigmatic. Due to the streamlined genome, which lacks classical secondary metabolite gene clusters[25], the biosynthesis of 7dSh is not yet clear. However, to the best of our knowledge, a specific biosynthetic gene cluster or pathway may not be necessary for the biosynthesis of 7dSh. It has been shown for another cyanobacterial strain with a small genome, that enzymatic promiscuity enables the production of a large variety of secondary metabolites without the need of specific enzymes[23]. One of the enzymes known for enzymatic promiscuity is the transketolase, the enzyme we used for chemoenzymatic synthesis of 7dSh. The transketolase plays a fundamental role in cyanobacterial metabolism, e.g., in the Calvin cycle, and exhibits a wide substrate specificity. To shed light on the biosynthesis of 7dSh, we screened *S. elongatus* cultures for the presence of a potential 7dSh precursor. The screening resulted in the isolation of the monosaccharide 5-deoxy-D-ribose (**2**), a metabolite never isolated from nature before (Supplementary Fig. 10a, b, Supplementary Fig. 17–21).

The effective in vitro conversion of 5-deoxy-D-ribose (**2**) to 7dSh (**1**), carried out by the *S. elongatus* transketolase in our chemoenzymatic synthesis, suggests this reaction is the final step in the biosynthesis of 7dSh. The affinity of the cyanobacterial transketolase to 5-deoxy-D-ribose was about 100-fold lower than the affinity to the natural transketolase substrate D-ribose 5-phosphate (Supplementary Fig. 10c, d), enough to explain the minute levels of 7dSh produced by *S. elongatus* in later stages of growth, where CO_2 fixation and consequently D-ribose 5-phosphate levels decrease. Nevertheless, the synthesis of the assumed precursor 5-deoxy-D-ribose remains enigmatic. Future studies shall clarify whether this compound is a side product of a primary metabolic pathway or whether yet unidentified enzymes are involved.

The biological role of 7dSh (**1**) for the producer strain remains obscure. Since 7dSh shows allelochemical characteristics and is excreted to the medium, its production could also be a strategy of *S. elongatus* to protect its niches against other competitors. Even though the low production level of 7dSh in laboratory test conditions questions this hypothesis, the 7dSh concentration could be higher under certain natural conditions, such as in biofilms. Although *S. elongatus* laboratory strains usually grow planktonically, the re-isolated wild-type grows in a biofilm[44]. When growing in a biofilm or a microbial mat, the concentration of 7dSh could increase to a level sufficient to provide physiological effects such as controlling the surrounding microbial community.

Discussion

This paper reports the first natural compound—the rare sugar 7-deoxy-sedoheptulose (7dSh; **1**)—that acts as an in vivo inhibitor of the DHQ synthase as part of the shikimate pathway. Even though various inhibitors of DHQ synthase have been described in the literature[38,45–47] (Supplementary Fig. 11), none of these metabolites were reported to show strong in vivo activity against microbes or plants. Furthermore, in contrast to the known DHQ synthase inhibitors, 7dSh is comparatively simple to synthesize and production could be easily scaled up. Notably, 7dSh shows in vivo activity, especially against autotrophically growing organisms. We expect that 7dSh would also inhibit the growth of microorganisms in habitats with minimal nutrient concentrations. In nutrient-saturated habitats, microorganisms can take up aromatic metabolites from their environment and thereby mitigate the effect of 7dSh. The promising in vivo activity confers 7dSh antibacterial, antifungal, and herbicidal characteristics, which could enable its deployment as an agent in agriculture, water management, veterinary medicine, and even human medicine. Additional studies are needed to determine the medical and economic potential of 7dSh.

Methods

Strains and culture conditions. Cyanobacterial strains (*Synechococcus elongatus* PCC 7942, *Anabaena variabilis* ATCC 29413, and *Synechocystis* sp. PCC 6803) were routinely cultivated under photoautotrophic conditions with continuous illumination at 30–60 µE (Lumilux de Lux, Daylight, Osram) at 27 °C. Cells were cultivated in flasks with shaking at 120–130 rpm. Unless indicated otherwise, cells were cultivated in BG11 medium[48] supplemented with 5 mM $NaHCO_3$. For BG11 solid medium, 15 g L^{-1} Bacto agar (Difco) was autoclaved separately and combined with BG11 liquid medium.

Large-scale batch cultures of *S. elongatus* were cultivated in 1 L flasks containing 700 mL BG11 medium for 14 days under illumination at 55 µE. The cultures were gassed with air supplemented with 2% CO_2. Batch cultures were inoculated with densely grown pre-cultures to an OD_{750} of 0.2.

For cultivation of nitrogen-starved *Synechocystis* sp., $NaNO_3$ was omitted from BG11 medium as previously described[34]: Nitrogen starvation was initiated by centrifugation of the cells at room temperature at less than 3500 × *g* (Hereaus Megafuge 1.0 R). Cell pellets were washed, resuspended (desired $OD_{750} = 0.4$) and cultivated in BG11 without $NaNO_3$ for two weeks (shaken in 500 mL Erlenmeyer flasks). Resuscitation of chlorotic cells was initialized by the centrifugation of the cells at less than 3500 xg (Hereaus Megafuge 1.0 R) followed by the resuspension of the cell pellets in BG11.

Streptomyces setonensis SF666 (NBRC No. 13797) and *Gluconobacter oxydans* subsp. *suboxydans* (VTT E-97003) were cultivated as previously described[33]. Briefly, *S. setonensis* was grown in complex media containing 2.5% (w/v) glucose, 3.5% (w/v) soy flour (soybean meal), 0.5% (w/v) soluble vegetable protein and 0.25% (w/v) NaCl at pH 7.0 and 28 °C for 7 days. Cultures were grown under constant shaking (250 rpm) in 500 mL Erlenmeyer flasks covered by foam caps. *G. oxydans* was grown in complex media containing 0.2% (w/v) Na-glutamate, 0.2% (w/v) K_2HPO_4, 2% (w/v) sucrose, 0.2% (w/v) peptone, 0.5% (w/v) yeast extract, 0.01% (w/v) $MgCl_2$, 0.001% (w/v) $FeSO_4$ and 0.001% (w/v) $MnSO_4$ at pH 6.8 and 30 °C. Cultures were tested for their sensitivity against 7dSh on agar plates (1.5% (w/v) agar) and in liquid media in 96 well plates. 96 well plates were analyzed by a microplate reader (Tecan Spark®10 M) at a wavelength of 600 nm.

Saccharomyces cerevisiae was grown in yeast extract-peptone-dextrose (YPD)[49] medium or yeast nitrogen base (YNB) without amino acids (Sigma-Aldrich) medium supplemented with 0.5 g L^{-1} fructose and 1 g L^{-1} casamino acids with continuous shaking at 30 °C.

For agar plate experiments seeds of *Arabidopsis thaliana* accession Col-0 were germinated in half-strength Murashige and Skoog (MS) salts basal medium (Sigma Aldrich) agar plates (1.5%, w/v, Bacto agar) under constant illumination (60 µE) at 24 °C. For simultaneous growth of seedlings, seeds were stored at 4 °C overnight prior to initiation of germination. Subsequent, seedlings were grown for 7 days. To achieve growth of seedlings along the agar, plates were mounted vertically and illuminated from above.

For *Arabidopsis thaliana* experiments in soil, 24-well plates (three plates for each condition) were filled half with autoclaved and dried GS90 standard soil (Patzer GmbH, Germany) and vermiculite. Subsequently, wells were filled with 750 µL water (control), 7dSh or glyphosate (each 260 µM in aqueous solution, for glyphosate pH 7 was adjusted with NaOH). Each well was planted with a single seed of *A. thaliana* and the plate was incubated at 4 °C in the dark for five days to ensure a simultaneous growth of the seedlings. After that the seedlings were transferred to a growth chamber (air humidity 40%) with a 16 h day (20 °C) and 8 h night (18 °C) cycle with a light intensity of 85 µE. After 18 days the seedlings were harvested and weighted.

Extraction of *S. elongatus* culture lyophilisates. For lyophilisate extraction, 100 mL of *S. elongatus* batch cultures (grown for 14 days) were lyophilized. Lyophilisate was solved in 1 mL methanol, chloroform, acetone, or ethyl acetate. A 10 µL aliquot of each extract was applied to agar diffusion plates spread with *A. variabilis*.

Correlation of OD_{750} and inhibitor production level. At each time point, 25 mL of each *S. elongatus* batch culture was centrifuged at room temperature at 4500 × *g* for 5 min. The supernatant was evaporated to dryness, and the residue was dissolved in 80 µL methanol. A 40 µL aliquot of each extract was applied to agar diffusion plates spread with *A. variabilis*.

***A. variabilis* growth inhibition assays**. The inhibition of the growth of *A. variabilis* by *S. elongatus* extracts was assayed in BG11 liquid medium and on BG11 solid medium. In agar diffusion tests, paper discs containing dried samples of *S. elongatus* extracts were applied to agar plates freshly inoculated with *A. variabilis*. Agar plates were incubated under constant illumination at 40 µE and 27 °C for 5–6 days.

For growth inhibition assays in liquid medium, *A. variabilis* was grown in 24-well plates in 1 mL BG11 (initial OD = 0.05, unless stated otherwise). Test samples and controls were applied in water. The cultures were shaken at 100 rpm and 27 °C for 2–3 days under constant illumination at 40 µE.

Summary of 7dSh purification from *S. elongatus*. Culture supernatants were adjusted to pH 4 with 0.5 M HCl and then lyophilized. The lyophilisate was extracted with methanol and concentrated in vacuo. The methanol extract was applied to a gel filtration/size-exclusion column (Sephadex LH20, 1.6 × 80 cm, flow rate 0.5 mL min^{-1}, in methanol). The active fractions (t_R ca. 8 h) were pooled, evaporated to dryness and loaded in silica gel onto a Si 35, SF10–4g cartridge for separation of metabolites by normal phase medium-pressure liquid chromatography (MPLC) at a flow rate of 10 mL min^{-1} with a chloroform (solvent A) /methanol (solvent B) gradient as follows: 100% A, then solvent B in solvent A increased by 10% every 5 min to a total of 40% B in 25 min. The active fractions (elution after about t_R = 18–21 min) were pooled, evaporated to dryness, re-dissolved in water and loaded onto a ligand/ion-exchange high-performance liquid chromatography (HPLC) column (HiPlex Ca, 300 mm × 7.7 mm, Agilent). HPLC with isocratic water elution (flow 0.5 mL min^{-1}, temperature column oven: 85 °C) for 20 min led to the chromatographically pure 7dSh (**1**) (t_R = 15 min).

Physiochemical characterization of 7dSh from *S. elongatus*. For high-resolution mass spectrometry (HR-MS) data, purified 7dSh (**1**) was applied to a HiPlex Ca column of a Dionex Ultimate 3000 HPLC system (Thermo Fisher Scientific) coupled to a maXis 4 G ESI-QTOF mass spectrometer (Bruker Daltonics). 7dSh was eluted isocratically with water (flow rate 0.5 mL min^{-1}, temperature column oven: 85 °C) for 20 min. The ESI source was operated at a nebulizer pressure of 2.0 bar, and dry gas was set to 8.0 L min^{-1} at 200 °C. MS/MS spectra were recorded in auto MS/MS mode with collision energy stepping enabled. The scan rates for full scan and MS/MS spectra were set to 1 Hz and 7 Hz, respectively. Sodium formate was used as internal calibrant in each analysis. The molecular formula was calculated from monoisotopic masses using the SmartFormula function of DataAnalysis (Bruker Daltonics).

NMR measurements were recorded on a Bruker AMX600-, Avance III HDX700-, and AVI400 instruments. Deuterated methanol or water was used as solvent and internal standard. All spectra were recorded at room temperature. Chemical shifts are reported as δ values relative to the respective solvent as an internal reference. Coupling constants (*J*) were reported in Hertz (Hz). Abbreviations of multiplicity: *s* = singlet, *d* = doublet, *dd* = doublet of doublet, *m* = multiplet. Optical rotations were measured with a Perkin–Elmer 241. *Rf* values on TLC were determined on silica gel 60 F254 plates (Merck, 0.2 mm). Compounds were detected with orcinol staining reagent (10 mL sulfuric acid containing 0.1 g Fe (III)-chloride and 1 mL orcinol solution (in 6% ethanol)).

Cloning and purification of *S. elongatus* transketolase. The ORF *Synpcc7942_0538* of *Synechococcus elongatus* PCC 7942 was PCR amplified using the primer combination 5′-CATCACAGCAGCGGCCTGGTGCCGCGCGGCAG CCATATGCTCG AGATGGTTGTTGCGGCTCAATC-3′ and 5′-AGCAGCCA ACTCAGCTTCCTTTCG GGCTTTGTTA GCAGCCGGATCCTAGCCGATCA CTGCTTTCG-3′. After restriction of the pET15b vector with *Bam*HI, the fragment was fused with the vector backbone using Gibson assembly[50]. The final construct was introduced into *E. coli* BL21 (DE3) cells by transformation. Overexpression of *Synpcc7942_0538* was induced by addition of 0.5 mM IPTG. After 12 h of induction at 37 °C, cells were harvested by centrifugation. All subsequent steps were carried out at 0–4 °C. The pellet was resuspended in 10 mL of lysis buffer (50 mM Tris-HCl, 300 mM NaCl, 10 mM imidazole, pH 7.5, protease inhibitor (complete ULTRA tablets, Roche), lysozyme, and DNAse), and cells were lysed by sonification. Cell debris and insoluble material were removed by centrifugation (25 min at 4 °C and 35,000 × *g*). The cleared cell lysate was applied to a HisTrap HP column (GE Healthcare Life Science). After column washing, the bound proteins were eluted in fractions with 10 mL elution buffer (50 mM Tris-HCl, 300 mM NaCl, 500 mM imidazole, pH 7.5). Transketolase-containing fractions were combined, dialyzed in dialysis buffer (50 mM Tris-HCl pH 8.0, 100 mM NaCl, 5 mM $MgCl_2$, 1 mM DTT, 0.5 mM ETDA, 50% glycerol) and stored at −20 °C.

Chemoenzymatic synthesis of 7-deoxy-D-*altro*-2-heptulose. The synthesis of 7dSh (**1**) was inspired by the chemoenzymatic synthesis of sedoheptulose 7-phosphate[51]. 5-Deoxy-D-ribose (**2**) (Glentham Life Sciences) (50 mg, 250 mM) was dissolved in 1.5 mL HEPES buffer (100 mM, pH 7.5) containing thiamine pyrophosphate (1.3 mg, 2 mM) and $MgCl_2$ (0.4 mg, 3 mM). β-Hydroxypyruvate (**3**) as its lithium salt hydrate (54 mg, 285 mM) was added, and the pH was adjusted to 7.5. The reaction was initiated by addition of 4 mg transketolase (EC 2.2.1.1), and the mixture was shaken at 400 rpm and 30 °C for 24 h (Thriller®, Peqlab). The reaction was stopped by the addition of 6 mL methanol, followed by centrifugation (2500 × *g*, 10 min). The supernatant was evaporated to dryness, and 7dSh was purified as described in our purification protocol for extraction of 7dSh from *S. elongatus* cultures, except that size-exclusion chromatography on Sephadex LH20 was omitted.

Photosynthetic oxygen evolution and PAM fluorometry. Photosynthetic oxygen evolution was determined in vivo using a Clark-type oxygen electrode (Hansatech Instruments RS232, Norfolk, UK). Two milliliters of treated or untreated cultures were transferred to the measurement chamber. Oxygen formation was measured for 10 min at room temperature under illumination at 50 µE. PSII activity was analyzed in vivo with a WATER- pulse amplitude modulation (PAM) chlorophyll fluorometer (Walz GmbH, Effeltrich, Germany). All samples were dark-adapted for 5 min before measurement. Measurement of the PSII quantum yield (F_v/F_m) was performed at room temperature with WinControl Data Acquisition software.

Analysis of cyanobacterial and herbal metabolite patterns. Aliquots (2 mL) of cyanobacterial cultures were centrifuged (30 s, 20,817 × *g*), and the pellets were immediately frozen in liquid nitrogen. *A. thaliana* plants were crushed in a mortar under liquid nitrogen cooling. The pellets or plant materials were extracted with 600 µL methanol, followed by a second extraction of the material with 600 µL 20% methanol containing 0.1% formic acid. Both supernatants of each material extraction were combined and lyophilized, and the residue was dissolved in 100 µL 20% methanol containing 0.1% formic acid. Extracts (10 µL) were examined by LC-HRMS (Dionex Ultimate 3000 HPLC system from Thermo Fisher Scientific, coupled to a maXis 4 G ESI-QTOF mass spectrometer from Bruker Daltonics). LC-HRMS settings were adopted from[52]. Obtained mass spectra were compared and processed using MetaboliteDetect (Bruker Daltonics). Molecular formulas were calculated from monoisotopic masses using the SmartFormula function of DataAnalysis (Bruker Daltonics).

Quantification of amino acids and DAHP in *A. variabilis*. For the quantification of amino acids (Trp, Tyr, Phe, Val, Arg, Leu, and Ile) and DAHP the freeze dried sample material (10 mL, OD_{750} = 0.5) was homogenized with a Retsch ball mill (two cycles, 30 s each). Extraction was done with 400 µl 80% methanol containing 0.1% formic acid followed by a second extraction step with 400 µl 20% methanol also containing 0.1% formic acid. Both supernatants were combined and brought to dryness in a vacuum concentrator. The dried samples were redissolved in 150 µl 0.1 M hydrochloric acid for analyses.

Amino acid analyses were done with a Water UPLC-SynaptG2 LC-MS system. Chromatography was carried out on a 2.1 × 100 mm Waters Acquity HSST3 column. For separation a 10 min gradient from 99% water to 99% methanol (both solvents with 0.1% formic acid) was used. The mass spectrometer was operated in ESI positive mode and scanned from 50 to 2000 *m/z* with a scan rate of 0.5 s. For quantification extracted ion chromatograms were generated and integrated. An external calibration function was used for the calculation of absolute amounts.

DAHP analyses were done on a Thermo Scientific/Dionex ICS 5000 system. Chromatography was carried out on a 3.0 × 150 mm Carbopac PA 20 column. For separation a 32 min gradient from 75 mM sodium hydroxide to a 75 mM sodium hydroxide/500 mM sodium acetat mixture was used. Quantification was done by integration of the signal and absolute amounts were calculated with an external calibration function.

Supplementation with aromatic amino acids. *A. variabilis* in BG11 liquid medium (initial OD_{750} = 0.2) was supplemented with aromatic amino acids to a final concentration of 1 mM tryptophan, 1 mM tyrosine, 1 mM phenylalanine, 1 µg mL^{-1} *p*-aminobenzoate, or 1 µg mL^{-1} *p*-hydroxybenzoate.

Cytotoxicity of 7dSh on mammalian cells. Human THP1 cells (DSMZ, ACC 16) were grown in RPMI 1640 medium with 2 mM glutamine, 10% heat-inactivated FBS, 2% HEPES, 1% penicillin-streptomycin (10000 U mL^{-1}, Gibco) and 1 mM sodium pyruvate. To induce differentiation, cells were seeded in RPMI medium containing 1% penicillin-streptomycin and treated with 160 nM phorbol-12-myristate-13-acetate for 24 h. A546 cells, HepG2 cells, and HEK 293 cells were grown in Dulbecco's Modified Eagle's Medium (DMEM) with 10% Fetal Bovine Serum (FCS) and 1% penicillin-streptomycin. Human neutrophils were isolated from healthy blood donors by biocoll/histopaque density gradient centrifugation and resuspended in RPMI + 2% human serum albumin (HSA) + 2 mM sodiumpyruvat + 10 mM HEPES. THP1 cells (1×10^5 or 3×10^5) were seeded in 96-well cell culture plates in a final volume of 100 µL or in 8-well µ-slides in a final volume of 300 µL, respectively. After differentiation, the cells adhered to the culture dishes. A546 (ATCC CCL-185) cells, HepG2 (ATCC HB-8065) cells, HEK 293 (InvivoGen 293-null) cells (0.5×10^5) and human neutrophils (1×10^6) were seeded in 96-well cell culture plates in a final volume of 200 µL.

To evaluate the cytotoxic potential of 7dSh (**1**) and glyphosate, human THP1 macrophages were treated with 5 mM of the respective compounds in RPMI medium with 1% penicillin-streptomycin for 24 h. A546 cells, HepG2 cells, and HEK 293 cells were treated with 5 mM of the respective compounds for 24 h in DMEM medium (without phenol red) + 10% FCS + 1% penicillin-streptomycin.

Human neutrophils were treated in RPMI + 2% HSA + 2 mM sodium pyruvate + 10 mM HEPES for 5 h. Cells in medium were used as negative control, and cells treated with 1% Triton X-100 were used as positive control (100% cytotoxicity). After the indicated time points the cytotoxic potential of the compounds was determined according to the release of lactate dehydrogenase into the supernatant using the Cytotoxicity Detection Kit (Roche) following instructions of the manufacturer. The data represent the mean of three independent experiments.

For microscopic analysis, THP1 macrophages in 8-well µ-slides were treated with 5 mM 7dSh in RPMI medium with 1% penicillin-streptomycin or were untreated for 24 h. Cells were fixed with 150 µl icecold PBS containing 3.7% formaldehyde for 30 min. Wells were washed three times with HBSS, and incubated with 2.5 µl Alexa Fluor 647 Phalloidin (Thermo Fisher) in 100 µl PBS containing 1% BSA for 30 min. Cells were stained with one drop of NucBlue® Fixed Cell ReadyProbes® reagent (DAPI, Thermo Fisher) and mounted using fluorescence mounting medium (DAKO). Image acquisition was performed in the confocal mode of an inverted Zeiss LSM 710 NLO microscope employing Zeiss Plan-Apochromat ×63/1.40 oil DIC M27 objective with the following excitation wavelengths: DAPI: 405 nm; Phalloidin: 633 nm. Images were exported in overlays as 16-bit tagged image files for further analysis. Overlays were batch processed for intensity and color balance.

Isolation and structural elucidation of 5-deoxy-D-ribose. 5-Deoxy-D-ribose (**2**) was isolated from cultures of *S. elongatus* as described for the isolation of 7dSh (**1**) from *S. elongatus* except that pooling of the fractions from chromatography was adapted to 5-deoxy-D-ribose. On Sephadex LH20, 5-deoxy-D-ribose co-eluted with 7dSh. On MPLC, 5-deoxy-D-ribose eluted after 14–15 min. On HPLC with a HiPlex Ca column, the compound showed a retention time of 25.5 min. The isolated compound and commercially available 5-deoxy-D-ribose (Glentham Life Sciences) were analyzed by NMR spectroscopy and mass spectrometry as described for 7dSh.

Kinetic characterization of the *S. elongatus* transketolase. The kinetics of the *S. elongatus* transketolase were characterized for D-ribose 5-phosphate (Sigma Aldrich) or 5-deoxy-D-ribose (**2**) (Glentham Life Sciences) as acceptors of the transferred C1-C2 ketol unit. Reaction mix contained 0.1 mM glycylglycine buffer pH 7.5, 3 mM $MgCl_2$, 2 mM thiamine pyrophosphate (TPP), 0.5 mM NADH, 100 mM-L-erythrulose, 10 units yeast ADH and 5.75 µg mL^{-1} *S. elongatus* transketolase. For determination of K_M and V_{max}, the substrate concentrations were varied: D-ribose 5 phosphate (0.1 mM to 2.0 mM) or 5-deoxy-D-ribose (75 mM to 600 mM). Absorption at 340 nm was recorded. The reaction was performed in a final volume of 200 µL or 400 µL. Michaelis–Menten kinetic profiles were determined using GraphPad prism.

Reporting summary. Further information on experimental design is available in the Nature Research Reporting Summary linked to this article.

Data availability

Data supporting the findings of this work are available within the paper and its Supplementary Information files and from the corresponding authors upon reasonable request. The source data underlying Figs. 1, 3–6 and Supplementary Figs 3, 5, 6, 7, 9, and 10 are provided in Source Data file.

Received: 10 July 2018 Accepted: 9 January 2019
Published online: 01 February 2019

References

1. Nagle, D. G. & Paul, V. J. Chemical defense of a marine cyanobacterial bloom. *J. Exp. Mar. Bio. Ecol.* **225**, 29–38 (1998).
2. Leão, P. N., Engene, N., Antunes, A., Gerwick, W. H. & Vasconcelos, V. The chemical ecology of cyanobacteria. *Nat. Prod. Rep.* **29**, 372–391 (2012).
3. Sharif, D. I., Gallon, J., Smith, C. J. & Dudley, E. Quorum sensing in Cyanobacteria: N-octanoyl-homoserine lactone release and response, by the epilithic colonial cyanobacterium Gloeothece PCC6909. *ISME J.* **2**, 1171–1182 (2008).
4. Schaeffer, D. J. & Krylov, V. S. Anti-HIV activity of extracts and compounds from Algae and Cyanobacteria. *Ecotoxicol. Environ. Saf.* **45**, 208–227 (2000).
5. Singh, R. K., Tiwari, S. P., Rai, A. K. & Mohapatra, T. M. Cyanobacteria: an emerging source for drug discovery. *J. Antibiot.* **64**, 401–412 (2011).
6. Singh, I. P., Milligan, K. E. & Gerwick, W. H. Tanikolide, a Toxic and Antifungal Lactone from the Marine Cyanobacterium Lyngbya majuscula. *J. Nat. Prod.* **62**, 1333–1335 (1999).
7. Berry, J. P., Gantar, M., Perez, M. H., Berry, G. & Noriega, F. G. Cyanobacterial toxins as allelochemicals with potential applications as algaecides, herbicides and insecticides. *Mar. Drugs* **6**, 117–146 (2008).
8. Rastogi, R. P. & Sinha, R. P. Biotechnological and industrial significance of cyanobacterial secondary metabolites. *Biotechnol. Adv.* **27**, 521–539 (2009).
9. Cox, P. A., Banack, S. A. & Murch, S. J. Biomagnification of cyanobacterial neurotoxins and neurodegenerative disease among the Chamorro people of Guam. *Proc. Natl Acad. Sci.* **100**, 13380–13383 (2003).
10. Dunlop, R. A., Cox, P. A., Banack, S. A. & Rodgers, K. J. The non-protein amino acid BMAA Is Misincorporated into Human Proteins in Place of l-Serine Causing Protein Misfolding and Aggregation. *PLoS One* **8**, e75376 (2013).
11. Bentley, R. & Haslam, E. The shikimate pathway—a metabolic tree with many branche. *Crit. Rev. Biochem. Mol. Biol.* **25**, 307–384 (1990).
12. Ducati, R., Basso, L. & Santos, D. Mycobacterial shikimate pathway enzymes as targets for drug design. *Curr. Drug. Targets* **8**, 423–435 (2007).
13. Herrmann, K. M. & Weaver, L. M. The shikimate pathway. *Annu. Rev. Plant. Physiol. Plant. Mol. Biol.* **50**, 473–503 (1999).
14. Duke, S. O. & Powles, S. B. Glyphosate: a once-in-a-century herbicide. *Pest. Manag. Sci.* **64**, 319–325 (2008).
15. Motta, E. V. S., Raymann, K., Moran, N. A. Glyphosate perturbs the gut microbiota of honey bees. *Proc. Natl Acad. Sci.* **115**, 10305–10310 (2018).
16. Benbrook, C. M. Trends in glyphosate herbicide use in the United States and globally. *Environ. Sci. Eur.* **28**, 3 (2016).
17. Steinrücken, H. C. & Amrhein, N. The herbicide glyphosate is a potent inhibitor of 5-enolpyruvylshikimic acid-3-phosphate synthase. *Biochem. Biophys. Res. Commun.* **94**, 1207–1212 (1980).
18. Lonhienne, T. et al. Structural insights into the mechanism of inhibition of AHAS by herbicides. *Proc. Natl Acad. Sci.* **115**, E1945–E1954 (2018).
19. Daniel, G. M., Jian-Guo, W., Thierry, L. & William, G. L. Crystal structure of plant acetohydroxyacid synthase, the target for several commercial herbicides. *FEBS J.* **284**, 2037–2051 (2017).
20. Leão, P. N. et al. Synergistic allelochemicals from a freshwater cyanobacterium. *Proc. Natl Acad. Sci.* **107**, 11183–11188 (2010).
21. Paul, D. G. N. & Valerie, J. Production of secondary metabolites by filamentous tropical marine cyanobacteria: ecological functions of the compounds. *J. Phycol.* **35**, 1412–1421 (1999).
22. Shih, P. M. et al. Improving the coverage of the cyanobacterial phylum using diversity-driven genome sequencing. *Proc. Natl Acad. Sci.* **110**, 1053–1058 (2013).
23. Li, B. et al. Catalytic promiscuity in the biosynthesis of cyclic peptide secondary metabolites in planktonic marine cyanobacteria. *Proc. Natl Acad. Sci.* **107**, 10430–10435 (2010).
24. Golden, S. S., Brusslan, J. & Haselkorn, R. Genetic engineering of the cyanobacterial chromosome. *Methods Enzymol.* **153**, 215–231 (1987).
25. Copeland, A. et al. *Complete sequence of chromosome 1 of Synechococcus elongatus PCC 7942* (2014).
26. Cohen, A., Sendersky, E., Carmeli, S. & Schwarz, R. Collapsing Aged Culture of the Cyanobacterium Synechococcus elongatus Produces Compound(s) Toxic to Photosynthetic Organisms. *PLoS One* **9**, e100747 (2014).
27. Wang, X. & Woods, R. J. Insights into furanose solution conformations: beyond the two-state model. *J. Biomol. NMR* **64**, 291–305 (2016).
28. Collins, P. Ch. 8-H. *Dictionary of Carbohydrates*. (Chapman and Hall/CRC, 2005).
29. Turner, N. J. Applications of transketolases in organic synthesis. *Curr. Opin. Biotechnol.* **11**, 527–531 (2000).
30. Kobori, Y., Myles, D. & Whitesides, G. Substrate specificity and carbohydrate synthesis using transketolase. *J. Org. Chem.* **57**, 5899–5907 (1992).
31. Sprenger, G. A., Schorken, U., Sprenger, G. & Sahm, H. Transketolase A of Escherichia coli K12. Purification and properties of the enzyme from recombinant strains. *Eur. J. Biochem.* **230**, 525–532 (1995).
32. Ezaki, N., Tsuruoka, T., Ito, T. & Niida, T. Studies on new antibiotics, SF-666 A and B. I. Isolation and characterization of SF-666 A and B. *Sci. Rept Meiji Seika Kaisha* **11**, 15–20 (1970).
33. Shomura, T. et al. Studies on new antibiotics, SF-666 A and B. II. Some biological characteristics of SF-666 A and B. *Sci. Rept Meiji Seika Kaisha* **11**, 21–25 (1970).
34. Klotz, A. et al. Awakening of a Dormant Cyanobacterium from Nitrogen Chlorosis Reveals a Genetically Determined Program. *Curr. Biol.* **26**, 2862–2872 (2016).
35. Schreiber, U., Bilger, W., Neubauer, C. Chlorophyll fluorescence as a nonintrusive indicator for rapid assessment of in vivo photosynthesis. In: *Ecophysiology of Photosynthesis* (eds. Schulze E. -D., Caldwell M. M.) (Springer Berlin Heidelberg, 1995).
36. Wolf, S., Schmidt, S., Muller-Hannemann, M. & Neumann, S. In silico fragmentation for computer assisted identification of metabolite mass spectra. *BMC Bioinforma.* **11**, 148 (2010).
37. Oldiges, M. *Metabolomanalyse zur Untersuchung der Dynamik im Aromatenbiosyntheseweg in L-Phenylalanin Produzenten von Escherichia coli* (2005).
38. Montchamp, J. L., Piehler, L. T. & Frost, J. W. Diastereoselection and in vivo inhibition of 3-dehydroquinate synthase. *J. Am. Chem. Soc.* **114**, 4453–4459 (1992).

39. Carpenter, E. P., Hawkins, A. R., Frost, J. W. & Brown, K. A. Structure of dehydroquinate synthase reveals an active site capable of multistep catalysis. *Nature* **394**, 299–302 (1998).
40. Vivancos, P. D. et al. Perturbations of Amino Acid Metabolism Associated with Glyphosate-Dependent Inhibition of Shikimic Acid Metabolism Affect Cellular Redox Homeostasis and Alter the Abundance of Proteins Involved in Photosynthesis and Photorespiration. *Plant Physiol.* **157**, 256–268 (2011).
41. Powell, H. A., Kerbby, N. W. & Rowell, P. Natural tolerance of cyanobacteria to the herbicide glyphosate. *New Phytol.* **119**, 421–426 (1991).
42. Fischer, R. S., Berry, A., Gaines, C. G. & Jensen, R. A. Comparative action of glyphosate as a trigger of energy drain in eubacteria. *J. Bacteriol.* **168**, 1147–1154 (1986).
43. Fait, A. et al. Arabidopsis seed development and germination is associated with temporally distinct metabolic switches. *Plant Physiol.* **142**, 839–854 (2006).
44. Parnasa, R. et al. Small secreted proteins enable biofilm development in the cyanobacterium Synechococcus elongatus. *Sci. Rep.* **6**, 32209 (2016).
45. Liu, J. S., Cheng, W. C., Wang, H. J., Chen, Y. C. & Wang, W. C. Structure-based inhibitor discovery of Helicobacter pylori dehydroquinate synthase. *Biochem. Biophys. Res. Commun.* **373**, 1–7 (2008).
46. Le Marechal, P., Froussios, C., Level, M. & Azerad, R. The interaction of phosphonate and homophosphonate analogues of 3-deoxy-D-arabino heptulosonate 7-phosphate with 3-dehydroquinate synthetase from Escherichia coli. *Biochem. Biophys. Res. Commun.* **92**, 1104–1109 (1980).
47. Tian, F., Montchamp, J.-L. & Frost, J. W. Inhibitor Ionization as a Determinant of Binding to 3-Dehydroquinate Synthase. *J. Org. Chem.* **61**, 7373–7381 (1996).
48. Rippka, R., Deruelles, J., Waterbury, J. B., Herdman, M. & Stanier, R. Y. Generic Assignments, Strain Histories and Properties of Pure Cultures of Cyanobacteria. *Microbiology* **111**, 1–61 (1979).
49. Yeast Extract–Peptone–Dextrose (YPD) Medium (Liquid or Solid). *Cold Spring Harbor Protocols* 2017, pdb.rec090563 (2017).
50. Gibson, D. G. et al. Enzymatic assembly of DNA molecules up to several hundred kilobases. *Nat. Methods* **6**, 343 (2009).
51. Charmantray, F., Helaine, V., Legeret, B. & Hecquet, L. Preparative scale enzymatic synthesis of D-sedoheptulose-7-phosphate from beta-hydroxypyruvate and D-ribose-5-phosphate. *J. Mol. Catal. B-Enzym* **57**, 6–9 (2009).
52. Zettler, J., Zubeil, F., Kulik, A., Grond, S. & Kaysser, L. Epoxomicin and Eponemycin Biosynthesis Involves gem-Dimethylation and an Acyl-CoA Dehydrogenase-Like Enzyme. *Chembiochem* **17**, 792–798 (2016).

Acknowledgements

Work of the authors is supported and funded by the RTG 1708 "Molecular principles of bacterial survival strategies", the Institutional Strategy of the University of Tübingen (Deutsche Forschungsgemeinschaft, ZUK 63) and the "Glycobiotechnology" initiative (Ministry for Science, Research and Arts Baden-Württemberg). We thank Dr. Klaus Eichele, Anorganic Chemistry, University of Tübingen for NMR-predictions. Thanks to Dr. Sandra Richter, ZMBP University of Tübingen, Dr. Dorothee Wistuba, University of Tübingen and Dr. Timo Niedermeyer, University of Halle and Dr. Christiane Wolz, IMIT Tübingen for helpful discussions. We are indebted to Karen Brune for critically reading the manuscript.

Author contributions

K.B. performed culture cultivation, isolated 7dSh (**1**) and 5-deoxy-D-ribose (**2**), designed and performed synthesis of 7dSh and HPLC-MS experiments of the metabolite pattern and the biological test systems, wrote manuscript with input from all authors. J.R. designed and performed plant assays on soil and performed statistical analysis. P.R. performed NMR analysis and interpreted NMR data. A.S. designed and performed cloning, purification and kinetic characterization of transketolase. L.B. and E.W. designed and performed cytotoxicity studies on mammalian cells. M.S. designed and performed DAHP and amino acid quantification. S.G. designed and interpreted chemical experiments, edited manuscript. K.F. designed and interpreted biological experiments, edited manuscript.

Additional information

Supplementary Information accompanies this paper at https://doi.org/10.1038/s41467-019-08476-8.

Competing interests: University of Tübingen has filed a patent application that covers 7dSh, 7dSh analogs and their use (EKUT-0365, German patent application number DE10 2017 01 898.1, International patent application number PCT/EP2018/082440). The remaining authors declare no competing interests.

Reprints and permission information is available online at http://npg.nature.com/reprintsandpermissions/

Journal peer review information: *Nature Communications* thanks William Dyer, William Gerwick, and the other anonymous reviewer(s) for their contribution to the peer review of this work. Peer reviewer reports are available.

Publisher's note: Springer Nature remains neutral with regard to jurisdictional claims in published maps and institutional affiliations.

Supplementary Information for:

Cyanobacterial antimetabolite 7-deoxy-sedoheptulose blocks the shikimate pathway to inhibit the growth of prototrophic organisms

Brilisauer et al.

Supplementary Table 1: Physicochemical data of 7dSh (1) and 5-deoxy-D-ribose (2).

Name	**7-Deoxy-D-*altro*-heptulose (1)** **7-Deoxy-D-sedoheptulose**	**5-Deoxy-D-ribose (2)**
Appearance	white solid	white oil
Sum formula	$C_7H_{14}O_6$ (M_R = 194.18)	$C_5H_{10}O_4$ (M_R = 134.13)
TLC (Rf, colour reaction)	R_f = 0.58 ($CHCl_3$:MeOH 8:5), Orcinol	R_f = 0.71 ($CHCl_3$:MeOH 8:5), Orcinol
HR ESI(+) MS	Calculated for $C_7H_{14}O_6$: 194.0785, found: 217.0688 $[M+Na]^+$ Δ 1.0 ppm	Calculated for $C_5H_{10}O_4$: 134.0574, found: 157.0474 $[M+Na]^+$ Δ 1.5 ppm
Optical rotation value	$[\alpha]_D^{25}$= +11° (*c* = 0.1 in MeOH)	$[\alpha]_D^{25}$= +35° (*c* = 0.1 in MeOH)
^{1}H-NMR	^{1}H-NMR (D_2O, 298 K, 600 MHz): δ = 1.23 (d, 7-H, *J* = 6.6 Hz, 3H), 3.58 (d, 1-H, *J* = 12.2 Hz, 2H), 3.72 (dd, 5-H, *J* = 7.5, 4.4 Hz, 1H), 3.97 (dd, 6-H, *J* = 6.6, 4.4 Hz, 1H), 4.10 (d, 3-H, *J* = 7.8 Hz, 1H), 4.24 (dd, 4-H, *J* = 7.8, 7.5 Hz, 1H) ppm. ^{1}H-NMR (MeOD, 25 °C, 600 MHz): δ = 1.22 (s, 7-H, *J* = 6.6 Hz, 3H), 3.50 (s, 1-H, *J* = 11.48 Hz, 2H), 3.65 (dd, 5-H, *J* = 6.5, 4.1 Hz, 1H), 3.90 (dd, 6-H, *J* = 6.6, 4.1 Hz, 1H), 4.02 (d,3-H, *J* = 7.4 Hz, 1H), 4.23 (dd, 4-H, *J* = 7.4, 6.5 Hz, 1H) ppm.	^{1}H-NMR (D_2O, 298 K, 400 MHz): δ = 1.35/1.26 (d, 5-H, *J* = 6.1/6.5 Hz, 3H), 4.01/4.16 (m, 2-H, 1H), 4.01/3.83 (m/t, 3-H, *J* = 5.7 Hz, 1H), 4.01/4.16 (m, 4-H, 1H), 5.21/5.38 (d, 1-H, *J* = 1.7/4.3 Hz, 1H) ppm. ^{1}H-NMR (MeOD, 25 °C, 600 MHz): δ = 1.30/1.21 (d, 5-H, *J* = 6.3 Hz, 3H), 3.81/3.98 (dd, 2-H, *J* = 1.0, 4.7/4.3, 5.7 Hz, 1H), 3.58/3.82 (dd, 3-H, *J* = 5.7, 5.7/4.7, 6.3 Hz, 1H), 3.89/4.00 (dd, 4-H, *J* = 4.3, 5.7/6.3. 6.3 Hz, 1H), 5.06/5.22 (d, 1-H, *J* =1.0/4.3 Hz, 1H) ppm.
^{13}C-NMR	^{13}C-NMR (D_2O, 298 K, 150.9 MHz): δ = 17.0 (C-7), 62.5 (C-1), 67.6 (C-6), 74.6 (C-4), 75.8 (C-3), 83.5 (C-5), 101.3 (C-2) ppm.	^{13}C-NMR (D_2O, 298 K, 100.6 MHz): δ = 19.1/17.9 (C-5), 75.2/74.9 (C-3), 75.5/70.4 (C-2), 78.2/78.1 (C-4), 100.8/95.7 (C-1) ppm.

Data are obtained from synthesis products.

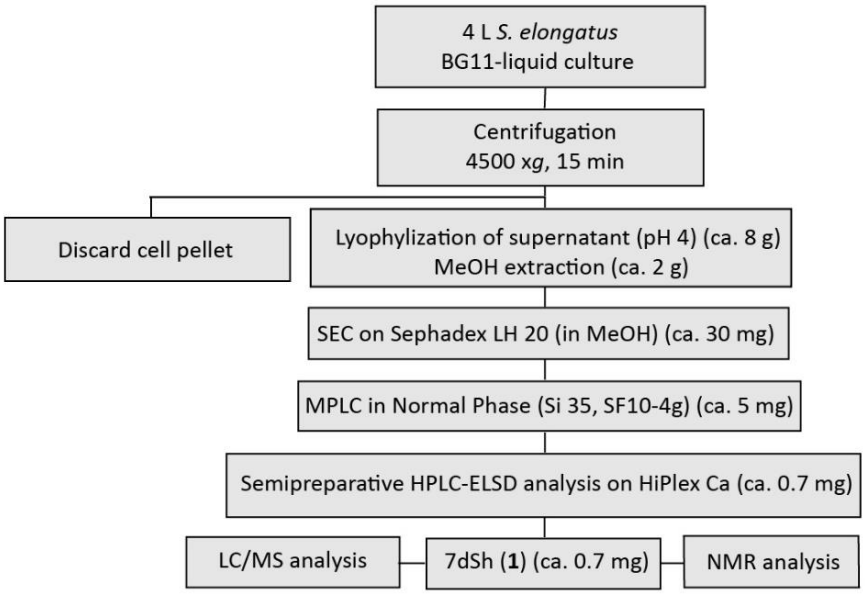

Supplementary Figure 1*:* Isolation scheme for bioactivity-guided purification of 7dSh from *S. elongatus*
The high polarity of 7dSh (**1**) required an optimization of the purification steps from the culture extract prior to final HPLC isolation. Purity was monitored via HPLC-UV-ELSD, NMR and LC-HRMS. HPLC on the ligand/ion-exchange HPLC column HiPlex Ca (Agilent) led to chromatographically pure 7dSh. The yield of the bioactive fractions in each step is indicated in parentheses. Abbreviations: MeOH, methanol; SEC, size-exclusion chromatography; MPLC, medium-pressure liquid chromatography; HPLC, high-performance liquid chromatography; ELSD, evaporative light-scattering detection; LC/MS, liquid chromatography mass spectrometry; NMR, nuclear magnetic resonance.

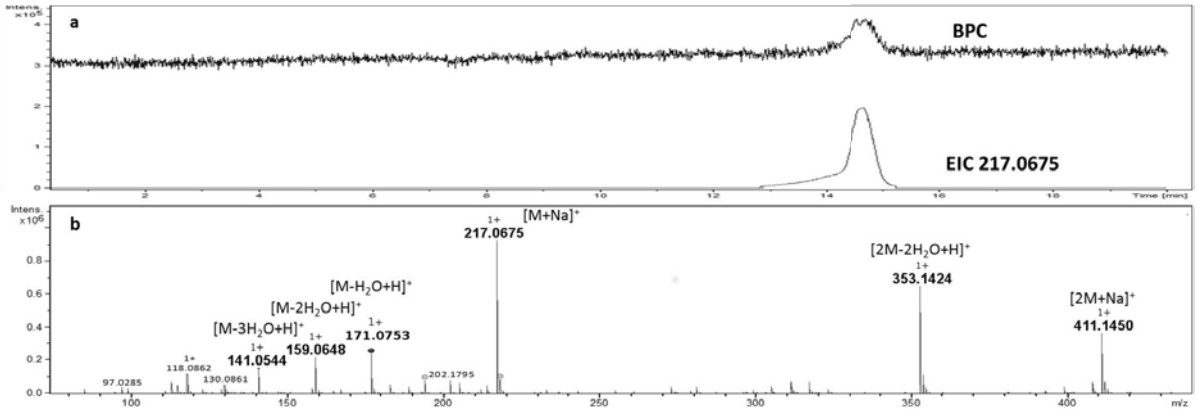

Supplementary Figure 2: HPLC-HRMS chromatogram and MS spectrum of 7dSh.

(**a**) High performance liquid chromatography coupled with high-resolution electrospray ionization mass spectrometry (HR-ESI(+)-MS) of isolated 7dSh (**1**) on a HiPlex Ca column. The base peak chromatogram (BPC) in positive mode and extracted ion chromatogram (EIC) of the isolated inhibitor revealed a mass of 217.0675 ($[M+Na]^+$, $C_7H_{14}O_6Na^+$) and chromatographic purity. (**b**) In the corresponding mass spectrum (R_t = 14.8 min), 7dSh exhibited the characteristic signal of *m/z* = 217.0675 $[M+Na]^+$ ($C_7H_{14}NaO_6^+$). Additional labelled signals correspond to 7dSh fragment ions, which resemble the typical H_2O-loss of carbohydrates and underline the sum formula of 7dSh as $C_7H_{14}O_6$ (molecular weight, M_R = 194.1825).

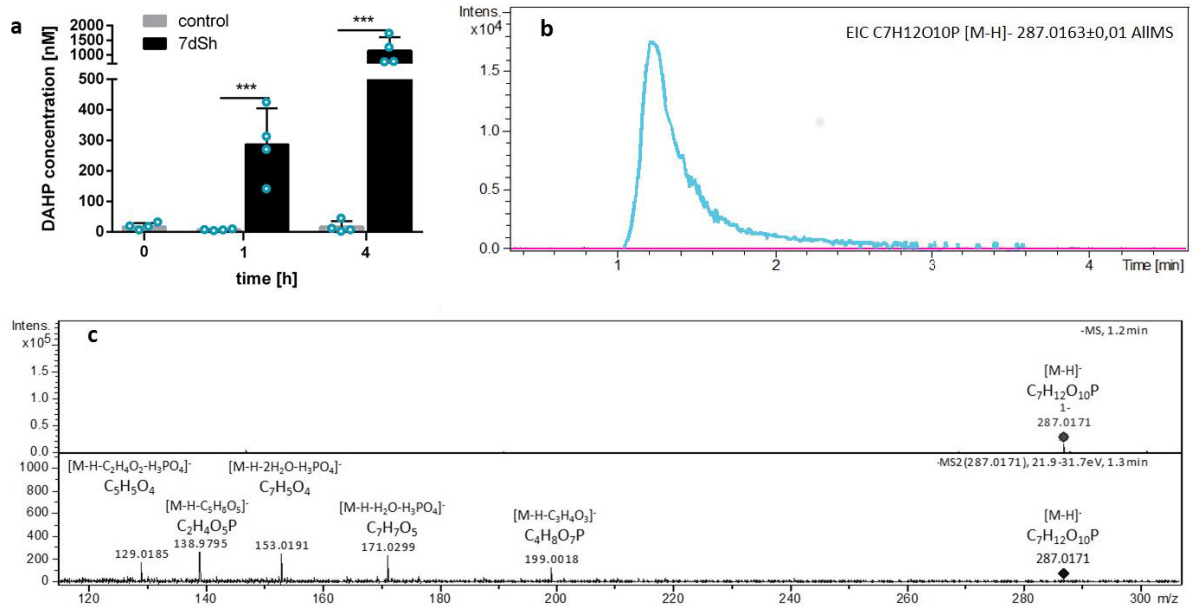

Supplementary Figure 3: DAHP accumulation in 7dSh-treated *A. variabilis* cultures.
Accumulation of 3-deoxy-D-arabinoheptulosonate 7-phosphate (**4**) (DAHP, $C_7H_{13}O_{10}P$) in 7dSh (**1**)-treated (40 µg mL^{-1}, ca. 206 µM) *A. variabilis* cultures (initial OD_{750} = 0.4) determined via LC-HRMS and electrochemical detector (ECD). (**a**) Increase in DAHP in 7dSh-treated *A. variabilis* cultures (detected by ECD). Significant differences between 7dSh treatment and untreated control for each timepoint were analyzed in an unpaired *t*-test (* *p*-value < 0.05; ** *p*-value < 0.01; *** *p*-value < 0.001; NS, not significant). Values represent the mean values of four biological replicates; standard deviations are indicated. Dots indicate data distribution. Source data are provided as a Source Data file. (**b**) LC-HRMS chromatogram with extracted mass signal of DAHP (ESI negative mode: $C_7H_{12}O_{10}P^-$ [M-H]$^-$) of *A. variabilis* culture treated with 7dSh for 1 h (turquoise) and of an untreated control culture (magenta). (**c**) Fragmentation pattern (ESI negative mode) of characteristic DAHP ions.

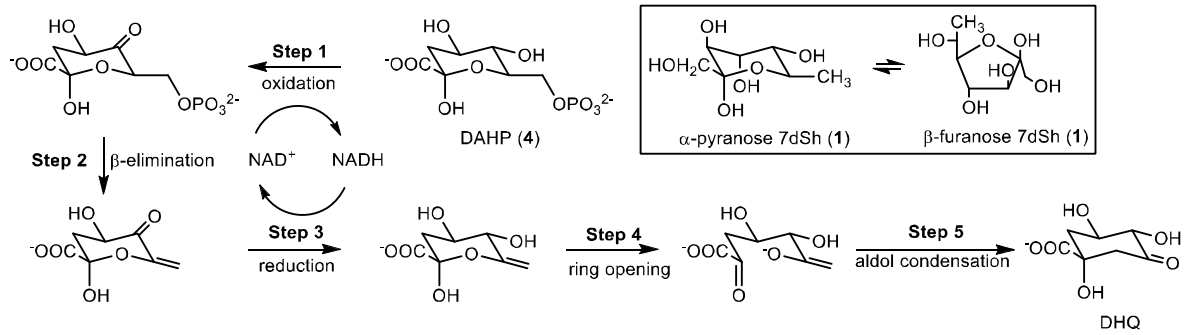

Supplementary Figure 4: Simplified mechanism of the conversion of DAHP to 3-dehydroquinate (DHQ) by DHQ synthase.

Modified from [1]. The pyranose and furanose forms of 7dSh (**1**) are depicted in the box.

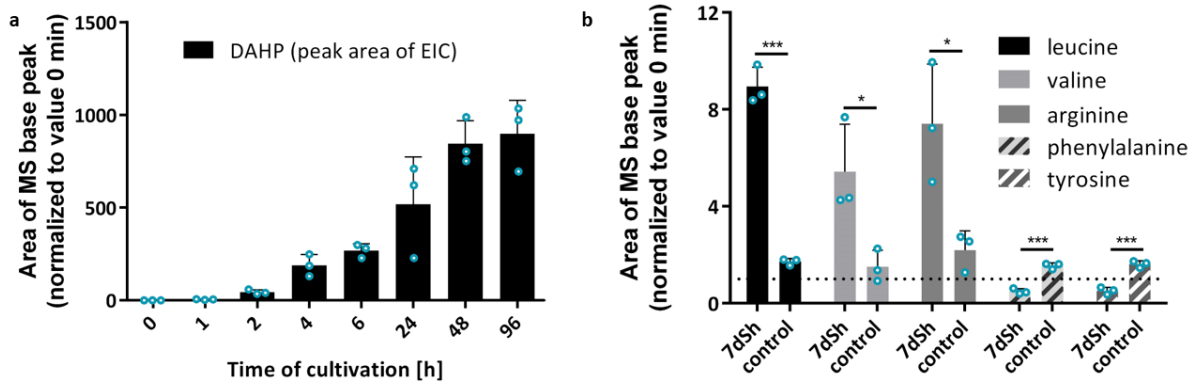

Supplementary Figure 5: Effects of 7dSh on DAHP and amino acid ratios in resuscitating *Synechocystis*. At time 0, nitrogen-starved cultures of *Synechocystis* sp. (initial OD = 0.2) were regenerated by adding $NaNO_3$ (17.3 mM) in the presence of 7dSh (**1**) (40 µg mL^{-1}, ca. 206 µM) or its absence. DAHP (**4**) and amino acid ratios were determined by LC-HRMS and are indicated by the peak areas of extracted ion chromatograms (EIC) normalized to respective value at time 0. (**a**) Increase of DAHP (ESI positive mode: $C_7H_{14}O_{10}P^+$) in 7dSh-treated cultures. (**b**) Changes in amino acid ratios (24 h after addition of $NaNO_3$ and 7dSh). The dashed line indicates the content of respective free amino acids present at time 0 before the addition of $NaNO_3$ and 7dSh. Significant differences between 7dSh treatment and untreated control for each timepoint were analyzed in an unpaired *t*-test (* *p*-value < 0.05; ** *p*-value < 0.01; *** *p*-value < 0.001; NS, not significant). Values in both graphs represent the mean values of three biological replicates; standard deviations are indicated. Dots indicate data distribution. Source data are provided as a Source Data file.

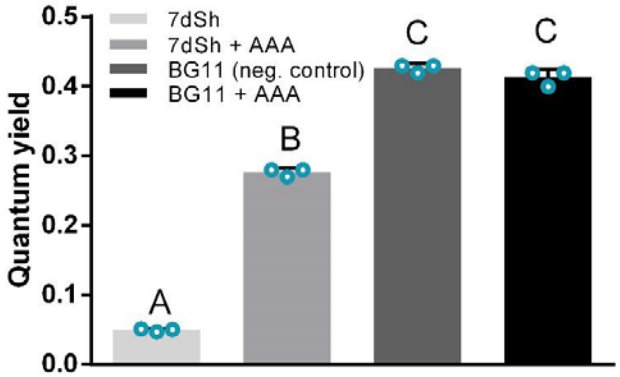

Supplementary Figure 6: Supplementation with aromatic amino acids alleviates effects of 7dSh on *A. variabilis.*

Effect of 7dSh (**1**) (ca. 50 µM) on the quantum yield of *A. variabilis* cultures (initial OD = 0.2) grown for 24 h with or without supplementation with a mixture of aromatic amino acids (AAA; tryptophan, tyrosine, and phenylalanine, 1 mM each; *p*-aminobenzoate and β-hydroxybenzoate, 1 µg mL^{-1} each). Statistical analysis was performed by using a one-way ANOVA. Tukey's multiple comparison test was used as the post-hoc test. Means that were significantly different (*p*-value <0.05) are marked with different capital letters in the diagram. Values represent the mean values of three biological replicates; standard deviations are indicated. Dots indicate data distribution. Source data are provided as a Source Data file.

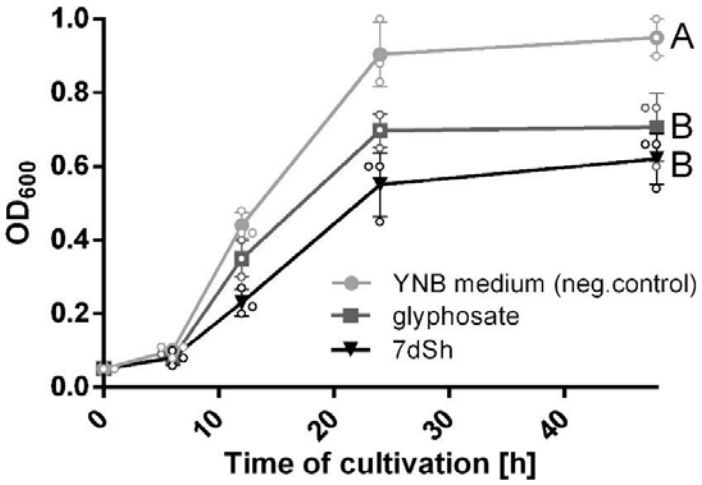

Supplementary Figure 7: Comparison of effects of 7dSh and glyphosate on *S. cerevisiae* grown in minimal medium.

S. cerevisiae was grown in YNB minimal medium in the presence of glyphosate (100 µg mL^{-1}, ca. 590 µM) or 7dSh (**1**) (10 µg mL^{-1}, ca. 50 µM) for 48 h (initial OD_{600} = 0.05). Statistical analysis was performed by using a one-way ANOVA. Tukey's multiple comparison test was used as a post-hoc test to figure out the differences between OD_{600} at timepoint 48h. Means that were significantly different ($p<0.05$) are marked with different capital letters in the diagram. Optical density values represent the mean values of three biological replicates; standard deviations are indicated. Dots indicate data distribution. Source data are provided as a Source Data file.

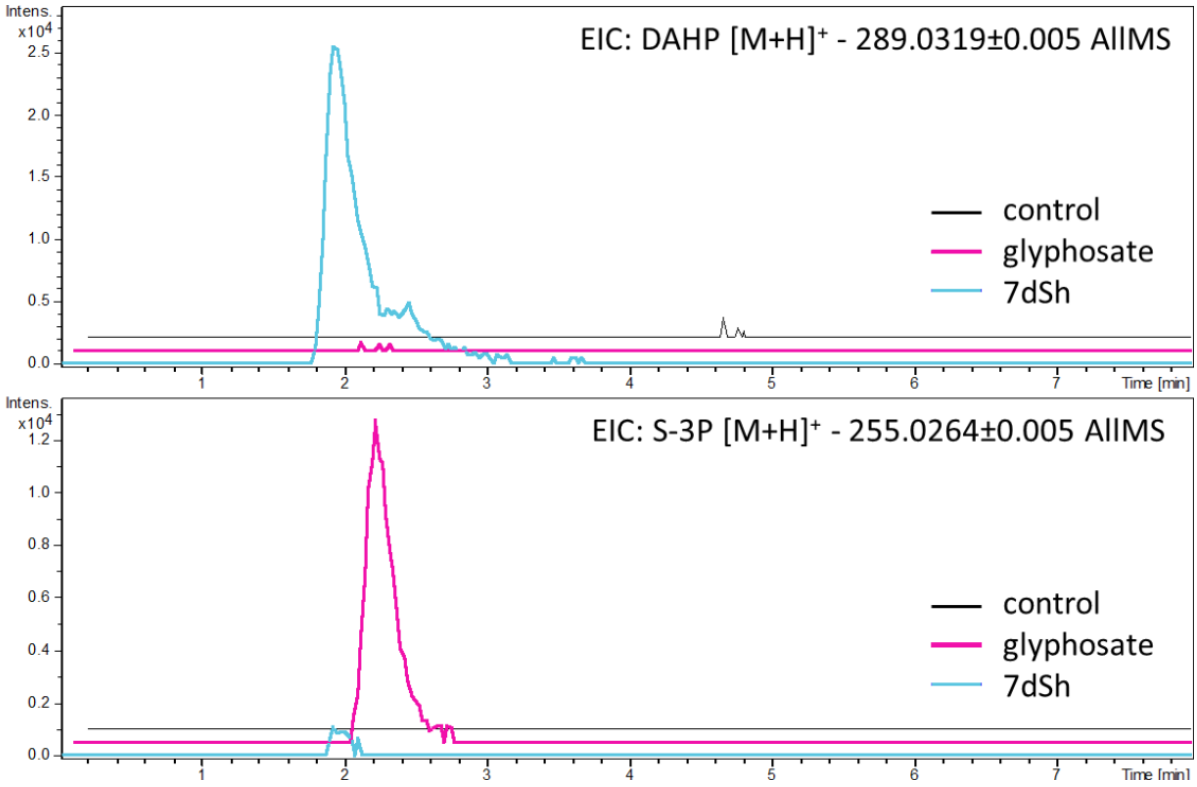

Supplementary Figure 8: LC-HRMS chromatograms show accumulation of shikimate pathway intermediates in *A. thaliana* seedlings treated with 7dSh or glyphosate.

A. thaliana seedlings were grown in presence or absence of 7dSh (**1**) or glyphosate (each 260 µM) for 7 days. The whole plant extracts of 10 seedlings were analyzed by LC-HRMS for the shunt products DAHP (**4**) and shikimate-3-phosphate (S-3P); shown are the stacked EIC chromatograms in positive mode (control in black, shikimate in magenta, 7dSh in turquoise).

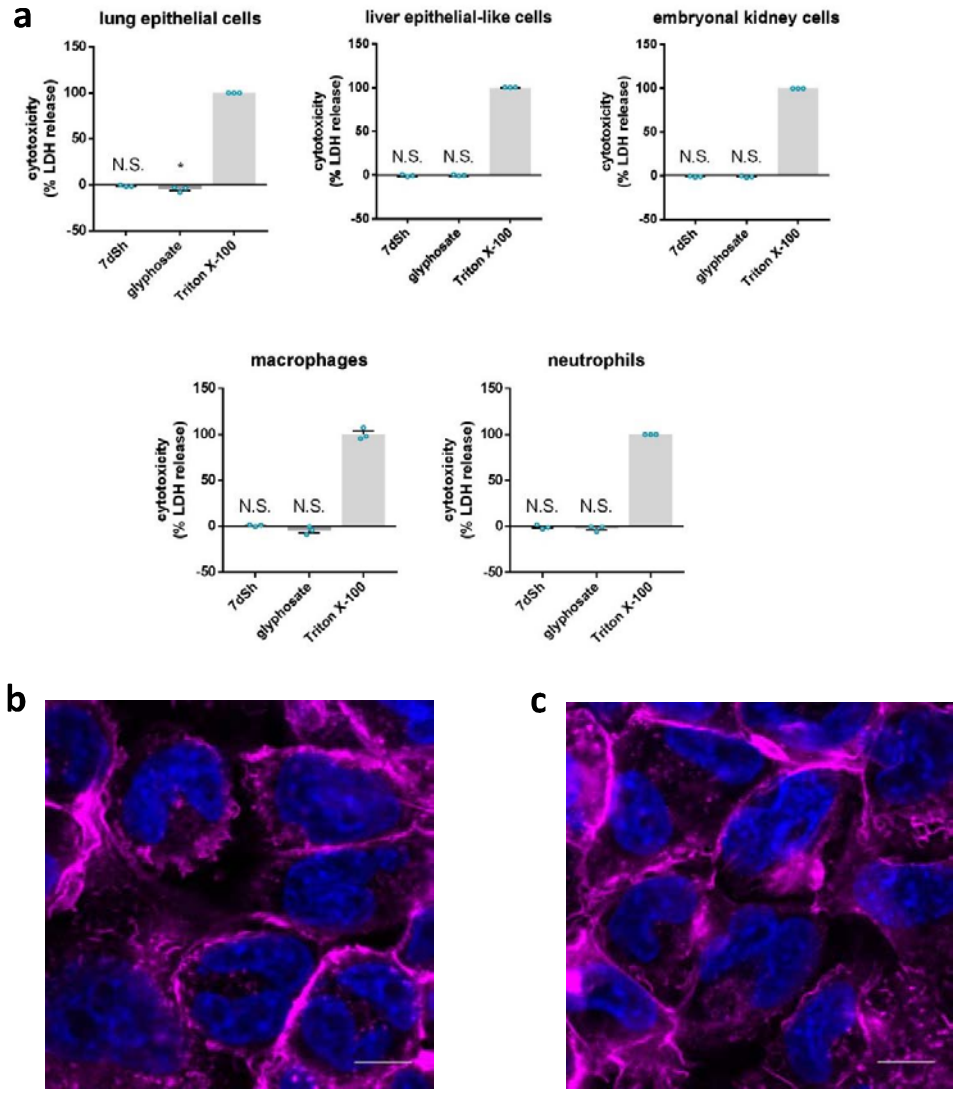

Supplementary Figure 9: Cytotoxic potential of 7dSh and glyphosate on human cell lines and primary cells.

(**a**) Effect of 7dSh (**1**) (970 µg mL^{-1}, 5 mM) and glyphosate (845 µg mL^{-1}, 5 mM) on human cell lines and primary cells. Cells were incubated in respective medium with 7dSh or glyphosate. After 24 h (5 h for neutrophils), cytotoxicity was measured according to the release of lactate dehydrogenase and compared to untreated control. The data represent the mean of three independent experiments; standard deviations are indicated. Dots indicate data distribution. Significant differences between 7dSh/glyphosate treatment and untreated control cells were analysed in a one-way ANOVA and a following Tukey's multiple comparisons test (*p-value < 0.05; ** p-value < 0.01; *** p-value < 0.001; N.S., not significant). Source data are provided as a Source Data file. (**b,c**) Cell morphology of untreated human THP1 macrophages (**b**) and those treated with 5 mM 7dSh (**c**) for 24 h. Cells were stained with phalloidin (pink: actin filaments) and DAPI (blue: DNA). Scales bars, 10 µm.

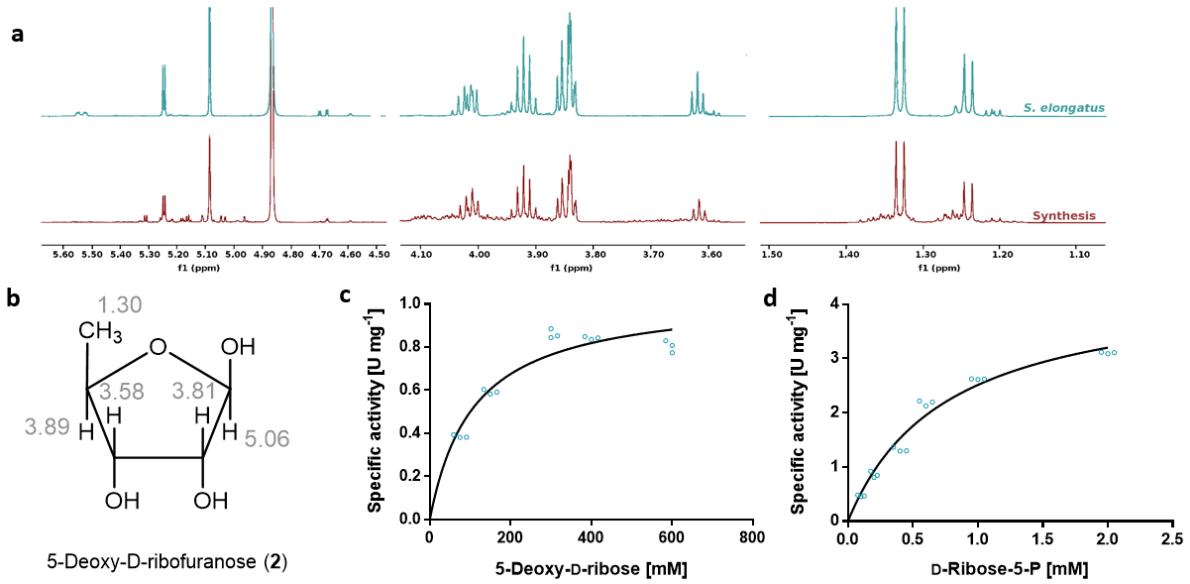

Supplementary Figure 10: ^{1}H NMR analysis of 5-deoxy-D-ribose and enzyme kinetics of the *S. elongatus* transketolase.

a) ^{1}H NMR spectra of 5-deoxy-D-ribose (**2**) (CD_3OD, 600 MHz) purified by chromatography from *S. elongatus* (turquoise) and from chemical synthesis (Glentham Life Sciences) as a control (red). (**b**) Chemical structure of 5-deoxy-D-ribofuranose (**2**) with given assignments (chemical shifts in ppm, gray). (**c**) Michaelis–Menten kinetic profile of the conversion of 5-deoxy-D-ribose by the *S. elongatus* transketolase (K_m = 108.3 mM ± 20.6; V_{max} = 1.04 U mg^{-1} ± 0.06). (**d**) Michaelis–Menten kinetic profile of the conversion of D-ribose 5-phosphate by the *S. elongatus* transketolase (K_m = 0.75 mM ± 0.09; V_{max} = 4.41 U mg^{-1} ± 0.23). Dots in (**c**) and (**d**) represent data distribution of three replicates. Source data are provided as a Source Data file.

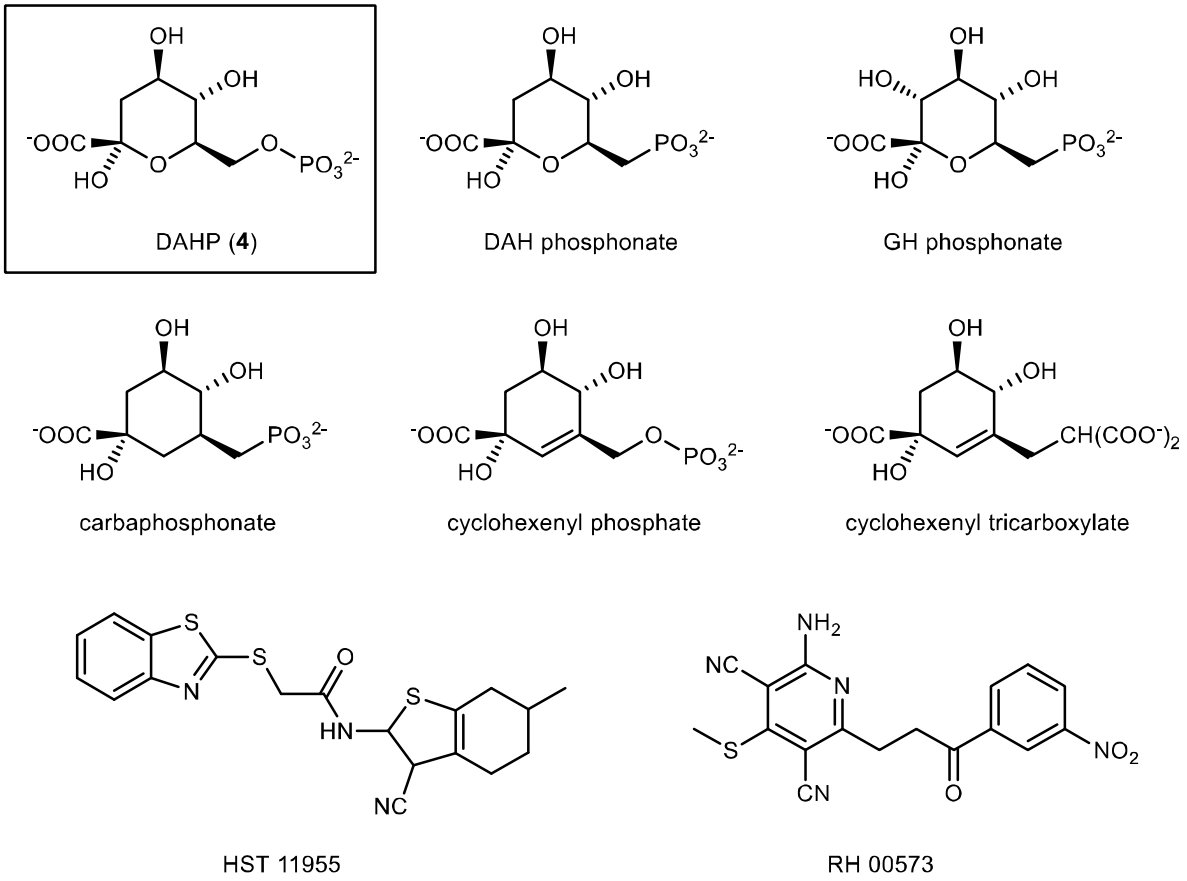

Supplementary Figure 11: Chemical structure of selected known DHQ synthase inhibitors.
The natural 3-dehydroquinate (DHQ) synthase substrate DAHP (**4**) is depicted in the box. DAH phosphonate (3-deoxy-D-*arabino*-heptulosonate 7-phosphonate) and GH phosphonate (D-*gluco*-heptulosonate 7-phosphonate) are phosphonate analogues of DAHP. Carbaphosphonate and its cyclohexenyl derivatives are all substrate analogues of DAHP.

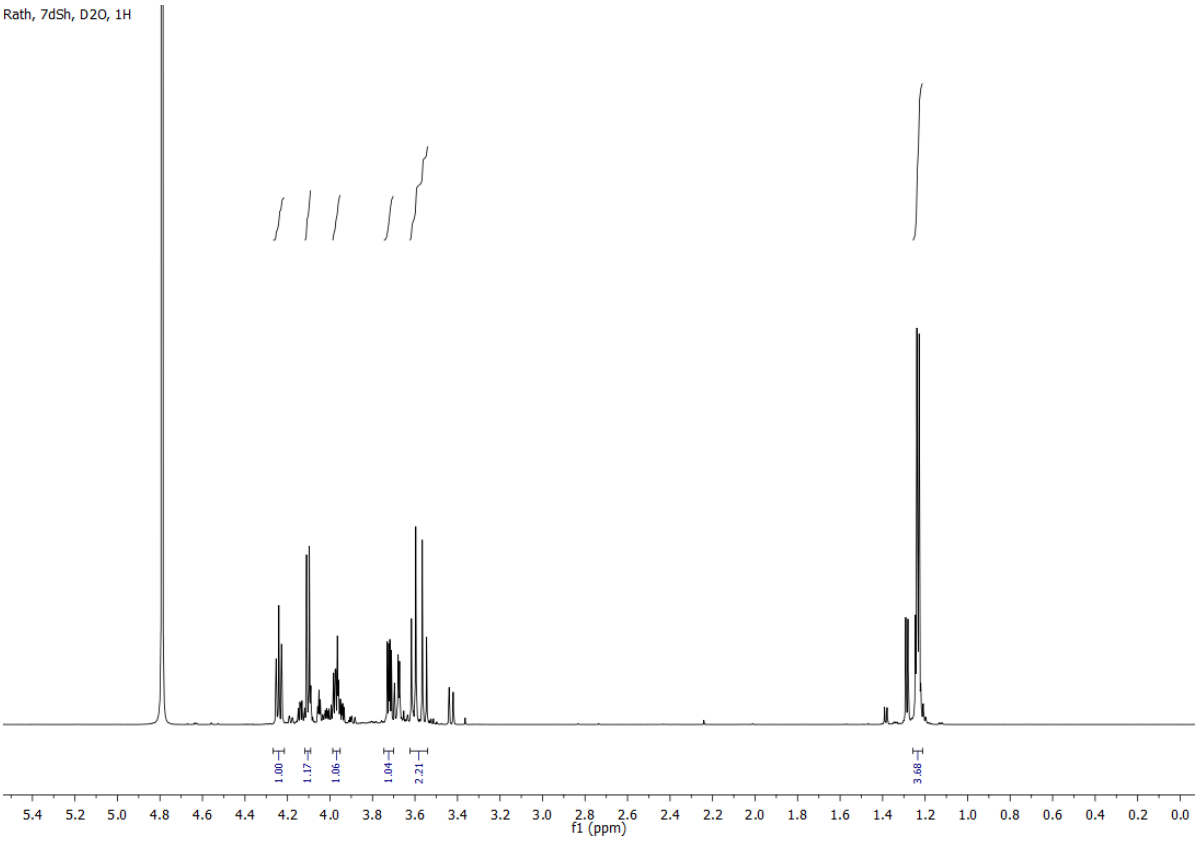

Supplementary Figure 12: ^{1}H NMR spectrum of 7-deoxy-sedoheptulose (7dSh, 1).
D_2O, 298 K, 600 MHz.

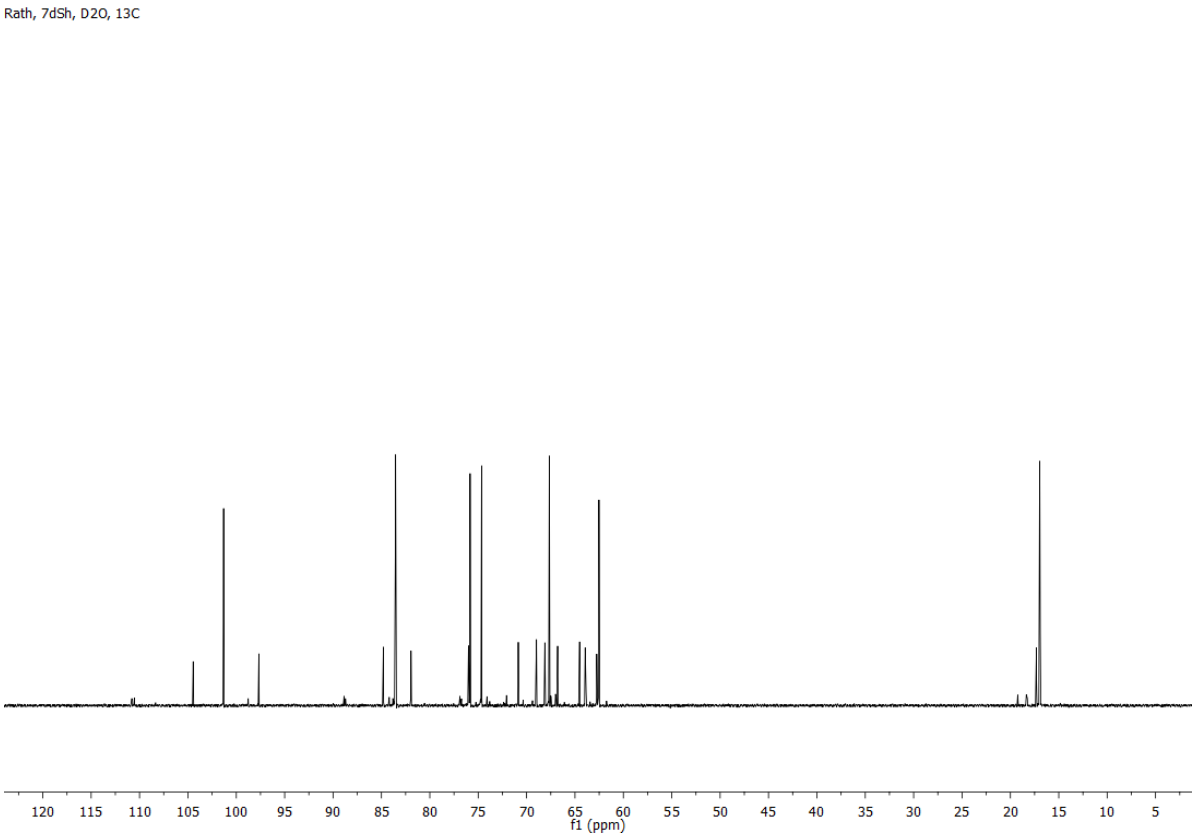

Supplementary Figure 13: ^{13}C NMR spectrum of 7-deoxy-sedoheptulose (7dSh, 1).
D_2O, 298 K, 150.9 MHz.

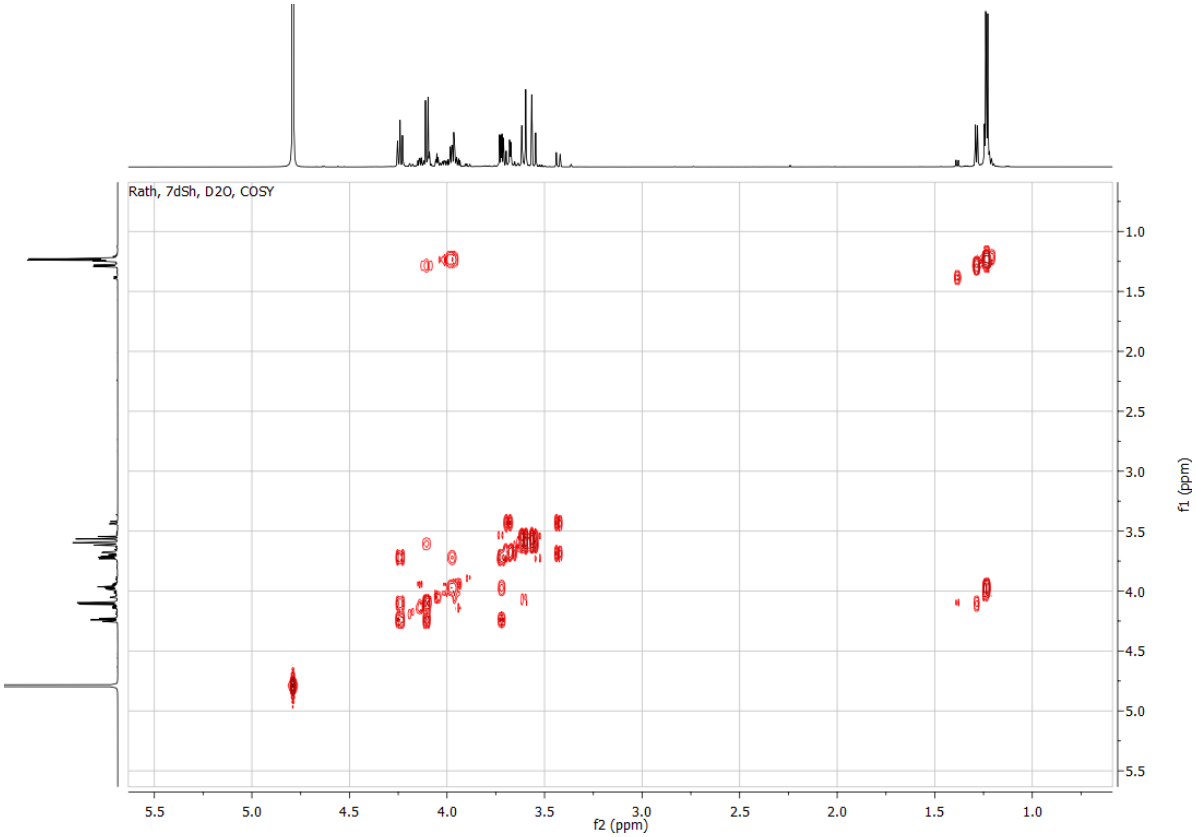

Supplementary Figure 14: H-H-correlation (COSY) spectrum of 7-deoxy-sedoheptulose (7dSh, 1). D_2O, 298 K, 600 MHz.

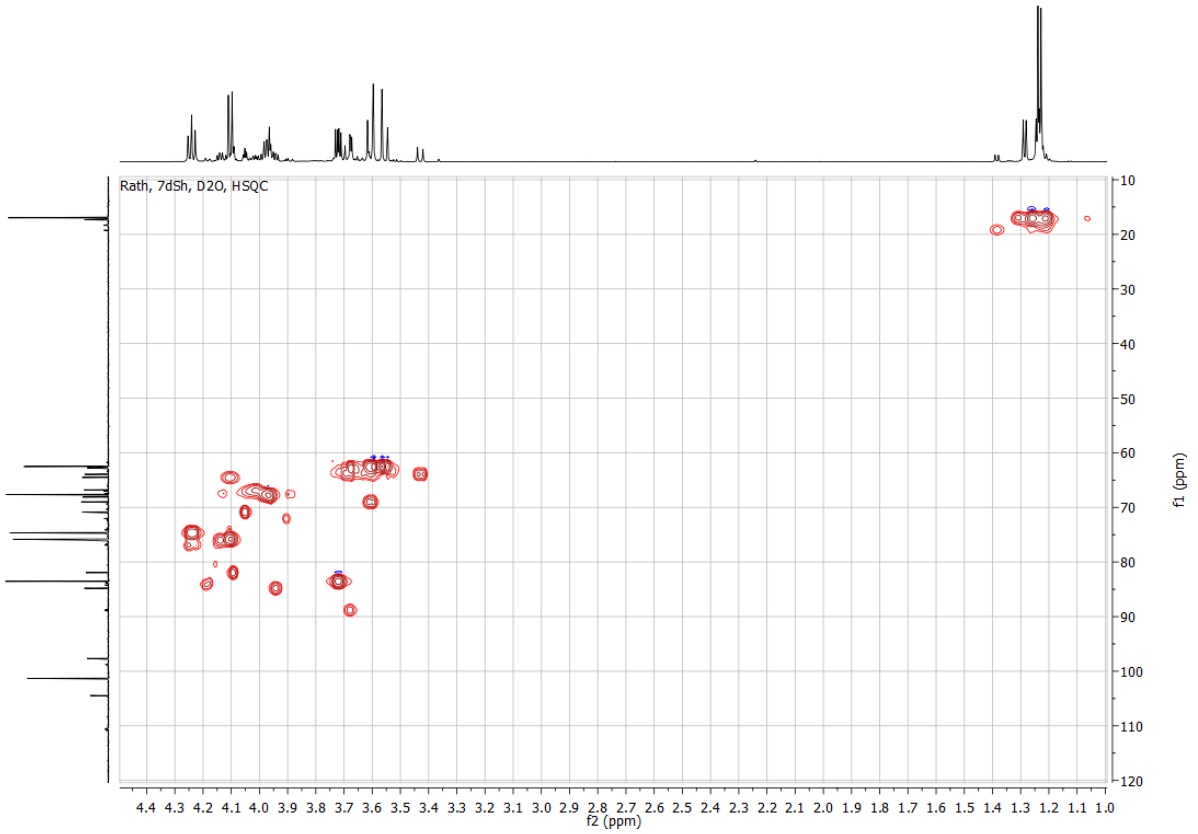

Supplementary Figure 15: CH-correlation (HSQC) spectrum of 7-deoxy-sedoheptulose (7dSh, 1). D_2O, 298 K, 600 MHz (150.9 MHz).

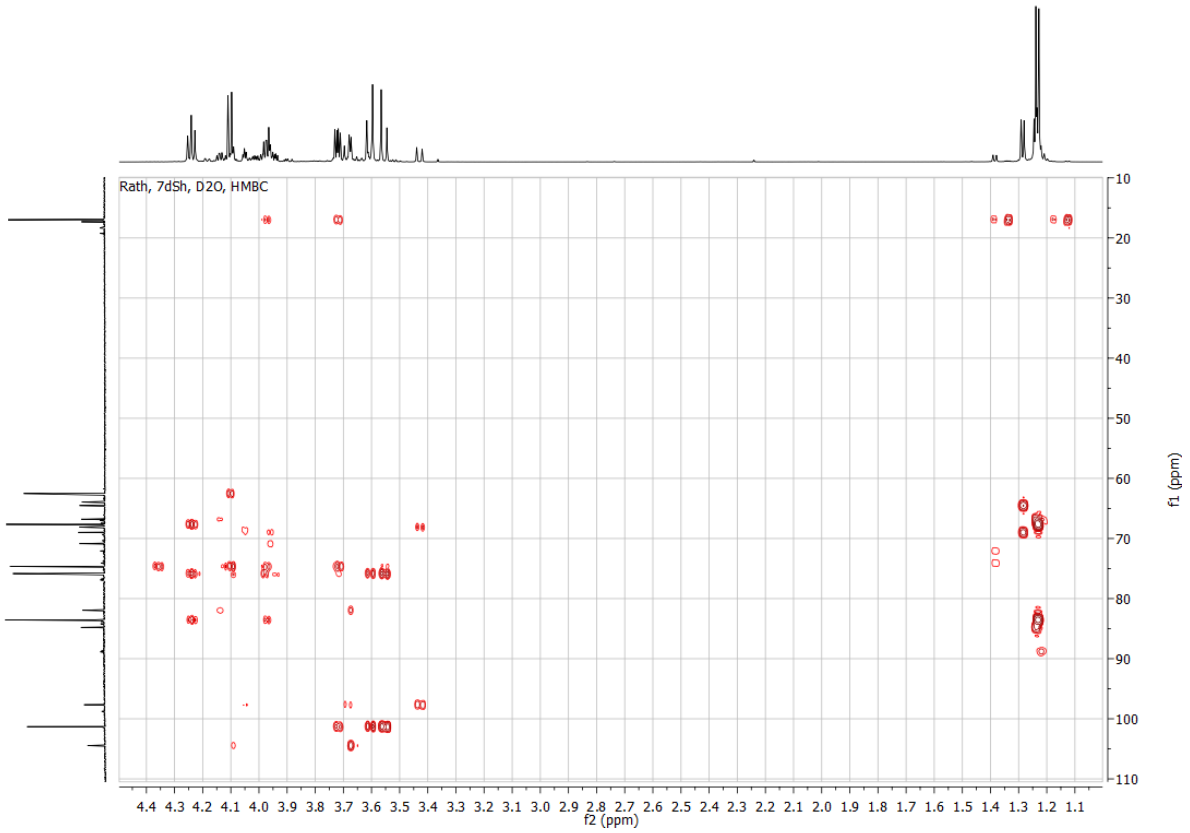

Supplementary Figure 16: Multiple bond CH-correlation (HMBC) spectrum of 7-deoxy-sedoheptulose (7dSh, 1).
D_2O, 298 K, 600 MHz (150.9 MHz).

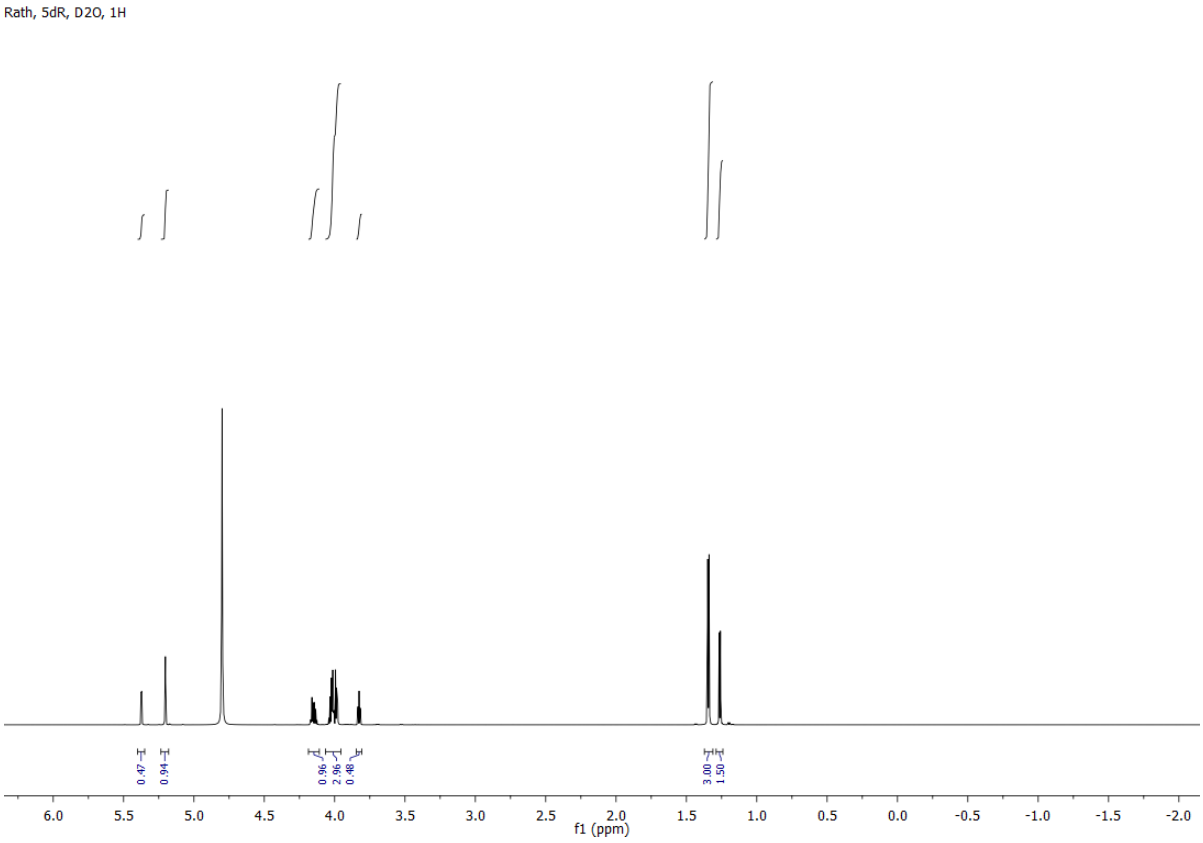

Supplementary Figure 17: ^{1}H NMR spectrum of 5-deoxy-D-ribose (2).
D_2O, 298 K, 700 MHz.

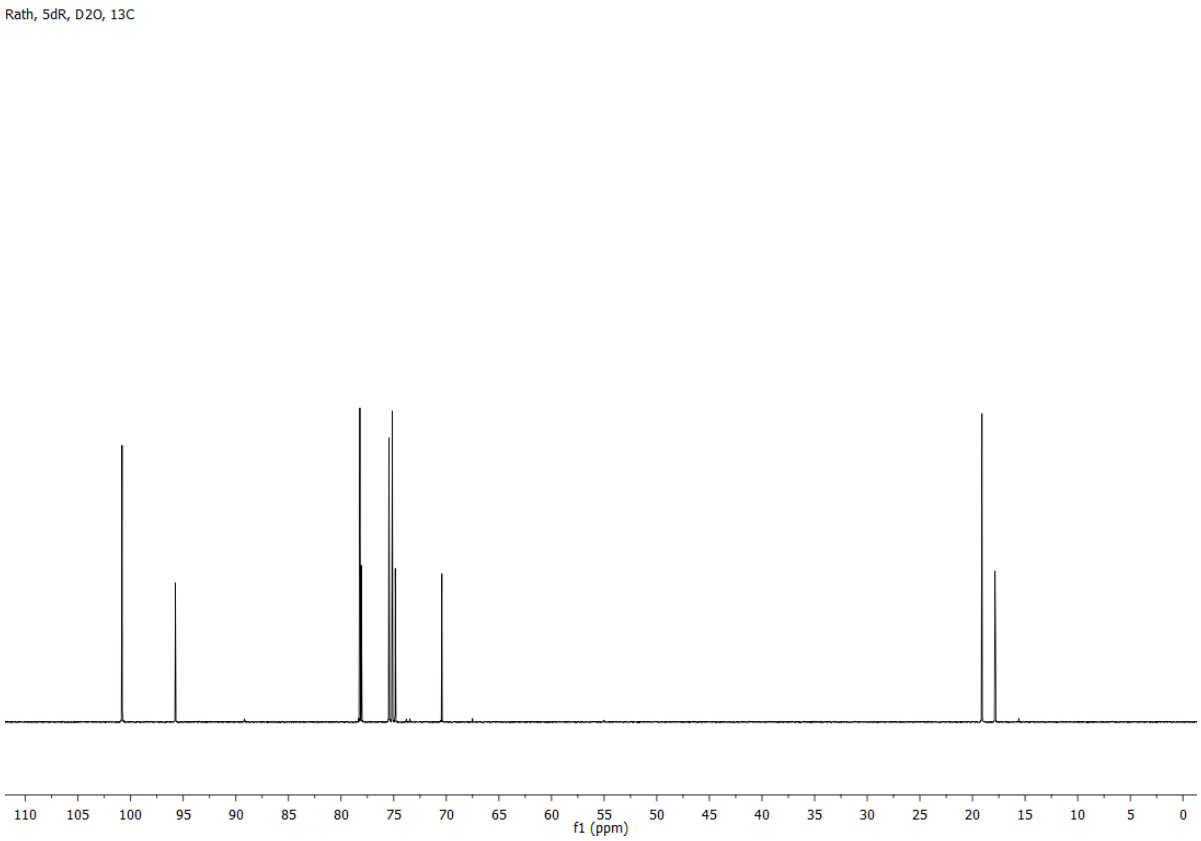

Supplementary Figure 18: ^{13}C NMR spectrum of 5-deoxy-D-ribose (2).
D_2O, 298 K, 176.1 MHz.

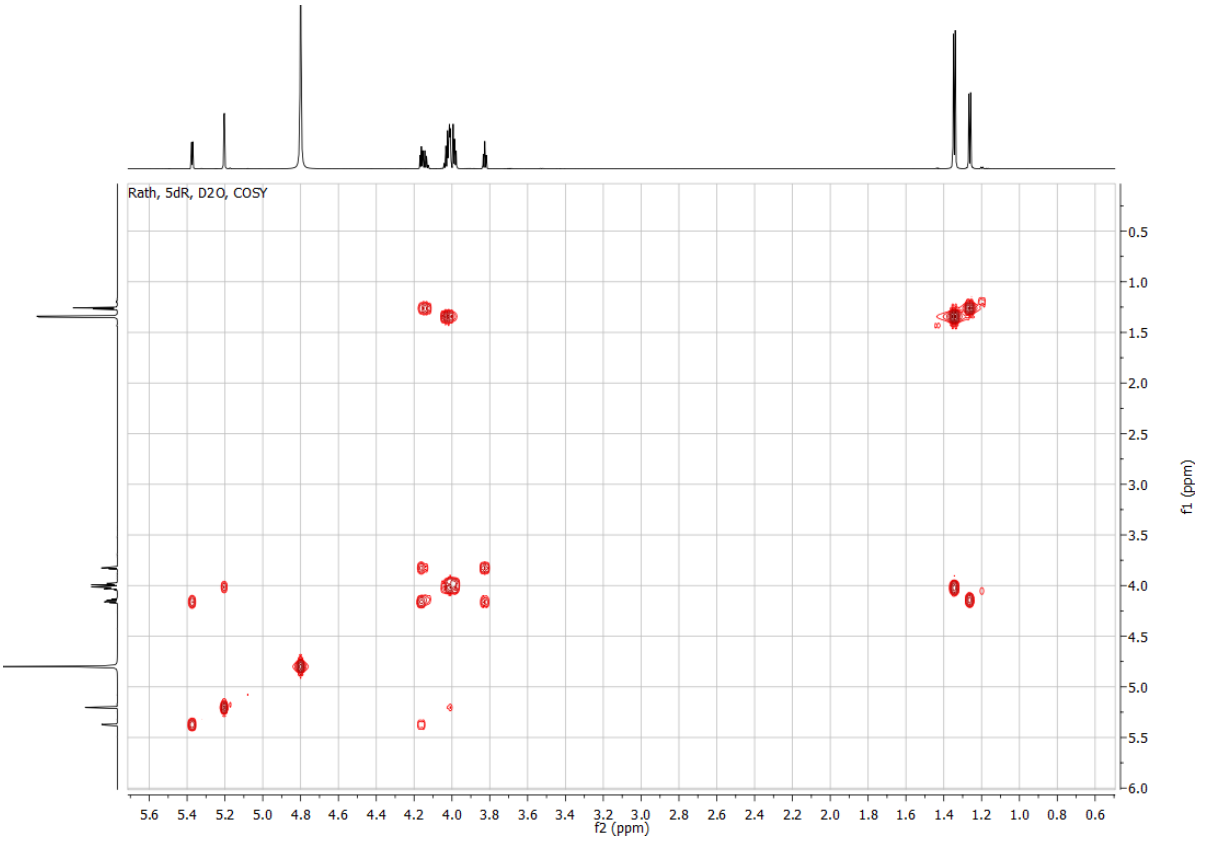

Supplementary Figure 19: H-H-correlation (COSY) spectrum of 5-deoxy-D-ribose (2).
D_2O, 298 K, 700 MHz.

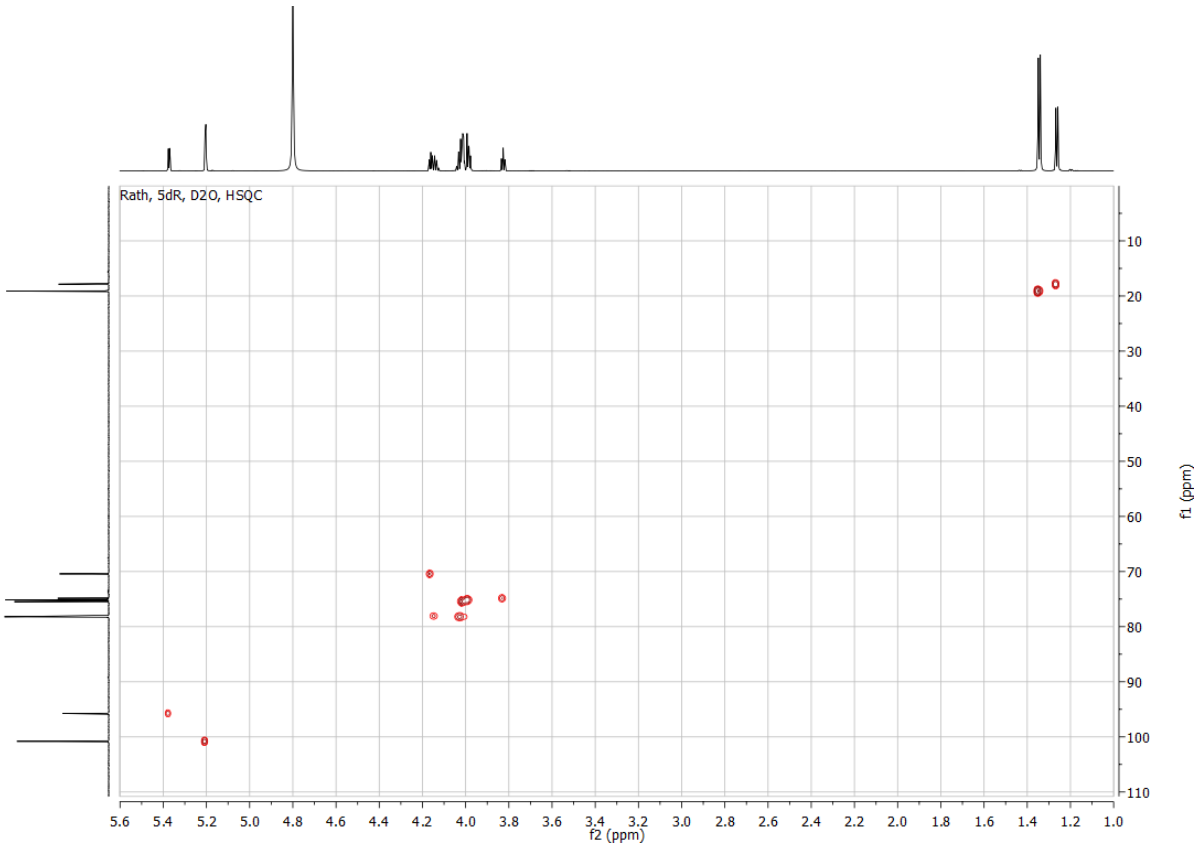

Supplementary Figure 20: CH-correlation (HSQC) spectrum of 5-deoxy-D-ribose (2).
D_2O, 298 K, 700 MHz (176.1 MHz).

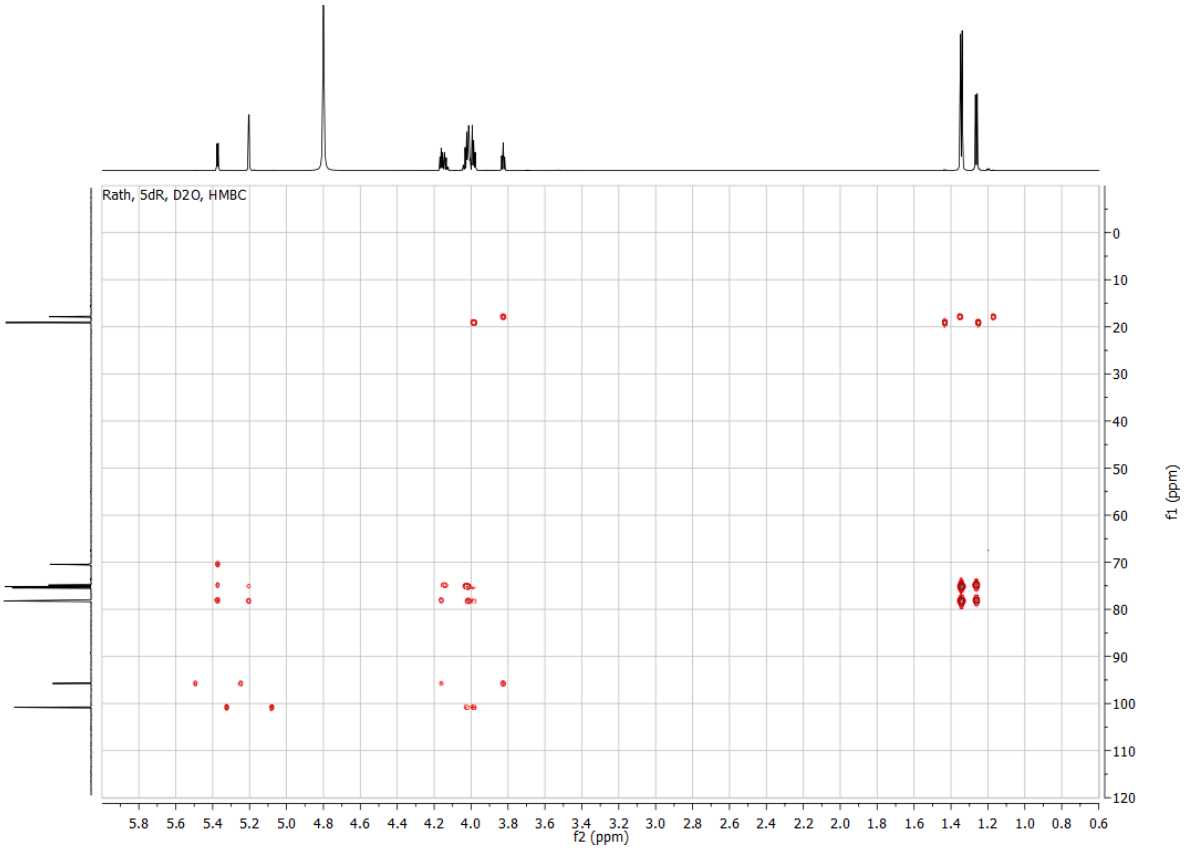

Supplementary Figure 21*:* Multiple bond CH-correlation (HMBC) spectrum of 5-deoxy-D-ribose (2). D_2O, 298 K, 700 MHz (176.1 MHz).

Supplementary References:

1. Carpenter EP, Hawkins AR, Frost JW, Brown KA. Structure of dehydroquinate synthase reveals an active site capable of multistep catalysis. *Nature* **394**, 299-302 (1998).

Publication 2:

Rapp, Johanna; Rath, Pascal; Kilian, Joachim; Brilisauer, Klaus; Grond, Stephanie; Forchhammer, Karl (2021): A bioactive molecule made by unusual salvage of radical SAM enzyme by-product 5-deoxyadenosine blurs the boundary of primary and secondary metabolism. *Journal of Biological Chemistry*, 296 (100621), https://doi.org/10.1016/j.jbc.2021.100621, © The Authors.

Corrigendum:

Experimental procedures - Quantification of metabolites in the culture supernatant via GC–MS: “The mass spectrometer was operated in ~~exposure index~~ mode.” “The mass spectrometer was operated in electron ionization mode.”

JBC RESEARCH ARTICLE

A bioactive molecule made by unusual salvage of radical SAM enzyme byproduct 5-deoxyadenosine blurs the boundary of primary and secondary metabolism

Received for publication, January 29, 2021, and in revised form, March 25, 2021 Published, Papers in Press, March 31, 2021,
https://doi.org/10.1016/j.jbc.2021.100621

Johanna Rapp[1], **Pascal Rath**[2], **Joachim Kilian**[3], **Klaus Brilisauer**[1], **Stephanie Grond**[2], **and Karl Forchhammer**[1,*]

From the [1]*Interfaculty Institute of Microbiology and Infection Medicine, Microbiology/Organismic Interactions,* [2]*Institute of Organic Chemistry, and* [3]*Center for Plant Molecular Biology, Eberhard Karls Universität Tübingen, Tübingen, Germany*

Edited by Chris Whitfield

5-Deoxyadenosine (5dAdo) is the byproduct of many radical *S*-adenosyl-L-methionine enzyme reactions in all domains of life. 5dAdo is also an inhibitor of the radical *S*-adenosyl-L-methionine enzymes themselves, making it necessary for cells to construct pathways to recycle or dispose of this toxic metabolite. However, the specific pathways involved have long remained unexplored. Recent research demonstrated a growth advantage in certain organisms by using 5dAdo or intermediates as a sole carbon source and elucidated the corresponding salvage pathway. We now provide evidence using supernatant analysis by GC–MS for another 5dAdo recycling route. Specifically, in the unicellular cyanobacterium *Synechococcus elongatus* PCC 7942 (*S. elongatus*), the activity of promiscuous enzymes leads to the synthesis and excretion first of 5-deoxyribose and subsequently of 7-deoxysedoheptulose. 7-Deoxysedoheptulose is an unusual deoxy-sugar, which acts as an antimetabolite of the shikimate pathway, thereby exhibiting antimicrobial and herbicidal activity. This strategy enables organisms with small genomes and lacking canonical gene clusters for the synthesis of secondary metabolites, like *S. elongatus*, to produce antimicrobial compounds from primary metabolism and enzymatic promiscuity. Our findings challenge the view of bioactive molecules as sole products of secondary metabolite gene clusters and expand the range of compounds that microorganisms can deploy to compete for their ecological niche.

S-Adenosyl-L-methionine (SAM; AdoMet), which is formed by ATP and the amino acid methionine, is an essential cofactor of various enzymatic reactions in all domains of life. SAM can serve as a methyl group donor for the methylation of DNA, RNA, and proteins in reactions that release *S*-adenosylhomocysteine (SAH) as a byproduct (1). SAM can also serve as an aminopropyl donor for polyamine synthesis and as a homoserine lactone donor for the synthesis of quorum-sensing compound *N*-acetylhomoserine lactone, both of which result in the release of 5-methylthioadenosine (MTA). Furthermore, SAM is a source of the 5-deoxyadenosylradical (5dAdo$^{\bullet}$), which is formed by the activity of radical SAM enzymes (1–5). 5dAdo$^{\bullet}$ is formed by the reductive cleavage of SAM and can abstract a hydrogen atom from its substrate to form a substrate radical as well as 5-deoxyadenosine (5dAdo), which is released as a byproduct (3, 6). Radical SAM enzymes, a superfamily with over 100,000 members, are present in all domains of life (2, 7). They are catalyzing various complex chemical reactions, including sulfur insertion, anaerobic oxidations, unusual methylations, and ring formations (8). Prominent members are, for example, involved in biotin, thiamine, and lipoate biosynthesis. Other members are involved in DNA repair or in the biosynthesis of secondary metabolites, for example, antibiotics (3). MTA, SAH, and 5dAdo are product inhibitors of these reactions (8–12). Therefore, and because of the high bioenergetic costs of these compounds, salvage pathways are necessary. SAH is rescued *via* the methionine cycle (13). MTA salvage *via* the methionine salvage pathway (MSP) is also well characterized (14, 15) (Fig. 1*B*). In the classical and aerobic MSP, MTA is either processed by a two-step reaction by the MTA nucleosidase (MtnN), followed by a phosphorylation by the methylthioribose (MTR) kinase or by the MTA phosphorylase (MtnP). The subsequent reactions consist of a dehydration (MtnB, methylthioribose-1-phosphate [MTR-1P] dehydratase), enolization and phosphorylation (either by MtnC: DK-MTP-1P enolase/phosphatase or by MtnW: DK-MTP-1P enolase and MtnX: HK-MTPene-1P phosphatase; DK-MTP-1P: 2,3-diketo-5-methylthiopentyl-1-phosphate, HK-MTPene-1P: 2-hydroxy-3-keto-5-methylthiopentenyl-1-phosphate), deoxygenation (MtnD: acireductone dioxygenase), and a final transamination step (MtnE: aminotransferase).

Despite the high abundance of radical SAM enzymes and thereby of 5dAdo, less is known about 5dAdo salvage. *In vitro* experiments showed that 5dAdo can be processed by a two-step reaction, in which 5dAdo is cleaved by promiscuous MtnN resulting in the release of adenine and 5-deoxyribose (5dR) (9, 10). The subsequent phosphorylation of 5dR by MTR kinase results in the formation of 5-deoxyribose 1-phosphate (5dR-1P). The second option is the direct conversion of 5dAdo into 5dR-1P and adenine *via* promiscuous MtnP

* For correspondence: Karl Forchhammer, karl.forchhammer@uni-tuebingen.de.

Bioactive compound formation by 5-deoxyadenosine salvage

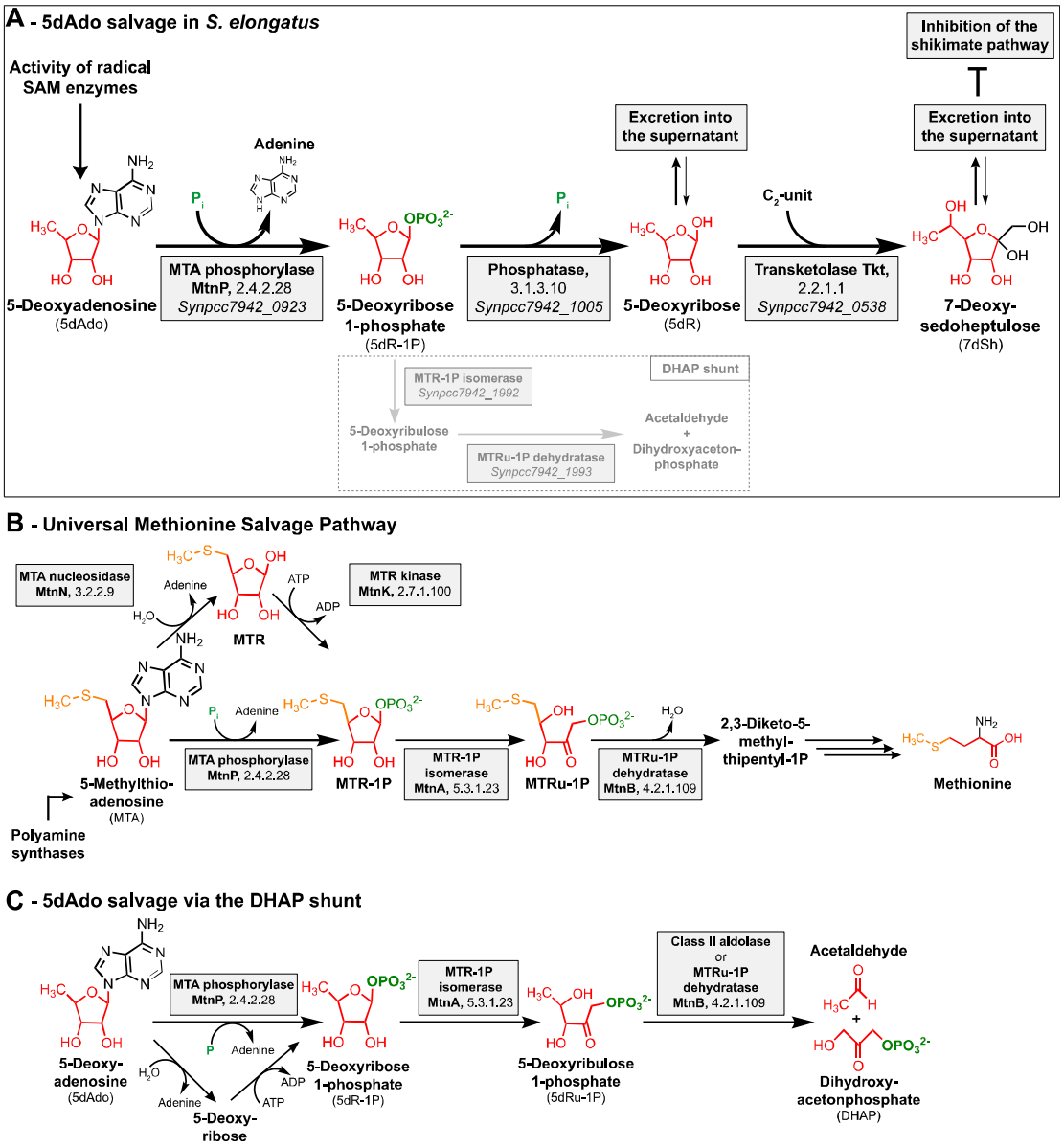

Figure 1. Overview of the 5dAdo and MTA salvage pathways. *A*, 5dAdo salvage in *Synechococcus elongatus via* the excretion of the bioactive deoxy-sugars 5dR and 7dSh (this study). 5dR-1P is partially also metabolized *via* the DHAP shunt (shown by *dashed line*), especially under low carbon conditions. *B*, universal methionine salvage pathway (16). *C*, 5dAdo salvage *via* the DHAP shunt (13, 19). MTA, 5-methylthioadenosine; MTR, methylthioribose; MTRu-1P, methylthioribulose-1P; SAM, *S*-adenosyl-L-methionine.

(16). Therefore, it is suggested that 5dAdo salvage is paralogous to the MSP and is driven by the promiscuous activity of the enzymes of the MSP (17). Recently, a pathway for 5dR salvage was elucidated in *Bacillus thuringiensis* involving the sequential activity of a kinase, an isomerase, and a class II aldolase, which are encoded by a specific gene cluster (18). The authors propose that 5dR is phosphorylated to 5dR-1P, which is then isomerized into 5-deoxyribulose 1-phosphate (5dRu-1P) and subsequently cleaved by an aldolase into acetaldehyde and dihydroxyacetone phosphate (DHAP) for primary metabolism. In organisms that lack the specific gene cluster, the cleavage of 5dAdo into DHAP and acetaldehyde is proposed to occur *via* the promiscuous activity of enzymes of the MSP. In support of this hypothesis, it was shown that *Arabidopsis thaliana* DEP1, an MTR-1P dehydratase of the MSP, is promiscuous and can also cleave 5dRu-1P into DHAP and

acetaldehyde, suggesting that a specific aldolase is not required for 5dAdo salvage (18). In agreement with this, the promiscuous activity of MSP enzymes in the 5dAdo salvage was recently reported in *Methanocaldococcus jannaschii* (*M. jannaschii*), where methylthioribose 1-phosphate isomerase uses MTR-1P, 5dR-1P, and 5dR as substrates (19). Only recently, 5dAdo was shown to be processed to DHAP and acetaldehyde by a gene cluster consisting of the first enzymes of the MSP as well as a class II aldolase in *Rhodospirillum rubrum* and pathogenic *Escherichia coli* strains, in a process termed "DHAP shunt" (13) (Fig. 1*C*).

In our previous work, we isolated the rare deoxy-sugar—namely, 7-deoxysedoheptulose (7-deoxy-D-*altro*-2-heptulose, 7-deoxy-sedoheptulose [7dSh])—from the supernatant of the unicellular cyanobacterium *Synechococcus elongatus* PCC 7942 (*S. elongatus*) (20). This compound showed bioactivity toward various prototrophic organisms, for example, other cyanobacteria, especially *Anabaena variabilis* American Type Culture Collection (ATCC) 29413 (*A. variabilis*), *Saccharomyces*, and *Arabidopsis*. It blocks the shikimate pathway presumably by inhibiting the enzyme dehydroquinate synthase (20). Because of the streamlined genome of *S. elongatus* and the lack of specific gene clusters for secondary metabolite synthesis (21, 22), the pathway for 7dSh formation remained enigmatic. Of note, 7dSh was also isolated from the supernatant of *Streptomyces setonensis* (20, 23), but the synthesis pathway remained unresolved. Therefore, we speculated that 7dSh synthesis might involve promiscuous enzymes of primary metabolism. Enzyme promiscuity, the ability of an enzyme to use various substrates, is especially important for organisms with a small genome. Previously, it was described that the marine cyanobacterium *Prochlorococcus* uses a single promiscuous enzyme that can transform up to 29 different ribosomally synthesized peptides into an arsenal of polycyclic bioactive products (24). As from the 7dSh-containing supernatant of *S. elongatus*, we in addition isolated the deoxy-sugar 5dR. We hypothesized that 5dR could serve as a precursor molecule of 7dSh (20). *In vitro*, 5dR can serve as a substrate for a transketolase-based reaction, in which a C_2 unit is transferred to the C_5 unit leading to the formation of 7dSh (20).

In this work, we identified the pathway for 7dSh biosynthesis, which involves a new salvage route for 5dAdo resulting in the release of 5dR and 7dSh into the culture medium (Fig. 1*A*). Therefore, *S. elongatus* can synthesize a bioactive compound from the products of the primary metabolism simply by using promiscuous enzymes.

Results

5dR and 7dSh accumulation in supernatants of S. elongatus *is strongly promoted by CO_2 supplementation*

Previously, we estimated the content of 7dSh in the supernatant of *S. elongatus* cultures *via* a bioassay based on the size of the inhibition zone of *A. variabilis* exposed to the supernatant of *S. elongatus* (20). To quantify the amounts of 5dR and 7dSh formed by *S. elongatus*, we developed a GC–MS–based method that enables the detection and absolute quantification of low micromolar concentrations of these metabolites in the culture supernatant. In cultures supplemented with 2% CO_2 (Fig. 2, *black dots*), 5dR gradually accumulated during growth (Fig. 2, *A* and *B*), whereas 7dSh accumulation only occurred during a later growth phase (Fig. 2*C*). After 30 days of cultivation, the supernatant contained four times more 5dR than 7dSh. Under ambient air conditions (Fig. 2, *gray squares*), small amounts of 5dR were formed, whereas 7dSh could not be detected (Fig. 2, *B* and *C*), despite that the optical density of the air-supplied cultures in the final stage of the experiment reached values similar to those of the CO_2-supplemented cultures, where 7dSh accumulation could be detected (Fig. 2*A*). This suggests that the formation of the deoxy-sugars is not only growth phase dependent but also related to a specific metabolic state.

To gain further insights into 5dR/7dSh metabolism, we measured the intracellular concentration of 5dR and 7dSh over the whole cultivation process. Surprisingly, only small intracellular amounts, close to detection limit of either deoxy-sugar, could be detected (Fig. S1), whereas the extracellular concentration gradually increased. This strongly suggests that extracellular 5dR/7dSh accumulation is not because of cell lysis but involves immediate secretion after their formation. Removal of these metabolites from the cytoplasm is probably essential for *S. elongatus* as both molecules showed growth

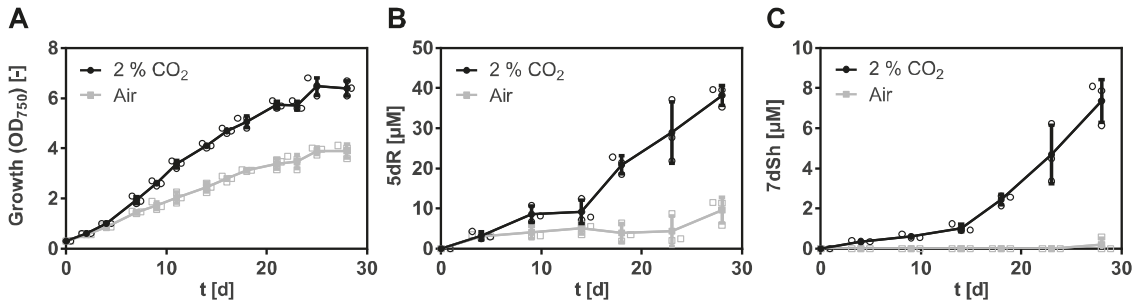

Figure 2. 5-Deoxyribose (5dR) and 7-deoxysedoheptulose (7dSh) accumulation in the supernatant of *Synechococcus elongatus* is strongly promoted by high CO_2 concentrations. *S. elongatus* cultures aerated either with ambient air (*gray squares*) or with air supplemented with 2% CO_2 (*black dots*). *A*, over time, growth of *S. elongatus* (indicated by an absorbance at 750 nm). Over time, concentration of 5dR (*B*) or 7dSh (*C*) in the supernatant of *S. elongatus* cultures. Note the different values of the *y*-axis. Data shown represent mean and standard deviation of three independent biological replicates.

inhibition toward the producer strain at elevated concentrations (Fig. 3). 7dSh is bactericidal at concentrations of 100 μM, whereas 5dR is bacteriostatic at concentrations of 250 μM.

5dR is a precursor molecule for 7dSh biosynthesis in vivo

In our previous work, we reported the *in vitro* synthesis of 7dSh by converting 5dR into 7dSh by a transketolase-based reaction with hydroxypyruvate as a C_2 unit donor (20). To determine whether 5dR might also be a precursor molecule for 7dSh *in vivo*, a 5dR-feeding experiment was performed (Fig. 4). To unambiguously distinguish the naturally formed and the supplemented 5dR, uniformly labeled [U-$^{13}C_5$]-5dR ($^{13}C_5$-5dR) was synthesized and added at a final concentration of 20 μM to *S. elongatus* cultures at the beginning of the cultivation. The concentration of labeled (Fig. 4, *B* and *C*), unlabeled, (Fig. 4, *D* and *E*), and the total amount of 5dR and 7dSh (Fig. 4, *F* and *G*) was determined by GC–MS at different time points over a period of 30 days.

Neither the growth of *S. elongatus* nor the excretion of unlabeled and intracellular synthesized 5dR and 7dSh was affected by the addition of exogenous $^{13}C_5$-5dR (Fig. 4, *A*, *D*, and E). We found that $^{13}C_5$-5dR is taken up by the cultures as its concentration in the supernatant continuously decreased (Fig. 4*B*, *gray squares*). Already within 2 days, $^{13}C_5$-7dSh could be detected in the supernatant of these cultures (Fig. 4*C*, *gray squares*), clearly proving that $^{13}C_5$-7dSh was formed from the precursor molecule $^{13}C_5$-5dR. However, only a small amount of exogenously added $^{13}C_5$-5dR was converted into 7dSh. At the end of the experiment, 10% of the initially applied $^{13}C_5$-5dR (20 μM) was converted into $^{13}C_5$-7dSh (~2 μM). Around 30% of $^{13}C_5$-5dR remained in the supernatant (6.5 μM). The residual amount is assumed to be metabolized *via* (an)other pathway(s). Because unlabeled 5dR was excreted at the same time as $^{13}C_5$-5dR was taken up (Fig. 4, *B* and *D*), 5dR must be imported and exported in parallel.

5dAdo as a precursor molecule of 7dSh

Next, we asked the question where 5dR is derived from. This drew our attention to 5dAdo, a byproduct of radical SAM enzymes (3). The compound has to be removed because of its intracellular toxicity (9), and its cleavage can result in the formation of 5dR (9, 18) (Fig. 1*C*). To prove that 7dSh is formed from 5dAdo salvage in *S. elongatus*, 5dAdo-feeding experiments were performed, and the supernatants were analyzed by GC–MS (Fig. 5). Notably, the growth of *S. elongatus* was not affected by supplementation with 5dAdo, which was taken up very quickly (Fig. 5, *A* and *B*). After 4 days, almost all 5dAdo was taken up. A control experiment showed that the rapid decline in the amount of 5dAdo in the supernatant was not caused by the instability of 5dAdo in the medium. Feeding of the cells with 5dAdo immediately led to an enhanced accumulation of 5dR in the culture supernatant (Fig. 5*C*). After 14 days, 7dSh levels in 5dAdo-supplemented cultures were clearly enhanced compared with control cultures (Fig. 5*D*), supporting our hypothesis that 5dAdo is a precursor molecule of 7dSh. However, only about half of the supplemented 5dAdo (initial concentration: 25 μM) was converted into 5dR and 7dSh: at the end of the experiment, the 5dR concentration in the supplemented cultures was increased by around 10 μM and that of 7dSh by 2 μM, suggesting additional pathway(s) for 5dAdo salvage.

5dAdo is known to be cleaved by either the MtnN or the MtnP (9, 10, 16). The former reaction leads to the release of adenine and 5dR, whereas the latter leads to phosphate-dependent release of adenine and 5dR-1P. In *S. elongatus*, no homologous gene for a MtnN was found, but gene *Synpcc7942_0923* is annotated as a MtnP. Therefore, an insertion mutant was generated *via* the replacement of the gene by an antibiotic resistance cassette (*S. elongatus mtnP*::*spec*$_R$). Polar effects because of the insertion of the antibiotic resistance cassette were excluded by monitoring the

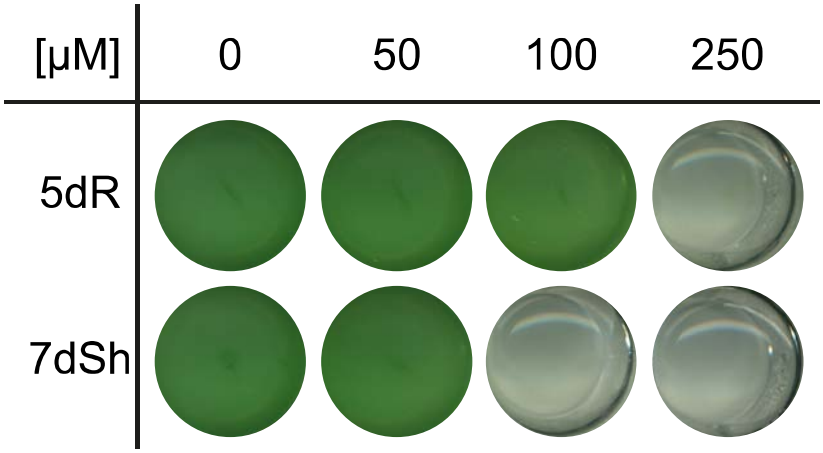

Figure 3. 5-Deoxyribose (5dR) and 7-deoxysedoheptulose (7dSh) are inhibiting the growth of the producer strain. Effect of different concentrations of 5dR and 7dSh on the growth of *Synechococcus elongatus*. The cultures were inoculated at an optical density of 750 nm of 0.1 in 1 ml BG11 medium in the absence (0) or the presence of either 5dR or 7dSh at the indicated concentrations and grown in a 24-well plate for 3 days. The experiment was performed in triplicates. The results of one replicate are shown.

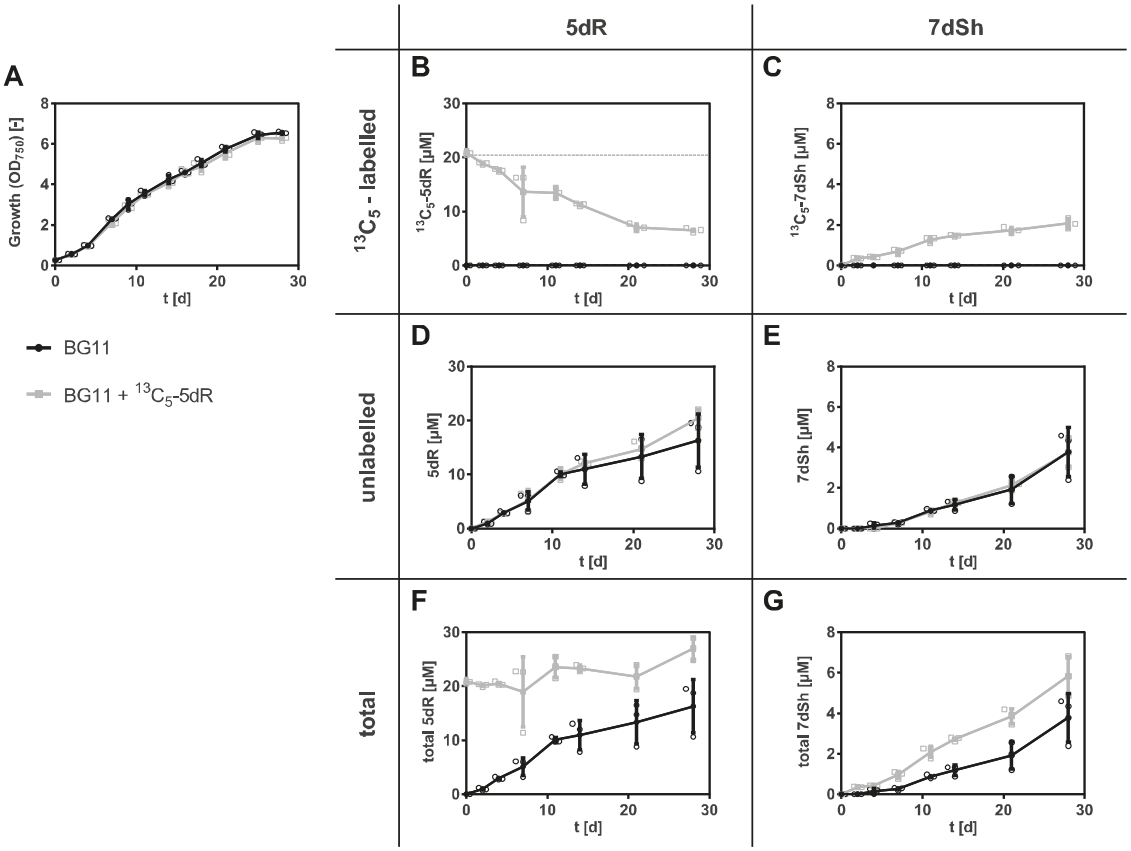

Figure 4. 5-Deoxyribose (5dR) is the precursor molecule of 7-deoxysedoheptulose (7dSh). Effects of $^{13}C_5$-5dR supplementation over the time on the growth of *Synechococcus elongatus* (*A*) or on the concentration of $^{13}C_5$-5dR (*B*), $^{13}C_5$-7dSh (*C*), unlabeled 5dR (*D*), unlabeled 7dSh (*E*), total 5dR (*F*), and total 7dSh (*G*) in the culture supernatant. About 20 µM $^{13}C_5$-5dR (indicated by *dashed line*) was added at the beginning of the cultivation (*gray squares*). Control cultures (*black dots*) were cultivated in BG11 without supplemented $^{13}C_5$-5dR. All cultures were aerated with air supplemented with 2% CO_2. Values shown in the graphs represent mean and standard deviation of three biological replicates.

expression of the genes with a semiquantitative RT-PCR (Fig. S2). Under conditions favorable for 5dR/7dSh production, the mutant grew like the wildtype (Fig. 6*A*). A GC–MS analysis of the culture supernatant revealed that the mutant neither excreted 5dR nor 7dSh (Fig. 6, *C* and *D*). Instead, while undetectable in the supernatant of the wildtype strain, 5dAdo strongly accumulated in the supernatant of *S. elongatus mtnP::spec$_R$* cultures (Fig. 6*B*). This confirmed that 5dR/7dSh are derived from 5dAdo in a MtnP-dependent manner. Because of the detoxification *via* excretion, the *mtnP::spec$_R$* mutant escapes the toxic effect of 5dAdo and does not show any growth disadvantage (Fig. 6*A*). It has previously been reported that a *mtnP* knockout mutant in *Saccharomyces cerevisiae* as well as MtnP-deficient mammalian tumor cells excreted MTA (25, 26). Both MTA and 5dAdo are known to be cleaved by MtnP (16). Consistently, the *mtnP::spec$_R$* mutant excretes MTA as well as 5dAdo (Fig. 6*E*). Since 5dR/7dSh formation strongly depends on elevated CO_2 conditions, we measured the amount of 5dAdo and MTA in cultures of the *mtnP::spec$_R$* mutant supplied with ambient air or with air enriched with 2% CO_2. However, the amounts of excreted 5dAdo and MTA (normalized to the optical density of the cultures) were almost identical under both conditions (Fig. 6*E*). This clearly indicates that 5dAdo salvage *via* 5dR/7dSh formation and excretion at high CO_2 conditions is not triggered by an increased synthesis of the precursor molecule 5dAdo compared with ambient CO_2 concentrations. Rather, it appears that 5dAdo is actively metabolized into 5dR/7dSh under elevated CO_2 conditions, whereas 5dAdo salvage under ambient CO_2 conditions is conducted by (an)other pathway(s). Since the MTA formation is also unaltered (Fig. 6*E*), we conclude that 5dAdo salvage *via* 5dR/7dSh formation is not triggered by an enhanced demand of MTA salvage *via* the MSP pathway.

5dR and 7dSh formation is not ubiquitous

To clarify how widespread the synthesis of 7dSh or 5dR is in cyanobacteria, we analyzed the supernatants of other cyanobacterial strains *via* GC–MS (*Synechococcus* sp. PCC 6301, *Synechococcus* sp. PCC 7002, *Synechococcus* sp. PCC 6312, *Synechococcus* sp. PCC 7502, *Synechocystis* sp. PCC 6803, *A. variabilis* ATCC 29413, *Nostoc punctiforme* ATCC 29133,

Bioactive compound formation by 5-deoxyadenosine salvage

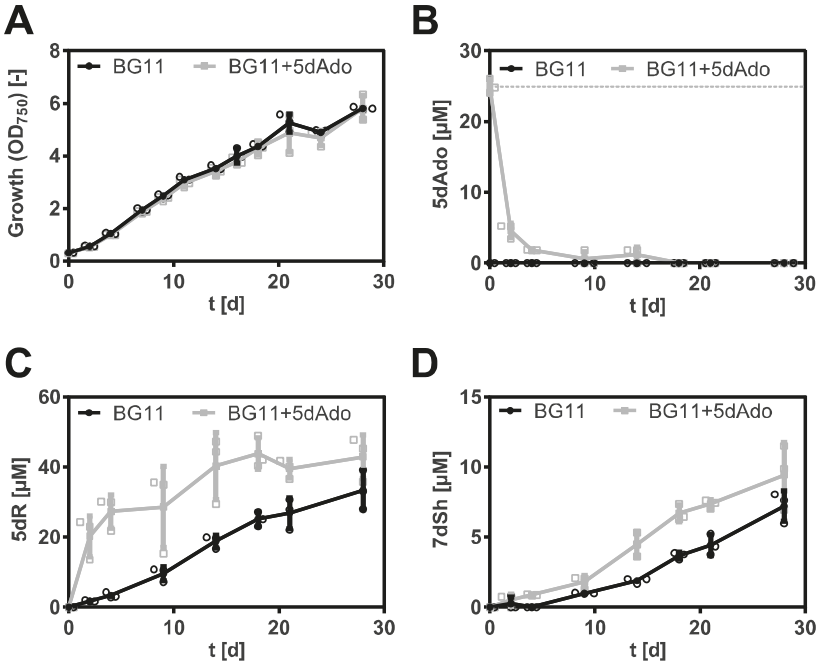

Figure 5. 5-Deoxyadenosine (5dAdo) feeding experiment. Effect of 5dAdo supplementation on the growth of *Synechococcus elongatus* (*A*) or on the concentration of 5dAdo (*B*), 5-deoxyribose (5dR) (*C*), and 7-deoxy-sedoheptulose (7dSh) (*D*) in the culture supernatant. About 25 µM 5dAdo (indicated by *dashed line*) was added at the beginning of the cultivation (*gray squares*). Control cultures (*black dots*) were cultivated in BG11 in the absence of exogenous 5dAdo. All cultures were aerated with air supplemented with 2% CO_2. Note the different values of the *y*-axis. Values shown in the graphs represent mean and standard deviation of three biological replicates.

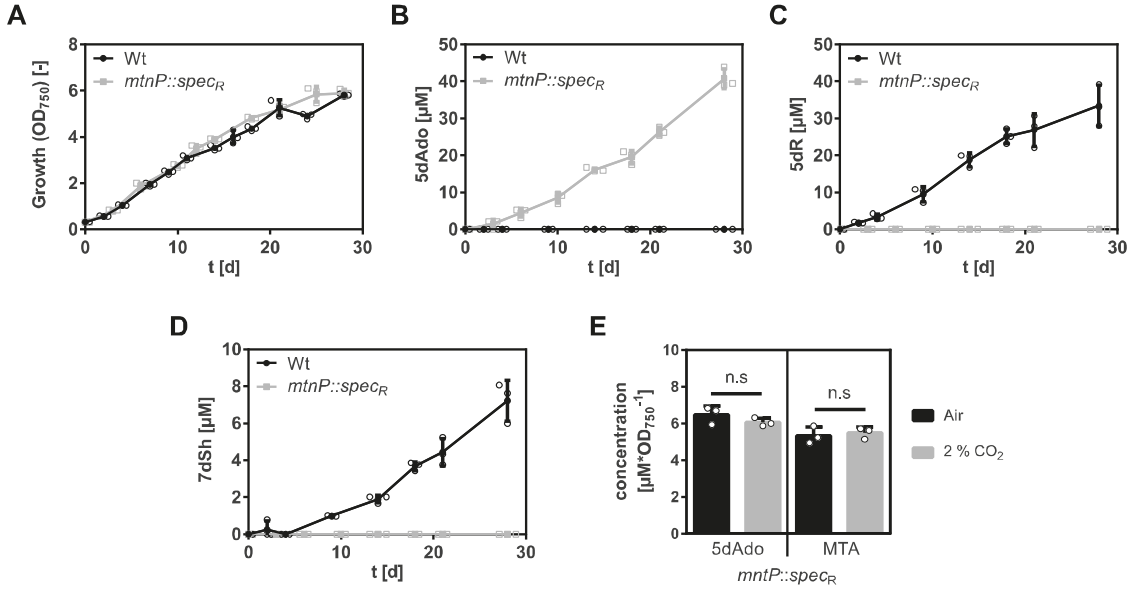

Figure 6. 5-Deoxyadenosine (5dAdo) is cleaved by 5-methylthioadenosine (MTA) phosphorylase (MtnP) and then metabolized into 5-deoxyribose (5dR) and 7-deoxysedoheptulose (7dSh) in *Synechococcus elongatus* at high CO_2 concentrations. Growth (*A*), concentrations of 5dAdo (*B*), 5dR (*C*), and 7dSh (*D*) in the supernatant of *S. elongatus* wildtype (*black dots*) or *mtnP::spec*$_R$ mutant (*gray squares*). All cultures were aerated with air supplemented with 2% CO_2. Note the different values of the *y*-axis. *E*, 5dAdo and MTA concentrations in the supernatant of the *mtnP::spec*$_R$ mutant normalized on the optical density after 11 days of cultivation (cultures were either aerated with atmospheric air [*black*] or with air supplemented with 2% CO_2 [*gray*]). Significant differences between the concentrations of 5dAdo or MTA during cultivation at 2% CO_2 and ambient air were analyzed by using an unpaired *t* test (*$p < 0.05$; **$p < 0.01$; and ***$p < 0.001$). Values shown in the graphs represent mean and standard deviation of three biological replicates. ns, not significant.

and *Anabaena* sp. PCC 7120). Only in three of five *Synechococcus* strains, the deoxy-sugars 5dR and 7dSh were detectable. All the other strains accumulated neither 5dR nor 7dSh. In the freshwater strain *Synechococcus* sp. PCC 6301, the amounts of 7dSh and 5dR were in a similar concentration range to those in *S. elongatus*. This is not surprising since the genome of *Synechococcus* sp. PCC 6301 is nearly identical to that of *S. elongatus* PCC 7942 (27). Very small amounts of 5dR and 7dSh were detected in the marine strain *Synechococcus* sp. PCC 7002. In *S. setonensis*, which was shown to produce 7dSh (20, 23), we detected 113 ± 7 μM 7dSh but no 5dR in the supernatant of cultures grown for 7 days.

5dAdo cleavage is strictly dependent on phosphorylase activity

To reveal whether 5dAdo is converted to 5dR *via* MtnP activity, crude extracts of *S. elongatus* wildtype and MtnP-deficient *mtnP*::*spec*$_R$ mutant cells were incubated with 5dAdo in the presence or the absence of potassium phosphate buffer. Analysis of the extracts *via* TLC revealed that 5dAdo cleavage and, thereby, adenine release is strictly dependent on the presence of phosphate (Fig. 7, *white label*) and only occurred in wildtype cell extracts but not in extracts of *mtnP*::*spec*$_R$ mutant cells. Therefore, 5dAdo cleavage in *S. elongatus* is strictly dependent on the presence of the MtnP. Other enzymes, for example, purine nucleosidase phosphorylases (28), apparently do not process 5dAdo in the cell extract. This result implies that the first product of 5dAdo cleavage is 5dR-1P, which is subsequently converted into 5dR. 5dR-1P seemed quite stable because LC-MS analysis revealed that a compound with an *m/z* ratio that corresponds to the sum formula of 5dR-1P ([M + H, M + Na]+ [*m/z* 215.0315; 237.0135]) accumulated in the crude extract (Fig. S3). Furthermore, no 5dR formation was observed in the crude extracts (Fig. S4). With this, we exclude a spontaneous hydrolysis of 5dR-1P, which is in accordance to the literature, where 5dR-1P is reported to be metabolically stable (29).

5dR-1P is dephosphorylated by a specific phosphatase

As 5dR-1P is metabolically stable, we assumed that for 5dR formation, a specific phosphatase must be involved. To identify this phosphatase, we analyzed the genome of *S. elongatus* regarding the presence of phosphoric monoester hydrolases (Table S3). *Synpcc7942_1005*, annotated as glucose-1-phosphatase, belonging to the haloacid dehalogenase (HAD)–like hydrolase superfamily subfamily IA (30, 31), seemed a promising candidate as only *S. elongatus* and *Synechococcus* sp. PCC 6301, which both produce larger amounts of 5dR/7dSh, possess a homologous gene. The other cyanobacteria mentioned previously do not possess it. Furthermore, phosphatases from the HAD-like hydrolase superfamily are known to be promiscuous enzymes dephosphorylating various phosphate sugars (32, 33). To examine whether this gene is essential for 5dR-1P dephosphorylation and thereby 5dR/7dSh synthesis, a corresponding mutant was created by replacing the *Synpcc7942_1005* gene with a spectinomycin resistance cassette (*S. elongatus Synpcc7942_1005*::*spec*$_R$). Polar effects because of the insertion of the antibiotic resistance cassette were excluded by monitoring the expression of the genes with a semiquantitative RT-PCR (Fig. S2). Under 5dR/7dSh production conditions, the mutant grew like the wildtype (Fig. 8*A*). The wildtype excreted 5dR and 7dSh, whereas the mutant only excreted trace amounts of 5dR and not 7dSh (Fig. 8, *C* and *D*). Instead, the mutant excreted 5dAdo, which was never detected in the supernatant of the wildtype (Fig. 8*B*). This clearly shows that the gene product of *Synpcc7942_1005* is the major enzyme for the dephosphorylation of 5dR-1P. However, since in the mutant, small quantities of 5dR were detectable, other phosphatases may also contribute to minor 5dR-1P dephosphorylation. In agreement with this, *Synechoccoccus* sp. PCC 7002, which does not possess a homolog

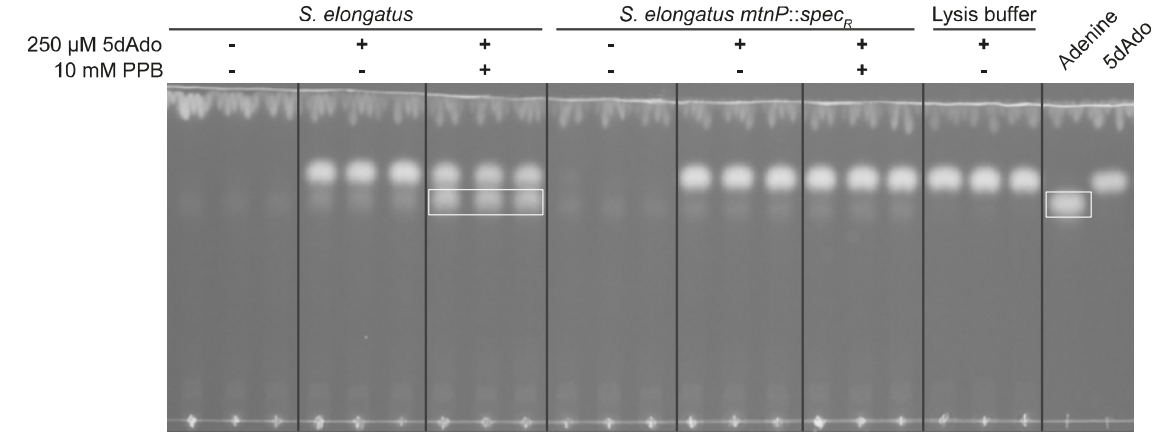

Figure 7. 5-Deoxyadenosine (5dAdo) cleavage in *Synechococcus elongatus* is phosphate dependent. Crude extracts from *S. elongatus* or *S. elongatus mtnP*::*spec*$_R$ were incubated with 5dAdo in the presence or the absence of potassium phosphate buffer (PPB) and then analyzed *via* TLC on silica gel. 5dAdo (R_f = 0.68) and adenine (R_f = 0.76) analytes were visualized *via* absorption at 254 nm. Pure adenine and 5dAdo were used as standards (*right*). Spots corresponding to adenine are highlighted with a *white box*. Three independent replicates are shown for each condition. The stability of 5dAdo in the buffer is shown with the lysis buffer control.

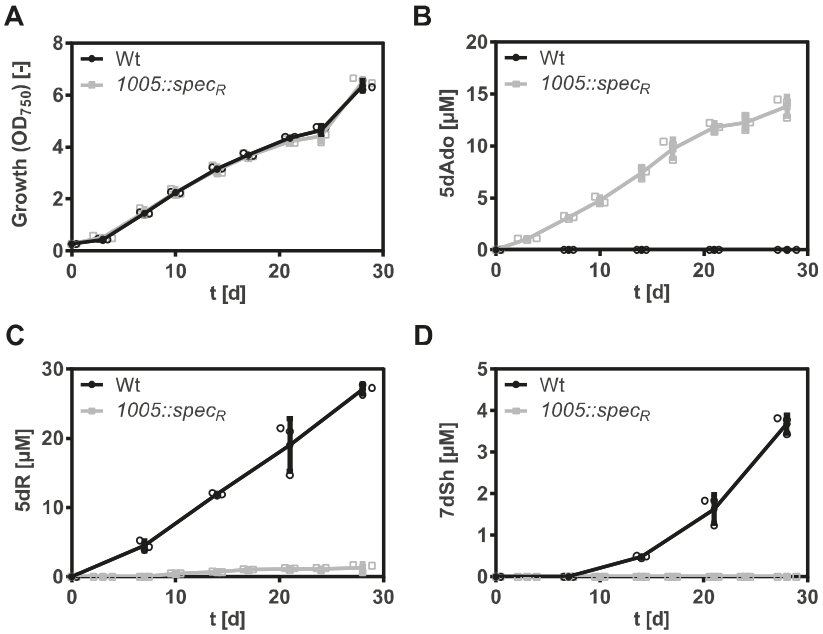

Figure 8. 5-Deoxyribose 1-phosphate (5dR-1P) is dephosphorylated by a phosphatase from the haloacid dehalogenase hydrolase superfamily (*Synpcc7942_1005*, Enzyme Commission number: 3.1.3.10). Growth (*A*), concentrations of 5-deoxyadenosine (5dAdo) (*B*), 5-deoxyribose (5dR) (*C*), and 7-deoxy-sedoheptulose (7dSh) (*D*) in the supernatant of *Synechococcus elongatus* wildtype (*black dots*) or *1005::spec$_R$* mutant (*gray squares*). All cultures were aerated with air supplemented with 2% CO_2. Note the different values of the *y*-axis. Values shown in the graphs represent mean and standard deviation of three biological replicates.

of *Synpcc7942_1005*, also excreted minor amounts of 5dR and 7dSh.

5dR/7dSh producers possess complete MSP gene clusters

By analyzing the genomes of all examined cyanobacteria in this study, it turned out that those strains that do not produce 5dR and 7dSh only possess annotated genes for the first two reactions of the MSP (*mtnP* and *mtnA*), whereas the producer strains possess annotated genes for the whole MSP pathway (Table S1). This suggests that the 5dR/7dSh producers might be able to rescue 5dAdo also *via* the DHAP shunt, as the third enzyme of the MSP, MTRu-1P-dehydratase (MtnB), can also act as a promiscuous aldolase, when no specific class II aldolase, as DrdA (*B. thuringiensis*) or Ald2 (*R. rubrum*), is present (13, 18). None of the analyzed strains possess an Ald2 homolog; therefore, the 5dR/7dSh nonproducer strains must employ another pathway of 5dAdo salvage.

With this, it appears that the pathway for 5dR and 7dS synthesis is clarified and based on the activity of seemingly promiscuous enzymes, which together catalyze the specific synthesis of the bioactive sugars. Moreover, as suggested by the CO_2-promoted synthesis, the cells are apparently able to tune the metabolic flow in this pathway in response to environmental conditions.

Discussion

Radical SAM enzymes are important enzymes in all domains of life (2). A byproduct of the activity of these enzymes is 5dAdo (3). Its accumulation inhibits the activity of the radical SAM enzymes themselves (9–12). Therefore, 5dAdo salvage pathways are essential. In this study, we showed that the unicellular cyanobacterium *S. elongatus* PCC 7942 has a special salvage route for 5dAdo, which was never reported before (Fig. 1*A*). We show that 5dAdo salvage can be achieved by the excretion of 5-deoxyribose and 7-deoxysedoheptulose. 5dR as a product of 5dAdo cleavage was postulated (8, 17) or observed before but only in *in vitro* assays (9, 17). 5dR excretion was suggested as a detoxification strategy for organisms that do not possess a specific gene cluster for 5dAdo salvage (18) (analogous to MTR excretion in *E. coli*, which does not possess a complete MSP (34, 35)). Therefore, 5dR accumulation in the supernatant of *S. elongatus* as an *in vivo* phenomenon was first reported by our previous publication (20) and here identified as a result of 5dAdo salvage.

We propose the following model for a possible 5dAdo salvage route in *S. elongatus* by the activity of promiscuous enzymes leading to the synthesis of the bioactive deoxy-sugars 5dR and 7dSh (Fig. 1*A*). In brief, 5dAdo is processed by the promiscuous MtnP into 5dR-1P. Under elevated CO_2 conditions, this molecule is dephosphorylated to 5dR by the presumably promiscuous phosphatase, the *Synpcc7942_1005* gene product, to 5dR, part of which is excreted and further metabolized by the activity of a promiscuous transketolase to 7dSh, which is also excreted to avoid the inhibition of the shikimate pathway (20). The producer strain tolerates high concentrations of 7dSh (Fig. 3), whereas other strains such as

A. variabilis are highly sensitive toward 7dSh treatment (20), implying that 7dSh is a potent allelopathic inhibitor.

Although most bacteria possess the enzymes for a two-step reaction of 5dAdo cleavage (MtnN and MTR kinase) (36, 37), all examined cyanobacteria possess an MtnP (Table S1), which is normally present in eukaryotes (except for plants). The phenotype of the insertion mutant (*mtnP::spec*$_R$), which excretes 5dAdo instead of 5dR/7dSh, demonstrates that 5dR and 7dSh are products of 5dAdo salvage (Fig. 6). The 5dAdo salvage routes previously reported suggest that the phosphorylation of 5dR or the 5dR moiety of 5dAdo is essential to further metabolize the molecules *via* specific enzymes or by promiscuous activity of the enzymes of the MSP (13, 17, 18). By contrast, in *S. elongatus*, 5dR-1P is dephosphorylated to 5dR or further processed to 7dSh to yield bioactive secreted metabolites. Our data imply that the dephosphorylation of 5dR-1P is not because of spontaneous hydrolysis but is mainly conducted by the gene product of *Synpcc7942_1005* (Fig. 8). *Synpcc7942_1005* belongs to Mg^{2+}-dependent class IA HAD-like hydrolase superfamily (31) and is annotated as a glucose-1-phosphatase, which catalyzes the dephosphorylation of glucose 1-phosphate (38). As these phosphatases can also exhibit phytase activity (39, 40), we assume that the gene product of *Synpcc7942_1005* might also exhibit promiscuous activity, including 5dR-1P dephosphorylation. The dephosphorylation of a similar molecule (5-fluoro-5-deoxyribose 1-phosphate) by a specific phosphoesterase (FdrA) is also conducted by *Streptomyces* sp. MA37 during the production of a specific secondary fluorometabolite (41) (Fig. S5).

In later growth phases, part of 5dR is transformed into 7dSh, which is then also immediately excreted into the supernatant (Figs. 2*C* and 4, *C* and *E*). In our previous work, we showed that the affinity of *S. elongatus* transketolase for 5dR is 100-fold lower than for the natural substrate D-ribose-5-phosphate (20). This is in accordance with the fact that 7dSh is only formed when relatively high extracellular 5dR concentrations are reached (either in later growth phases or because of the addition of externally added 5dR; note that 5dR is continuously imported and exported). Furthermore, only one-tenth of $^{13}C_5$-5dR is converted into $^{13}C_5$-7dSh. 7dSh formation from 5dR is therefore an impressive example how a more potent "derivative" (7dSh) is formed by promiscuous enzyme activity. Interestingly, a promiscuous transketolase reaction was also suggested in later steps of anaerobic 5dAdo salvage in *M. jannaschii*, in which 5dRu-1P is cleaved into lactaldehyde and methylglyoxal (19). As our analysis showed, *S. setonensis* (not yet sequenced) accumulates much higher concentrations of 7dSh in the supernatant than *S. elongatus* but no 5dR at all. If *S. setonensis* synthesizes 7dSh *via* the same pathway than *S. elongatus*, the complete conversion of 5dR could be due to a more specific transketolase.

In high concentrations, 5dR exhibited toxicity toward the producer strain (Fig. 3). 5dR toxicity was also reported in *B. thuringiensis* (18), but the intracellular target is not yet known. Therefore, *S. elongatus* has to steadily excrete 5dR into the supernatant to avoid intracellular toxicity. Because $^{13}C_5$-5dR was taken up at the same time as unlabeled 5dR was excreted (Fig. 4, *B* and *D*), specific transport systems have to be present, which are probably essential for the survival of the producer strain.

5dAdo salvage *via* 5dR and 7dSh excretion was only observed when cultures were aerated with air supplemented with 2% CO_2 (Fig. 2, *B* and *C*). Since equal amounts of 5dAdo were formed under ambient CO_2 as under high CO_2 conditions (Fig. 6*E*), we assumed that under ambient conditions, 5dAdo salvage is conducted *via* (an)other pathway(s). The occurrence of (an) additional 5dAdo salvage pathway(s) in *S. elongatus* is underlined by the fact that 5dAdo is not completely metabolized into 5dR/7dSh even under high CO_2 conditions (Fig. 5). Because *S. elongatus* and the other 5dR/7dSh producers are equipped with the enzymes for the whole MSP (Table S1), we hypothesize that 5dAdo can be also metabolized *via* promiscuous activity of the enzymes of the MSP *via* the "DHAP-shunt" resulting in the formation of DHAP and acetaldehyde (Fig. 1, *A* and *C*) as suggested for organisms that do not possess a specific gene cluster for 5dAdo salvage (13, 17, 18). The formation of MTA, the starting molecule of the MSP, is almost identical under atmospheric and high carbon conditions (Fig. 6*E*). This indicates that 5dAdo salvage *via* 5dR/7dSh excretion under high CO_2 conditions is not triggered by an increased demand of MTA salvage. It is known that intracellular CO_2/HCO_3^- (C_i) exhibits regulatory functions at the metabolic and transcriptomic levels (42), and it is known to regulate virulence and toxin production in pathogens, for example, in *Vibrio cholerae* (43). In particular, cyanobacteria strongly respond to the ambient C_i supply by a multitude of metabolic adaptations such as carbon concentrating mechanisms (44) and the synthesis of cAMP (45). As we hypothesize that the fate of 5dAdo is a regulated process, we assume that the dephosphorylation of 5dR and the subsequent formation of 7dSh molecules is not an "accident". They are rather purposely formed metabolites, which however derive from toxic byproducts of the primary metabolism. The regulation how 5dAdo is directed toward 5dR/7dSh formation has to be further investigated.

With 18 radical SAM enzymes (Table S2), *S. elongatus* only possesses a relatively small number of radical SAM enzymes compared with other prokaryotes (*B. thuringiensis*: 15; other Firmicutes: more than 40 (18); *R. rubrum*: 25; and *M. jannaschii*: 30 (13)). Probably the most important radical SAM enzymes under the cultivation conditions applied here are involved in cofactor biosynthesis and presumably equally important under ambient or high carbon conditions resulting in the unaltered 5dAdo formation.

7dSh can inhibit the growth of not only other cyanobacteria but also plants and was therefore suggested to be an allelopathic inhibitor by inhibiting the dehydroquinate synthase, the second enzyme of the shikimate pathway (20). In addition, 5dR is toxic for various organisms (Fig. 3; (18)). Despite the low concentrations of 5dR/7dSh observed under laboratory conditions, it is imaginable that excretion of 5dR and 7dSh plays a role in protecting the ecological niche of the producer strains. 7dSh is a more potent inhibitor, for example, for *A. variabilis* than for the producer strain. A bactericidal effect for

A. variabilis was observed at concentrations of 13 μM 7dSh (20), whereas *S. elongatus* is affected by 100 μM (Fig. 3). Although it is not obvious from isolated *in vitro* studies, we speculate that 7dSh might play a role in niche competition. In its natural environment, *S. elongatus* can live planktonically, but it is also able to form biofilms or microbial mats, which also contain the colonization of caves and humid stonewalls (46–50). In the latter habitats, the dilution of excreted compounds is prevented, and therefore, the activity of 7dSh as an allelopathic inhibitor is imaginable. In addition, cyanobacteria tend to excrete exopolysaccharides in biofilms (51), which can be used as a carbon source by heterotrophic members of the microbial community, thereby causing locally elevated CO_2 concentrations. This could lead to a local enrichment of 5dR and 7dSh, thereby providing a growth advantage to the producer strains protecting their niches against competing microalgae.

5dAdo salvage is a less noticeable and overlooked research topic in comparison to methionine salvage from MTA. Hence, it should be further investigated above all because 5dAdo is present in all domains of life, whereas MTA is only produced by specific organisms. Since 5dAdo disposal pathways seem to differ from species to species, our findings suggest that other noncanonical 5dAdo salvage pathways may exist, encouraging the search of "cryptic" metabolites derived from this pathway.

Overall, this study shows a unique example of a synthesis pathway of bioactive molecules solely catalyzed by promiscuous enzymes of primary metabolism, which challenges the current view on the synthesis of bioactive molecules. The involvement of enzyme multifunctionality extends the range of possible bioactive compounds far beyond what can be predicted from standard genome mining biased for secondary metabolite gene clusters.

Experimental procedures

Cultivation

S. elongatus PCC 7942 was cultivated under photoautotrophic conditions in BG11 medium (52) supplemented with 5 mM $NaHCO_3$. Precultures were cultivated in shaking flasks at 30 to 50 μE at 125 rpm (27 °C). Main cultures were cultivated in 500 to 700 ml BG11 at 27 °C in flasks that were either aerated with air or air supplemented with 2% CO_2. For this purpose, cultures were inoculated with an optical density at 750 nm of 0.2 to 0.5 and then cultivated for the first 3 days at 10 μE (Lumilux de Lux; Daylight; Osram). Later, the light intensity was set to around 30 μE. Growth was determined by measuring the absorbance at 750 nm (Specord 205; Analytik Jena). For feeding experiments, the cultures were supplemented at the beginning of the cultivation with 5dR, [U-$^{13}C_5$]-5dR, or 5dAdo (Carbosynth Ltd) at the respective concentrations (see Results section). The other cyanobacterial strains (*Synechococcus* sp. PCC 6301, *Synechococcus* sp. PCC 6312, *Synechococcus* sp. PCC 7502, *Synechocystis* sp. PCC 6803, *A. variabilis* ATCC 29413, *N. punctiforme* ATCC 29133, and *Anabaena* sp. PCC 7120) were cultivated as described previously. *Synechococcus* sp. PCC 7002 was cultivated in a 1:1 mixture of BG11 and ASN III + vitamin B_{12} (10 μg/ml) (52).

S. setonensis SF666 was cultivated for 7 days as described in our previous work (20).

Synthesis of 5-deoxyribose and 7-deoxysedoheptulose

5dR and [U-$^{13}C_5$]-5dR **5** were synthesized in a four-step synthesis based on the literature (53, 54) with an additional optimization. All synthetic intermediates shown in the reaction scheme (Fig. S6) were verified by TLC, MS, and NMR. Detailed data for the ^{13}C-labeled compounds are presented in the Supporting Information. The synthesis starts with the reaction of D-ribose (Sigma) or [U-$^{13}C_5$]-D-ribose **1** (500.1 mg, 3.22 mmol; Eurisotop) in a 4:1 mixture of acetone:methanol with $SnCl_2$×2 H_2O (1 eq) and catalytic amounts of concentrated H_2SO_4 at 45 °C for 20 h. After cooling to room temperature, the mixture was filtered, neutralized with $NaHCO_3$ solution, once again filtered, and the organic solvent was evaporated. The remaining aqueous solution was extracted with ethylacetate, dried over Na_2SO_4, and evaporated *in vacuo* to yield the acetonide-protected ribose **2** as a colorless oil (399.7 mg, 1.91 mmol, 59%).

Envisaging the following deoxygenation reaction, the protected pentose **2** (399.7 mg, 1.91 mmol) was diluted in dilated cardiomyopathy with addition of triethylamine (2.5 eq). After cooling on ice, mesylchloride (2.5 eq) was slowly added and then stirred for 5 h on ice. The reaction mixture was washed with 1 N HCl, ultrapure water, $NaHCO_3$ solution, NaCl solution, and again with ultrapure water. The organic solvent was dried over Na_2SO_4 and evaporated *in vacuo* to give **3** as an yellowish oil (556.5 mg, 1.97 mmol, 103%, mesylchloride as impurity), which becomes crystalline at 4 °C.

For the reduction as the third step **3** (556.1 mg, 1.91 mmol, maximum educt amount) was diluted in dimethyl sulfoxide. After cooling on ice, $NaBH_4$ (5 eq) was added slowly. Afterward, the reaction mixture was heated slowly to 85 °C and reacting for 12 h. After cooling on ice, 5% AcOH was added to quench remaining $NaBH_4$. The aqueous solution was extracted with dilated cardiomyopathy, washed with ultrapure water, dried over Na_2SO_4, and evaporated *in vacuo* (40 °C, 750 mbar) to get **4** as a colorless oil (357.7 mg, 1.85 mmol, 86%).

Deprotecting to the target **5** was achieved by diluting the acetonide-protected ω-deoxy-sugar **4** (357.7 mg, 1.85 mmol) in 0.04 N H_2SO_4 and heating to 85 °C for 3 h. After cooling to room temperature, the reaction mixture was neutralized with $NaHCO_3$ solution and evaporated by lyophilization. The final product was first purified by medium-pressure liquid chromatography (gradient: start $CHCl_3$:MeOH 10:0; end $CHCl_3$:MeOH 7:3) and HPLC (column: HiPlexCa, 85 °C, 250 × 10.7 mm, 1.5 ml/min, solvent: ultrapure water) to get [U-$^{13}C_5$]-5-deoxy-D-ribofuranose **5** as a colorless oil (115.7 mg, 1.12 mmol, 61%).

7dSh or [3,4,5,6,7-$^{13}C_5$]-7dSh was synthesized in a transketolase-based reaction with 5dR or [U-$^{13}C_5$]-5dR as substrate as described in our previous publication (20) with slight modifications. The reaction was performed in water

instead of Hepes buffer to ensure an enhanced stability of hydroxypyruvate (very unstable in Hepes (55)). The reaction was performed for 7 days, and fresh hydroxypyruvate was added every day. Purification was done as described for 5dR.

Construction of insertion mutants

To create an insertion mutant of the 5-methylthioadenosine phosphorylase (Enzyme Commission number: 2.4.2.28, MtnP, *Synpcc7942_0932*) and glucose-1-phosphatase (Enzyme Commission number: 3.1.3.10, *Synpcc7942_1005*) in *S. elongatus* PCC 7942, a spectinomycin resistance cassette was introduced inside the respective gene. An integrative plasmid was constructed in *E. coli* and then transformed into *S. elongatus*. For this purpose, flanking regions on both sides of the respective gene were amplified from *S. elongatus* colonies with primers adding an overlapping fragment (46_0923_up_fw, 47_0923_up_rev; 48_Δ0923_down_fw and 49_0923_down_rev for *Synpcc7942_0923*::$spec_R$; 85_1005_up_fw, 86_1005_up_rev; 87_1005_down_fw and 88_1005_down_rev for *Synpcc7942_1005*::$spec_R$; sequences are shown in Table S4). The spectinomycin resistance cassette was amplified with primers 32_Spec_fw and 33_Spec_rev. All PCR amplification products were introduced into a pUC19 vector cut with XbaI and PstI by using Gibson assembly (56). The plasmid was verified by Sanger sequencing (Eurofins Genomics). The plasmid was then transformed into *S. elongatus* using natural competence as described elsewhere (57). Segregation was confirmed by colony PCR (50_0923_rev_seg and 51_0923_fw_seg for *Synpcc7942_0923*::$spec_R$; 85_1005_up_fw and 88_1005_down_rev for *Synpcc7942_1005*::$spec_R$). Precultures of these strains, in the following named as *S. elongatus mtnP*::$spec_R$ or *S. elongatus 1005*::$spec_R$ were cultivated in the presence of 20 μg/ml spectinomycin, main cultures without antibiotic.

Quantification of metabolites in the culture supernatant via *GC–MS*

Culture supernatant was collected by centrifugation of 1.5 ml culture (16.000*g*, 10 min, 4 °C). About 200 μl of the supernatant was immediately frozen on liquid nitrogen and stored at −80 °C. Before extraction, the supernatant was lyophilized. For intracellular measurements, the cell pellets were also frozen in liquid nitrogen. Samples were extracted as described in the literature (58) with slight modifications: 700 μl of ice-cold extraction solution ($CHCl_3$/MeOH/H_2O in a ratio of 1/2.5/0.5 v/v/v) were either added to 200 μl of the lyophilized supernatant or to cell pellets. Samples were homogenized by vortexing, ultrasonic bath (Bandelin, Sonorex) treatment (10 min), and shaking (10 min, 1.000 rpm). After that, the samples were cooled on ice for 5 min and then centrifuged (10 min, 16.000*g*, 4 °C). The supernatant was transferred into a new reaction tube. The pellet was again extracted with 300 μl extraction solvent as described before. The supernatants were pooled, and 300 μl ice-cold water was added for phase separation. The samples were vortexed, incubated on ice (5 min), and then centrifuged (10 min, 16.000*g*, 4 °C). About 900 μl of the upper polar phase was transferred into a new 2 ml reaction tube and dried in a vacuum concentrator (Eppendorf, Concentrator plus, mode: V-AQ, 30 °C) for approximately 4.5 h. The samples were immediately closed and then derivatized as described in the literature (59) with slight modifications. Therefore, the pellets were resolved in 60 μl methoxylamine hydrochloride (Acros Organics) in pyridine (anhydrous, Sigma–Aldrich) (20 mg/ml), homogenized by vortexing, a treatment in an ultrasonic bath (15 min), and an incubation at 30 °C on a shaker (1.400 rpm) for 1.5 h. After that, 80 μl *N*-methyl-*N*-(trimethylsilyl)trifluoroacetamide (Macherey-Nagel) was added, and the samples were incubated at 37 °C for 30 min (1.200 rpm). The samples were centrifuged (16.000*g*, 2 min), and 120 μl was transferred into a glass vial with microinsert. The samples were stored at room temperature for 2 h before GC–MS measurement.

GC–MS measurements were performed on a Shimadzu GC–MS TQ 8040 (injector: AOC-20i; sampler: AOC-20s) with an SH-Rxi-5Sil-MS column (Restek; 30 m, 0.25 mm ID, 0.25 μm). For GC measurement, the initial oven temperature was set to 60 °C for 3 min. After that, the temperature was increased by 10 °C/min up to 320 °C, which was then held for 10 min. The GC–MS interface temperature was set to 280 °C, and the ion source was heated to 200 °C. The carrier gas flow (helium) was 1.28 ml/min. The injection was performed in split mode 1:10. The mass spectrometer was operated in exposure index mode. Metabolites were detected in multiple reaction monitoring mode. Quantification of the metabolites was performed with a calibration curve of the respective substances (5dAdo, 5dR, 7dSh, $^{13}C_5$-5dR, and $^{13}C_5$-7dSh). The recovery efficiency of exogenously added standards ($^{13}C_5$-5dR and $^{13}C_5$-7dSh) during the extraction of the cell pellets, as well as during extraction of the supernatant, is shown in the Supporting Information (Fig. S7 and Supporting text).

Quantification of MTA and 5dAdo

For the quantification of MTA and 5dAdo (Fig. 6*E*), 25 μl of culture supernatant was mixed with 75 μl aqueous solution of 20% MeOH (v/v) + 0.1% (v/v) formic acid. Samples were analyzed on an LC–HR-MS system (Dionex Ultimate 3000 HPLC system coupled to maXis 4G ESI-QTOF mass spectrometer). 5dAdo and MTA were separated on a C18 column with an MeOH/H_2O gradient (10%–100% in 20 min). The concentration was calculated from peak areas of extracted ion chromatograms of a calibration curve of the respective standards (MTA was obtained from Cayman Chemicals).

Crude extract assays

Crude extract assays were performed by harvesting 10 ml of the cultures after 14 days of cultivation (air supplemented with 2% CO_2) by centrifugation (3.200*g*, 10 min, 4 °C). The supernatant was discarded, and the pellet was washed with 10 ml fresh medium. The pellet was resuspended in 2.5 ml lysis buffer (25 mM Hepes pH 7.5, 50 mM KCl, 1 mM DTT). Cell

disruption was performed in a FastPrep-24 instrument (MP Biomedicals, 5 m/s, 20 s, 3× with 5 min break) by adding glass beads (⌀ = 0.1–0.11 mm). Cell debris was removed by centrifugation (25.000*g*, 10 min, 4 °C). About 200 µl of the extract was either used alone or supplemented with 5dAdo (final concentration: 250 µM) or in combination with potassium phosphate buffer pH 7.5 (final concentration: 10 mM). The extracts were incubated at 28 °C for 7 h, frozen in liquid nitrogen, and lyophilized. About 100 µl MeOH was added, and the samples were homogenized and centrifuged. About 50 µl was applied on a TLC plate (ALUGRAM Xtra SIL G UV_{254}; Macherey-Nagel). For the mobile phase, $CHCl_3$/MeOH in a ratio of 9:5 (v/v) with 1% (v) formic acid was used. Visualization was performed at 254 nm (Fig. 7) or spraying with anisaldehyde (Fig. S4).

Bioinformatics

Annotations of the different genes were obtained from the Kyoto Encyclopedia of Genes and Genomes database (60). Also, radical SAM enzyme (pf: Radical_SAM, PF04055) search was done in Kyoto Encyclopedia of Genes and Genomes database. Searching for homologous genes was performed by using BlastP (BLOSUM 62). Searching for Ald2 homologs, *R. rubrum* protein sequence (rru:Rru_A0359) was used as a query sequence, and an e value <10e-20 was used for positive results.

Data availability

All data are presented in the article, in the supporting information, or are available upon request (please contact: Karl Forchhammer, karl.forchhammer@uni-tuebingen.de).

Supporting information—This article contains supporting information (15, 18, 41, 53, 54, 60, 61).

Acknowledgments—The work is supported and funded by the "Glycobiotechnology" initiative (Ministry for Science, Research and Arts Baden-Württemberg), the Research Training Group 1708 "Molecular principles of bacterial survival strategies", and the Institutional Strategy of the University of Tübingen (Deutsche Forschungsgemeinschaft, ZUK 63). The work was further supported by infrastructural funding from the DFG Cluster of Excellence EXC 2124 Controlling Microbes to Fight Infections (project ID 390838134). We thank Dr Libera Lo Presti for critical reading of the article. We especially thank Tim Orthwein for fruitful discussions and Michaela Schuppe for the cultivation of *Streptomyces setonensis*.

Author contributions—J. R. designed, performed, interpreted experiments, and wrote the article. P. R. synthesized labeled and unlabeled 5dR and 7dSh. J. K. optimized the GC–MS method and supported with GC–MS measurements. K. B. supported initial experiments and proofread the article. S. G. supported chemical analytics and proofread the article. K. F. supervised the study and supported article writing.

Conflict of interest—The authors declare that they have no conflicts of interest with the contents of this article.

Abbreviations—The abbreviations used are: 5dAdo, 5-deoxyadenosine; 5dAdo•, 5-deoxyadenosylradical; 5dR, 5-deoxyribose; 5dR-1P, 5-deoxyribose 1-phosphate; 5dRu-1P, 5-deoxyribulose 1-phosphate; 7dSh, 7-deoxysedoheptulose; ATCC, American Type Culture Collection; DHAP, dihydroxyacetone phosphate; HAD, haloacid dehalogenase; MSP, methionine salvage pathway; MTA, 5-methylthioadenosine; MtnN, MTA nucleosidase; MtnP, MTA phosphorylase; MTR, methylthioribose; MTR-1P, methylthioribose-1-phosphate; SAH, *S*-adenosylhomocysteine; SAM, *S*-adenosyl-L-methionine.

References

1. Fontecave, M., Atta, M., and Mulliez, E. (2004) *S*-adenosylmethionine: Nothing goes to waste. *Trends Biochem. Sci.* **29**, 243–249
2. Sofia, H. J., Chen, G., Hetzler, B. G., Reyes-Spindola, J. F., and Miller, N. E. (2001) Radical SAM, a novel protein superfamily linking unresolved steps in familiar biosynthetic pathways with radical mechanisms. Functional characterization using new analysis and information visualization methods. *Nucleic Acids Res.* **29**, 1097–1106
3. Wang, S. C., and Frey, P. A. (2007) *S*-adenosylmethionine as an oxidant: The radical SAM superfamily. *Trends Biochem. Sci.* **32**, 101–110
4. Booker, S. J., and Grove, T. L. (2010) Mechanistic and functional versatility of radical SAM enzymes. *F1000 Biol. Rep.* **2**, 52
5. Broderick, J. B., Duffus, B. R., Duschene, K. S., and Shepard, E. M. (2014) Radical *S*-adenosylmethionine enzymes. *Chem. Rev.* **114**, 4229–4317
6. Marsh, E. N. G., Patterson, D. P., and Li, L. (2010) Adenosyl radical. Reagent and Catalyst in enzyme reactions. *ChemBioChem* **11**, 604–621
7. Holliday, G. L., Akiva, E., Meng, E. C., Brown, S. D., Calhoun, S., Pieper, U., Sali, A., Booker, S. J., and Babbitt, P. C. (2018) Atlas of the radical SAM superfamily: Divergent Evolution of function using a "Plug and play" domain. *Meth Enzymol.* **606**, 1–71
8. Parveen, N., and Cornell, K. A. (2011) Methylthioadenosine/*S*-adenosylhomocysteine nucleosidase, a critical enzyme for bacterial metabolism. *Mol. Microbiol.* **79**, 7–20
9. Choi-Rhee, E., and Cronan, J. E. (2005) A nucleosidase required for in vivo function of the *S*-Adenosyl-L-Methionine radical enzyme, biotin synthase. *Chem. Biol.* **12**, 589–593
10. Challand, M. R., Ziegert, T., Douglas, P., Wood, R. J., Kriek, M., Shaw, N. M., and Roach, P. L. (2009) Product inhibition in the radical *S*-adenosylmethionine family. *FEBS Lett.* **583**, 1358–1362
11. Farrar, C. E., Siu, K. K. W., Howell, P. L., and Jarrett, J. T. (2010) Biotin synthase exhibits burst kinetics and multiple turnovers in the absence of inhibition by products and product-related biomolecules. *Biochemistry* **49**, 9985–9996
12. Palmer, L. D., and Downs, D. M. (2013) The thiamine biosynthetic enzyme ThiC catalyzes multiple turnovers and is inhibited by *S*-adenosylmethionine (AdoMet) metabolites. *J. Biol. Chem.* **288**, 30693–30699
13. North, J. A., Wildenthal, J. A., Erb, T. J., Evans, B. S., Byerly, K. M., Gerlt, J. A., and Tabita, F. R. (2020) A bifunctional salvage pathway for two distinct *S*-adenosylmethionine by-products that is widespread in bacteria, including pathogenic *Escherichia coli*. *Mol. Microbiol.* **113**, 923–937
14. Wray, J. W., and Abeles, R. H. (1995) The methionine salvage pathway in *Klebsiella pneumoniae* and rat liver. Identification and characterization of two novel dioxygenases. *J. Biol. Chem.* **270**, 3147–3153
15. Sekowska, A., and Danchin, A. (2002) The methionine salvage pathway in *Bacillus subtilis*. *BMC Microbiol.* **2**, 8
16. Savarese, T. M., Crabtree, G. W., and Parks, R. E. (1981) 5′-methylthioadenosine phosphorylase—I. Substrate activity of 5′-deoxyadenosine with the enzyme from Sarcoma 180 cells. *Biochem. Pharmacol.* **30**, 189–199
17. Sekowska, A., Ashida, H., and Danchin, A. (2018) Revisiting the methionine salvage pathway and its paralogues. *Microb. Biotechnol.* **12**, 77–97
18. Beaudoin, G. A. W., Li, Q., Folz, J., Fiehn, O., Goodsell, J. L., Angerhofer, A., Bruner, S. D., and Hanson, A. D. (2018) Salvage of the 5-deoxyribose byproduct of radical SAM enzymes. *Nat. Commun.* **9**, 3105

19. Miller, D. V., Rauch, B. J., Harich, K., Xu, H., Perona, J. J., and White, R. H. (2018) Promiscuity of methionine salvage pathway enzymes in *Methanocaldococcus jannaschii*. *Microbiology* **164**, 969–981
20. Brilisauer, K., Rapp, J., Rath, P., Schöllhorn, A., Bleul, L., Weiß, E., Stahl, M., Grond, S., and Forchhammer, K. (2019) Cyanobacterial antimetabolite 7-deoxy-sedoheptulose blocks the shikimate pathway to inhibit the growth of prototrophic organisms. *Nat. Commun.* **10**, 545
21. Shih, P. M., Wu, D., Latifi, A., Axen, S. D., Fewer, D. P., Talla, E., Calteau, A., Cai, F., Tandeau de Marsac, N., Rippka, R., Herdman, M., Sivonen, K., Coursin, T., Laurent, T., Goodwin, L., *et al.* (2013) Improving the coverage of the cyanobacterial phylum using diversity-driven genome sequencing. *Proc. Natl. Acad. Sci. U. S. A.* **110**, 1053–1058
22. Copeland, A., Lucas, S., Lapidus, A., Barry, K., Detter, J. C., Glavina, T., Hammon, N., Israni, S., Pitluck, S., Schmutz, J., Larimer, F., Land, M. M., Kyrpides, N., Lykidis, A., Golden, S., *et al.* (2014) *Complete Sequence of Chromosome 1 of* Synechococcus elongatus *PCC 7942*, National Library of Medicine (US), National Center for Biotechnology Information, Bethesda, MD
23. Ito, T., Ezaki, N., Tsuruoka, T., and Niida, T. (1971) Structure of SF-666 A and SF-666 B, new monosaccharides. *Carbohydr. Res.* **17**, 375–382
24. Li, B., Sher, D., Kelly, L., Shi, Y., Huang, K., Knerr, P. J., Joewono, I., Rusch, D., Chisholm, S. W., and van der Donk, W. A. (2010) Catalytic promiscuity in the biosynthesis of cyclic peptide secondary metabolites in planktonic marine cyanobacteria. *Proc. Natl. Acad. Sci. U. S. A.* **107**, 10430–10435
25. Chattopadhyay, M. K., Tabor, C. W., and Tabor, H. (2006) Methylthioadenosine and polyamine biosynthesis in a *Saccharomyces cerevisiae meu1*Δ mutant. *Biochem. Biophys. Res. Commun.* **343**, 203–207
26. Kamatani, N., and Carson, D. A. (1980) Abnormal regulation of methylthioadenosine and polyamine metabolism in methylthioadenosine phosphorylase-deficient human leukemic cell lines. *Cancer Res.* **40**, 4178–4182
27. Sugita, C., Ogata, K., Shikata, M., Jikuya, H., Takano, J., Furumichi, M., Kanehisa, M., Omata, T., Sugiura, M., and Sugita, M. (2007) Complete nucleotide sequence of the freshwater unicellular cyanobacterium *Synechococcus elongatus* PCC 6301 chromosome: Gene content and organization. *Photosynth Res.* **93**, 55–67
28. Lee, J. E., Settembre, E. C., Cornell, K. A., Riscoe, M. K., Sufrin, J. R., Ealick, S. E., and Howell, P. L. (2004) Structural comparison of MTA phosphorylase and MTA/AdoHcy nucleosidase explains substrate preferences and identifies regions exploitable for inhibitor design. *Biochemistry* **43**, 5159–5169
29. Plagemann, P. G., and Wohlhueter, R. M. (1983) 5′-Deoxyadenosine metabolism in various mammalian cell lines. *Biochem. Pharmacol.* **32**, 1433–1440
30. Koonin, E. V., and Tatusov, R. L. (1994) Computer analysis of bacterial haloacid dehalogenases defines a large superfamily of hydrolases with diverse specificity. Application of an iterative approach to database search. *J. Mol. Biol.* **244**, 125–132
31. Burroughs, A. M., Allen, K. N., Dunaway-Mariano, D., and Aravind, L. (2006) Evolutionary genomics of the HAD superfamily: Understanding the structural adaptations and catalytic diversity in a superfamily of phosphoesterases and allied enzymes. *J. Mol. Biol.* **361**, 1003–1034
32. Pradel, E., and Boquet, P. L. (1988) Acid phosphatases of *Escherichia coli*: Molecular cloning and analysis of *agp*, the structural gene for a periplasmic acid glucose phosphatase. *J. Bacteriol.* **170**, 4916–4923
33. Kuznetsova, E., Proudfoot, M., Gonzalez, C. F., Brown, G., Omelchenko, M. V., Borozan, I., Carmel, L., Wolf, Y. I., Mori, H., Savchenko, A. V., Arrowsmith, C. H., Koonin, E. V., Edwards, A. M., and Yakunin, A. F. (2006) Genome-wide analysis of substrate specificities of the *Escherichia coli* haloacid dehalogenase-like phosphatase family. *J. Biol. Chem.* **281**, 36149–36161
34. Schroeder, H. R., Barnes, C. J., Bohinski, R. C., Mumma, R. O., and Mallette, M. F. (1972) Isolation and identification of 5-methylthioribose from *Escherichia coli* B. *BBA Gen. Subjects* **273**, 254–264
35. Hughes, J. A. (2006) *In vivo* hydrolysis of *S*-adenosyl-L-methionine in *Escherichia coli* increases export of 5-methylthioribose. *Can. J. Microbiol.* **52**, 599–602
36. Albers, E. (2009) Metabolic characteristics and importance of the universal methionine salvage pathway recycling methionine from 5′-methylthioadenosine. *IUBMB Life* **61**, 1132–1142
37. Zappia, V., Della Ragione, F., Pontoni, G., Gragnaniello, V., and Cartenì-Farina, M. (1988) Human 5′-deoxy-5′-methylthioadenosine phosphorylase: Kinetic studies and catalytic mechanism. In: Zappia, V., Pegg, A. E., eds. *Progress in Polyamine Research. Novel Biochemical, Pharmacological, and Clinical Aspects*, Springer US, Boston, MA: 165–177
38. Turner, D. H., and Turner, J. F. (1960) The hydrolysis of glucose monophosphates by a phosphatase preparation from pea seeds. *Biochem. J.* **74**, 486–491
39. Herter, T., Berezina, O. V., Zinin, N. V., Velikodvorskaya, G. A., Greiner, R., and Borriss, R. (2006) Glucose-1-phosphatase (AgpE) from *Enterobacter cloacae* displays enhanced phytase activity. *Appl. Microbiol. Biotechnol.* **70**, 60–64
40. Suleimanova, A. D., Beinhauer, A., Valeeva, L. R., Chastukhina, I. B., Balaban, N. P., Shakirov, E. V., Greiner, R., and Sharipova, M. R. (2015) Novel glucose-1-phosphatase with high phytase activity and unusual metal ion Activation from Soil Bacterium *Pantoea* sp. strain 3.5.1. *Appl. Environ. Microbiol.* **81**, 6790–6799
41. Ma, L., Bartholome, A., Tong, M. H., Qin, Z., Yu, Y., Shepherd, T., Kyeremeh, K., Deng, H., and O'Hagan, D. (2015) Identification of a fluorometabolite from *Streptomyces* sp. MA37: (*2R3S4S*)-5-fluoro-2,3,4-trihydroxypentanoic acid. *Chem. Sci.* **6**, 1414–1419
42. Blombach, B., and Takors, R. (2015) CO_2 - Intrinsic product, essential substrate, and regulatory trigger of microbial and mammalian production processes. *Front. Bioeng. Biotechnol.* **3**, 108
43. Abuaita, B. H., and Withey, J. H. (2009) Bicarbonate Induces *Vibrio cholerae* virulence gene expression by enhancing ToxT activity. *Infect. Immun.* **77**, 4111–4120
44. Burnap, R. L., Hagemann, M., and Kaplan, A. (2015) Regulation of CO_2 concentrating mechanism in cyanobacteria. *Life* **5**, 348–371
45. Selim, K. A., Haase, F., Hartmann, M. D., Hagemann, M., and Forchhammer, K. (2018) P_{II}-like signaling protein SbtB links cAMP sensing with cyanobacterial inorganic carbon response. *Proc. Natl. Acad. Sci. U. S. A.* **115**, E4861–E4869
46. Yang, Y., Lam, V., Adomako, M., Simkovsky, R., Jakob, A., Rockwell, N. C., Cohen, S. E., Taton, A., Wang, J., Lagarias, J. C., Wilde, A., Nobles, D. R., Brand, J. J., and Golden, S. S. (2018) Phototaxis in a wild isolate of the cyanobacterium *Synechococcus elongatus*. *Proc. Natl. Acad. Sci. U. S. A.* **115**, E12378–E12387
47. Golden, S. S. (2019) The international journeys and aliases of *Synechococcus elongatus*. *N.Z. J. Bot.* **57**, 70–75
48. Czerwik-Marcinkowska, J., and Mrozińska, T. (2011) Algae and cyanobacteria in caves of the polish Jura. *Polish Bot. J.* **56**, 203–243
49. Mattern, H., and Mareš, J. (2018) Cyanobacteria. In: Stutz, S., Mattern, H., eds. *Beiträge zu den Algen Baden-Württembergs. Band 1. Allgemeiner Teil & Cyanobacteria, Glaucobionta, Rhodobionta und Chlorobionta*, Verlag Manfred Hennecke
50. Conradi, F. D., Mullineaux, C. W., and Wilde, A. (2020) The role of the cyanobacterial type IV Pilus Machinery in finding and Maintaining a favourable environment. *Life* **10**, 252
51. Rossi, F., and Philippis, R de (2015) Role of cyanobacterial exopolysaccharides in phototrophic biofilms and in complex microbial mats. *Life* **5**, 1218–1238
52. Rippka, R., Deruelles, J., Waterbury, J. B., Herdman, M., and Stanier, R. Y. (1979) Generic Assignments, strain Histories and Properties of pure cultures of cyanobacteria. *J. Gen. Microbiol.* **111**, 1–61
53. Sairam, P., Puranik, R., Sreenivasa Rao, B., Veerabhadra Swamy, P., and Chandra, S. (2003) Synthesis of 1,2,3-tri-*O*-acetyl-5-deoxy-D-ribofuranose from D-ribose. *Carbohydr. Res.* **338**, 303–306
54. Zhang, J. T., Chen, S. P., Feng, J. M., Liu, D. W., Tang, L. J., Wang, X. J., and Huang, S. P. (2013) Synthetic study of 1, 2, 3-tri-*O*-Acetyl-5-Deoxy-D-Ribofuranose. *Adv. Mat Res.* **781-784**, 1184–1186
55. Kobori, Y., Myles, D. C., and Whitesides, G. M. (1992) Substrate specificity and carbohydrate synthesis using transketolase. *J. Org. Chem.* **57**, 5899–5907

56. Gibson, D. G. (2011) Enzymatic assembly of overlapping DNA fragments, p. 349–361. In Voigt, C., ed., *Methods in Enzymology: Synthetic Biology, Part B* **498**. Academic Press, San Diego, CA
57. Clerico, E. M., Ditty, J. L., and Golden, S. S. (2007) Specialized Techniques for Site-directed Mutagenesis in cyanobacteria, p. 155–171. In: Rosato, E., ed. *Circadian Rhythms. Methods and Protocols*, Humana Press, Totowa, NJ
58. Fürtauer, L., Weckwerth, W., and Nägele, T. (2016) A Benchtop Fractionation Procedure for Subcellular analysis of the plant Metabolome. *Front Plant Sci.* **7**, 1912
59. Weckwerth, W., Wenzel, K., and Fiehn, O. (2004) Process for the integrated extraction, identification and quantification of metabolites, proteins and RNA to reveal their co-regulation in biochemical networks. *Proteomics* **4**, 78–83
60. Kanehisa, M., and Goto, S. (2000) Kegg: Kyoto Encyclopedia of genes and genomes. *Nucleic Acids Res.* **28**, 27–30
61. Sekowska, A., Denervaud, V., Ashida, H., Michoud, K., Haas, D., Yokota, A., and Danchin, A. (2004) Bacterial variations on the methionine salvage pathway. *BMC Microbiol* **4**, 9

Supporting information for:

A bioactive molecule made by unusual salvage of radical SAM enzyme by-product 5-deoxyadenosine blurs the boundary of primary and secondary metabolism

Johanna Rapp, Pascal Rath, Joachim Kilian, Klaus Brilisauer, Stephanie Grond, Karl Forchhammer

Results

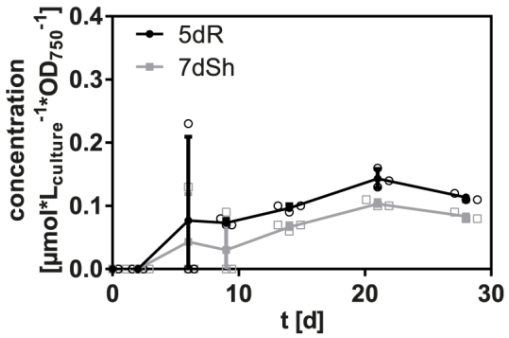

Figure S1: Only small intracellular 5dR and 7dSh accumulation in *S. elongatus.* Concentration of 5dR (black dots) and 7dSh (grey squares) in *S. elongatus* cells [µmol*$L^{-1}_{culture}$*OD_{750}^{-1}] aerated with air supplemented with 2 % CO_2.

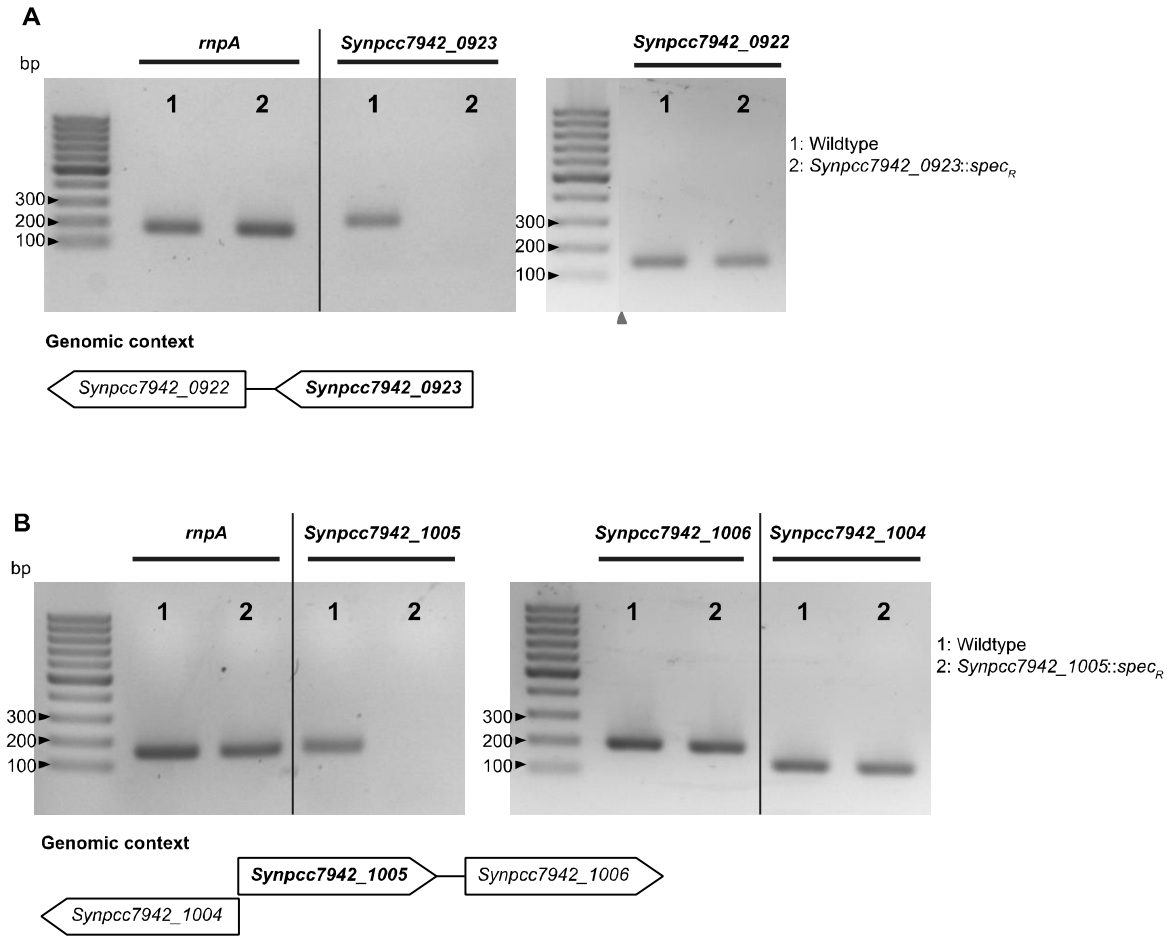

Figure S2: Gene expression of selected genes in *S. elongatus* wildtype and in the insertion mutants *Synpcc7942_0923*::*spec*$_R$ (A) and *Synpcc7942_1005*::*spec*$_R$ (B) determined by semi-quantitative RT-PCR and genomic context of the deleted genes. RNA was extracted from the cell pellets, converted into cDNA by using reverse transcriptase. Gene expression was determined by amplifying the deleted gene and down- or upstream genes by using gene-specific primers (see Table S4) resulting in fragments of 100-200 bp. Amplified fragments were analysed by using agarose gel-electrophoresis. Splice borders are labelled with grey triangle, but marker and samples were run on the same gel. The expression of the house-keeping gene *rnpA* served as a control.

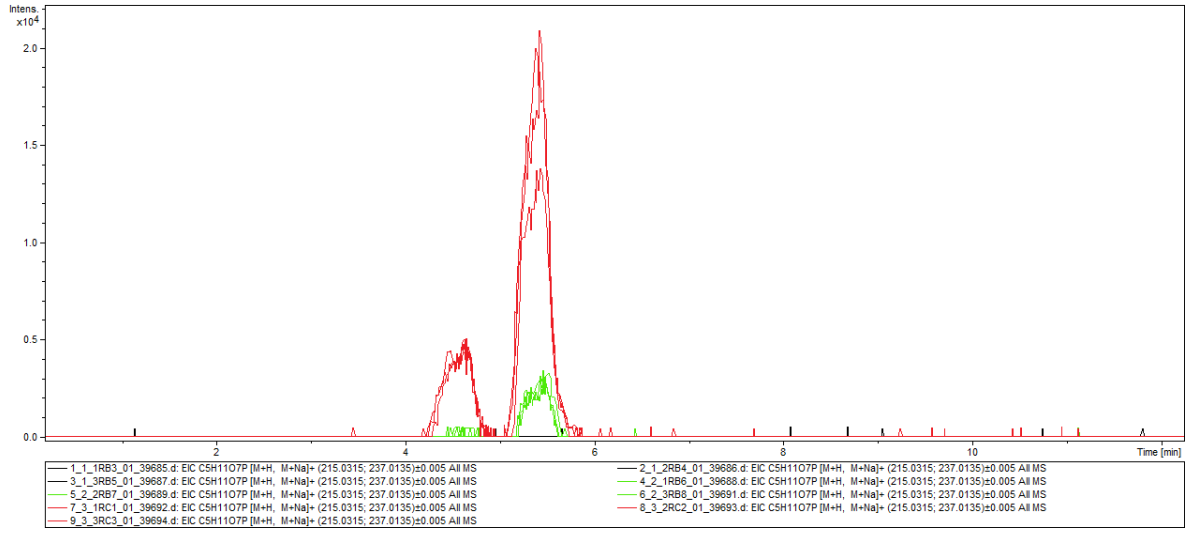

Figure S3: 5dR-1P accumulates in crude extracts of *S. elongatus* that were incubated in the presence of phosphate. Accumulation of 5dR-1P shown as extracted ion chromatogram [M+H, M+Na]+ (*m/z* 215.0315; *m/z* 237.0135) in crude extracts of *S. elongatus*, (Red – with 5dAdo+potassium phosphate buffer (PPB); green – with 5dAdo, no PPB; black – without 5dAdo, PPB). Three independent replicates are shown for each treatment. One part of the samples of the crude extract assays was analysed via high resolution LC-MS (C18 Gemini, solvent A: ACN+0.1 %TFA, solvent B: H_2O, 1% - 20% B in 20 min, Maxis 4G ESI-QTOF).

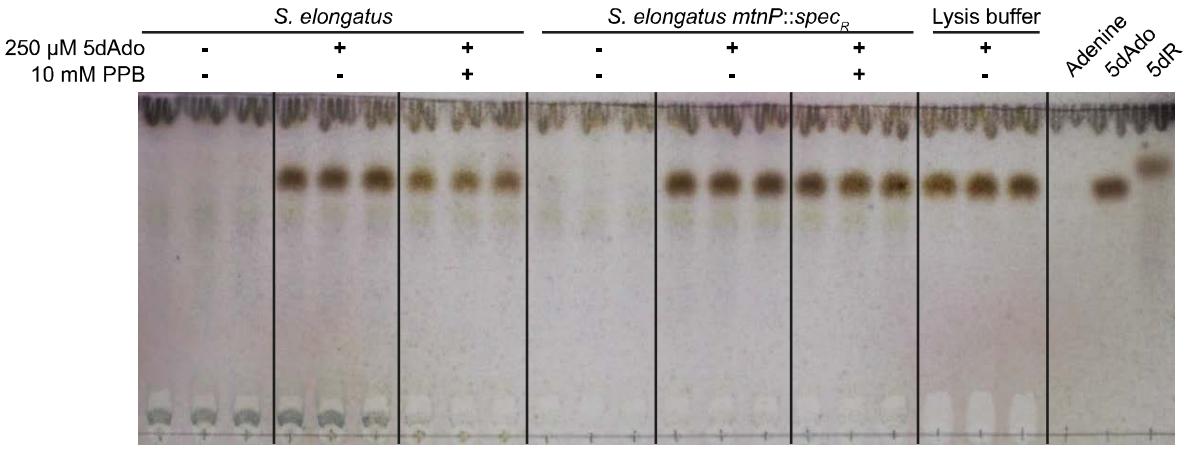

Figure S4: 5dR does not accumulate in crude extracts which were incubated with 5dAdo. Crude extracts from *S. elongatus* or *S. elongatus mtnP*::*spec*$_R$ were incubated with 5dAdo in the presence or absence of potassium phosphate buffer (PPB) and then analysed via thin layer chromatography (TLC). TLC plate from Figure 7 (main text) was sprayed with anisaldehyde after UV-visualisation. Pure adenine, 5dAdo and 5dR were used as standards (right). Adenine is only visible with UV-visualisation (see Figure 7, main text). Three independent replicates are shown for each condition.

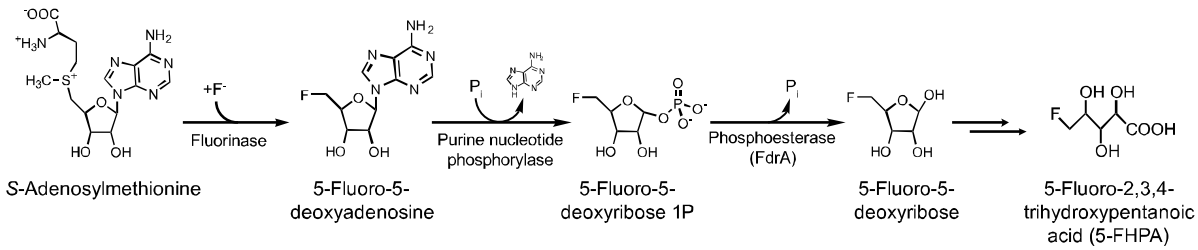

Figure S5: Biosynthesis of the fluoro-metabolite 5-FHPA in *Streptomyces* sp. MA37 (modified after (1)).

Table S1: Overview of MSP genes present in different cyanobacteria.

Gene name in *B. subtilis*		MtnN	MtnK	MtnP*	MtnA	MtnB	MtnC***	MtnX	MtnW	MtnD	MtnE
Gene Product		MTA nucleosidase	MTR kinase	MTA phosphory-lase	MTR-1P isomerase	MTRu-1P dehydratase **	enolase/ phosphatase[*1]	phospha-tase[*2]	enolase[*3]	dioxygenase[*4]	amino transferase ****
Strain	Identifier	EC 3.2.2.9	EC 2.7.1.100	EC 2.4.2.28	EC 5.3.1.23	EC 4.2.1.109	EC 3.1.3.77	EC 3.1.3.87	EC 5.3.2.5	EC 1.13.11.53/54	EC 2.6.1.117
PCC 7942	syf: Synpcc7942_	-	-	0923	1992	1993	1994	0510	-	0608	2.6.1.-
PCC 6301	syc: syc	-	-	0619_d	2104_d	2103_c	2102_c	1010_d	-	0916_c	2.6.1.-
PCC 7002	syp: SYNPCC7002_	-	-	A0108	A2308	A0554	A0552	A0257	-	A0553	2.6.1.-
PCC 6803	syn:	-	-	sll0135	slr1938	-	-	-	-	-	2.6.1.-
PCC 7120	ana:	-	-	alr4054	all3566	-	-	-	-	all2724	2.6.1.-
PCC 7502	synp: Syn7502_	-	-	03055	00983	-	-	-	-	-	2.6.1.-
PCC 6312	syne: Syn6312_	-	-	2991	2219	-	-	-	-	-	2.6.1.-
ATCC 29431	ava:	-	-	Ava_1653	Ava_3544	-	-	-	-	Ava_4291	2.6.1.-
ATCC 29133	npu: Npun_	-	-	F6610	F5471	-	F4952	-	-	-	2.6.1.-

Gene abbreviations according to *B. subtilis* annotation in which the MSP was discovered (2, 3). Gene identifiers are referred to KEGG (4).

* not in *B. subtilis*

** For *A. thaliana* MTR-1P dehydratase (DEP1) moonlighting aldolase activity on 5-deoxyribulose 1-phosphate was shown (5).

*** not in *B. subtilis*. MtnC (EC 3.1.3.77) is a bifunctional enzyme, which has enolase and phosphatase activity. In *B. subtilis* this step is performed by two enzymes (MtnW: 2,3-diketo-5-methylthiopentyl-1-phosphate enolase (EC 5.3.2.5) and MtnX: 2-hydroxy-3-keto-5-methylthiopentenyl-1-phosphate phosphatase (EC 3.1.3.87).

**** aminotransferases are normally broad specificity enzymes (3)

[*1] 2,3-dioxomethio-pentane-1P enolase/phosphatase

[*2] 2-hydroxy-3-keto-5-methylthiopentenyl-1-phosphate phosphatase

[*3] 2,3-diketo-5-methylthiopentyl-1-phosphate enolase

[*4] 1,2-dihydroxy-3-keto-5-methylthiopentene dioxygenase

Table S2: Genes encoding for SAM radical enzymes in *S. elongatus* PCC 7942. KEGG genes were examined for the presence of the Pfam motif PF04055 (SAM_radical), which is a distinctive feature of radical SAM enzymes. Table shows accession number and annotations from KEGG. GenBank annotations are only shown if using another annotation.

Accesion No.	Annotation
Synpcc7942_0419	K01012 biotin synthase [EC:2.8.1.6]
Synpcc7942_0542	K03644 lipoyl synthase [EC:2.8.1.8]
Synpcc7942_0686	K11781 5-amino-6-(D-ribitylamino)uracil---L-tyrosine 4-hydroxyphenyl transferase [EC:2.5.1.147] | (GenBank) FO synthase subunit 2
Synpcc7942_0799	no KO assigned | (GenBank) Elongator protein 3
Synpcc7942_0838	no KO assigned | (GenBank) Elongator protein 3/MiaB/NifB
Synpcc7942_0877	no KO assigned | (GenBank) Elongator protein 3/MiaB/NifB
Synpcc7942_0892	K11780 7,8-didemethyl-8-hydroxy-5-deazariboflavin synthase [EC:4.3.1.32] | (GenBank) FO synthase subunit 1
Synpcc7942_0945	no KO assigned | (GenBank) conserved hypothetical protein
Synpcc7942_1229	K05936 precorrin-4/cobalt-precorrin-4 C11-methyltransferase [EC:2.1.1.133 2.1.1.271]
Synpcc7942_1282	K03639 GTP 3',8-cyclase [EC:4.1.99.22] | (GenBank) GTP cyclohydrolase subunit MoaA
Synpcc7942_1332	K10026 7-carboxy-7-deazaguanine synthase [EC:4.3.99.3] | (GenBank) conserved hypothetical protein
Synpcc7942_1507	K03644 lipoyl synthase [EC:2.8.1.8] | (GenBank) lipoic acid synthetase
Synpcc7942_1621	no KO assigned | (GenBank) Elongator protein 3/MiaB/NifB
Synpcc7942_1652	no KO assigned | (GenBank) Elongator protein 3/MiaB/NifB
Synpcc7942_1758	K06941 23S rRNA (adenine2503-C2)-methyltransferase [EC:2.1.1.192] | (GenBank) conserved hypothetical protein
Synpcc7942_2374	K06168 tRNA-2-methylthio-N6-dimethylallyladenosine synthase [EC:2.8.4.3] | (GenBank) tRNA-i(6)A37 thiotransferase enzyme MiaB
Synpcc7942_2382	no KO assigned | (GenBank) coproporphyrinogen III oxidase, anaerobic
Synpcc7942_2512	K14441 ribosomal protein S12 methylthiotransferase [EC:2.8.4.4] | (GenBank) Protein of unknown function UPF0004

Table S3: Genes encoding for phosphoric monoester hydrolases [EC: 3.1.3.-] in *S elongatus* PCC 7942. Table shows accession number and annotations from KEGG. GenBank annotations are only shown if using another annotation.

Accesion No.	Annotation
Synpcc7942_0173	K01082 3'(2'), 5'-bisphosphate nucleotidase [EC:3.1.3.7] | (GenBank) 3'-Phosphoadenosine 5'-phosphosulfate (PAPS) 3'-phosphatase-like
Synpcc7942_0463	K01104 protein-tyrosine phosphatase [EC:3.1.3.48] | (GenBank) protein tyrosine phosphatase
Synpcc7942_0485	K22305 phosphoserine phosphatase [EC:3.1.3.3] | (GenBank) phosphoglycerate mutase
Synpcc7942_0505	K11532 fructose-1,6-bisphosphatase II / sedoheptulose-1,7-bisphosphatase [EC:3.1.3.11 3.1.3.37]
Synpcc7942_0510	K08966 2-hydroxy-3-keto-5-methylthiopentenyl-1-phosphate phosphatase [EC:3.1.3.87]
Synpcc7942_0613	K08296 phosphohistidine phosphatase [EC:3.1.3.-] | (GenBank) phosphohistidine phosphatase, SixA
Synpcc7942_0693	K01091 phosphoglycolate phosphatase [EC:3.1.3.18] | (GenBank) conserved hypothetical protein
Synpcc7942_0791	K00974 tRNA nucleotidyltransferase (CCA-adding enzyme) [EC:2.7.7.72 3.1.3.- 3.1.4.-] | (GenBank) polyA polymerase
Synpcc7942_0965	K01082 3'(2'), 5'-bisphosphate nucleotidase [EC:3.1.3.7] | (GenBank) ammonium transporter protein Amt1-like
Synpcc7942_0976	K00974 tRNA nucleotidyltransferase (CCA-adding enzyme) [EC:2.7.7.72 3.1.3.- 3.1.4.-] | (GenBank) CBS
Synpcc7942_1005	K20866 glucose-1-phosphatase [EC:3.1.3.10] | (GenBank) HAD-superfamily hydrolase subfamily IA, variant 3
Synpcc7942_1130	K01090 protein phosphatase [EC:3.1.3.16] | (GenBank) protein serine/threonine phosphatase
Synpcc7942_1515	K01090 protein phosphatase [EC:3.1.3.16] | (GenBank) protein serine/threonine phosphatase
Synpcc7942_1553	K07053 3',5'-nucleoside bisphosphate phosphatase [EC:3.1.3.97] | (GenBank) Phosphoesterase PHP-like
Synpcc7942_1763	K01092 myo-inositol-1(or 4)-monophosphatase [EC:3.1.3.25] | (GenBank) inositol monophosphate family protein
Synpcc7942_1931	K07313 serine/threonine protein phosphatase 1 [EC:3.1.3.16] | (GenBank) probable serine/threonine protein phosphatase
Synpcc7942_1994	K09880 enolase-phosphatase E1 [EC:3.1.3.77] | (GenBank) 2,3-diketo-5-methylthio-1-phosphopentane phosphatase
Synpcc7942_2063	K03787 5'-nucleotidase [EC:3.1.3.5] | (GenBank) exopolyphosphatase / 5'-nucleotidase / 3'-nucleotidase
Synpcc7942_2076	K06949 ribosome biogenesis GTPase / thiamine phosphate phosphatase [EC:3.6.1.- 3.1.3.100] | (GenBank) GTPase EngC
Synpcc7942_2288	K03270 3-deoxy-D-manno-octulosonate 8-phosphate phosphatase (KDO 8-P phosphatase) [EC:3.1.3.45] | (GenBank) Phosphatase kdsC
Synpcc7942_2335	K03841 fructose-1,6-bisphosphatase I [EC:3.1.3.11] | (GenBank) D-fructose 1,6-bisphosphatase
Synpcc7942_2473	K07315 phosphoserine phosphatase RsbU/P [EC:3.1.3.3] | (GenBank) serine phosphatase
Synpcc7942_2582	K01092 myo-inositol-1(or 4)-monophosphatase [EC:3.1.3.25]
Synpcc7942_2589	K05979 2-phosphosulfolactate phosphatase [EC:3.1.3.71]
Synpcc7942_2613	K01091 phosphoglycolate phosphatase [EC:3.1.3.18] | (GenBank) HAD-superfamily hydrolase subfamily IA

Material & Methods

Table S4: Oligonucleotides for PCR amplification (G), sequencing (S) and semi-quantitative RT-PCR (qPCR). Overlapping fragments for Gibson cloning are labelled in bold.

Name	Sequence (5‘ → 3‘)
46_0923_up_fw (G)	**AGCTCGGTACCCGGGGATCCT**GGCCTCTACCGAATGGAAGC
47_0923_up_rev (G)	**CTGCGTTCGGTCAAGAGCT**TTGCCAAAGAAGGTCGAAGG
32_Spec_fw (G)	GAGCTCTTGACCGAACGCAG
33_Spec_rev (G)	TTATTTGCCGACTACCTTGGTGATCTC
48_0923_down_fw (G)	**GAGATCACCAAGGTAGTCGGCAAATAA**CCCAGATTATCGGCATGACC
49_0923_down_rev (G)	**ACGCCAAGCTTGCATGCCTGCA**TGCAGGAGTAGTGCCAAACG
1064_pUC19_fw (S)	TGCTGCAAGGCGATTAAGTTGGG
1065_pUC19_rev (S)	CGACAGGTTTCCCGACTGGAAAG
50_0923_rev_seg (S)	CTAGTCGACCCGCTTCAACC
51_0923_fw_seg (S)	GCCACCAAGGATCCCAGATG
85_1005_up_fw	**AGCTCGGTACCCGGGGATCCT**TACAACCGCCTCAAGTGC
86_1005_up_rev	**CTGCGTTCGGTCAAGAGCT**ATGGAGCGTCCCGAAGTAAG
87_1005_down_fw	**GAGATCACCAAGGTAGTCGGCAAATAA**ATGCTTGCTCGTCTTGG
88_1005_down_rev	**ACGCCAAGCTTGCATGCCTGCA**GCTGCTCCAAAGGCAAAC
77_rnpA_fw (qPCR)	GAGTCCGTCAACGAAAGTC
78_rnpA_rev (qPCR)	GTGAGCAGGCCATCAAAG
107_0922_fw (qPCR)	CTGAGCTTGTCGCCATTC
108_0922_rev (qPCR)	GGCAAGGCATTACGGAAG
91_0923_fw (qPCR)	TTCTTTCGGCCTCAGCAG
92_0923_rev (qPCR)	TCGGCCAGTAGTTGACTC
79_1005_fw (qPCR)	GACTGGCACGCTCTTTAC
80_1005_rev (qPCR)	GGCATTCCAAGCCGTATC
105_1006_fw (qPCR)	TCTGCGATCGGCTATCTC
106_1006_rev (qPCR)	TCGCTTGTTGTCCAATCG
109_1004_fw (qPCR)	CGCTTGGGTGTAGTTGAC
110_1004_rev (qPCR)	CCGAGTTCGTGCTGATTC

Chemical synthesis of 5-deoxyribose and 7-deoxysedoheptulose

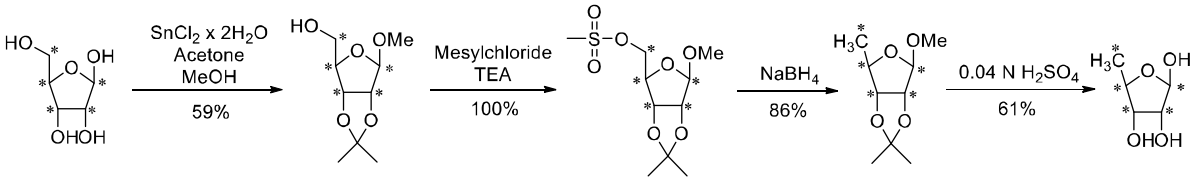

Figure S6: Four step synthesis of [U-$^{13}C_5$]-5dR modified after(6, 7). (1): $^{13}C_5$-D-Ribose, (2): Methyl-2,3-*O*-isopropylidene-$^{13}C_5$-β-D-ribofuranoside, (3): Methyl-2,3-*O*-isopropylidene-5-*O*-mesyl-$^{13}C_5$-β-D-ribofuranoide, (4): Methyl-2,3-*O*-isopropylidene-$^{13}C_5$-5-deoxy-β-D-ribofuranoide, (5): [U-$^{13}C_5$]-5-Deoxy-D-ribofuranose.

Physiochemical data of intermediates of the chemical synthesis

Abbreviations: TLC: thin layer chromatography; R_f: retention factor; NMR: nuclear magnetic resonance; MHz: megahertz; $CDCl_3$: deuterated chloroform; δ: chemical shift; ppm: part per million; dm: doublet of multiplet; *J*: coupling constants; Hz: hertz; ddm: doublet of doublet of multiplet; d: doublet; s: singlet; m: multiplet; HR-(+)ESI-MS: High resolution-electrospray-mass spectrometry (positive mode); m/z: mass-to-charge ratio; calcd: calculated; ddd: doublet of doublet of doublet; D_2O; deuterium oxide.

Methyl-2,3-*O*-isopropylidene-$^{13}C_5$-β-D-ribofuranoside (2)

TLC: R_f 0.63 (cyclohexane/ethylacetate 1:1)

^{1}H-NMR (400 MHz, $CDCl_3$):
δ (ppm)=4.95 (dm, $J_{1,C\text{-}1}$=174.4 Hz, 1H, 1-H), 4.81 (dm, $J_{3,C\text{-}3}$=160.6 Hz, 1H, 3-H), 4.57 (dm, $J_{2,C\text{-}2}$=158.7 Hz, 1H, 2-H), 4.41 (dm, $J_{4,C\text{-}4}$=155.1 Hz, 1H, 4-H), 3.68 (ddm, $J_{5a,C\text{-}5}$=143.8 Hz, $J_{5a,5b}$=12.6 Hz, 1H, 5a-H), 3.59 (ddm, $J_{5b,C\text{-}5}$=142.0 Hz, $J_{5b,5a}$=12.6 Hz, 1H, 5b-H), 3.42 (d, $J_{\text{-}OCH3,C\text{-}1}$=4.4 Hz, 3H, -O$CH_3$), 1.47 and 1.30 (s, 3H, C$(CH_3)_2$)

^{13}C-NMR (100 MHz, $CDCl_3$):
δ (ppm)=112.2 ($C(CH_3)_2$), 109.8 (d, $J_{C\text{-}1,C\text{-}2}$=48.5 Hz, C-1), 88.4 (dd, $J_{C\text{-}4,C\text{-}3}$=39.8 Hz, $J_{C\text{-}4,C\text{-}5}$=38.9 Hz, C-4), 85.9 (dd, $J_{C\text{-}2,C\text{-}1}$=48.5 Hz, $J_{C\text{-}2,C\text{-}3}$=31.0 Hz, C-2), 81.5 (ddm, $J_{C\text{-}3,C\text{-}4}$=39.8 Hz, $J_{C\text{-}3,C\text{-}2}$=31.0 Hz, C-3), 64.1 (dm, $J_{C\text{-}5,C\text{-}4}$=38.9 Hz, C-5), 55.6 (m, -OCH_3), 26.4 and 24.8 (C$(CH_3)_2$)

HR-(+)ESI-MS: *m/z* calcd. for $[M+H]^+$: 210.1238, found: 210.1239; *m/z* calcd. for $[M+Na]^+$: 232.1058, found: 232.1058.

Methyl-2,3-*O*-isopropylidene-5-*O*-mesyl-$^{13}C_5$-β-D-ribofuranoide (3)

TLC: R_f 0.59 (cyclohexane/ethylacetate 1:1)

^{1}H-NMR (400 MHz, $CDCl_3$):
δ (ppm)=4.98 (ddd, $J_{1,C\text{-}1}$=173.9 Hz, $J_{1,C\text{-}2}$=7.5 Hz, $J_{1,2}$=3.0 Hz, 1H, 1-H), 4.69 (dm, $J_{3,C\text{-}3}$=154.5 Hz, 1H, 3-H), 4.60 (ddm, $J_{2,C\text{-}2}$=158.9 Hz, $J_{2,1}$=3.0 Hz, 1H, 2-H), 4.40 (dm, $J_{4,C\text{-}4}$=155.1 Hz, 1H, 4-H), 4.20 (dm, $J_{5a,C\text{-}5}$=152.1 Hz, 1H, 5a-H), 4.18 (dm, $J_{5b,C\text{-}5}$=154.1 Hz, 1H, 5b-H), 3.34 (d, $J_{\text{-}OCH3,C\text{-}1}$=4.5 Hz, 3H, -O$CH_3$), 3.06 (s, 1H, Mesyl-$CH_3$), 1.47 and 1.30 (s, 3H, C$(CH_3)_2$)

^{13}C-NMR (100 MHz, $CDCl_3$):

δ (ppm)=113.0 (*C*(CH_3)$_2$), 109.7 (d, $J_{C\text{-}1,C\text{-}2}$=49.3 Hz, C-1), 85.0 (dd, $J_{C\text{-}2,C\text{-}1}$=49.3 Hz, $J_{C\text{-}2,C\text{-}3}$=30.7 Hz, C-2), 83.9 (dd, $J_{C\text{-}4,C\text{-}5}$=42.5 Hz, $J_{C\text{-}4,C\text{-}3}$=39.1 Hz, C-4), 81.5 (ddd, $J_{C\text{-}3,C\text{-}4}$=39.1 Hz, $J_{C\text{-}3,C\text{-}2}$=30.7 Hz, $J_{C\text{-}3,C\text{-}5}$=5.5 Hz, C-3), 68.5 (dd, $J_{C\text{-}5,C\text{-}4}$=42.5 Hz, $J_{C\text{-}5,C\text{-}3}$=5.5 Hz, C-5), 55.4 (m, -O*C*H_3), 37.9 (Mesyl-CH_3), 26.5 and 25.0 (C(*C*H_3)$_2$)

HR-(+)ESI-MS: *m/z* calcd. for $[M+H]^+$: 288.1014, found: 288.1013; *m/z* calcd. for $[M+Na]^+$: 310.0833, found: 310.0831.

Methyl-2,3-*O*-isopropylidene-$^{13}C_5$-5-deoxy-β-D-ribofuranoide (4)

TLC: R_f 0.87 (cyclohexane/ethylacetate 1:1)

^{1}H-NMR (700 MHz, $CDCl_3$):
δ (ppm)=4.92 (ddd, $J_{1,C\text{-}1}$=172.3 Hz, $J_{1,C\text{-}2}$=7.5 Hz, $J_{1,2}$=2.6 Hz, 1H, 1-H), 4.61 (ddm, $J_{2,C\text{-}2}$=161.4 Hz, $J_{2,1}$=2.6 Hz, 1H, 2-H), 4.49 (dm, $J_{3,C\text{-}3}$=155.8 Hz, 1H, 3-H), 4.32 (dm, $J_{4,C\text{-}4}$=149.6 Hz, 1H, 4-H), 3.31 (d, $J_{\text{-}OCH3,C\text{-}1}$=4.4 Hz, 3H, -O*C*$H_3$), 1.46 and 1.29 (s, 3H, C(*C*H_3)$_2$), 1.27 (dm, $J_{5,C\text{-}5}$=126.3 Hz, 3H, 5-H)

^{13}C-NMR (176 MHz, $CDCl_3$):
δ (ppm)=112.2 (*C*(CH_3)$_2$), 109.6 (dm, $J_{C\text{-}1,C\text{-}2}$=48.1 Hz, C-1), 85.9 (dm, $J_{C\text{-}2,C\text{-}1}$=48.1 Hz, C-2), 85.3 (dm, $J_{C\text{-}3,C\text{-}4}$=37.7 Hz, C-3), 83.2 (ddm, $J_{C\text{-}4,C\text{-}3}$=$J_{C\text{-}4,C\text{-}5}$=37.7 Hz, C-4), 54,5 (m, -O*C*H_3), 26.6 and 25.1 (C(*C*H_3)$_2$), 21.0 (dm, $J_{C\text{-}5,C\text{-}4}$=37.7 Hz, C-5)

HR-(+)ESI-MS: *m/z* calcd. for $[M+H]^+$: 194.1289, found: 194.1294; *m/z* calcd. for $[M+Na]^+$: 216.1109, found: 216.1111.

[U-$^{13}C_5$]-5-Deoxy-D-ribofuranose (5)

TLC: R_f 0.46 (chloroform/methanol 4:1)

^{1}H-NMR (400 MHz, D_2O):
β-furanose: δ (ppm)=5.18 (dm, $J_{1,C\text{-}1}$=172.1 Hz, 1H, 1-H), 4.00-3.95 (m, 3H, 2-H, 3-H, 4-H), 1.33 (dm, $J_{3,C\text{-}3}$=126.8 Hz, 3H, 5-H)
α-furanose: δ (ppm)= 5.35 (dm, $J_{1,C\text{-}1}$=172.6 Hz, 1H, 1-H), 4.14 (dm, $J_{2,C\text{-}2}$=151.2 Hz, 1H, 2-H), 4.12 (dm, $J_{4,C\text{-}4}$=150.5 Hz, 1H, 4-H), 3.80 (dm, $J_{3,C\text{-}3}$=150.2 Hz 1H, 3-H), 1.24 (dm, $J_{3,C\text{-}3}$=126.8 Hz, 3H, 5-H)

^{13}C-NMR (100 MHz, D_2O):
β-furanose: δ (ppm)= 100.8 (m, C-1), 78.3 (dm, $J_{C\text{-}4,C\text{-}5}$=39.5 Hz, C-4), 75.2 (m, C-2 and C-3), 19.1 (d, $J_{C\text{-}5,C\text{-}4}$=39.5 Hz, C-5)
α-furanose: δ (ppm)= 95.7 (dm, $J_{C\text{-}1,C\text{-}2}$=42.2 Hz, C-1), 78.1 (dm, $J_{C\text{-}4,C\text{-}5}$=39.9 Hz, C-4), 74.8 (m, C-3), 70.4 (dm, $J_{C\text{-}2,C\text{-}1}$=42.2 Hz, C-2), 17.8 (d, $J_{C\text{-}5,C\text{-}4}$=39.9 Hz, C-5)

HR-(+)ESI-MS: *m/z* calcd. for $[M+Na]^+$: 162.0639, found: 162.0640.

[3,4,5,6,7-$^{13}C_5$]-7-Deoxy-D-*altro*-heptulose

TLC: R_f 0.56 (chloroform/methanol 8:5)

^{1}H-NMR (400 MHz, D_2O):
β-furanose δ (ppm)=4.21 (dm, $J_{4,C\text{-}4}$=110.7 Hz, 1H, 4-H), 4.07 (dm, $J_{3,C\text{-}3}$=145.4 Hz, 1H, 3-H), 3.94 (m, 1H, H-6), 3.69 (m, 1H, 5-H), 3.63 (dd, $J_{1a,1b}$=11.8 Hz, $J_{1a,C\text{-}3}$=4.3 Hz, 1H, 1a-H), 3.54 (d, $J_{1b,1a}$=11.8 Hz, $J_{1b,C\text{-}3}$=6.5 Hz, 1H, 1b-H), 1.20 (dm, $J_{7,C\text{-}7}$=126.8 Hz, 3H, 7-H)
α-pyranose δ (ppm)=4.07 (m, 1H, 6-H), 4.03 (m, 1H, 4-H), 3.69 (m, 1H, 3-H), 3.66 (m, 1H, 1a-H), 3.57 (m, 1H, 5-H), 3.40 (m, 1H, 1b-H), 1.26 (dm, $J_{7,C\text{-}7}$=127.1 Hz, 3H, 7-H)
α-furanose δ (ppm)=4.14 (m, 1H, 4-H), 4.06 (m, 1H, 3-H), 3.99 (m, 1H, 6-H), 3.91 (m, 1H, 5-H), 3.92 (m, 1H, 1a-H), 3.64 (m, 1H, 1b-H), 1.20 (dm, $J_{7,C\text{-}7}$=126.8 Hz, 3H, 7-H)

^{13}C-NMR (100 MHz, D_2O):

β-furanose δ (ppm)=101.3 (dm, $J_{C\text{-}2,C\text{-}3}$=44.4 Hz, C-2), 83.5 (dm, ^{1}J=43.4 Hz, 39.0 Hz, ^{2}J=5.4 Hz, C-5), 75.8 (m, C-3); 74.7 (m, C-4), 67.7 (m, C-6), 62.4 (C-1), 17.0 (d, $J_{C\text{-}7,C\text{-}6}$=38.4 Hz, C-7)
α-pyranose δ (ppm)=98.0 (m, C-2), 70.8 (dm, ^{1}J=38.9 Hz, C-4), 68.9 (m, C-5), 67.6 (m, C-3), 64.5 (dm, ^{1}J=41.1 Hz, C-6), 63.8 (C-1), 16.9 (m, C-7)
α-furanose δ (ppm)= 104.4 (m, C-2), 84.7 (dm, ^{1}J=40.9 Hz, C-5), 82.0 (dm, $J_{C\text{-}3,C\text{-}4}$=40.5 Hz, C-3), 75.8 (m, C-4), 66.7 (dm, ^{1}J=38.4 Hz, C-6), 62.9 (m, C-1), 17.0 (d, $J_{C\text{-}7,C\text{-}6}$=37.4 Hz, C-7)

HR-(+)ESI-MS: *m/z* calcd. for $[M+Na]^{+}$: 222.0850, found: 222.0852.

Quantification of metabolites in the culture supernatant via GC-MS

To determine the recovery efficiency of the extraction method from the cell pellets (Figure S7 A), as well as from the supernatant (Figure S7 B), we performed spiking experiments with $^{13}C_5$-5dR and $^{13}C_5$-7dSh.

Recovery efficiency in the cell pellet:
For the standard, we added 5dR, $^{13}C_5$-5dR, 7dSh and $^{13}C_5$-7dSh (1000 pmol each) to 700 µL of the extraction solution and proceeded with extraction, derivatization and GC-MS measurement as described in the Materials & Methods section. Additionally, we added $^{13}C_5$-5dR and $^{13}C_5$-7dSh (1000 pmol each) to cell pellets from day 7 (received from 1.5 mL culture) and analogously performed the extraction, derivatization, and GC-MS measurement. The mean of the peak areas of each compound in the standard was set to 100 %. Peak areas of each compound in the cell pellet were normalized to this. Figure S7 A clearly shows that the recovery efficiency of exogenously added $^{13}C_5$-5dR and $^{13}C_5$-7dSh in the cell pellet (grey bars) does not differ from that of the standard (black bars). Besides the measurement of exogenously added ^{13}C-labelled compounds, we simultaneously also measured the unlabeled endogenously produced compounds in these cell pellets. Only 5.34 % of unlabeled 5dR and 1.43 % of unlabeled 7dSh (in relation to the applied 1000 pmol) were found, which corresponds to concentrations measured in Figure S1.

Recovery efficiency in the supernatant:
To determine the recovery efficiency in the supernatant, we added $^{13}C_5$-5dR and $^{13}C_5$-7dSh (1000 pmol each) to 200 µL of culture supernatant, lyophilized the supernatant and proceeded with extraction, derivatization, and GC-MS measurement as described in the Materials & Methods section. The standard, containing 5dR, $^{13}C_5$-5dR, 7dSh and $^{13}C_5$-7dSh (1000 pmol each) was also lyophilized and then treated as the supernatant sample. The mean of the peak area of each compound in the standard was set to 100 %. Peak areas of each compound in the cell pellet were normalized to this. Figure S7 B clearly shows that the recovery efficiency of exogenously added $^{13}C_5$-5dR and $^{13}C_5$-7dSh in the supernatant (grey bars) does not differ from that of the standard (black bars). Besides the measurement of exogenously added ^{13}C-labelled compounds, we simultaneously also measured the unlabeled endogenously produced compounds in the supernatant of day 14. 218 % of unlabeled 5dR and 6 % of unlabeled 7dSh were found (in relation to the applied 1000 pmol), which corresponds to concentrations measured at this time point.

These experiments show that the extraction and derivatization method described in the Material & Methods section is applicable to culture supernatant as well as cell pellets.

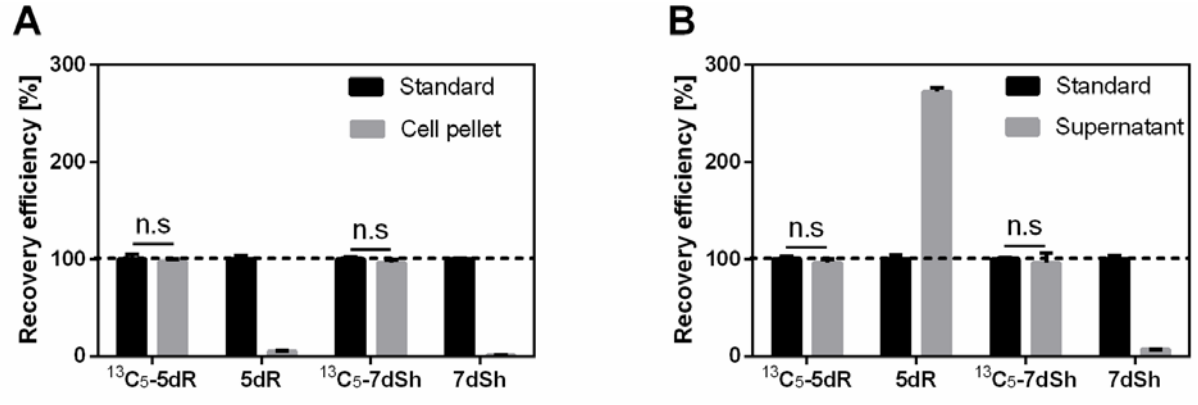

Figure S7: Recovery efficiency of exogenously added $^{13}C_5$-5dR and $^{13}C_5$-7dSh and the amount of unlabeled, endogenously formed 5dR and 7dSh (in relation to the standard containing 1000 pmol of the respective substance) during extraction and derivatization of the cell pellet (A) and the supernatant (B). Mean of peak areas of each compound in the standard was set to 100 %. Values shown in the graph represent mean and standard deviation of three replicates. Significant differences between the recovery efficiency of exogenously added $^{13}C_5$-5dR and $^{13}C_5$-7dSh in the standard and in the cell pellet (A) or in the supernatant (B) were analyzed by using an unpaired t-test (* *p*-value < 0.05; ** *p*-value < 0.01; *** *p*-value < 0.001; n.s.: not significant).

References

1. Ma L, Bartholome A, Tong MH, Qin Z, Yu Y, Shepherd T, Kyeremeh K, Deng H, O'Hagan D. 2015. Identification of a fluorometabolite from *Streptomyces* sp. MA37: (2*R*3*S*4*S*)-5-fluoro-2,3,4-trihydroxypentanoic acid. Chem. Sci. 6:1414–1419. doi:10.1039/C4SC03540B.
2. Sekowska A, Danchin A. 2002. The methionine salvage pathway in *Bacillus subtilis*. BMC Microbiol 2:8. doi:10.1186/1471-2180-2-8.
3. Sekowska A, Denervaud V, Ashida H, Michoud K, Haas D, Yokota A, Danchin A. 2004. Bacterial variations on the methionine salvage pathway. BMC Microbiol 4:9. doi:10.1186/1471-2180-4-9.
4. Kanehisa M, Goto S. 2000. KEGG: Kyoto Encyclopedia of Genes and Genomes. Nucleic Acids Res 28:27–30. doi:10.1093/nar/28.1.27.
5. Beaudoin GAW, Li Q, Folz J, Fiehn O, Goodsell JL, Angerhofer A, Bruner SD, Hanson AD. 2018. Salvage of the 5-deoxyribose byproduct of radical SAM enzymes. Nat Commun 9:3105. doi:10.1038/s41467-018-05589-4.
6. Sairam P, Puranik R, Sreenivasa Rao B, Veerabhadra Swamy P, Chandra S. 2003. Synthesis of 1,2,3-tri-*O*-acetyl-5-deoxy-D-ribofuranose from D-ribose. Carbohydr. Res. 338:303–306. doi:10.1016/S0008-6215(02)00464-0.
7. Zhang JT, Chen SP, Feng JM, Liu DW, Tang LJ, Wang XJ, Huang SP. 2013. Synthetic Study of 1, 2, 3-Tri-*O*-Acetyl-5-Deoxy-D-Ribofuranose. Adv Mat Res 781-784:1184–1186. doi:10.4028/www.scientific.net/AMR.781-784.1184.

Publication 3:

Rapp, Johanna; Wagner, Berenike; Brilisauer, Klaus; Forchhammer, Karl (2021): *In vivo* inhibition of the 3-dehydroquinate synthase by 7-deoxysedoheptulose depends on promiscuous uptake by sugar transporters in cyanobacteria. *Frontiers in Microbiology*, 12 (692986), https://doi.org/10.3389/fmicb.2021.692986, © The Authors.

frontiers in Microbiology

ORIGINAL RESEARCH
published: 23 June 2021
doi: 10.3389/fmicb.2021.692986

In vivo Inhibition of the 3-Dehydroquinate Synthase by 7-Deoxysedoheptulose Depends on Promiscuous Uptake by Sugar Transporters in Cyanobacteria

*Johanna Rapp, Berenike Wagner, Klaus Brilisauer and Karl Forchhammer**

Interfaculty Institute of Microbiology and Infection Medicine, Organismic Interactions, Eberhard Karls Universität Tübingen, Tübingen, Germany

7-Deoxysedoheptulose (7dSh) is a bioactive deoxy-sugar actively excreted by the unicellular cyanobacterium *Synechococcus elongatus* PCC 7942 (*S. elongatus*) but also *Streptomyces setonensis*. In our previous publications we have shown that in *S. elongatus*, 7dSh is exclusively synthesized by promiscuous enzyme activity from an inhibitory by-product of radical SAM enzymes, without a specific gene cluster being involved. Additionally, we showed that 7dSh inhibits the growth of cyanobacteria, but also the growth of plants and fungi, presumably by inhibiting the 3-dehydroquinate synthase (DHQS), the second enzyme of the shikimate pathway, as the substrate of this enzyme strongly accumulates in cells treated with 7dSh. In this study, by using purified DHQS of *Anabaena variabilis* ATCC 29413 (*A. variabilis*) we biochemically confirmed that 7dSh is a competitive inhibitor of this enzyme. By analyzing the effect of 7dSh on a subset of cyanobacteria from all the five subsections, we identified different species whose growth was inhibited by 7dSh. We also found that in some of the susceptible cyanobacteria import of 7dSh is mediated by structurally different and promiscuous transporters: 7dSh can be taken up by the fructose ABC-transporter in *A. variabilis* and via the glucose permease in *Synechocystis* sp. PCC 6803 (*Synechocystis* sp.). In both cases, an effective uptake and thereby intracellular enrichment of 7dSh was essential for the inhibitory activity. Importantly, spontaneous mutations in the sugar transporters of *A. variabilis* and *Synechocystis* sp. not only disabled growth of the two strains on fructose and glucose, respectively, but also almost abolished their sensitivity to 7dSh. Although we have clearly shown in these examples that the effective uptake plays an essential role in the inhibitory effect of 7dSh, questions remain about how 7dSh resistance works in other (cyano)bacteria. Also, the involvement of a putative ribokinase in 7dSh resistance in the producer strain *S. elongatus* remained to be further investigated. Overall, these data establish 7dSh as the first allelochemical targeting the shikimate pathway in other cyanobacteria and plants and suggest a role of 7dSh in niche competition.

Keywords: 7-deoxysedoheptulose, allelopathy and allelochemicals, sugar uptake, 3-dehydroquinate synthase, shikimate pathway inhibitors, cyanobacteria, fructose ABC-transporter, glucose permease

OPEN ACCESS

Edited by:
Wendy Schluchter, University of New Orleans, United States

Reviewed by:
Enrique Flores, Consejo Superior de Investigaciones Científicas Spanish National Research Council (CSIC), Spain
Nir Keren, Hebrew University of Jerusalem, Israel

****Correspondence:***
Karl Forchhammer
karl.forchhammer@uni-tuebingen.de

Specialty section:
This article was submitted to Microbial Physiology and Metabolism, a section of the journal Frontiers in Microbiology

Received: *09 April 2021*
Accepted: *03 June 2021*
Published: *23 June 2021*

Citation:
Rapp J, Wagner B, Brilisauer K and Forchhammer K (2021) In vivo Inhibition of the 3-Dehydroquinate Synthase by 7-Deoxysedoheptulose Depends on Promiscuous Uptake by Sugar Transporters in Cyanobacteria. Front. Microbiol. 12:692986. doi: 10.3389/fmicb.2021.692986

INTRODUCTION

Cyanobacteria colonize the highly diverse habitats of the entire illuminated biosphere. They are found in aquatic habitats–either in salt- or freshwater–but also in the terrestrial environment on rocks and soil, from desert to Antarctica. They may propagate in planktonic lifestyle or may live in microbial mats or biofilms. Their ubiquitous presence in the biosphere is based on various survival strategies, including the production of over 1,100 secondary metabolites (Dittmann et al., 2015), enabling them to compete for their ecological niches or to survive under difficult environmental conditions. Chemically mediated interactions, either positive or negative, between plants, plants and microbes, or microbe–microbe are termed as allelopathic (Rice, 1984; Weir et al., 2004). Among others, allelopathy is a strategy to fight competitors and predators (Leflaive and Ten-Hage, 2007). The ability of cyanobacteria to excrete allelopathic compounds, or allelochemicals, was discovered over 50 years ago in field-studies of freshwater cyanobacteria (Keating, 1977, 1978), but also described for marine cyanobacteria (Paz-Yepes et al., 2013). Allelochemicals from cyanobacteria, such as cyanobacterin from *Scytonema hofmanii* (Gleason and Paulson, 1984) and fischerellin A from *Fischerella muscicola* (Gross et al., 1991) often inhibit the photosystem II. The target organisms are other cyanobacteria, micro- and macro-algae as well as angiosperms (Leão et al., 2009). The majority of bioactive compounds, isolated mostly from few genera (*Lyngbya*, *Microcystis*, *Nostoc*, and *Hapalosiphon*), often have complex chemical structures and are mainly synthesized by gene clusters containing nonribosomal peptide synthetases (NRPS) and or polyketide synthases (PKS) (Dittmann et al., 2015). Although a variety of bioactive compounds have been isolated from cyanobacteria, only a few are considered to act as allelopathic inhibitors in the natural habitat of the producer strains [overview of allelopathic inhibitors from cyanobacteria by Leflaive and Ten-Hage (2007)]. Classification of a bioactive compound as an allelochemical can be controversial in certain cases, because it is difficult to simulate a complex ecosystem in the laboratory (Gross, 2003; Inderjit and Duke, 2003). The following aspects are important, when speculating about a possible role in allelopathic interactions: Allelopathic inhibitors must be excreted by the producer strain and not released by cell lysis, as it is the case for microcystins, which are regularly stored intracellularly (Schatz et al., 2007; Jüttner and Lüthi, 2008; Leão et al., 2009). Another aspect is the capability of the target organisms to take up the inhibitory compound, which is a less addressed topic (Inderjit and Duke, 2003). In the context of allelopathic interactions between cyanobacteria mediated by polar/hydrophilic compounds, the structure of their envelope plays an important role. Although cyanobacteria are regarded as Gram-negative bacteria, possessing an outer membrane, they also possess a thick peptidoglycan layer with a degree of crosslinking that resembles that from Gram-positive bacteria (Hansel and Tadros, 1998; Hoiczyk and Hansel, 2000; Castenholz, 2015). Molecules can pass the outer membrane via relatively unspecific porins, whereas transport over the cytoplasmic membrane is carried out via specific transporter, for example the fructose ABC-transporters (ATP-binding cassette transporters) (Ungerer et al., 2008) or transporters belonging to the major facilitator superfamily like the glucose permease Gtr (Schmetterer, 1990). The allelochemical microcin C possesses a peptide moiety, which is required for the uptake via an ABC-transporter into sensitive cells. Intracellularly, the peptide moiety is cleaved and converted to the mature inhibitor (Metlitskaya et al., 2006; Novikova et al., 2007).

The common unicellular model organism *Synechococcus elongatus* PCC 7942 (thereafter *S. elongatus*) has a small, streamlined genome, which has no known gene cluster for the production of secondary metabolites (Shih et al., 2013; Copeland et al., 2014). Nevertheless, we have recently isolated and characterized a bioactive compound from the supernatant of this strain, which inhibits not only the growth of other cyanobacteria, but also the growth of fungi and plants (Brilisauer et al., 2019). The compound was characterized as a rare deoxy sugar–namely 7-deoxy-D-*altro*-2-heptulose (7-deoxysedoheptulose, 7dSh) (Brilisauer et al., 2019). Recently, we showed that 7dSh derives from 5-deoxyadenosine (5dAdo) (Rapp et al., 2021), an inhibitory by-product of radical SAM enzymes, which are involved in a multitude of reactions (Sofia et al., 2001), for example in the synthesis of the essential cofactors biotin and thiamine (Choi-Rhee and Cronan, 2005; Challand et al., 2010). 5dAdo is metabolized into 5-deoxyribose (5dR) and subsequently converted to 7dSh, by the sole activity of promiscuous enzymes, without a specific gene cluster being involved (Rapp et al., 2021). Therefore, 7dSh is not a "classical" secondary metabolite as it derives from a toxic waste product of the primary metabolism. 5dAdo is only converted to 7dSh under certain environmental conditions, suggesting an unknown regulatory mechanism for the formation of the "secondary" metabolite 7dSh (Rapp et al., 2021). 7dSh is most likely an antimetabolite of the shikimate pathway, as 7dSh treated cells strongly accumulate the structurally similar molecule 3-deoxy-D-*arabino*-heptulosonate 7-phosphate (DAHP), the substrate of the 3-dehydroquinate synthase (DHQS) (see **Figure 1**; Brilisauer et al., 2019). This NAD^+-dependent enzyme catalyzes the conversion of DAHP into 3-dehydroquinate by the release of phosphate (**Figure 1A**). The shikimate pathway consists of seven enzymatic steps that convert erythrose 4-phosphate and phosphoenolpyruvate into chorismate, a precursor molecule for the synthesis of aromatic amino acids, folate cofactors and isoprenoid quinones. Additionally, 7dSh treated *Anabaena variabilis* cells had a significantly reduced content of aromatic amino acids (Brilisauer et al., 2019), further indicating that 7dSh is an inhibitor of this pathway. The pathway is only present in bacteria, including cyanobacteria, fungi, plants, and apicomplexans (Bentley, 1990; Roberts et al., 1998), thereby being a useful target for antibiotics, fungicides, and herbicides.

In this study we confirmed the intracellular target of 7dSh biochemically using purified protein and identified the competitive nature of the inhibitor. Furthermore, we screened the spectrum of sensitive cyanobacteria and elucidated the uptake of 7dSh by two different types of transporters. Effective uptake of 7dSh leading to an intracellular enrichment is essential for the inhibitory effect of 7dSh. The characterization of the target but also the uptake mode is interesting for the ecological function of

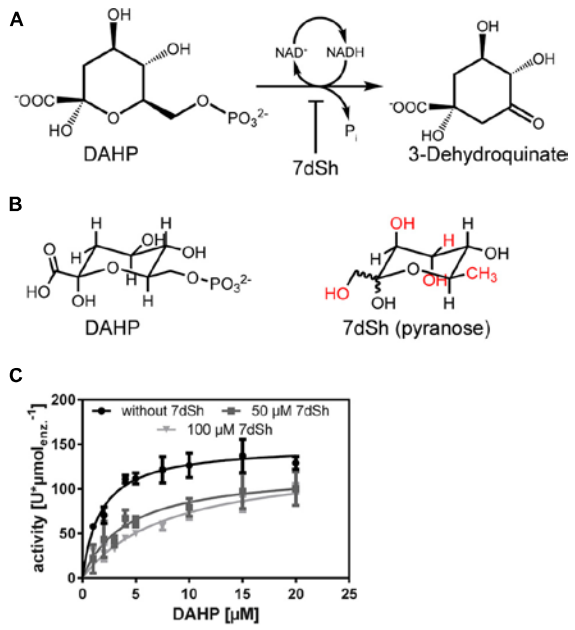

FIGURE 1 | The NAD^+-dependent 3-dehydroquinate synthase (DHQS) mediates the conversion of 3-deoxy-D-*arabino*-heptulosonate 7-phosphate (DAHP) into 3-dehydroquinate by the release of phosphate. 7dSh is an inhibitor of the DHQS-mediated reaction. **(A)** Schematic representation of the DHQS mediated reaction. **(B)** Structural comparison of DAHP and 7-deoxysedoheptulose (7dSh) in its pyranose form. **(C)** Michaelis-Menten of the *Av*DHQS-mediated conversion of DAHP into 3-dehydroquinate in the absence of 7dSh (black dots) or in the presence of 7dSh (dark grey squares–50 µM 7dSh, light grey triangles–100 µM 7dSh). Kinetic parameters are depicted in **Table 3**. Values represent mean and standard deviation of three independent replicates.

TABLE 1 | Cyanobacterial strains used in this study.

Strain
Synechococcus elongatus PCC 7942
Synechococcus elongatus PCC 7942-7dSh^R
Synechococcus elongatus PCC 7942 *Synpcc7942_0116::spec*^{R}
Synechococcus sp. PCC 6301
Synechocystis sp. PCC 6803 GT
Synechocystis sp. PCC 6803 GT-7dSh^R
Synechocystis sp. PCC 6803 GT *sll0771::spec*^{R}
Synechococcus sp. PCC 7002
Synechococcus sp. PCC 6312
Pleurocapsa minor SAG 4.99
Stanieria cyanosphaera SAG 33.87
Phormidium molle SAG 26.99
Leptolyngbya boryana PCC 6306
Oscillatoria acuminata PCC 6304
Anabaena sp. PCC 7120
Anabaena sp. PCC 7120 (pRL1049-*frtRABC*)
Anabaena variabilis ATCC 29413
Anabaena variabilis ATCC 29413-7dSh^R
Nodularia sphaerocarpa SAG 50.79
Nostoc muscorum SAG 1453-12a
Scytonema hofmanii PCC 7110
Chlorogloeopsis fritschii PCC 6912
Fischerella muscicola PCC 7414
Mastigocladus laminosus SAG 4.84

the inhibitor, but also relevant for potential application of 7dSh as an herbicide.

MATERIALS AND METHODS

Cultivation

Cyanobacterial strains (see **Table 1**) were cultivated under photoautotrophic conditions in BG11-medium (Rippka et al., 1979) supplemented with 5 mM $NaHCO_3$, except for *Synechococcus* sp. PCC 7002 which was cultivated in a 1:1 mixture of BG11 and ASN III + vitamin B_{12} (10 µg*mL^{-1}) (Rippka et al., 1979). Cultivation was conducted at 27°C, constant illumination with light intensity of 30–50 µE (Lumilux de Lux, Daylight, Osram) and continuous shaking (125 rpm). Bioactivity assays were performed in a 24-well plate (except for *A. variabilis* and *Anabaena* sp. from **Figure 2**). The respective strains were inoculated with an optical density of OD_{750} = 0.05 in 1 mL BG11 and cultivated for 3–7 days at the conditions mentioned above. Stock solutions of 7dSh, fructose and glucose were set up in water and then applied to the cultures. Final concentrations are shown in the figures. 7dSh was synthesized as described in our previous publications (Brilisauer et al., 2019; Rapp et al., 2021). Cell density of the unicellular strains was determined by the measurement of the absorbance at 750 nm (Specord, Analytik Jena).

Bioactivity assays with *A. variabilis* and *Anabaena* sp. PCC 7120 were performed in shaking flasks with a cultivation volume of 5 mL (**Figure 2**). Flasks were inoculated with a chlorophyll *a* content of around 1.0–1.5 µg*mL^{-1}. Cell density of the filamentous cyanobacteria was determined by measuring the content of chlorophyll *a* as the determination of this is more precise in filamentous strains. In short: 1 mL of the culture was centrifuged (16.000×*g*, 5 min) and the supernatant was discarded. The pellet was extracted with 1 mL 90% (v/v) MeOH and incubated for 30 min in the dark. The cell debris was removed by centrifugation (16.000×*g*, 2 min). Chlorophyll *a* content was measured by the absorbance at 665 nm and the amount was calculated as described elsewhere (Mackinney, 1941).

For heterotrophic growth experiments, the cultures were incubated with fructose or glucose in the presence of the photosystem II-inhibitor DCMU [3-(3,4-dichlorophenyl)-1,1-dimethylurea] (Rippka, 1972). DCMU was dissolved in acetone and adjusted to a final concentration of 5 µM.

Spontaneous 7dSh-resistant mutants (7dSh^R) of *A. variabilis*, *Synechocystis* sp. and *S. elongatus* were isolated from cultures that were cultivated at sublethal concentrations of 7dSh (10 µg*mL^{-1} 7dSh for *A. variabilis* and 20 µg*mL^{-1} for *Synechocystis* sp. and *S. elongatus*) and then plated on agar plates containing the same

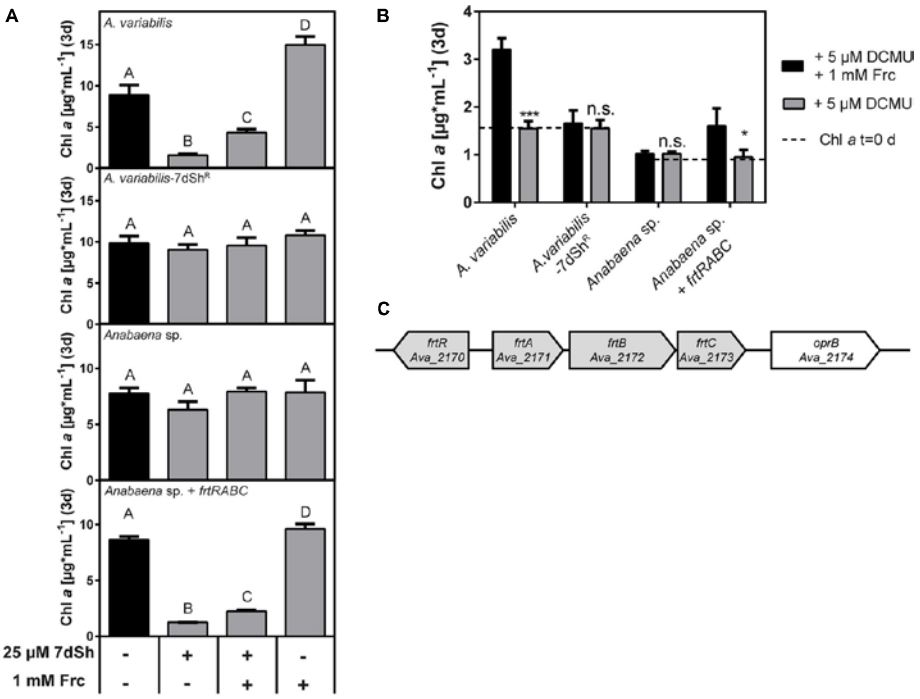

FIGURE 2 | 7-deoxysedoheptulose is taken up via the fructose ABC-transporter in *A. variabilis*. **(A)** Effect of 7dSh, 7dSh in combination with fructose and fructose alone on the growth of *A. variabilis*, *A. variabilis*-7dSh^R, *Anabaena* sp. and *Anabaena* sp. expressing the fructose ABC transporter operon of *A. variabilis* (*Anabaena* sp. + *frtRABC*). The strains were inoculated with a chlorophyll *a* content of around 1 µg*mL^{-1} and cultivated for 3 days. Values shown in the graphs represent mean and standard deviation of three biological replicates. Statistical analysis was performed by using a one-way ANOVA followed by Tukey's multiple comparison test. Means that were significantly different (p-value < 0.05) are marked with different capital letters. **(B)** Photoheterotrophic growth on fructose in the presence of the photosystem II inhibitor DCMU. The strains were inoculated with the indicated chlorophyll *a* content (dashed line) and cultivated for 3 days. Values shown in the graphs represent mean and standard deviation of three biological replicates. Significant photoheterotrophic growth was analyzed by comparing the growth in the presence of DCMU with or without fructose using an unpaired *t*-test (*p-value < 0.05; **p-value < 0.01; ***p-value < 0.001; n.s., not significant). **(C)** Genomic context of the fructose ABC-transporter *frtABC* operon including the regulator *frtR* in *A. variabilis*. The operon is clustered with the putative carbohydrate porin *oprB*.

concentration of 7dSh. One single colony per strain was isolated and then used for bioactivity assays and sequencing (single genes: *gtr*/*sll0771* in *Synechocystis* sp., *frtRABC* in *A. variabilis*, and whole genome sequencing in *S. elongatus*).

Cloning, Expression, Purification, and Activity of the DHQS From *A. variabilis*

The 3-dehydroquinate synthase (EC 4.2.3.4) of *A. variabilis* (Ava_4386) was amplified from genomic DNA with primers 1 and 2 (**Table 2**). Vector pET22b and the amplified gene was cut with NdeI/XhoI and ligated as described elsewhere and then transformed into *Escherichia coli* Top10. With vector pET22b, a His-Tag was introduced on the C-terminus of the protein. The vector was verified by sequencing (LightRun Tube, Eurofins Genomics, Ebersberg, Germany) and then transformed into *E. coli* BL21 (DE3). For protein expression the strain was cultivated in 400 mL LB at 37°C (150 rpm) until an optical density of around $OD_{600} \approx 0.8$. Protein expression was induced with IPTG with a final concentration of 500 µM. After overnight cultivation at 20°C (150 rpm), the cells were harvested by centrifugation (6,000×*g*, 10 min, 4°C). The pellet was resuspended in 40 mL lysis buffer (50 mM *Tris*–HCl pH 7.5, 300 mM NaCl, 10 mM imidazole, protease inhibitor (complete ULTRA tablets, Roche) and DNAseI). Cell disruption was conducted via sonification (Branson, 5 mm tip). Cell debris was removed by centrifugation (40.000×*g*, 45 min, 4°C). The cell lysate was filtered with a syringe filter (0.45 µm) and applied to a HisTrap HP column (1 mL, GE Healthcare Life Science). After washing of the column, the protein was eluted with elution buffer (50 mM *Tris*–HCl, 300 mM NaCl, 250 mM imidazole, pH 7.5). Protein containing fractions were pooled and dialyzed overnight (ZelluTrans MWCO 3500 Da, Roth; in 50 mM *Tris*–HCl pH 8.0, 100 mM NaCl, 5 mM $MgCl_2$, 1 mM DTT, 0.5 mM ETDA, 50% glycerol) and stored at −20°C. Purity was confirmed by SDS-PAGE. Protein concentration was determined with the Bradford method (RotiQuant, Roth).

In the 3-dehydroquinate synthase mediated reaction DAHP is converted into 3-dehydroquinate by the release of phosphate (see **Figure 1A**). The activity of DHQS was determined by phosphate

TABLE 2 | Oligonucleotides used in this study.

Name	Sequence (5′ → 3′)
1_Avar AroB	**GAGAGACATATG**ATGACTTCTGTAATTAATGTGAATCTA
2_Avar AroB rev	**GAGAGACTCGAG**CATCTGCTGTAAAACTTGCCGAA
3_frtR_fw	**ACGGTTTCCCTCTACCGGGATCC**CACAGACCGAAGT GGAAATG
4_frtC_rev	**CGCAAGAGGCCCTTTCGTCTTCAAGAATTC**TGTTCAC GCAACGAGAAACC
5_pRL1049_fw	CGATCCCGCGAAATTAATAC
6_Ava2170_rev	TAGTTGACTTGTAAAGTTTTGCGTACTGAG
7_Gtr_rev	TTTGGGCCTCACTGGGTATC
8_Gtr_fw	GCAACTTGCCATAGGCTAAC
9_0771_up_fw	**AGCTCGGTACCCGGGGATCCT**GGGAAAGGAATTGAT CGG
10_0771_up_rev	**CTGCGTTCGGTCAAGAGCT**GTAAAGCTGAAATTGA AGAAG
11_0771_down_fw	**GAGATCACCAAGGTAGTCGGCAAATAA**TTAATTTTTTAT TTTGAGGGG
12_0771_down_rev	**ACGCCAAGCTTGCATGCCTGCA**CCACCAAACTTTGCA GAG
13_0116_up_fw	**AGCTCGGTACCCGGGGATCCT**TCCGCACCACTTCCC GTTTG
14_0116_up_rev	**CTGCGTTCGGTCAAGAGCT**CCCCGCTTCCCCCGTGG
15_0116_down_fw	**GAGATCACCAAGGTAGTCGGCAAATAA**CTATCTAAAC AGCAAATTAAC
16_0116_down_rev	**ACGCCAAGCTTGCATGCCTGCA**GAGGTTCCATCAGC ATAC
17_0116_seq_fw	TGTGGGTCGTTCGATTCC
18_0116_seq_rev	ATCGGAAGCCAAGTTAGC
19_Spec_fw	GAGCTCTTGACCGAACGCAG
20_Spec_rev	TTATTTGCCGACTACCTTGGTGATCTC
21_2170_fw	ACATTCGTTGGCTGACTG
22_2170_rev	AGCAGGCGTTTCTCATTC
23_2171_fw	ACGGCTGCTGACACTGATAC
24_2171_rev	GATCGCTTCTATGGCTTCTG
25_2172_rev	GATGCTCCAGTTGCATAGTG
26_2172_fw	TTTCTCCACCTGCGACTG
27_2173_fw	ACGAGCATCCCAAATCAC
28_2173_rev	CTGCGGAGTCTGTCAATC

Overlapping fragments for Gibson Assembly are labelled in bold. Underlined sections indicate restriction sites.

release as described by Zhu et al. (2018) with malachite green (Phosphate Assay Kit, abcam, Cambridge, United Kingdom). The reaction was performed in a total volume of 200 µL in a 96-well plate. For this purpose, the prewarmed buffer (25 mM *Tris*–HCl pH 7.5 50 mM KCl) was mixed with 10 µM NAD^+ (Roth), 1 mM DTT (Roth), 2 nM of the enzyme, and varying concentrations of DAHP (Carbosynth, Berkshire, United Kingdom). The reaction was conducted at 29°C. The reaction was stopped by the addition of 30 µL malachite green solution. After 30 min incubation in the dark at room temperature, phosphate release was measured by the absorbance at 650 nm in a microplate reader (Tecan Spark, Männedorf, Switzerland). For the determination of the kinetic parameters of the natural reaction, phosphate release was monitored after 5, 7, and 10 min of reaction. With the slope through this time points, v_{max} and k_M was calculated. Enzyme activities were therefore expressed as phosphate release in micromoles per minute per µmol of the enzyme ($U^*\mu mol_{enz.}{}^{-1}$). The kinetic parameters were determined with GraphPad prism by fitting the data into the following equation: $v = \frac{v_{max} \times [S]}{(k_m + [S])}$.

The inhibition constant k_i was calculated by using the following model: $k_{M\,Obs} = k_M \times \left(\frac{1+[I]}{k_i}\right)$ and $Y = \frac{v_{max} \times X}{(k_{M\,Obs} + X)}$, where $k_{M\ Obs}$ is the Michalis-Menten constant in the presence of a competitive inhibitor.

(Partial) Sequencing of Spontaneous 7dSh-Resistant Mutants

To analyze the genomic background of the spontaneous *A. variabilis*-7dSh^R mutant, genomic DNA of the mutant and the wildtype was isolated and the genomic environment of the fructose ABC-transporter operon (*Ava_2170-Ava_2173*) was investigated (see **Supplementary Figure 2**). Gene specific primers were designed for each single gene of the operon, but also for the whole operon. A PCR with a Taq polymerase (RedTaq Mastermix, Genaxxon bioscience, Ulm, Germany) was performed to amplify these regions. The products were analyzed on an agarose gel.

Genomic DNA of the *Synechocystis* sp.-7dSh^R mutant and wildtype was amplified with a Q5-Polymerase (New England Biolabs, Ipswich, MA, United States) using primers 7+8 (sequence in **Table 2**). The product was analyzed by Sanger sequencing (LightRun Tube, Eurofins).

To obtain high quality genomic DNA of *S. elongatus* wildtype and *S. elongatus*-7dSh^R, the extraction was performed with the DNeasy PowerLyzer Microbial Kit (Qiagen). Whole genome sequencing was performed by CD Genomics ("Microbial Whole Genome Sequencing", New York, NY, United States).

Construction of *Anabaena* sp. (pRL1049-*frtRABC*)

The fructose transporter operon from *A. variabilis* (*Ava_2170-Ava_2173*) was amplified from genomic DNA with the Gibson primers 3+4 (sequence in **Table 2**), adding overlapping fragments to the operon. Vector pRL1049, which is self-replicating in *Anabaena* sp. (Black and Wolk, 1994) was digested with EcoRI and BamHI. After that, the fragments were fused using Gibson Assembly (Gibson, 2011) and transformed in *E. coli* TOP10. The construct was verified by sequencing (LightRun Tube, Eurofins Genomics). Transformation in *Anabaena* sp. was performed by conjugation as previously described (Elhai and Wolk, 1988). The presence of the replicative plasmid in *Anabaena* sp. PCC 7120 was verified by a colony PCR using the primers 5+6 (sequence in **Table 2**). The strain was cultivated in the presence of 5 $\mu g^* mL^{-1}$ spectinomycin and 5 $\mu g^* mL^{-1}$ streptomycin.

Construction of *Synechocystis* sp. *sll0771*::*spec*^{R} and *S. elongatus Synpcc7942_0116*::*spec*^{R}

For the construction of the insertion mutants *Synechocystis* sp. *sll0771*::*spec*^{R} and *S. elongatus Synpcc7942_0116*::*spec*^{R} the

respective gene was replaced with a spectinomycin resistance cassette. For this, flanking regions of both sides of the respective gene, 300–400 bp in length, were amplified from genomic DNA of the respective strain with primers adding overlapping fragments to the backbone vector or the spectinomycin resistance cassette. Primer 9+10 (for *Synechocystis* sp.) and 13+14 (for *S. elongatus*) were used to amplify the upstream fragments, primer 11+12 (for *Synechocystis* sp.) and 15+16 (for *S. elongatus*) for the downstream fragments (primer sequence see **Table 2**). The spectinomycin resistance cassette was amplified with the primer 19+20. For the replacement of the respective gene, the vector pUC19 (non-replicative in cyanobacteria) was digested with XbaI and PstI. All fragments (digested vector, upstream fragment, spectinomycin cassette, and downstream fragment) were fused using Gibson assembly (Gibson, 2011) and transformed into *E. coli* TOP 10. The plasmid was verified by Sanger sequencing (LightRun Tube, Eurofins Genomics). The plasmid was transformed into *Synechocystis* sp. or *S. elongatus* by using the natural competence of this strains. The exact procedure is described in our previous publication (Rapp et al., 2021). Integration of the plasmid and segregation was confirmed by colony PCR (9+12 for *Synechocystis* sp., 17+18 for *S. elongatus*, see **Table 2**). Both strains were cultivated in the presence of 20 $\mu g^{*}mL^{-1}$ spectinomycin.

RESULTS

7dSh Is a Competitive Inhibitor of the 3-Dehydroquinate Synthase

Anabaena variabilis ATCC 29413 (thereafter *A. variabilis*) cultures treated with 7dSh strongly accumulate 3-deoxy-D-*arabino*-heptulosonate 7-phosphate (DAHP), which is the substrate of the 3-dehydroquinate synthase, the second enzyme in the shikimate pathway (Brilisauer et al., 2019; **Figure 1A**). Additionally, the content of aromatic amino acids is strongly decreased in 7dSh treated cells, whereas the pools of the non-aromatic amino acids are significantly elevated (Brilisauer et al., 2019). DAHP shows a similar structure as 7dSh in its pyranose form (**Figure 1B**, differences are labelled in red), suggesting that 7dSh is a structural analogue/antimetabolite of DAHP. To confirm the intracellular target and the inhibitory mode of 7dSh, an *in vitro* enzymatic inhibition assay was performed. Therefore, we cloned the DHQS gene from *A. variabilis* (*Ava_4386*, *Av*DHQS) into an *E. coli* overexpression vector, expressed it in *E. coli* BL21 (DE3) and purified the enzyme via its His-tag. Purity was confirmed by SDS-PAGE, where a band corresponding to the expected molecular weight of ∼39 kDa was observed (**Supplementary Figure 1**). In the DHQS mediated reaction, DAHP is converted into 3-dehydroquinate by the release of phosphate, which can be measured by means of the malachite green assay (**Figure 1A**). First, the kinetic parameters of the standard reaction were measured (**Figure 1C**, black dots; **Table 3**). For DAHP we obtained a k_M-value of 1.8 ± 0.3 μM and a v_{max}-value of 149.3 ± 6.1 $U^{*}\mu mol_{enz.}{}^{-1}$. Following the addition of 50 or 100 μM 7dSh to the standard reaction, the k_M-value drastically increased although v_{max} remained nearly constant (see **Table 3** and **Figure 1C**, dark grey squares and light grey triangle). This confirmed the competitive nature of the DHQS inhibitor 7dSh and clearly showed that 7dSh, presumably in its furanose form, is a structural analogue of DAHP. From this data we calculated a k_i of 17.6 μM for 7dSh towards the DHQS from *A. variabilis*. Additionally, an IC_{50}-value of 21.3 μM was determined (data not shown).

TABLE 3 | Kinetic parameters of the *Av*DHQS mediated conversion of DAHP into 3-dehydroquinate in the absence or presence of the inhibitor 7dSh.

7dSh (μM)	k_M (μM)	v_{max} ($U^{*}\mu mol_{enz.}{}^{-1}$)
–	1.8 ± 0.3	149.3 ± 6.1
50	4.3 ± 1.1	121.2 ± 10.9
100	8.2 ± 1.5	133.9 ± 10.9

Sensitivity of Different Cyanobacterial Strains Towards 7dSh Treatment

To elucidate the allelopathic potential of 7dSh, we examined the effect of the inhibitor on various cyanobacterial species belonging to all subsections of the phylum (Rippka et al., 1979). Therefore, we inoculated the strains in a 24-well plate in the presence of different 7dSh concentrations (0, 10, 50, and 250 μM) and cultivated them in continuous light until the control showed proper growth (**Figure 3**). Two of the strains, *A. variabilis* and *Oscillatoria acuminata* PCC 6304 were almost completely lysed by 10 μM 7dSh. *Synechocystis* sp. PCC 6803 GT (thereafter *Synechocystis* sp.), *Leptolyngbya boryana* PCC 6306 and *Nodularia sphaerocarpa* SAG 50.79 were moderately inhibited by 50 μM 7dSh. Growth inhibition in the 7dSh producer strains *S. elongatus* and *Synechococcus* sp. PCC 6301 was observed only at high 7dSh concentrations (250 μM). *Nostoc muscorum* SAG 1453-12a was slightly affected by showing a more yellowish phenotype at concentrations above 50 μM. Other cyanobacteria, especially those growing in macroscopic filaments, for example *Chlorogloeopsis fritschii* PCC 6912 and *Fischerella muscicola* PCC 7414, but also *Anabaena* sp. PCC 7120 (thereafter *Anabaena* sp.) and some unicellular cyanobacteria like *Synechococcus* sp. PCC 7002, *Synechococcus* sp. PCC 6312 and the two strains of subsection II (*Pleurocapsa minor* SAG 4.99, *Staniera cyanosphaera* SAG 33.87) were not affected by 7dSh even at high concentrations.

Taken together, these data indicate that the sensitivity to 7dSh may greatly vary from a cyanobacterial species to another. As some cyanobacteria are capable of heterotrophic growth (Rippka et al., 1979) and thereby endowed with the ability of sugar uptake (Schmetterer, 1990; Ungerer et al., 2008; **Figure 3**), we hypothesized that 7dSh sensitivity might be correlated with this ability, at least partially. Hence, we set out to test this hypothesis.

Uptake of 7dSh in *A. variabilis* via the Fructose ABC-Transporter

To find a reason for the different sensitivities, we first focused on the highly sensitive *A. variabilis* and the close relative, but 7dSh insensitive *Anabaena* sp. strain (**Figure 3**). While the overall

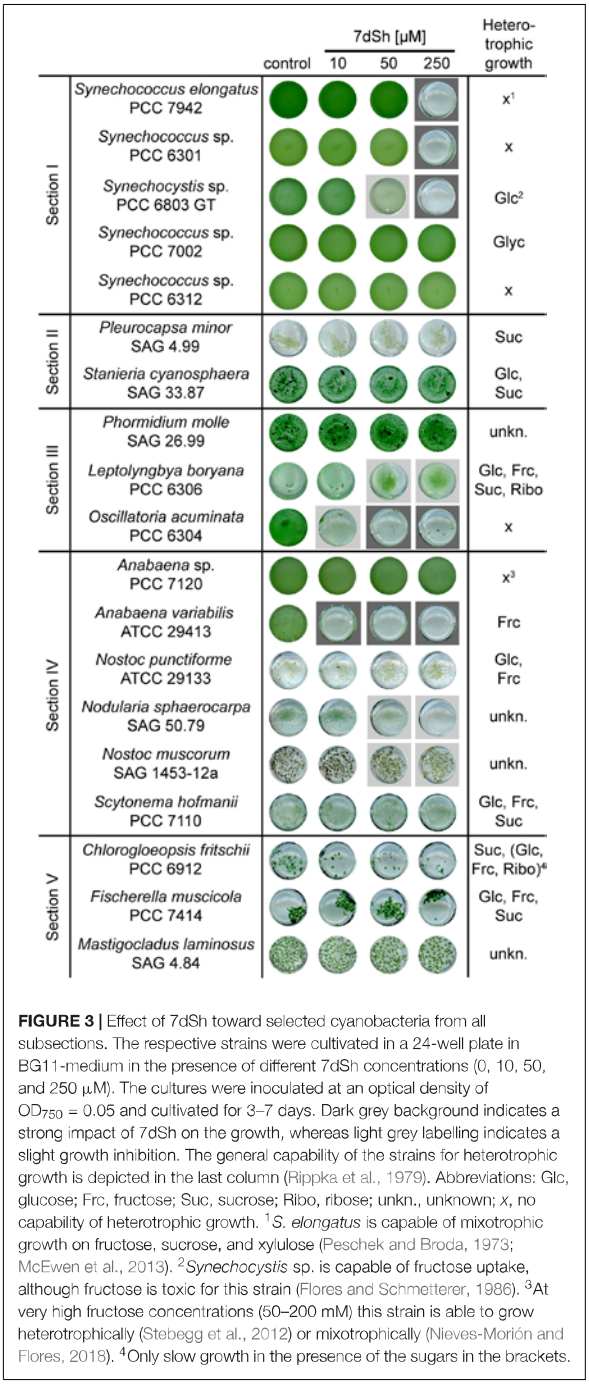

FIGURE 3 | Effect of 7dSh toward selected cyanobacteria from all subsections. The respective strains were cultivated in a 24-well plate in BG11-medium in the presence of different 7dSh concentrations (0, 10, 50, and 250 µM). The cultures were inoculated at an optical density of OD_{750} = 0.05 and cultivated for 3–7 days. Dark grey background indicates a strong impact of 7dSh on the growth, whereas light grey labelling indicates a slight growth inhibition. The general capability of the strains for heterotrophic growth is depicted in the last column (Rippka et al., 1979). Abbreviations: Glc, glucose; Frc, fructose; Suc, sucrose; Ribo, ribose; unkn., unknown; *x*, no capability of heterotrophic growth. [1]*S. elongatus* is capable of mixotrophic growth on fructose, sucrose, and xylulose (Peschek and Broda, 1973; McEwen et al., 2013). [2]*Synechocystis* sp. is capable of fructose uptake, although fructose is toxic for this strain (Flores and Schmetterer, 1986). [3]At very high fructose concentrations (50–200 mM) this strain is able to grow heterotrophically (Stebegg et al., 2012) or mixotrophically (Nieves-Morión and Flores, 2018). [4]Only slow growth in the presence of the sugars in the brackets.

similarity of the two strains in homologous genes is 95% (Ungerer et al., 2008), their sequence similarity in the target of 7dSh, the DHQS enzyme, is around 99% (only four amino acids of the 363 are different). *A. variabilis* is known for its ability to use fructose as an additional carbon source or even grow heterotrophically on fructose (Haury and Spiller, 1981) as the strain contains an operon for a fructose ABC-transporter (Ungerer et al., 2008). *Anabaena* sp. has no homologous operon and is not able of heterotrophic growth at reasonable fructose concentrations (Rippka et al., 1979; Ungerer et al., 2008). Therefore, we assumed that this sugar transporter might play a role in the uptake of 7dSh. To verify this assumption, we performed bioactivity assays in the presence of 7dSh, fructose and a combination of both. After 3 days, the cell density (expressed as chlorophyll *a* content) was determined (**Figures 2A,B**). *A. variabilis* cells treated with 25 µM 7dSh showed a significantly reduced cell density, whereas the cell density of *Anabaena* sp. was not affected. The addition of a 40-fold higher concentration of fructose to *A. variabilis* alleviated the inhibitory effect of 7dSh to a certain extent but the culture did not regain the cell density of untreated cells. Additionally, we isolated a spontaneous 7dSh resistant *A. variabilis* mutant by cultivating an *A. variabilis* culture at sublethal concentrations of 7dSh (hereafter termed *A. variabilis*-7dSh^R). The cell density of this mutant was not affected by the addition of 25 µM 7dSh. Furthermore, unlike the wildtype, the mutant was no longer capable of using fructose as an additional carbon source (**Figure 2A**) or of photoheterotrophic growth in the presence of the PS II inhibitor DCMU [3-(3,4-dichlorophenyl)-1,1-dimethylurea] (**Figure 2B**). To finally prove that the fructose ABC-transporter operon *frtRABC* is responsible for 7dSh uptake, we cloned this operon into a replicative plasmid (pRL1049) and introduced it into *Anabaena* sp. (thereafter named *Anabaena* sp. + *frtRABC*). The resulting strain gained sensitivity towards 7dSh, which could be alleviated by the addition of fructose as also shown for *A. variabilis* wildtype. Furthermore, this strain also gained the ability to use fructose as an additional carbon source (**Figure 2A**) or to grow photoheterotrophically on fructose in the presence of DCMU (**Figure 2B**), as also described in the literature (Ungerer et al., 2008). Additionally, we analyzed the genomic context of the *frtRABC* operon in *A. variabilis* wildtype and in *A. variabilis*-7dSh^R. Therefore, we designed gene specific primers and amplified parts of the respective genes, but also the whole operon and analyzed the PCR fragments via agarose gel electrophoresis (see **Supplementary Figure 2**). The wildtype clearly showed the anticipated fragments for all the amplified genes (*Ava_2170*, *Ava_2171*, *Ava_2172*, and *Ava_2173*) as well as the fragment of the whole operon (*Ava_2170-Ava_2173*), whereas the mutant did not show any of the fragments, indicating a deletion of the whole operon in *A. variabilis*-7dSh^R (**Supplementary Figure 2**).

Uptake of 7dSh in *Synechocystis* sp. via the Glucose Permease Gtr

The unicellular cyanobacterium *Synechocystis* sp., a frequently used model strain, also showed sensitivity towards 7dSh treatment (**Figure 3**). The glucose-tolerant lab-strain can use glucose as an additional carbon source and can even grow heterotrophically on glucose (Rippka et al., 1979; Anderson and McIntosh, 1991). On the contrary, fructose is toxic for

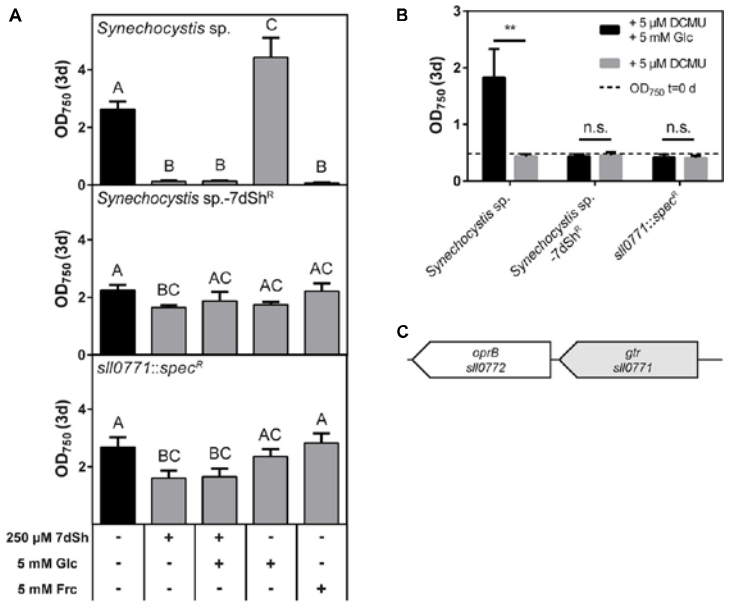

FIGURE 4 | 7-deoxysedoheptulose is taken up via the glucose permease Gtr in *Synechocystis* sp. **(A)** Effect of 7dSh, 7dSh in combination with glucose, glucose or fructose on the growth of wildtype *Synechocystis* sp., the 7dSh resistant mutant *Synechocystis* sp.-7dSh^R and the *gtr* insertion mutant *Synechocystis* sp. *sll0771*::*spec*^{R}. The strains were inoculated at an optical density of OD_{750} = 0.05 and cultivated for 3 days. Values shown in the graphs represent mean and standard deviation of three biological replicates. Statistical analysis was performed by using a one-way ANOVA followed by Tukey's multiple comparison test. Means that were significantly different (p-value < 0.05) are marked with different capital letters. **(B)** Heterotrophic growth on glucose by using the photosystem II inhibitor DCMU. The strains were inoculated at an optical density of 0.5 and cultivated for 3 days. Values shown in the graphs represent mean and standard deviation of three biological replicates. Significant heterotrophic growth was analyzed by comparing the growth in the presence of DCMU with or without fructose using an unpaired t-test (*p-value < 0.05; **p-value < 0.01; *** p-value < 0.001; n.s., not significant). **(C)** Genomic context of the glucose permease in *Synechocystis* sp. A putative carbohydrate porin is located downstream of *gtr*.

this strain (Flores and Schmetterer, 1986). Both, glucose and fructose are taken up by the glucose permease Gtr (also called GlcP or Sll0771), which belongs to the major facilitator superfamily (Joset et al., 1988; Zhang et al., 1989; Schmetterer, 1990). With this knowledge, we performed bioactivity assays with *Synechocystis* sp. in the presence of 7dSh, glucose, the combination of them and fructose and determined the cell density after 3 days (**Figure 4**). The addition of 250 µM 7dSh led to a significantly reduced cell density. Even the addition of the 20-fold amount of glucose did not alleviate the inhibitory effect of 7dSh. Additionally, we isolated a spontaneous 7dSh-resistant mutant by cultivating *Synechocystis* sp. at sublethal concentrations of 7dSh (hereafter termed *Synechocystis* sp.-7dSh^R). The growth of this mutant was only slightly affected by the addition of 7dSh, but the mutant was no longer capable of using glucose as an additional carbon source or of photoheterotrophic growth (**Figure 4A**) on glucose in the presence of DCMU (**Figure 4B**). The wildtype showed a significantly enhanced optical density in the presence of glucose and during photoheterotrophic growth in the presence of glucose and DCMU. Furthermore, the *Synechocystis* sp.-7dSh^R was not inhibited by the addition of fructose, which showed toxicity in the wildtype. These findings suggest that the glucose permease is responsible for the uptake of 7dSh in *Synechocystis* sp. To confirm this assumption, we amplified and sequenced the gene of the glucose permease (*sll0771*) of wildtype and resistant mutant. It turned out that the mutant had acquired a single point mutation on position 1,174, containing a transition of thymine to cytosine. This results in an amino acid exchange from tryptophane to arginine located in a membrane-spanning helix at amino acid position 392, and therefore, of functional importance (Schmetterer, 1990). To confirm that the glucose permease Gtr is responsible for 7dSh uptake, the respective gene *sll0771* was replaced by a spectinomycin resistance cassette resulting in strain *Synechocystis* sp. *sll0771*::*spec*^{R}. The growth of the mutant was only slightly affected by the addition of 7dSh, and the strain was no longer capable of using glucose as an additional carbon source or of heterotrophic growth on glucose (**Figure 4**). These findings clearly indicate that 7dSh is mainly imported via the glucose permease Gtr, but there might be also other transporters with lower affinity that can import 7dSh.

7dSh-Sensitivity of the Producer Strain *S. elongatus*

Synechococcus elongatus is a natural producer of 7dSh and its precursor molecule 5-deoxyribose (5dR) (Brilisauer et al., 2019; Rapp et al., 2021). In our previous work we showed that both

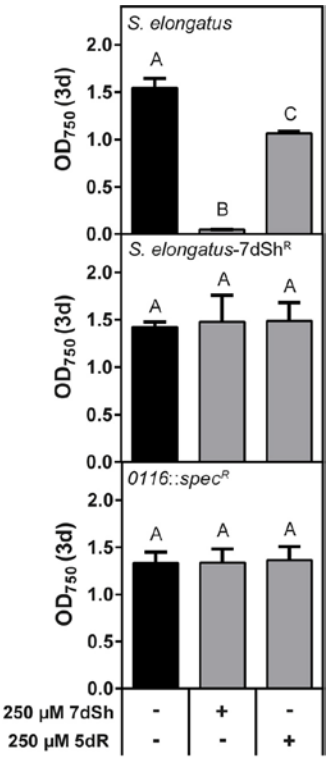

FIGURE 5 | The putative ribokinase Synpcc7942_0116 is responsible for 5dR and 7dSh sensitivity in *S. elongatus*. Effect of 7dSh and 5dR on the growth on wildtype *S. elongatus*, the 7dSh resistant mutant *S. elongatus*-7dSh^R and the putative ribokinase insertion mutant *S. elongatus Synpcc7942_0116*::*spec*^{R}. The strains were inoculated at an optical density of OD_{750} = 0.05 and cultivated for 3 days. Values shown in the graphs represent mean and standard deviation of three biological replicates. Statistical analysis was performed by using a one-way ANOVA followed by Tukey's multiple comparison test. Means that were significantly different (p-value < 0.05) are marked with different capital letters.

compounds are immediately excreted after formation, as none of these compounds accumulates intracellularly (Rapp et al., 2021). We furthermore showed that at the same time as 5dR is excreted, it is also imported and that both substances showed an inhibitory effect towards the producer at high concentrations (Rapp et al., 2021), indicating that there is also a mechanism for the uptake of both substances. By cultivating *S. elongatus* at sublethal 7dSh concentrations we isolated a spontaneous resistant mutant (*S. elongatus*-7dSh^R), which was no longer sensitive towards 250 µM 7dSh, but also not sensitive towards 250 µM 5dR (**Figure 5B**). This suggests a common mechanism for the inhibitory effect of 5dR and 7dSh in *S. elongatus*. In contrast to the other strains analyzed above, *S. elongatus* is not able to grow heterotrophically (Rippka et al., 1979) and no sugar transporter is identified so far, although various ABC-type transporters and permeases are annotated in the genome of this strain. To elucidate the mechanism for 7dSh insensitivity, we performed a whole genome sequencing of the *S. elongatus*-7dSh^R and the wildtype. Compared to the annotated genome (GenBank accession No.: CP000100.1), our laboratory wildtype strain possesses three point mutations on the chromosome, leading to amino acid exchanges (see Supporting information, **Table 1**). In *S. elongatus*-7dSh^R four point mutations were identified, three of which also present in the wildtype. The additional point mutation, an exchange of thymine to adenine (position 923), resulting in an amino acid exchange from isoleucine to proline, is located at amino acid position 308 in gene *Synpcc7942_0116*. The gene is annotated as a sugar or nucleosidase kinase or belonging to ribokinase family (COG annotation) and it contains the PFAM motive pfkB of family carbohydrate kinase (PF00294). In the KEGG database it is annotated as a fructokinase (EC: 2.7.1.4) (Kanehisa and Goto, 2000). To confirm the role of this gene in 5dR/7dSh sensitivity, we replaced the gene with a spectinomycin resistance (*S. elongatus Synpcc7942_0116*::*spec*^{R}) and performed growth experiments in the presence of 5dR and 7dSh (**Figure 5C**). Interestingly, the strain was no longer affected by 5dR or 7dSh (**Figure 5**), indicating an essential role of this gene product in the sensitivity of this strain regarding these two compounds.

DISCUSSION

Only few bioactive compounds from cyanobacteria are regarded as allelopathic inhibitors (Legrand et al., 2003; Leão et al., 2009). Here, we confirmed the allelopathic potential of 7dSh, a bioactive compound, which is actively formed and excreted by the unicellular cyanobacterium *S. elongatus*. 7dSh derives from a toxic waste product of the primary metabolism by solely promiscuous enzyme activity (Brilisauer et al., 2019; Rapp et al., 2021). First, we biochemically verified that 7dSh is an antimetabolite of the DHQS-mediated reaction, by mimicking the natural substrate DAHP (**Figure 1**). This is to the best of our knowledge the first example of an allelochemical targeting the shikimate pathway. Although a variety of allelochemicals are targeting the photosystem II (Gross, 2003), the shikimate pathway is an attractive target as all niche competitors of cyanobacteria possess this pathway (cyanobacteria, plants, but also other bacteria). The DHQS from *A. variabilis* was inhibited by 7dSh in a competitive manner and exhibited an inhibition constant (k_i) of 17.6 µM or an IC_{50}-value of 23.3 µM. 7dSh is most likely only active in its pyranose form, as the structural similarity to DAHP is obvious in this conformation (**Figure 1B**), although the majority of it is present in the furanose form (Brilisauer et al., 2019). For this reason, we assume, that only a minor part of 7dSh, the part, which is present in the pyranose form, is involved in the inhibition of the DHQS. According to literature, the hydroxyl group at C_5, which has the same configuration in 7dSh and in the natural substrate DAHP, is important for binding in the active side of the enzyme. In this first step the hydroxyl group at C_5 is oxidized by enzyme bound NAD^+ (Carpenter et al., 1998). This ketone-NADH intermediate is bound very tightly to the enzyme (Bender et al., 1989), before β-elimination of the phosphate group occurs, which is blocked by various inhibitors, presumably also by 7dSh. The activity of 7dSh

is comparable with other synthetic oxacyclic DHQS inhibitors (f.e. phosphonate), which display k_i-values also in the lower μM range (Bender et al., 1989). Furthermore, the kinetic parameters of *A. variabilis* DHQS were similar to other organisms, for example *Actinidia chinensis*, which has a k_M-value for DAHP of 1.3 μM (Mittelstädt et al., 2013).

Not all cyanobacteria are affected by 7dSh treatment: while several species are only affected in high concentrations (**Figure 3**), others are completely growth inhibited or even lysed at low μM concentrations of 7dSh (*A. variabilis*, *Oscillatoria accuminata*, **Figure 3**; Brilisauer et al., 2019). In complex communities involving different species, it is common that some species remain sensitive towards allelopathic inhibitors, whereas others develop strategies to tolerate the compounds (Bubak et al., 2020). The isolation of spontaneous 7dSh-resistant mutants demonstrates that cyanobacteria can easily adapt to the inhibitor. However, this goes hand in hand with the loss of the ability to use sugars as a(n) (additional) carbon source (see *A. variabilis*-7dSh^R and *Synechocystis* sp.-7dSh^R), thereby losing a feature which could favor growth under certain nutritional conditions or in plant symbiosis (Ekman et al., 2013). We hypothesize that *S. elongatus* might compensate its inability to grow heterotrophically by excreting 7dSh, which then inhibits other cyanobacteria thereby hindering their overgrowth when sugars are present. Interestingly, some strains capable of heterotrophic growth on sugars, thereby necessarily possessing sugar uptake systems, are not affected by 7dSh (e.g., *Staniera cyanosphera*), suggesting that these strains might have developed mechanisms to grow heterotrophically while avoiding 7dSh inhibition. Additionally, heterotrophic bacteria are at most weakly affected by 7dSh [e.g., *Gluconobacter oxydans* is not inhibited by 7dSh (Brilisauer et al., 2019)]. For *E. coli* a weak growth inhibition could be observed when cultivated in minimal medium, but not in complex medium (**Supplementary Figure 3**). It might be possible that some heterotrophic bacteria are able to metabolize 7dSh, as it is reported that the cocultivation of cyanobacteria with heterotrophic bacteria can support the growth of the cyanobacteria (Zheng et al., 2018; Gao et al., 2020).

With growth experiments in the presence of 7dSh and/or fructose (**Figure 2**), we identified the *frtRABC* operon, encoding for the ABC-type fructose transporter and a *lacI*-like regulatory gene *frtR* (Ungerer et al., 2008), as the transporter for 7dSh uptake in *A. variabilis*. The promiscuous uptake of 7dSh by this transporter is quite effective as strong DAHP accumulation could be observed within 1 h, whereas in control cultures no DAHP was detectable (Brilisauer et al., 2019). Additionally, fructose in a 40-fold higher concentration does only partly alleviate the toxic effect of 25 μM 7dSh, indicating an effective and rapid uptake of 7dSh in *A. variabilis* cells. With this, we assume that either 7dSh has a high affinity towards the fructose transporter [k_M-value for fructose 140 μM (Haury and Spiller, 1981)] or 7dSh quickly increases the expression of the transporter as also reported for fructose (Ungerer et al., 2008). The effect of 7dSh, whether it shows bacteriostatic or bactericidal activity, is strongly dependent on the optical density of the cultures (Brilisauer et al., 2019), which clearly showed that the effect of 7dSh strongly depends on the amount of 7dSh per cell. This indicates that the intracellular concentration of 7dSh should be by orders of magnitude higher than the applied extracellular concentration and explains that extracellular concentrations of 7dSh, which were far below the k_i-value, can have detrimental effects on *A. variabilis*. The effective and rapid uptake of 7dSh leading to a strong intracellular enrichment is thereby essential for the inhibitory activity of 7dSh. Although 7dSh is a competitive inhibitor, which should be displaced by increasing DAHP concentrations, we assume that the bactericidal effects of 7dSh are additionally caused by strong metabolic perturbations, which are also described for other compounds targeting the shikimate pathway. The physiological effects of glyphosate (targeting aromatic amino acid synthesis) or the acetolactate synthase (ALS) inhibitor Imazamox (targeting branched-chain amino acid synthesis) are broader than the sole depletion of amino acids, resulting for example in the use of less efficient metabolic pathways (Orcaray et al., 2012; Zulet et al., 2015). Additionally, we cannot exclude that 7dSh has also other, unknown side targets. 7dSh can sneak into cells of target organisms not only via the fructose ABC-transporter: it can also be imported by a structural and functional different sugar transporter–the well-characterized glucose permease of *Synechocystis* sp. (Flores and Schmetterer, 1986; Joset et al., 1988; Schmetterer, 1990). Besides its ability to transport glucose (k_M = 0.58 mM), also the glucose analogue 3-*O*-methyl-D-glucose (k_M = 1.66 mM) and fructose, which is even toxic for *Synechocystis* sp., can be taken up (Joset et al., 1988). It is obvious that *Synechocystis* sp. possesses also other transporters, which can take up 7dSh with a poorer efficiency as the growth of the *gtr* insertion mutant (*Synechocystis* sp. *sll0771::spec*^{R}) is slightly impaired by 7dSh (**Figure 4A**). This is underlined by the fact that a *gtr*$^-$ mutant gained the ability to grow heterotrophically on fructose, although for the wildtype fructose is toxic (Stebegg et al., 2019). Directly adjacent to the *frtRABC* operon in *A. variabilis* and adjacent to the glucose permease in *Synechocystis* sp., we noted the presence of a gene encoding for a putative carbohydrate porin (*Ava_2174*, *sll0772*) (**Figures 2C**, **4C**) suggesting that porins might be responsible for the permeation via the outer membrane. *Sll0772* and *ava_2174* show high sequence similarity to a porin-encoding gene from *Nostoc punctiforme* ATCC 29133 (*N. punctiforme*), which is also clustered with a fructose ABC transporter and was shown to be responsible for permeation of the sugar through the outer membrane (Ekman et al., 2013). Interestingly, *N. punctiforme* is not affected by 7dSh treatment although it has a similar fructose ABC-transporter as *A. variabilis* and additionally a clustered glucose permease (Ekman et al., 2013). We hypothesize that this might be due to a different regulation, as the expression of the fructose transporter in *A. variabilis* is regulated by FrtR (Ungerer et al., 2008), whereas the homologue in *N. punctiforme* HrmR, does not appear to be involved in the regulation of the fructose transporter (Ekman et al., 2013). Besides lower uptake of 7dSh, there are also other possibilities which can result in insensitivity towards 7dSh, e.g., excretion systems, which might be especially present in strains with a large genome. This is underlined by the fact that also other complex, multicellular cyanobacteria (e.g., *Chlorogloeopsis fritschii* PCC 6912, *Fischerella muscicola* PCC 7414), which are able to use various sugars for heterotrophic growth are not

affected by 7dSh treatment. We have to add that 7dSh might be not exclusively transported by sugar transporters, but also by other transporters. The uptake of 7dSh in the producer strain *S. elongatus* remains unclear, especially as the strain also possesses an effective, but unidentified excretion system, which leads to an immediate excretion of intracellularly formed 7dSh (Rapp et al., 2021). However, it seems that the strain possesses unidentified sugar transporters, which presumably allow the strain to grow mixotrophically on fructose, glucose, sucrose and xylose to a certain extent (Peschek and Broda, 1973; McEwen et al., 2013). The involvement of the putative ribokinase in 7dSh and 5dR-sensitivity should be further investigated. It is possible that in this strain phosphorylated 5dR and 7dSh, which cannot be excreted, act as inhibitors. For *A. variabilis* we exclude that phosphorylated 7dSh plays a role in the 7dSh-triggered inhibition. By having a look in previous HRLC-MS data, where we examined the metabolome of 7dSh treated and untreated *A. variabilis* cells, we clearly see an accumulation of a compound with a *m/z* ratio corresponding to the sum formula of 7dSh ($C_7H_{14}O_6$ $[M+H, M+Na]^+$) in 7dSh treated cells, but not in untreated control cultures. A compound with a *m/z* ratio of phosphorylated 7dSh ($C_7H_{15}O_9P$ $[M+H, M+Na]^+$) neither accumulates in 7dSh treated nor in untreated cells (data not shown). We conclude that the extraction process does not destroy phosphorylated compounds, as we observe a strong accumulation of a phosphorylated compound with the sum formula $C_7H_{13}O_{10}P$ $[M+H, M+Na]^+$, corresponding to the *m/z* ratio of DAHP in 7dSh treated cells. Additionally, during the elucidation of the biosynthesis of 7dSh, we were able to measure phosphorylated 5dR in crude extracts incubated with 5dAdo, with this method (Rapp et al., 2021).

The main problem of allelopathic interactions in aquatic ecosystems is the dilution of the allelochemical, thereby causing a reduction of the effective concentrations (Gross, 2003). Although *S. elongatus* was originally isolated from freshwater and is commonly cultivated in its planktonic lifestyle in the laboratory (Golden, 2019), various authors reported that *S. elongatus* can also exhibit a terrestrial lifestyle, colonizing soil, rocks, humid stonewalls, and even caves in microbial mats and biofilms (Schlösser, 1994; Czerwik-Marcinkowska and Mrozińska, 2011; Mattern and Mareš, 2018; Yang et al., 2018; Conradi et al., 2020). Although 7dSh is isolated from planktonic cells, we suggest that 7dSh as an allelopathic inhibitor might play a more important role in its terrestrial and community-/biofilm-forming lifestyle, where it accumulates in high concentrations. One of the two most sensitive strains in this study, *Oscillatoria accuminata,* also colonizes soil (strain information for SAG 1449-3 on the website). The soil bacterium *Streptomyces setonensis* produces significantly higher amounts of 7dSh (more than 10-fold compared to *S. elongatus*) (Rapp et al., 2021), suggesting that 7dSh excretion is a more common strategy in allelopathic interactions in a terrestrial lifestyle. It is possible that *S. elongatus* might be able to produce greater amounts of 7dSh under other conditions, because in our laboratory conditions only a minor part of 5dAdo is converted into 7dSh (Rapp et al., 2021). Besides the competition with other cyanobacteria, *S. elongatus* might also compete with angiosperms regarding light. 7dSh also strongly inhibits the growth of germinating *A. thaliana* seedlings, either on agar plates, but also in soil, where a significant growth reduction was observed already at 25 μM (Brilisauer et al., 2019), suggesting that 7dSh might also play a role in niche protection or competition for light with angiosperms. It is obvious that 7dSh is also taken up by (a) sugar transporter(s) in *A. thaliana* as the effect of 7dSh on germinating seedlings is strongly alleviated when sucrose is present (**Supplementary Figure 4**). 7dSh showed a similar effect on *A. thaliana* seedlings as the commercially available herbicide glyphosate (Brilisauer et al., 2019). As plants possess monosaccharide transporters, belonging to the major facilitator superfamily, for the distribution of sugars (Williams et al., 2000), we speculate that 7dSh might exhibit systemic toxicity which is essential for being an effective herbicide. The verification of the target of 7dSh, and the deeper understanding how 7dSh is taken up might also help to further develop 7dSh as an herbicide, as the uptake of an herbicide is a suitable target for the development of resistant crops. The exact uptake mechanism of glyphosate in plants is not yet known, but only recently a transporter for glyphosate uptake in *B. subtilis* was identified (Wicke et al., 2019).

With the identification of different sugar transporters responsible for 7dSh uptake and the fact that 7dSh is actively excreted by *S. elongatus,* we identified the allelopathic function of this rare deoxy-sugar. As it is also excreted by *S. setonensis* we suggest that formation and excretion of 7dSh is a more common mechanism in niche protection.

DATA AVAILABILITY STATEMENT

The original contributions presented in the study are included in the article/**Supplementary Material**, further inquiries can be directed to the corresponding author.

AUTHOR CONTRIBUTIONS

JR designed, performed, interpreted the experiments, and wrote the manuscript. BW and KB performed, interpreted, and discussed the experiments. KF supervised the study and supported the manuscript writing. All authors contributed to the article and approved the submitted version.

FUNDING

JR was supported and funded by the "Glycobiotechnology" initiative (Ministry for Science, Research and Arts Baden-Württemberg), the RTG 1708 "Molecular principles of bacterial survival strategies". KB was supported and funded by the RTG 1708 "Molecular principles of bacterial survival strategies" and the Institutional Strategy of the University of Tübingen (Deutsche Forschungsgemeinschaft, ZUK 63). The work was further supported by infrastructural funding from the DFG Cluster of Excellence EXC 2124 Controlling Microbes to Fight Infections (project ID 390838134).

ACKNOWLEDGMENTS

We thank Libera Lo Presti (project ID 390838134) for critical reading and language-editing and Antje Bauer for the help with strain cultivation.

SUPPLEMENTARY MATERIAL

The Supplementary Material for this article can be found online at: https://www.frontiersin.org/articles/10.3389/fmicb.2021.692986/full#supplementary-material

REFERENCES

Anderson, S. L., and McIntosh, L. (1991). Light-activated heterotrophic growth of the cyanobacterium *Synechocystis* sp. strain PCC 6803: a blue-light-requiring process. *J. Bacteriol.* 173, 2761–2767. doi: 10.1128/jb.173.9.2761-2767.1991

Bender, S. L., Widlanski, T., and Knowles, J. R. (1989). Dehydroquinate synthase: the use of substrate analogues to probe the early steps of the catalyzed reaction. *Biochemistry* 28, 7560–7572. doi: 10.1021/bi00445a010

Bentley, R. (1990). The shikimate pathway - a metabolic tree with many branches. *Crit. Rev. Biochem. Mol. Biol.* 25, 307–384. doi: 10.3109/10409239009090615

Black, T. A., and Wolk, C. P. (1994). Analysis of a het$^-$ mutation in *Anabaena* sp. strain PCC 7120 implicates a secondary metabolite in the regulation of heterocyst spacing. *J. Bacteriol.* 176, 2282–2292. doi: 10.1128/jb.176.8.2282-2292.1994

Brilisauer, K., Rapp, J., Rath, P., Schöllhorn, A., Bleul, L., Weiß, E., et al. (2019). Cyanobacterial antimetabolite 7-deoxy-sedoheptulose blocks the shikimate pathway to inhibit the growth of prototrophic organisms. *Nat. Commun.* 10:545. doi: 10.1038/s41467-019-08476-8

Bubak, I., Śliwińska-Wilczewska, S., Głowacka, P., Szczerba, A., and Możdżeń, K. (2020). The importance of allelopathic Picocyanobacterium *Synechococcus* sp. on the abundance, biomass formation, and structure of phytoplankton assemblages in three freshwater lakes. *Toxins* 12:259. doi: 10.3390/toxins12040259

Carpenter, E. P., Hawkins, A. R., Frost, J. W., and Brown, K. A. (1998). Structure of dehydroquinate synthase reveals an active site capable of multistep catalysis. *Nature* 394, 299–302. doi: 10.1038/28431

Castenholz, R. W. (2015). "General characteristics of the cyanobacteria," in *Bergey's Manual of Systematics of Archaea and Bacteria*, eds M. E. Trujillo, S. Dedysh, P. DeVos, B. Hedlund, P. Kämpfer, F. A. Rainey, et al. (Hoboken, NJ: John Wiley & Sons Inc), 1–23.

Challand, M. R., Martins, F. T., and Roach, P. L. (2010). Catalytic activity of the anaerobic tyrosine lyase required for thiamine biosynthesis in *Escherichia coli*. *J. Biol. Chem.* 285, 5240–5248. doi: 10.1074/jbc.M109.056606

Choi-Rhee, E., and Cronan, J. E. (2005). A nucleosidase required for in vivo function of the S-Adenosyl-L-methionine radical enzyme, biotin synthase. *Chem. Biol.* 12, 589–593. doi: 10.1016/j.chembiol.2005.04.012

Conradi, F. D., Mullineaux, C. W., and Wilde, A. (2020). The role of the cyanobacterial type IV pilus machinery in finding and maintaining a favourable environment. *Life* 10:252. doi: 10.3390/life10110252

Copeland, A., Lucas, S., Lapidus, A., Barry, K., Detter, J. C., Glavina, T., et al. (2014). *Complete Sequence of Chromosome 1 of Synechococcus Elongatus* PCC 7942. Bethesda, MD: National Library of Medicine.

Czerwik-Marcinkowska, J., and Mrozińska, T. (2011). Algae and cyanobacteria in caves of the Polish Jura. *Pol. Bot. J.* 56, 203–243.

Dittmann, E., Gugger, M., Sivonen, K., and Fewer, D. P. (2015). Natural product biosynthetic diversity and comparative genomics of the cyanobacteria. *Trends Microbiol.* 23, 642–652. doi: 10.1016/j.tim.2015.07.008

Ekman, M., Picossi, S., Campbell, E. L., Meeks, J. C., and Flores, E. (2013). A *Nostoc punctiforme* sugar transporter necessary to establish a cyanobacterium-plant symbiosis. *Plant. Physiol.* 161, 1984–1992. doi: 10.1104/pp.112.213116

Elhai, J., and Wolk, C. P. (1988). Conjugal transfer of DNA to cyanobacteria. *Methods Enzymol.* 167, 747–754. doi: 10.1016/0076-6879(88)67086-8

Flores, E., and Schmetterer, G. (1986). Interaction of fructose with the glucose permease of the cyanobacterium *Synechocystis* sp. strain PCC 6803. *J. Bacteriol.* 166, 693–696. doi: 10.1128/jb.166.2.693-696.1986

Gao, S., Kong, Y., Yu, J., Miao, L., Ji, L., Song, L., et al. (2020). Isolation of axenic cyanobacterium and the promoting effect of associated bacterium on axenic cyanobacterium. *BMC Biotechnol.* 20:61. doi: 10.1186/s12896-020-00656-5

Gibson, D. G. (2011). "Enzymatic assembly of overlapping DNA fragments," in *Methods in Enzymology: Synthetic Biology*, ed. C. Voigt (San Diego, CA: Academic Press), 349–361.

Gleason, F. K., and Paulson, J. L. (1984). Site of action of the natural algicide, cyanobacterin, in the blue-green alga, *Synechococcus* sp. *Arch. Microbiol.* 138, 273–277. doi: 10.1007/BF00402134

Golden, S. S. (2019). The international journeys and aliases of *Synechococcus elongatus*. *N. Z. J. Bot.* 57, 70–75. doi: 10.1080/0028825X.2018.1551805

Gross, E. M. (2003). Allelopathy of aquatic autotrophs. *Crit. Rev. Plant Sci.* 22, 313–339. doi: 10.1080/713610859

Gross, E. M., Wolk, C. P., and Juttner, F. (1991). Fischerellin, a new allelochemical from the freshwater cyanobacterium *Fischerella muscicola*. *J. Phycol.* 27, 686–692. doi: 10.1111/j.0022-3646.1991.00686.x

Hansel, A., and Tadros, M. H. (1998). Characterization of two pore-forming proteins isolated from the outer membrane of *Synechococcus* PCC 6301. *Curr. Microbiol.* 36, 321–326. doi: 10.1007/s002849900316

Haury, J. F., and Spiller, H. (1981). Fructose uptake and influence on growth of and nitrogen fixation by *Anabaena variabilis*. *J. Bacteriol.* 147, 227–235. doi: 10.1128/JB.147.1.227-235.1981

Hoiczyk, E., and Hansel, A. (2000). Cyanobacterial cell walls: news from an unusual prokaryotic envelope. *J. Bacteriol.* 182, 1191–1199. doi: 10.1128/JB.182.5.1191-1199.2000

Inderjit, S., and Duke, S. O. (2003). Ecophysiological aspects of allelopathy. *Planta* 217, 529–539. doi: 10.1007/s00425-003-1054-z

Joset, F., Buchou, T., Zhang, C.-C., and Jeanjean, R. (1988). Physiological and genetic analysis of the glucose-fructose permeation system in two *Synechocystis* species. *Arch. Microbiol.* 149, 417–421. doi: 10.1007/BF00425581

Jüttner, F., and Lüthi, H. (2008). Topology and enhanced toxicity of bound microcystins in *Microcystis* PCC 7806. *Toxicon* 51, 388–397. doi: 10.1016/j.toxicon.2007.10.013

Kanehisa, M., and Goto, S. (2000). KEGG: kyoto encyclopedia of genes and genomes. *Nucleic Acids Res.* 28, 27–30. doi: 10.1093/nar/28.1.27

Keating, K. I. (1977). Allelopathic influence on blue-green bloom sequence in a eutrophic lake. *Science* 196, 885–887. doi: 10.1126/science.196.4292.885

Keating, K. I. (1978). Blue-green algal inhibition of diatom growth: transition from mesotrophic to eutrophic community structure. *Science* 199, 971–973. doi: 10.1126/science.199.4332.971

Leão, P. N., Vasconcelos, M. T. S. D., and Vasconcelos, V. M. (2009). Allelopathy in freshwater cyanobacteria. *Crit. Rev. Microbiol.* 35, 271–282. doi: 10.3109/10408410902823705

Leflaive, J., and Ten-Hage, L. (2007). Algal and cyanobacterial secondary metabolites in freshwaters: a comparison of allelopathic compounds and toxins. *Freshw. Biol.* 52, 199–214. doi: 10.1111/j.1365-2427.2006.01689.x

Legrand, C., Rengefors, K., Fistarol, G. O., and Granéli, E. (2003). Allelopathy in phytoplankton - biochemical, ecological and evolutionary aspects. *Phycologia* 42, 406–419. doi: 10.2216/i0031-8884-42-4-406.1

Mackinney, G. (1941). Absorption of light by chlorophyll solutions. *J. Biol. Chem.* 140, 315–322.

Mattern, H., and Mareš, J. (2018). "Cyanobacteria," in *Beiträge zu den Algen Baden-Württembergs. Band 1. Allgemeiner Teil & Cyanobacteria, Glaucobionta, Rhodobionta und Chlorobionta*, eds. S. Stutz, and H. Mattern (Verlag Manfred Hennecke).

McEwen, J. T., Machado, I. M. P., Connor, M. R., and Atsumi, S. (2013). Engineering *Synechococcus elongatus* PCC 7942 for continuous growth under diurnal conditions. *Appl. Environ. Microbiol.* 79, 1668–1675. doi: 10.1128/AEM.03326-12

Metlitskaya, A., Kazakov, T., Kommer, A., Pavlova, O., Praetorius-Ibba, M., Ibba, M., et al. (2006). Aspartyl-tRNA synthetase is the target of peptide nucleotide antibiotic Microcin C. *J. Biol. Chem.* 281, 18033–18042. doi: 10.1074/jbc.M513174200

Mittelstädt, G., Negron, L., Schofield, L. R., Marsh, K., and Parker, E. J. (2013). Biochemical and structural characterisation of dehydroquinate synthase from the New Zealand kiwifruit *Actinidia chinensis*. *Arch. Biochem. Biophys.* 537, 185–191. doi: 10.1016/j.abb.2013.07.022

Supporting information for:

In vivo inhibition of the 3-dehydroquinate synthase by 7-deoxysedoheptulose depends on promiscuous uptake by sugar transporters in cyanobacteria

Johanna Rapp, Berenike Wagner, Klaus Brilisauer, Karl Forchhammer

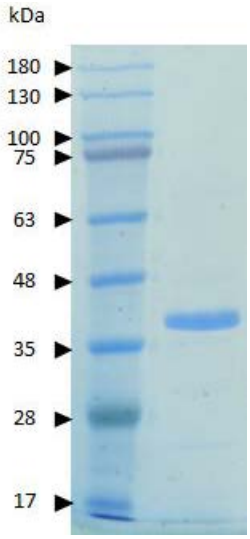

Figure S1: Coomassie-stained SDS-PAGE gel of purified *Av*DHQS. The protein was expressed in *E. coli* BL21 (DE3) with a C-terminal His-Tag and purified via Ni^{2+} affinity chromatography. ~0.5 µg of protein was applied to a 12 % SDS-PAGE gel.

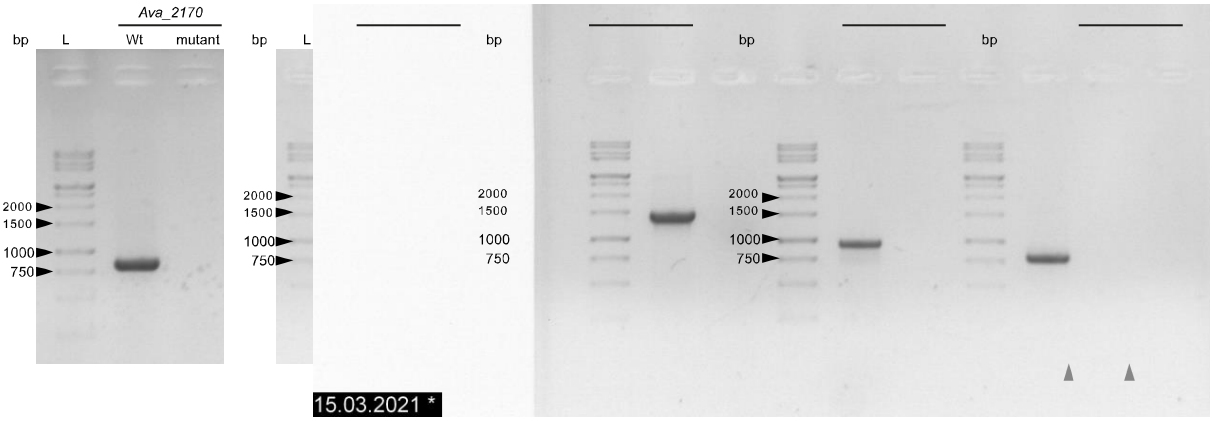

Figure S2: Analysis of PCR fragments of the *frtRABC* operon (*Ava_2170-2173*) from genomic DNA of *A. variabilis* (Wt) and a spontaneous 7dSh-resistant mutant (mutant) visualized by agarose gel electrophoresis. Gene specific primers were used in a PCR reaction with genomic DNA (50 ng DNA, Red Taq Mastermix, Genaxxon). *Ava_2170* – primer 21+22 (expected band size: 863 bp), *Ava_2171* – primer 23+24 (expected band size: 735 bp), *Ava_2172* – primer 25+26 (expected band size: 1510 bp), *Ava_2173* – primer 27+28 (expected band size: 946 bp), *Ava_2170-Ava_2173* – primer 3+4 (expected band size: 5574 bp). To analyse the presence of the single genes, primers lying inside the respective gene were used. For the amplification of the whole operon, primers lying 200 bp up- and downstream of the operon were used. Primer sequences are shown in Table 3. L - DNA ladder 1 kb (Genaxxon). Splice borders are labelled with grey triangle, but marker and samples were run on the same gel.

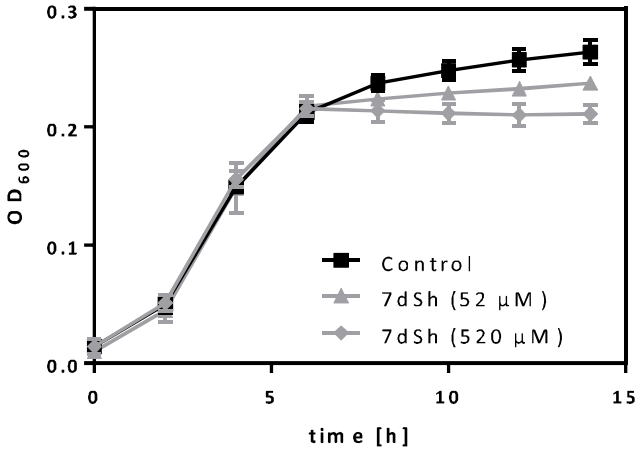

Figure S3: Growth of *E. coli* in minimal medium (M9) supplemented with 0.5 mg/mL fructose and 1 mg/mL casamino acids in the presence or absence of 7dSh. *E. coli* K12 was inoculated with an optical density of OD_{600}=0.02 in a 96-well plate and cultivated at 37 °C and constant shaking (120 rpm). Values represent mean and standard deviation of seven biological replicates. *E. coli* cells growing in complex media (LB) is not affected by the addition of 7dSh (data not shown).

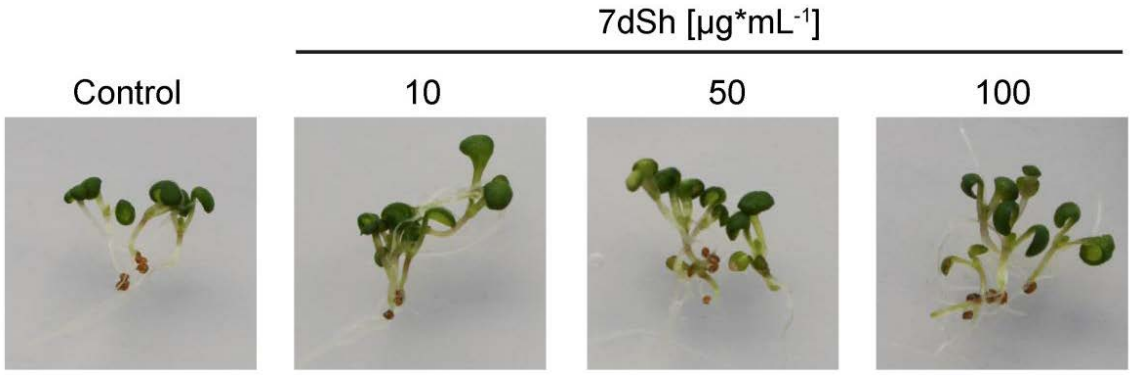

Figure S4: Effect of 7dSh on the germination of *A. thaliana* seedlings in liquid Murashige and Skoog Basal Medium containing 10 mg/mL sucrose after 7 days of cultivation in day/night cycle. In the absence of sucrose, the germination of *A. thaliana* seedlings in the presence of 7dSh is strongly decreased (Brilisauer et al., 2019).

Table 1: Results of the whole genome sequencing of *S. elongatus* and a spontaneous 7dSh-resistant mutant.

Position on chromosome	Gene	Nucleotide in sense direction			Affected base triplet and corresponding amino acid in			
		reference genome	wildtype	resistant mutant	reference genome		wildtype	resistant mutant
92978	Synpcc7942_0095 compl.	T	**C**	**C**	CA**G**	Q (Gln)	C**G**G	R (Arg)
115221	Synpcc7942_0116	T	T	**A**	A**T**C	I (Ile)	A**T**C	N (Asn)
924962	Synpcc7942_0918	T	**C**	**C**	C**T**G	L (Leu)	C**C**G	P (Pro)
2440364	Synpcc7942_2373 compl.	C	**T**	**T**	G**G**T	G (Gly)	GA**T**	D (Asp)

REFERENCES

Brilisauer, K., Rapp, J., Rath, P., Schöllhorn, A., Bleul, L., Weiß, E., et al. (2019). Cyanobacterial antimetabolite 7-deoxy-sedoheptulose blocks the shikimate pathway to inhibit the growth of prototrophic organisms. *Nat. Commun.* 10, 545. doi: 10.1038/s41467-019-08476-8

Publication 4:

Rapp, Johanna; Forchhammer, Karl: 5-Deoxyadenosine metabolism – more than “waste disposal” (2021). *Microbial Physiology*, https://doi.org/10.1159/000516105. © The Authors.

Microbial Physiology

Review Article

Microb Physiol
DOI: 10.1159/000516105

Received: January 8, 2021
Accepted: March 19, 2021
Published online: June 14, 2021

5-Deoxyadenosine Metabolism: More than "Waste Disposal"

Johanna Rapp Karl Forchhammer

Interfaculty Institute of Microbiology and Infection Medicine, Microbiology/Organismic Interactions, Eberhard Karls Universität Tübingen, Tübingen, Germany

Keywords
5-Deoxyadenosine salvage · Enzyme promiscuity · DHAP shunt · 7-Deoxysedoheptulose · 5-Deoxyribose

Abstract
5-Deoxyadenosine (5dAdo) is a by-product of many radical SAM enzyme reactions in all domains of life, and an inhibitor of the radical SAM enzymes themselves. Hence, pathways to recycle or dispose of this toxic by-product must exist but remain largely unexplored. In this review, we discuss the current knowledge about canonical and atypical 5dAdo salvage pathways that have been characterized in the last years. We highlight studies that report on how, in certain organisms, the salvage of 5dAdo via specific pathways can confer a growth advantage by providing either intermediates for the synthesis of secondary metabolites or a carbon source for the synthesis of metabolites of the central carbon metabolism. Yet, an alternative recycling route exists in organisms that use 5dAdo as a substrate to synthesize and excrete 7-deoxysedoheptulose, an allelopathic inhibitor of one enzyme of the shikimate pathway, thereby competing for their own niche. Remarkably, most steps of 5dAdo salvage are the result of the activity of promiscuous enzymes. This strategy enables even organisms with a small genome to synthesize bioactive compounds which they can deploy under certain conditions to gain a competitive growth advantage. We conclude emphasizing that, unexpectedly, 5dAdo salvage pathways seem not to be ubiquitously present, raising questions about the fate of such a toxic by-product in those species. This observation also suggests that additional 5dAdo salvage pathways, possibly relying on the activity of promiscuous enzymes, may exist. The future challenge will be to bring to light these "cryptic" 5dAdo recycling pathways.

Introduction

S-Adenosyl-L-methionine (SAM or AdoMet) is an essential cofactor and cosubstrate of various biological reactions in all domains of life (see Fontecave et al. [2004] for an overview). SAM is formed from the condensation of ATP and the amino acid methionine by the activity of the SAM synthetase/methionine adenosyltransferase (EC 2.5.1.6) [Chou and Talalay 1972; Tallan and Cohen 1976]. SAM is the major methyl-group donor for the methylation of proteins, nucleic acids, carbohydrates and lipids, which results in the release of the by-product *S*-adenosylhomocysteine (SAH/AdoHcy) [Cantoni 1975; Chiang et al., 1996] (Fig. 1 a). Furthermore, SAM is a source of aminoalkyl groups during the synthesis of polyamines, the bacterial quorum sensing signal *N*-acylhomoserine lac-

karger@karger.com
www.karger.com/mip

Correspondence to:
Karl Forchhammer, karl.forchhammer@uni-tuebingen.de

tone (Autoinducer 1) [Nealson and Hastings 1979], the plant hormone ethylene [Yang and Hoffman 1984] and phytosiderophores, which are excreted by plant roots for increasing metal ion availability [Negishi et al., 2002]. During these reactions, methylthioadenosine (MTA) is formed as a by-product (Fig. 1 a). Additionally, SAM is a source of 5-deoxyadenosyl radical, which takes part in various reactions that are catalyzed by the radical SAM enzyme superfamily [Sofia et al., 2001]. Over 100,000 homologous enzymes belong to this superfamily [Holliday et al., 2018], and they all generate a radical species, the 5-deoxyadenosyl radical (5dAdo•), by the reductive cleavage of SAM using an unusual Fe-S cluster [Sofia et al., 2001; Wang and Frey 2007]. Prominent members of the family take part in the biosynthesis of vitamins and cofactors (i.e., biotin and thiamine), but also in that of complex secondary metabolites like antibiotics [Sofia et al., 2001]. In most of these reactions, 5-deoxyadenosine is released as a by-product (Fig. 1 a). A scheme illustrating 5-deoxyadeonosine radical formation in radical SAM enzymes can be found in reference [Fontecave et al., 2004].

SAH, MTA and 5dAdo are by-products which have to be removed because they are product inhibitors [Challand et al., 2009; Parveen and Cornell 2011]. Since elimination via export would lead to a loss of valuable carbon, nitrogen, and sulphur, they are preferentially recycled. SAH and MTA salvage pathways are well characterized. The sulphur form of SAH is rescued via the two- or three-step methionine cycle (also called activated methyl cycle), which is present in almost all organisms (except some ob-

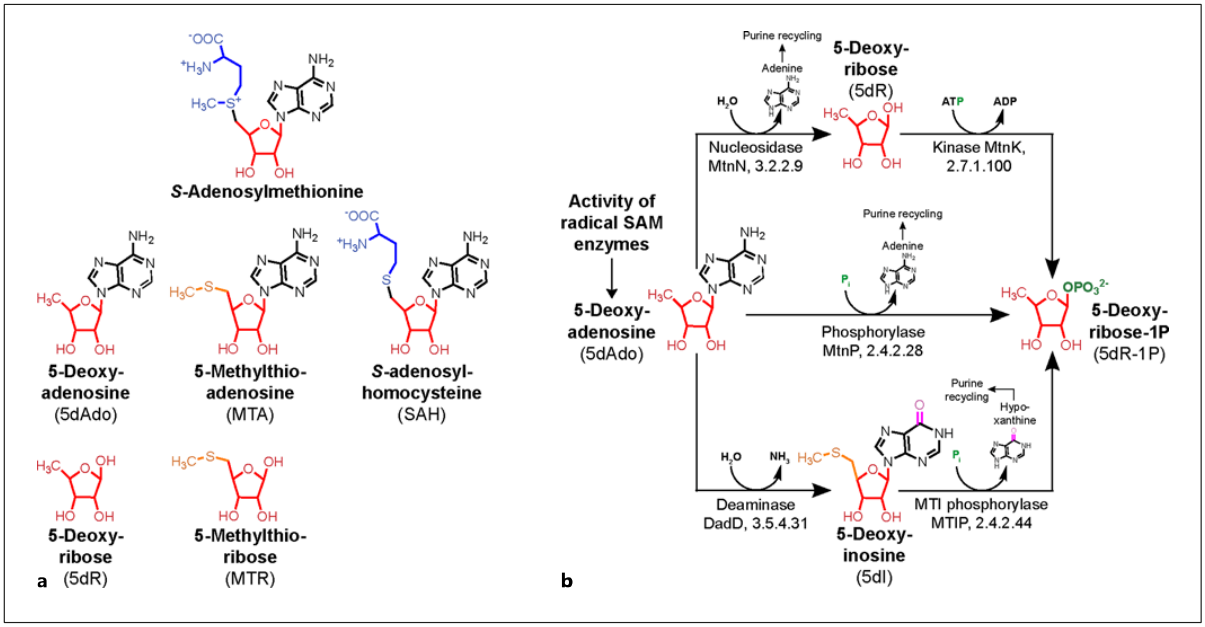

Fig. 1. a *S*-Adenosylmethionine-derived metabolites. **b** Overview of possible 5-deoxyadenosine cleavage steps.

Fig. 2. Overview of different 5dAdo salvage pathways and universal methionine salvage pathway. **a** 5dAdo salvage via the DHAP shunt. This pathway is either conducted by promiscuous enzymes of the MSP pathway (MtnP/MtnN and MtnK, MtnA, MtnB), e.g. in *R. rubrum*, or by an additional set of paralogous enzymes (DrdK, DrdI, DrdA), e.g. in *B. thuringiensis* [Beaudoin et al., 2018; North et al., 2020]. **b** In the unicellular cyanobacterium *S. elongatus* PCC 7942 5dAdo can be metabolized into 5-deoxyribose and the bioactive deoxy-sugar 7-deoxysedoheptulose. Depending on the environmental conditions, 5dAdo is presumably also metabolized via the DHAP shunt [Rapp et al., 2021]. **c** 5dAdo salvage by the formation of DKFP in the methanogenic archaeon *M. jannaschii* [Miller et al., 2014; Miller et al., 2018b]. **d** First steps of the universal methionine salvage pathway [Sekowska and Danchin 2002; Sekowska et al., 2004]. 5dAdo, 5-deoxyadenosine; 5dR, 5-deoxyribose; 5dR-1P, 5-deoxyribose 1-phosphate; 5dRu-1P, 5-deoxyribulose 1-phosphate; 5dI, 5-deoxyinosine; DKFP, 6-deoxy-5-keto-fructose 1-phosphate; DHK-MTPene, 1,2-dihydroxy-3-keto-5-(methylthio)pent(1)ene; KMTB, 2-keto-4-(methylthio)butyric acid.

(For figure see next page.)

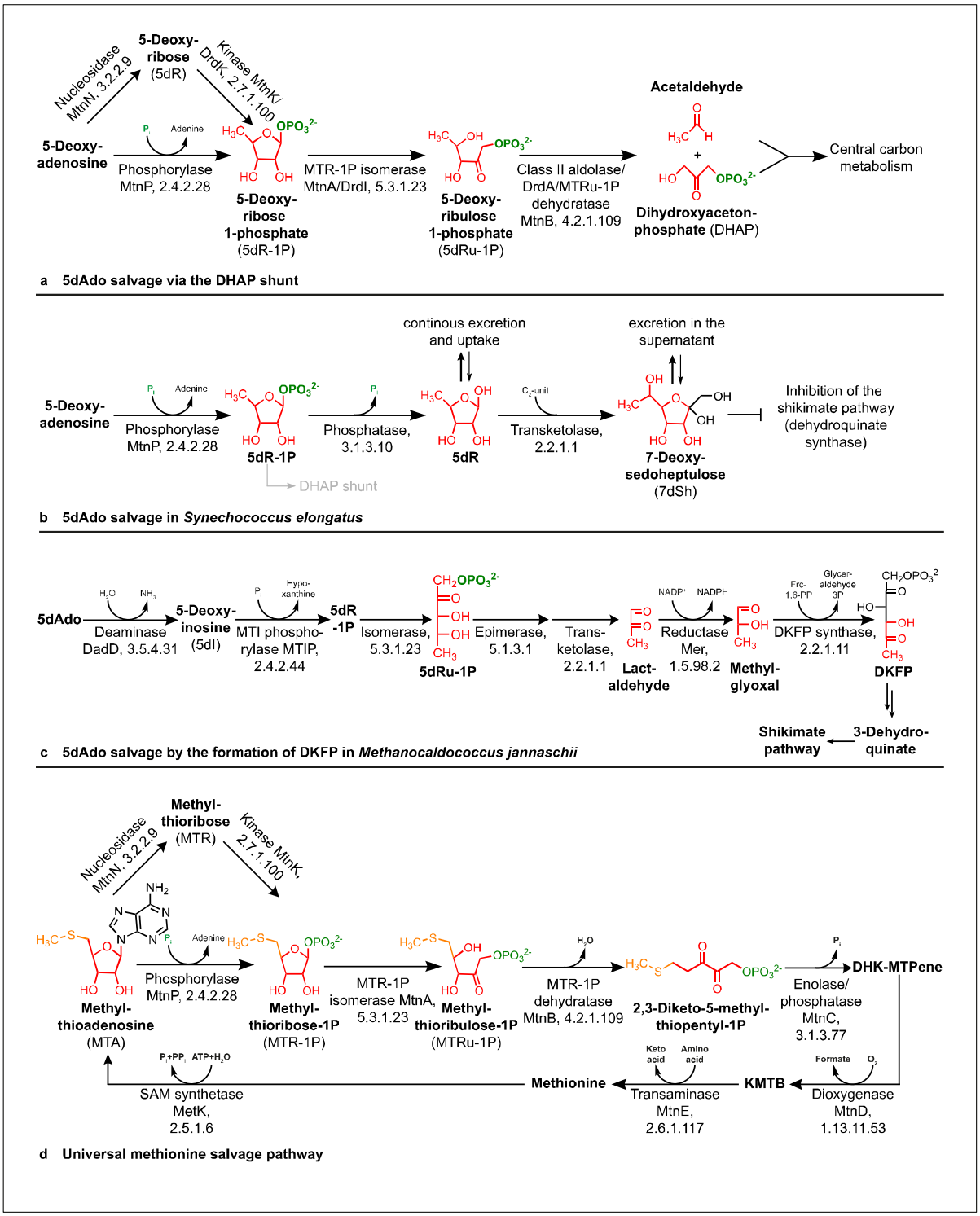
5-Deoxy-adenosine
Nucleosidase MtnN, 3.2.2.9
5-Deoxy-ribose (5dR)
Kinase MtnK/ DrdK, 2.7.1.100
Phosphorylase MtnP, 2.4.2.28
5-Deoxy-ribose 1-phosphate (5dR-1P)
MTR-1P isomerase MtnA/DrdI, 5.3.1.23
5-Deoxy-ribulose 1-phosphate (5dRu-1P)
Class II aldolase/ DrdA/MTRu-1P dehydratase MtnB, 4.2.1.109
Acetaldehyde
Dihydroxyaceton-phosphate (DHAP)
Central carbon metabolism
a 5dAdo salvage via the DHAP shunt
5-Deoxy-adenosine
Phosphorylase MtnP, 2.4.2.28
5dR-1P
Phosphatase, 3.1.3.10
5dR
continous excretion and uptake
Transketolase, 2.2.1.1
excretion in the supernatant
7-Deoxy-sedoheptulose (7dSh)
Inhibition of the shikimate pathway (dehydroquinate synthase)
DHAP shunt
b 5dAdo salvage in Synechococcus elongatus
5dAdo
Deaminase DadD, 3.5.4.31
5-Deoxy-inosine (5dI)
MTI phospho-rylase MTIP, 2.4.2.44
5dR-1P
Isomerase, 5.3.1.23
5dRu-1P
Epimerase, 5.1.3.1
Trans-ketolase, 2.2.1.1
Lact-aldehyde
Reductase Mer, 1.5.98.2
Methyl-glyoxal
DKFP synthase, 2.2.1.11
DKFP
Shikimate pathway
3-Dehydro-quinate
c 5dAdo salvage by the formation of DKFP in Methanocaldococcus jannaschii
Methyl-thioadenosine (MTA)
Nucleosidase MtnN, 3.2.2.9
Methyl-thioribose (MTR)
Kinase MtnK, 2.7.1.100
Phosphorylase MtnP, 2.4.2.28
Methyl-thioribose-1P (MTR-1P)
MTR-1P isomerase MtnA, 5.3.1.23
Methyl-thioribulose-1P (MTRu-1P)
MTR-1P dehydratase MtnB, 4.2.1.109
2,3-Diketo-5-methyl-thiopentyl-1P
Enolase/ phosphatase MtnC, 3.1.3.77
DHK-MTPene
Dioxygenase MtnD, 1.13.11.53
KMTB
Transaminase MtnE, 2.6.1.117
Methionine
SAM synthetase MetK, 2.5.1.6
d Universal methionine salvage pathway

ligate endosymbionts) [Vendeville et al., 2005; North et al., 2020]. The sulphur of MTA is rescued via the methionine salvage pathway (MSP, also MTA cycle or Yang cycle in plants). This pathway is well characterized in various bacterial species like *Klebsiella pneumoniae* [Wray and Abeles 1995] and *Bacillus subtilis* [Sekowska and Danchin 2002], but also in the rat liver [Wray and Abeles 1995]. The canonical MSP consists of six to eight enzymatic steps catalyzed by the nucleosidase/kinase (MtnN/MtnK) or the phosphorylase (MtnP), an isomerase (MtnA), a dehydratase (MtnB), an enolase/phosphatase (MtnC or MtnW/MtnX), a dioxygenase (MtnD), and a transaminase (MtnE) (see Fig. 2 d). MTA is thereby converted into adenine, formate, and L-methionine by consuming inorganic phosphate, molecular oxygen, and a suitable amino acid as an amine donor [Sekowska et al., 2004]. Apart from the canonical, universally oxygen-dependent MSP [see Sekowska et al. [2004]; Albers [2009]; Sekowska et al. [2018]], different alternative pathways have been described in the last years. For example, the aerobic/anaerobic "MTA-isoprenoid shunt" [Erb et al., 2012], the anaerobic "DHAP-ethylene shunt" [North et al., 2017], the aerobic "DHAP-methanethiol shunt" [Miller et al., 2018a], the "bifunctional DHAP shunt" [North et al., 2020] and a modified anaerobic MSP in methanogenic archaea [Miller et al., 2018b]. A nice overview of the different MSP pathways was recently provided by North et al. [2020] and Miller et al. [2018a]. In this review, we therefore focus on the metabolism of 5-deoxyadenosine, a nearly universal metabolite.

Overview of 5dAdo Salvage Pathways

While MTA salvage has been intensively studied in the last decades, 5dAdo metabolism has received little attention. This is quite surprising because MTA is only released in some reactions, whereas 5dAdo is the by-product of a multitude of enzymatic reactions. Some authors have suggested that 5dAdo is metabolized by enzymes of the MSP that display broad substrate specificity, and that the 5dAdo salvage pathway is paralogous to the MSP [Sekowska et al., 2018]. The utilization of different substrates by one enzyme has been referred to as enzyme promiscuity [Copley 2003]. In some studies, promiscuous enzymes are distinguished from broad-specificity or bifunctional enzymes in that the former catalyze a fortuitous reaction for which they did not evolve [Khersonsky and Tawfik 2010]. However, it is very unlikely that enzyme reactions in a physiological context are ever fortuitous, and therefore, we will use the term enzyme promiscuity in the same manner as bifunctional/broad-specificity enzymes. In the past, 5dAdo salvage was often only discussed as a side topic of MTA salvage. Earlier literature only focused on 5dAdo cleavage, but not on its further metabolization [Savarese et al., 1981; Plagemann and Wohlhueter 1983; Choi-Rhee and Cronan 2005]. Only recently some 5dAdo salvage pathways have been experimentally confirmed in different bacterial species [Beaudoin et al., 2018; North et al., 2020; Rapp et al., 2021] (Fig. 2 a, b). Recently, the first steps of 5dAdo salvage in the methanogenic archaeon *Methanocaldococcus jannaschii* were confirmed, but the later steps still remain hypothetical [Miller et al., 2018b] (Fig. 2 c). Interestingly, little is known about 5dAdo salvage in humans.

5dAdo Formation

Various authors have shown that 5-deoxyadenosine accumulation strongly inhibits the activity of radical SAM enzymes [Choi-Rhee and Cronan 2005; Challand et al., 2009; Farrar et al., 2010; Palmer and Downs 2013]. *Escherichia coli* mutants impaired in processing 5dAdo displayed a strong growth phenotype, which could be overcome by the addition of biotin and lipoate [Choi-Rhee and Cronan 2005]. These coenzymes are formed by radical SAM enzymes [Sofia et al., 2001; Berkovitch et al., 2004] and their synthesis is therefore inhibited by the accumulation of 5dAdo. The number of genes encoding radical SAM enzymes is quite diverse in different organisms. In *M. jannaschii*, 2% of the genome encodes radical SAM enzymes (35 of 1,811 protein-encoding genes), whereas other organisms possess less radical SAM enzymes (*Synechococcus elongatus*: 18 of 2,714 genes, ≙0.66%; *Bacillus thuringiensis*: 15 of 6,334 genes, ≙0.24%; *Rhodospirillum rubrum*: 25 of 3,916 genes, ≙0.64%, *Homo sapiens*: 8 of ~23,000≙0.035%) [Beaudoin et al., 2018; North et al., 2020; Rapp et al., 2021]. A large part of radical SAM enzymes is only active under anaerobic conditions [Challand et al., 2010; Beaudoin et al., 2018], but 5dAdo formation was also observed under aerobic conditions in *S. elongatus* [Rapp et al., 2021] and in *R. rubrum* [North et al., 2020]. We assume that under aerobic conditions, 5dAdo mostly derives from radical SAM enzymes which are involved in essential cofactor biosynthesis like the biotin synthase or the lipoic acid synthetase. Biotin is an essential cofactor, e.g. for the acetyl-CoA-carboxylase, whereas lipoic acid is an essential cofactor of the pyruvate dehydrogenase complex. In *R. rubrum* the amount of

5dAdo was however increased 75-fold under anaerobic conditions (see Δ*mtnP* mutant [North et al., 2020]).

5dAdo Cleavage

The first step of 5dAdo metabolism, the cleavage of 5dAdo, is well characterized and confirmed by various in vitro and in vivo studies (Fig. 1 b). 5-Deoxyadenosine can be cleaved in a phosphate-dependent manner by the activity of the MTA phosphorylase (MtnP, MTAP, EC 2.4.2.28), which results in the release of adenine and 5-deoxyribose 1-phosphate (5dR-1P) (Fig. 1b, middle part) [Savarese et al., 1981]. Alternatively, 5dAdo is cleaved by a MTA nucleosidase (MtnN, Pfs, EC 3.2.2.9), releasing 5dR and adenine [Choi-Rhee and Cronan 2005; Challand et al., 2009]. Subsequently, the adenine molecule is directed towards the purine salvage pathway [Nygaard 1993], while 5dR is phosphorylated by the MTR kinase (MtnK, 2.7.1.100), resulting also in the formation of 5dR-1P (Fig. 1 b, upper part) [Beaudoin et al., 2018]. With the exception of plants, most eukaryotic cells use the phosphorylase, whereas about 50% of all sequenced bacteria [North et al., 2020], as well as protozoa, use the two-step mechanism with the nucleosidase and kinase [Zappia et al., 1988; Albers 2009]. Other bacteria (≈30% [North et al., 2020]), like *Pseudomonas* and most cyanobacteria, but also trypanosomes [Ghoda et al., 1988] and most archaea use the phosphorylase. The enzymes involved in these first metabolic steps are well known for their promiscuous activity. The MTA nucleosidase of commensal *E. coli* is a variable SAH/MTA/5dAdo nucleosidase which catalyzes the cleavage of these by-products into *S*-ribosylhomocysteine, 5-methylthioribose and 5-deoxyribose with almost similar efficiency [Choi-Rhee and Cronan 2005; Challand et al., 2009; Parveen and Cornell 2011; North et al., 2020], although MTA is a slightly preferred substrate. Furthermore, the homologous nucleosidase of *Mycobacterium tuberculosis* has a preference for 5dAdo, but is also able to process MTA and SAH, albeit with less efficiency [Namanja-Magliano et al., 2016]. Because of the fact that mammals do not possess a MTA nucleosidase, this enzyme is an attractive target for antimicrobial drugs [Lee et al., 2001; Li et al., 2003]. The MTA kinase MtnK is promiscuous as it catalyzes 5dR and MTR phosphorylation with equal efficiency, whereas *S*-ribosylhomocysteine is a very poor substrate suggesting that SAH is preferentially processed by the specific SAH hydrolase [North et al., 2020]

The MTA phosphorylase MtnP is also known for its promiscuity [Savarese et al., 1981; Plagemann and Wohlhueter 1983; North et al., 2020], but it can only process MTA and 5dAdo with similar affinities, whereas SAH is cleaved by the SAH hydrolase in mammals [La Haba and Cantoni 1959; Parveen and Cornell 2011]. In *R. rubrum*, MtnP is a promiscuous MTA and 5dAdo phosphorylase, but is not able to use SAH as a substrate [North et al., 2020]. Likewise, the phosphorylase of *S. elongatus* appears to be a MTA/5dAdo phosphorylase, because a knockout mutant of this gene excretes 5dAdo as well as MTA [Rapp et al., 2021]. Defects in the activity of the MTA phosphorylase in human cells are furthermore strongly correlated with cancer development [Kamatani and Carson 1980; Christopher et al., 2002; Berasain et al., 2004; Bertino et al., 2011].

A third and less common mechanism of 5dAdo processing is present in anaerobic organisms like the methanogenic *M. jannaschii* where 5dAdo is first deaminated by a MTA/SAH deaminase (DadD, EC 3.5.4.31/.28), which results in the formation of 5-deoxyinosine (5dI) [Miller et al., 2014; Miller et al., 2018b]. Subsequently, a methylthioinosine phosphorylase (MTIP, EC 2.4.2.44) cleaves the molecule, resulting in the release of hypoxanthine and 5dR-1P (Fig. 1 b, lower part). In *M. jannaschii*, the methylthioinosine phosphorylase (MTIP) only accepts hypoxanthine-containing MTI and 5dI with similar affinity (it is unable to use MTA, 5dAdo, adenosine) [Miller et al., 2018b]. It has also been suggested that MTIP plays a broader role in the general salvage of hypoxanthine-containing purine nucleosides.

Although the cleavage of 5dAdo is well characterized, the further fate of 5dR/5dR-1P is more diverse and only poorly characterized, as discussed in the following paragraphs.

5dAdo Salvage via the DHAP (Dihydroxyaceton Phosphate) Shunt

In the last years, various authors have shown that 5dR/5dR-1P is metabolized via the "DHAP" shunt, named by North and colleagues [Beaudoin et al., 2018; North et al., 2020]. In the DHAP shunt, 5dR/5dR-1P is metabolized by the activity of a kinase (only for 5dR) and/or an isomerase, leading to 5dRu-1P. The subsequent activity of an aldolase results in the release of dihydroxyacetone phosphate (DHAP) and acetaldehyde which can be metabolized via primary metabolism (Fig. 2 a). This pathway is similar to L-fucose and L-rhamnose metabolism in

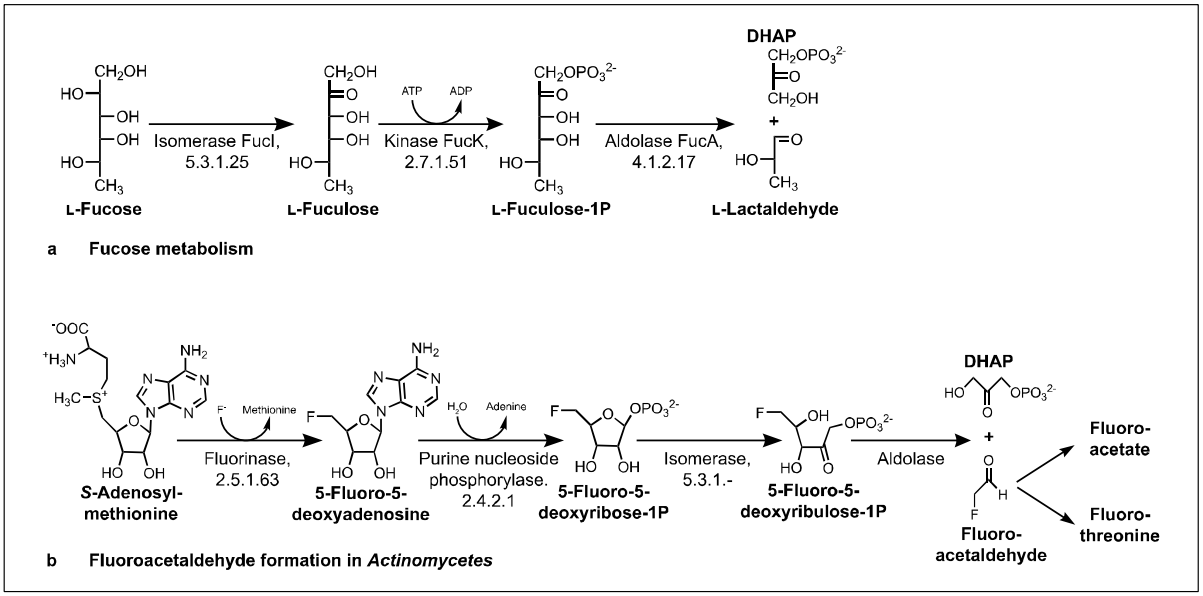

Fig. 3. Variants of the 5dAdo salvage pathway via the DHAP shunt (see Fig. 2 a). The molecules are processed by the activity of a phosphorylase/kinase, an isomerase, and an aldolase. **a** Fucose metabolism in *E. coli* [Chen et al., 1987]. **b** Fluoroacetaldehyde formation in *Actinomycetes* [Onega et al., 2007]. Fluoroacetaldehyde is the precursor molecule for the toxic fluorometabolites fluoroacetate and fluorothreonine which are produced by various *Actinomycetes* like *S. cattleya* [O'Hagan et al., 2002].

E. coli where these two molecules are processed by the activity of an isomerase, a kinase and an aldolase, leading to the formation of L-lactaldehyde and DHAP [Chen et al., 1987] (Fig. 3 a).

5dAdo salvage via the DHAP pathway can be either conducted by promiscuous enzyme activity of the first enzymes of the MSP pathway (e.g., *R. rubrum*) [North et al., 2020] or by paralogous genes (e.g., *B. thuringiensis*) [Beaudoin et al., 2018] (Fig. 2 a). By using comparative genomics, a specific gene cluster was first identified in *B. thuringiensis* for 5dR metabolism and subsequently verified its involvement biochemically [Beaudoin et al., 2018]. The gene cluster encodes the deoxyribose disposal (Drd) kinase DrdK, the isomerase DrdI and the aldolase DrdA. This gene cluster is present in this organism in addition to the gene cluster for the methionine salvage pathway (MSP), and are hence considered to be paralogous genes. Specific gene clusters for the DHAP shunt are present in at least six different bacterial phyla and occur in more than 10% of the sequenced species [North et al., 2017; Beaudoin et al., 2018; North et al., 2020]. Interestingly, some organisms possess a specific gene cluster for the DHAP shunt but lack genes for the MSP pathway (*Myxococcus xanthus*, *Clostridium botulinum*, various extraintestinal pathogenic *E. coli* (ExPEC) strains), whereas others, for example many *Bacillus* species, have both paralogous gene clusters [North et al., 2020]. It was also shown that the kinase, isomerase and aldolase that are responsible for 5dR cleavage (DrdK, DrdI, DrdA) are phylogenetically distinct from homologues that are responsible for canonical methionine salvage or fucose/rhamnose metabolism ([Beaudoin et al., 2018] supplementary information). It is very likely that, in organisms that do not possess a specific gene cluster for 5dAdo salvage, 5dR/5dR-1P can be metabolized by the promiscuous activity of enzymes of the MSP pathway. This is supported by the evidence that the MTR-1P isomerase (MtnA, EC 5.3.1.23) from the universal MSP of *B. subtilis*, which catalyzes the isomerization of MTR-1P to MTRu-1P, is able to isomerize 5dR-1P into 5dRu-1P, albeit with poor efficiency [North et al., 2020]. Furthermore, the next enzyme of the MSP, the MTRu-1P dehydratase MtnB (EC 4.2.1.109), can exhibit promiscuous aldolase activity on 5dRu-1P leading to the formation of DHAP and acetaldehyde. This promiscuity

was experimentally shown for DEP1 of *Arabidopsis thaliana* ([Beaudoin et al., 2018] supplementary information) and for MtnB of *B. subtilis* [North et al., 2020]. We have also suggested that *S. elongatus* is able to use the promiscuous enzymes of the MSP for 5dAdo salvage via the DHAP shunt under certain conditions [Rapp et al., 2021] (Fig. 2b, DHAP shunt).

Interestingly, the enzymes of the DHAP shunt can also be used to metabolize MTR, an intermediate of the MTA salvage pathway. In *R. rubrum*, MTR can be metabolized via the DHAP shunt leading to the formation of DHAP and (2-methylthio) acetaldehyde under both aerobic and anaerobic conditions [North et al., 2020]. The possibility of using the DHAP shunt for MTR salvage in *R. rubrum* is essential as this organism lacks most of the genes of the canonical MSP [Erb et al., 2012]. Furthermore, the canonical MSP, by using the dioxygenase MtnD, is strictly dependent on the presence of oxygen. Therefore, under anaerobic conditions the bifunctional DHAP shunt can be used for MTA salvage. This is underlined by the fact that DHAP shunt genes are enriched in anaerobic and facultative anaerobic bacteria. Nevertheless, also the aerobic *B. thuringiensis* can use the enzymes of the DHAP shunt (DrdK, DrdI, DrdA) for MTR metabolism [Beaudoin et al., 2018]. Furthermore, it was shown that the enzymes from the MSP are so promiscuous that they can even metabolize ribose into the homoserine precursor 2-keto-4-hydroxybutyrate (KHB) in *B. subtilis* [Nakano et al., 2013].

5dAdo Salvage in *Synechococcus elongatus* Leading to Bioactive Deoxy-Sugar Synthesis

Only recently we identified an unusual 5dAdo salvage pathway in the unicellular cyanobacterium *S. elongatus* PCC 7942, which has a small and stream-lined genome [Rapp et al., 2021]. In this organism, 5dAdo salvage can result in the excretion of 5-deoxyribose and 7-deoxysedoheptulose under certain conditions [Brilisauer et al., 2019; Rapp et al., 2021] (Fig. 2 b). In this pathway, 5dAdo is cleaved by promiscuous MTA/5dAdo phosphorylase (*Synpcc7942_0923*, EC 2.4.2.28), leading to the formation of 5dR-1P. During growth at high CO_2 concentrations, 5dR-1P is then dephosphorylated by a presumably promiscuous phosphatase belonging to the HAD-like hydrolase superfamily (*Synpcc7942_1005*, EC 3.1.3.10), resulting in the formation of 5dR. This is quite surprising, as in other 5dAdo salvage pathways 5dR must be phosphorylated for further metabolization. 5dR is immediately excreted into the supernatant because accumulation of 5dR is toxic for the producer strain *S. elongatus* [Rapp et al., 2021]. It is unclear where and how 5dR exerts its toxic effects, but the addition of 5dR is sufficient to strongly affect the growth of *B. thuringiensis*or or also *S. elongatus* in high concentrations [Rapp et al., 2021]. *S. elongatus* is able to take up exogenously added $^{13}C_5$-labelled 5dR and excrete endogenously produced, unlabelled 5dR at the same time [Rapp et al., 2021]. Therefore, 5dR is continuously exported out of and imported into the cells. At the transition to stationary growth, a portion of the 5dR is converted into the unusual and bioactive deoxy-sugar 7-deoxysedoheptulose (7dSh). This reaction is catalyzed by the promiscuous transketolase (*Synpcc7942_0538*, EC 2.2.1.1), which transfers a C_2-unit onto 5dR [Brilisauer et al., 2019; Rapp et al., 2021]. It is known that transketolase enzymes can transfer a C_2-ketol unit (e.g., from hydroxypyruvate or xylulose 5-phosphate) onto an acceptor aldehyde while accepting various aldehyde substrates with 3*S*, 4*R*-configuration [Kobori et al., 1992]. Accordingly, 5dR was used for the in vitro synthesis of 7dSh by the *S. elongatus* transketolase in the presence of hydroxypyruvate as artificial ketol-donor [Brilisauer et al., 2019]. However, it turned out that the affinity of the *S. elongatus* transketolase for 5dR is much lower than for the native substrate ribose 5-phosphate [Brilisauer et al., 2019]. Under ambient CO_2 conditions, *S. elongatus* only accumulates very small quantities of 5dR, and no detectable amounts of 7dSh [Rapp et al., 2021]. Since neither the levels of 5dAdo nor MTA were enhanced under high carbon conditions, we suggested that 5dAdo is presumably rescued via the DHAP-shunt under ambient carbon conditions by the promiscuous activity of the first enzymes of the MSP pathway [Rapp et al., 2021]. Despite its small genome size, *S. elongatus* possesses the whole set of genes of the MSP, whereas other cyanobacteria (for example *Synechocystis* sp. PCC 6803, *Synechococcus* sp. PCC 7502, *Synechococcus* sp. PCC 6312, *Anabaena* sp. PCC 7120, *Anabaena variabilis* ATCC 29413) only possess the first two enzymes (MtnP, MtnA) [see Rapp et al. [2021], supporting information]. Significantly, these other cyanobacteria do not excrete 5dR or 7dSh [Rapp et al., 2021]. Therefore, it is unclear how these organisms perform 5dAdo salvage. It could be speculated that they use MtnP and MtnA for the first steps resulting in 5dRu-1P formation. After that, 5dRu-1P may be cleaved by an aldolase, which are in general also known for their promiscuity [Fessner et al., 1991; Laurent et al., 2018]. The presence of a complete, canonical MSP is not necessary in the abovementioned cyanobacteria as they probably do not pro-

duce MTA. Spermidine synthesis via the spermidine synthase (EC 2.5.1.16) plays a major role in MTA formation, but spermidine can also be synthesized via the carboxyspermidine decarboxylase (CASDC, EC 1.5.1.7) and carboxyspermidine dehydrogenase (CASDH, EC 4.1.1.96), in a series of reactions that do not lead to MTA excretion. *Synechocystis* sp. PCC 6803, for example, uses CASDC and CASDH for spermidine synthesis [Zhu et al., 2015].

5dAdo Salvage via 6-Deoxy-5-Keto-Fructose 1-Phosphate Formation, a Precursor Molecule for the Synthesis of Aromatic Amino Acids in Methanogens

Miller and coworkers [Miller et al., 2014; Miller et al., 2018b] suggested a special pathway for 5dAdo salvage in the methanogenic archaeon *M. jannaschii,* leading first to the formation of methylglyoxal and then of 6-deoxy-5-keto-fructose 1-phosphate (DKFP) (Fig. 2 c). The authors even proposed that this pathway is essential for the synthesis of aromatic amino acids in archaea, which use DKFP for the synthesis of 3-dehydroquinate, a precursor of aromatic amino acids that is generally produced via the shikimate pathway. However, archaea do not possess the enzymatic equipment for the oxidative pentose phosphate pathway, which provides the precursor molecule for the canonical shikimate pathway, erythrose-4-phosphate [Grochowski et al., 2005]. Furthermore, in the genome of methanogenic archaea, the first two enzymes of the canonical shikimate pathway (DAHP synthase and dehydroquinate synthase) are missing. Therefore, archaea have evolved a different strategy to synthesize aromatic amino acids which starts with the condensation of DKFP and L-aspartate semialdehyde into 3-dehydroquinate, a common metabolite in the shikimate pathway [White 2004; Gulko et al., 2014]. As mentioned above, the first step of 5dAdo metabolism is conducted by a deaminase, followed by a phosphorylase reaction, leading to 5dR-1P which is then isomerized by MTRI to 5dRu-1P as in the DHAP shunt (Fig. 2 c). 5dRu-1P is then hypothesized to be further processed by the activity of an epimerase and a transketolase into lactaldehyde, which is reduced by the promiscuous reductase Mer [Miller et al., 2017] to methylglyoxal. Although this metabolite is quite toxic, it was shown that methylglyoxal is an intermediate in the synthesis of DKFP [White and Xu 2006], where the molecule is used in a transaldolase reaction with fructose 1,6-bisphosphate catalyzed by the DKFP synthase (EC 2.2.1.11), leading to the formation of glyceraldehyde 3-phosphate and DKFP. In contrast to that, North and coworkers hypothesized that, although archaea do not possess a homolog of an aldolase for the DHAP shunt, they might also use an analogous aldolase and thereby also apply the DHAP shunt [North et al., 2020].

5dAdo Salvage to Gain Growth Advantage

In some organisms, 5dAdo is more than a toxic byproduct, and the 5dAdo salvage pathway more than simply a means of "waste disposal." As a matter of fact, some species can use "unique" 5dAdo salvage pathways to gain a growth advantage over other members of a microbial community either by using 5dAdo as a substrate for the production of antimicrobial/bioactive compounds or as a sole carbon source in nutrient-limited habitats. In both scenarios, 5dAdo confers a fitness and colonization advantage to those organisms endowed with the ability to differently "recycle" this potentially toxic metabolite.

As mentioned above, the unicellular cyanobacterium *S. elongatus* PCC 7942 is able to excrete 5dR and 7dSh as a consequence of 5dAdo salvage [Rapp et al., 2021]. 7dSh is a competitive inhibitor of the dehydroquinate synthase, the second enzyme in the shikimate pathway, responsible for the synthesis of aromatic amino acids [Brilisauer et al., 2019]. Inhibitors of the shikimate pathway are generally attractive compounds for the development of antibacterial, antifungal, and herbicidal products, as the shikimate pathway is essential for these organisms but absent in mammals. It was shown that 7dSh acts as an allelopathic inhibitor towards other cyanobacteria, for example against the especially sensitive *A. variabilis* strains [Brilisauer et al., 2019]. Furthermore, it was shown that 7dSh can also inhibit the growth of *Saccharomyces cerevisiae* and more importantly, it showed herbicidal activity towards *A. thaliana* seedlings germinating on agar plates, but also on soil [Brilisauer et al., 2019]. Furthermore, 7dSh exhibited no toxic effects on human cell lines [Brilisauer et al., 2019] and did not alter the development of zebrafish (*Danio rerio*) [Schweizer et al., 2019]. Therefore, it could be applied as a harmless herbicide, which explains why the compound has attracted much attention [Brilisauer and Harter, 2020]. With respect to the physiological relevance of 7dSh production by *S. elongatus,* it should be noted that formation of 7dSh, as well as 5dR, is dependent on the cultivation conditions. Both molecules are mainly formed under elevated CO_2 conditions, and 7dSh formation occurs in late growth phases [Rapp et al., 2021]. As the amount of the precursor molecule 5dAdo is unaltered under high CO_2 conditions compared to ambi-

ent CO_2 conditions, we assume that 5dAdo is actively directed towards 5dR/7dSh synthesis under conditions in which competition with other community members, such as in biofilms, becomes important [Rapp et al., 2021]. In its natural habitat *S. elongatus* can form biofilms [Yang et al., 2018; Golden 2019] and tend to excrete exopolysaccharides [Rossi and Philippis 2015], which can be used as a carbon source by heterotrophic members of the microbial community thereby causing locally elevated CO_2 concentrations. It is remarkable that *S. elongatus* with a small, streamlined genome and no known gene cluster for the synthesis of secondary metabolites, can use a "waste product" of primary metabolism, 5dAdo, to synthesize a bioactive compound by promiscuous enzyme activity, thus competing against other species for the colonization of its own niche. This makes *S. elongatus* the archetypal organism able to derive bioactive compounds from primary, rather than the secondary metabolism. Interestingly, 7dSh had previously already been isolated from *Streptomyces setonensis* [Ito et al., 1971], which indicates that 5dAdo salvage via 7dSh excretion is not a feature unique to *S. elongatus*. As the genome of *S. setonensis* is currently unsequenced, it remains speculative whether 7dSh in this organism is also derived from 5dAdo.

Interestingly, it was shown that especially pathogenic strains of several organisms (e.g., *Clostridium tetani*, *C. botulinum*, *B. thuringiensis*, *Bacillus cereus* and *Bacillus anthracis*) possess putative DHAP shunt gene clusters, whereas the non-pathogenic strains of the genera do not [Beaudoin et al., 2018; North et al., 2020]. Furthermore, putative DHAP shunt gene clusters are present in nearly 50% of all extraintestinal pathogenic *E. coli* (ExPEC) isolates, whereas commensal *E. coli* strains neither possess a complete MSP pathway nor the DHAP shunt gene cluster [North et al., 2020]. Also, only 0.1% of intestinal pathogenic *E. coli* isolates harbour putative DHAP gene clusters [North et al., 2020]. In the intestinal environment, nutrients are normally not limiting. In comparison, in the extraintestinal environment (urine, blood, and cerebrospinal fluid) carbon and sulphur sources are often limiting or only present in compounds like urea, organic acids, purines and amino acids [North et al., 2020]. 5dAdo (also as 5-deoxyinosine) and MTA along with the degradation products 5dR/5dR-1P and MTR (methylthioribose), are common metabolites in this extraintestinal environment [Liebich et al., 1997; Lee et al., 2004; North et al., 2020], because mammals only metabolize 5dAdo beyond the phosphorylase step [Plagemann and Wohlhueter 1983; Savarese et al., 1981]. Furthermore, commensal *E. coli*, which do not possess a complete MSP, excrete MTR [Schroeder et al., 1972; Hughes 2006]. *E. coli* ExPEC strains harbouring gene clusters for the DHAP shunt are able to grow on these metabolites as sole carbon and sulphur sources, whereas commensal *E. coli* were not able to grow on these metabolites [North et al., 2020]. The presence of this gene cluster therefore leads to a growth advantage in this ecological niche. Because the putative DHAP shunt gene cluster was present in nearly half of all *E. coli* ExPEC strains, for example in the lineage ST 131, which is multidrug resistant and a pathogen with worldwide distribution, causing urinary tract and blood infections [Petty et al., 2014], the DHAP shunt might be a very suitable target for drug development [North et al., 2020]. Furthermore, a similar pathway to the DHAP shunt is used for the formation of toxic fluorometabolites in *Actinomycetes*, for example in *Streptomyces cattleya* [Sanada et al., 1986] (Figure 3 b). In this species, SAM serves as a precursor molecule for 5-fluoro-5-deoxyadenosine, which is formed by a specific fluorinase [O'Hagan et al., 2002]. This molecule is then also processed by a nucleotide phosphorylase [Cobb et al., 2004], an isomerase [Onega et al., 2007], and an aldolase [Moss et al., 2000], leading to fluoroacetaldehyde, the precursor molecule for the toxic fluorometabolites, fluoroacetate and fluorothreonine. These examples illustrate how, by salvaging 5dAdo, some organisms may acquire a growth advantage over others in specific niches and/or environmental conditions.

Export and Import of 5dAdo and Related Metabolites

Little is known about the export and import of 5dAdo and related metabolites. Various authors showed that strains deficient in the activity of the MTA phosphorylase excrete MTA and 5dAdo. This was shown for *S. elongatus* [Rapp et al., 2021], *R. rubrum* [North et al., 2020], *S. cerevisiae* (only MTA) [Chattopadhyay et al., 2006] and also mammalian cell lines (only MTA) [Kamatani and Carson 1980]. Feeding experiments with 5dAdo showed that not only bacterial strains, but also mammalian cell lines are capable of 5dAdo uptake [Rapp et al., 2021; North et al., 2020; Plagemann et al., 1988]. In mammalian cells, for example erythrocytes, which are deficient in de novo purine biosynthesis, 5dAdo and MTA are taken up by a nucleoside transporter with a broad substrate specificity [Plagemann et al., 1988]. 5dAdo uptake in bacteria, to the best of our knowledge, has not been further characterized. In *R. rubrum*, it is assumed that MTA is taken up via

the methionine transport complex (MetINQ) because proteins of this complex are enriched when cells grow on MTA as a sole sulphur source [North et al., 2016]. Furthermore, the MetINQ methionine transport complex is known for its substrate promiscuity [North et al., 2016]. However, it is not known if 5dAdo is also a possible substrate.

It is obvious that several organisms are capable of 5dR uptake. When supplemented into the medium of *B. thuringiensis*, 5dR strongly accumulates intracellularly, thereby causing growth retardation [Beaudoin et al., 2018]. It was also shown that *E. coli* ExPEC strain can use 5dR as a sole carbon source [North et al., 2020]. Interestingly, several organisms harboring gene clusters for the DHAP shunt also contain putative sugar transporters [Beaudoin et al., 2018] with the potential to take up 5dR, which, nonetheless, remains to be demonstrated. While it was shown that in rats 5dR can be reduced to 5-deoxyribitol and also be excreted [Ichihara et al., 1985], to our knowledge, 5dR excretion has only been reported for *S. elongatus* [Rapp et al., 2021]. Because *S. elongatus* is capable of 5dR uptake and excretion at the same time, we assume that two transporters are present in *S. elongatus* in analogy to the two different genes (MtrA/YfnA and MtrE) reported to code for efflux and influx transporters of MTR in *B. subtilis* [Borriss et al., 2018]. The authors also identified secondary MTR transporters, including an ABC transporter for ribose (RbsDACB) and a guanosine transporter (NupQ). It is conceivable that 5dR is imported via the same transporter as 7dSh in *S. elongatus*, which is supported by the demonstration that a spontaneous 7dSh-resistant mutant is also resistant towards 5dR treatment, but the mutant excretes as much 5dR and 7dSh as the wild type (Rapp, unpubl. data).

Conclusions

The mechanisms behind 5-deoxyadenosine salvage have mainly been addressed in the last years, and many aspects still remain elusive. Since several, unusual pathways for MTA salvage have recently been discovered, it is very likely that other, yet to be unravelled pathways for 5dAdo salvage exist. The fact that most steps of 5dAdo salvage are conducted by promiscuous enzymes makes it difficult to predict gene clusters with a putative role in this process. However, the use of comparative genomics coupled with biochemical validation promises to be a useful approach to identify 5dAdo recycling pathways.

Acknowledgements

We thank Dr. Libera Lo Presti for critical reading and linguistic editing of the manuscript.

Conflict of Interest Statement

The authors declare that there is no conflict of interest.

Funding Sources

The work of J.R. is funded by RTG 1708 "Molecular principles of bacterial survival strategies" and by the "Glycobiotechnology" initiative (Ministry for Science, Research and Arts Baden-Württemberg). The work was further supported by infrastructural funding from the DFG Cluster of Excellence EXC 2124 Controlling Microbes to Fight Infections (project ID 390838134).

Author Contributions

J.R. wrote the manuscript. K.F. supervised manuscript writing.

References

Albers E. Metabolic characteristics and importance of the universal methionine salvage pathway recycling methionine from 5'-methylthioadenosine. IUBMB Life. 2009;61(12):1132–42.

Beaudoin GAW, Li Q, Folz J, Fiehn O, Goodsell JL, Angerhofer A, et al. Salvage of the 5-deoxyribose byproduct of radical SAM enzymes. Nat Commun. 2018;9(1):3105.

Berasain C, Hevia H, Fernández-Irigoyen J, Larrea E, Caballería J, Mato JM, et al. Methylthioadenosine phosphorylase gene expression is impaired in human liver cirrhosis and hepatocarcinoma. Biochim Biophys Acta. 2004;1690(3):276–84.

Berkovitch F, Nicolet Y, Wan JT, Jarrett JT, Drennan CL. Crystal structure of biotin synthase, an S-adenosylmethionine-dependent radical enzyme. Science. 2004;303(5654):76–9.

Bertino JR, Waud WR, Parker WB, Lubin M. Targeting tumors that lack methylthioadenosine phosphorylase (MTAP) activity: current strategies. Cancer Biol Ther. 2011;11(7):627–32.

Borriss R, Danchin A, Harwood CR, Médigue C, Rocha EPC, Sekowska A, et al. Bacillus subtilis, the model Gram-positive bacterium: 20 years of annotation refinement. Microb Biotechnol. 2018;11(1):3–17.

Brilisauer K, Harter K. Biogener Zucker als nachhaltiges Herbizid. Biospektrum. 2020;26(5):561.

Brilisauer K, Rapp J, Rath P, Schöllhorn A, Bleul L, Weiß E, et al. Cyanobacterial antimetabolite 7-deoxy-sedoheptulose blocks the shikimate pathway to inhibit the growth of prototrophic organisms. Nat Commun. 2019;10(1):545.

Cantoni GL. Biological methylation: selected aspects. Annu Rev Biochem. 1975;44:435–51.

Challand MR, Martins FT, Roach PL. Catalytic activity of the anaerobic tyrosine lyase required for thiamine biosynthesis in Escherichia coli. J Biol Chem. 2010;285(8):5240–8.

Challand MR, Ziegert T, Douglas P, Wood RJ, Kriek M, Shaw NM, et al. Product inhibition in the radical S-adenosylmethionine family. FEBS Lett. 2009;583(8):1358–62.
Chattopadhyay MK, Tabor CW, Tabor H. Methylthioadenosine and polyamine biosynthesis in a Saccharomyces cerevisiae meu1delta mutant. Biochem Biophys Res Commun. 2006;343(1):203–7.
Chen YM, Zhu Y, Lin EC. The organization of the fuc regulon specifying L-fucose dissimilation in Escherichia coli K12 as determined by gene cloning. Mol Gen Genet. 1987;210(2):331–7.
Chiang PK, Gordon RK, Tal J, Zeng GC, Doctor BP, Pardhasaradhi K, et al. S-Adenosylmethionine and methylation. FASEB J. 1996; 10(4)471–80.
Choi-Rhee E, Cronan JE. A nucleosidase required for in vivo function of the S-adenosyl-L-methionine radical enzyme, biotin synthase. Chem Biol. 2005;12(5):589–93.
Chou TC, Talalay P. The mechanism of S-adenosyl-L-methionine synthesis by purified preparations of bakers' yeast. Biochemistry. 1972; 11(6):1065–73.
Christopher SA, Diegelman P, Porter CW, Kruger WD. Methylthioadenosine phosphorylase, a gene frequently codeleted with p16(cdkN2a/ARF), acts as a tumor suppressor in a breast cancer cell line. Cancer Res. 2002;62(22): 6639–44. Available online at https://cancerres.aacrjournals.org/content/62/22/6639.short.
Cobb SL, Deng H, Hamilton JT, McGlinchey RP, O'Hagan D. Identification of 5-fluoro-5-deoxy-D-ribose-1-phosphate as an intermediate in fluorometabolite biosynthesis in Streptomyces cattleya. Chem Commun (Camb). 2004(5):592–3.
Copley S. Enzymes with extra talents: moonlighting functions and catalytic promiscuity. Curr Opin Chem Biol. 2003;7(2):265–72.
Erb TJ, Evans BS, Cho K, Warlick BP, Sriram J, Wood BM, et al. A RubisCO-like protein links SAM metabolism with isoprenoid biosynthesis. Nat Chem Biol. 2012;8(11):926–32.
Farrar CE, Siu KK, Howell PL, Jarrett JT. Biotin synthase exhibits burst kinetics and multiple turnovers in the absence of inhibition by products and product-related biomolecules. Biochemistry. 2010;49(46):9985–96.
Fessner W-D, Sinerius G, Schneider A, Dreyer M, Schulz GE, Badia J, et al. Diastereoselective enzymatic aldol additions: L-rhamnulose and L-fuculose 1-phosphate aldolases from E. coli. Angew Chem Int Ed Engl. 1991;30(5):555–8.
Fontecave M, Atta M, Mulliez E. S-adenosylmethionine: nothing goes to waste. Trends Biochem Sci. 2004;29(5):243–9.
Ghoda LY, Savarese TM, Northup CH, Parks RE, Garofalo J, Katz L, et al. Substrate specificities of 5'-deoxy-5'-methylthioadenosine phosphorylase from Trypanosoma brucei brucei and mammalian cells. Mol Biochem Parasitol. 1988;27(2-3):109–18.
Golden SS. The international journeys and aliases of Synechococcus elongatus. N Z J Bot. 2019; 57(2):70–5.
Grochowski LL, Xu H, White RH. Ribose-5-phosphate biosynthesis in Methanocaldococcus jannaschii occurs in the absence of a pentose-phosphate pathway. J Bacteriol. 2005;187(21): 7382–9.
Gulko MK, Dyall-Smith M, Gonzalez O, Oesterhelt D. How do Haloarchaea synthesize aromatic amino acids? PLoS One. 2014;9(9): e107475.
Holliday GL, Akiva E, Meng EC, Brown SD, Calhoun S, Pieper U, et al. Atlas of the radical SAM superfamily: divergent evolution of function using a "plug and play" domain. Methods Enzymol. 2018;606:1–71.
Hughes JA. In vivo hydrolysis of S-adenosyl-L-methionine in Escherichia coli increases export of 5-methylthioribose. Can J Microbiol. 2006;52(6):599–602.
Ichihara S, Ichihara Y, Tomisawa H, Fukazawa H, Tateishi M. Identification of 5-deoxy-D-ribitol as a major metabolite of 5'-deoxy-5-fluorouridine in rats. Drug Metab Dispos. 1985; 13(4):520–1. Available online at http://dmd.aspetjournals.org/content/dmd/13/4/520.full.pdf.
Ito T, Ezaki N, Tsuruoka T, Niida T. Structure of SF-666 A and SF-666 B, new monosaccharides. Carbohydr Res. 1971;17(2):375–82.
Kamatani N, Carson DA. Abnormal regulation of methylthioadenosine and polyamine metabolism in methylthioadenosine phosphorylase-deficient human leukemic cell lines. Cancer Res. 1980;40(11):4178–82.
Khersonsky O, Tawfik DS. Enzyme promiscuity: a mechanistic and evolutionary perspective. Annu Rev Biochem. 2010;79:471–505.
Kobori Y, Myles DC, Whitesides GM. Substrate specificity and carbohydrate synthesis using transketolase. J Org Chem. 1992;57(22): 5899–907.
La Haba Gde, Cantoni GL. The enzymatic synthesis of S-adenosyl-L-homocysteine from adenosine and homocysteine. J Biol Chem. 1959; 234(3):603–8.
Laurent V, Darii E, Aujon A, Debacker M, Petit JL, Hélaine V, et al. Synthesis of branched-chain sugars with a DHAP-dependent aldolase: ketones are electrophile substrates of rhamnulose-1-phosphate aldolases. Angew Chem Int Ed Engl. 2018;57(19):5467–71.
Lee JE, Cornell KA, Riscoe MK, Howell PL. Structure of E. coli 5′-methylthioadenosine/S-adenosylhomocysteine nucleosidase reveals similarity to the purine nucleoside phosphorylases. Structure. 2001;9(10):941–53.
Lee SH, Jung BH, Kim SY, Chung BC. A rapid and sensitive method for quantitation of nucleosides in human urine using liquid chromatography/mass spectrometry with direct urine injection. Rapid Commun Mass Spectrom. 2004;18(9):973–7.
Li X, Chu S, Feher VA, Khalili M, Nie Z, Margosiak S, et al. Structure-based design, synthesis, and antimicrobial activity of indazole-derived SAH/MTA nucleosidase inhibitors. J Med Chem. 2003;46(26):5663–73.
Liebich HM, Di Stefano C, Wixforth A, Schmid HR. Quantitation of urinary nucleosides by high-performance liquid chromatography. J Chromatogr A. 1997;763(1–2):193–7.
Miller AR, North JA, Wildenthal JA, Tabita FR. Two distinct aerobic methionine salvage pathways generate volatile methanethiol in Rhodopseudomonas palustris. mBio. 2018a; 9(2).
Miller D, O'Brien K, Xu H, White RH. Identification of a 5'-deoxyadenosine deaminase in Methanocaldococcus jannaschii and its possible role in recycling the radical S-adenosylmethionine enzyme reaction product 5'-deoxyadenosine. J Bacteriol. 2014;196(5):1064–72.
Miller DV, Rauch BJ, Harich K, Xu H, Perona JJ, White RH. Promiscuity of methionine salvage pathway enzymes in Methanocaldococcus jannaschii. Microbiology (Reading). 2018b;164(7):969–81.
Miller DV, Ruhlin M, Ray WK, Xu H, White RH. N5,N10 -methylenetetrahydromethanopterin reductase from Methanocaldococcus jannaschii also serves as a methylglyoxal reductase. FEBS Lett. 2017;591(15):2269–78.
Moss SJ, Murphy CD, O'Hagan D, Schaffrath C, Hamilton JTG, McRoberts WC, et al. Fluoroacetaldehyde: a precursor of both fluoroacetate and 4-fluorothreonine in Streptomyces cattleya. Chem Commun. 2000(22): 2281–2.
Nakano T, Saito Y, Yokota A, Ashida H. Plausible novel ribose metabolism catalyzed by enzymes of the methionine salvage pathway in Bacillus subtilis. Biosci Biotechnol Biochem. 2013;77(5):1104–7.
Namanja-Magliano HA, Stratton CF, Schramm VL, Schramm VL. Transition state structure and inhibition of Rv0091, a 5'-deoxyadenosine/5'-methylthioadenosine nucleosidase from Mycobacterium tuberculosis. ACS Chem Biol. 2016;11(6):1669–76.
Nealson KH, Hastings JW. Bacterial bioluminescence: its control and ecological significance. Microbiol Rev. 1979;43(4):496–518. Available online at
Negishi T, Nakanishi H, Yazaki J, Kishimoto N, Fujii F, Shimbo K, et al. cDNA microarray analysis of gene expression during Fe-deficiency stress in barley suggests that polar transport of vesicles is implicated in phytosiderophore secretion in Fe-deficient barley roots. Plant J. 2002;30(1):83–94.
North JA, Miller AR, Wildenthal JA, Young SJ, Tabita FR. Microbial pathway for anaerobic 5'-methylthioadenosine metabolism coupled to ethylene formation. Proc Natl Acad Sci USA. 2017;114(48):E10455–64.

North JA, Sriram J, Chourey K, Ecker CD, Sharma R, Wildenthal JA, et al. Metabolic regulation as a consequence of anaerobic 5-methylthioadenosine recycling in Rhodospirillum rubrum. MBio. 2016;7(4).

North JA, Wildenthal JA, Erb TJ, Evans BS, Byerly KM, Gerlt JA, et al. A bifunctional salvage pathway for two distinct S-adenosylmethionine by-products that is widespread in bacteria, including pathogenic Escherichia coli. Mol Microbiol. 2020;113(5):923–37.

Nygaard P. Purine and pyrimidine salvage pathways. In: Sonenshein AL, Hoch JA, Losick R, editors. Bacillus subtilis and Other Gram-Positive Bacteria. Biochemistry, Physiology, and Molecular Genetics. Washington: American Society for Microbiology; 1993. p. 359–78.

O'Hagan D, Schaffrath C, Cobb SL, Hamilton JT, Murphy CD. Biochemistry: biosynthesis of an organofluorine molecule. Nature. 2002; 416(6878):279.

Onega M, McGlinchey RP, Deng H, Hamilton JTG, O'Hagan D. The identification of (3R,4S)-5-fluoro-5-deoxy-⍺-ribulose-1-phosphate as an intermediate in fluorometabolite biosynthesis in Streptomyces cattleya. Bioorg Chem. 2007;35(5):375–85.

Palmer LD, Downs DM. The thiamine biosynthetic enzyme ThiC catalyzes multiple turnovers and is inhibited by S-adenosylmethionine (AdoMet) metabolites. J Biol Chem. 2013;288(42):30693–9.

Parveen N, Cornell KA. Methylthioadenosine/S-adenosylhomocysteine nucleosidase, a critical enzyme for bacterial metabolism. Mol Microbiol. 2011;79(1):7–20.

Petty NK, Ben Zakour NL, Stanton-Cook M, Skippington E, Totsika M, Forde BM, et al. Global dissemination of a multidrug resistant Escherichia coli clone. Proc Natl Acad Sci USA. 2014;111(15):5694–9.

Plagemann PG, Wohlhueter RM. 5'-Deoxyadenosine metabolism in various mammalian cell lines. Biochem Pharmacol. 1983;32(8): 1433–40.

Plagemann PG, Wohlhueter RM, Woffendin C. Nucleoside and nucleobase transport in animal cells. Biochim Biophys Acta. 1988;947(3): 405–43.

Rapp J, Rath P, Kilian J, Brilisauer K, Grond S, Forchhammer K. A bioactive molecule made by unusual salvage of radical SAM enzyme by-product 5-deoxyadenosine blurs the boundary of primary and secondary metabolism. Journal of Biological Chemistry. 2021. https://doi.org/10.1016/j.jbc.2021.100621.

Rossi F, De Philippis R. Role of cyanobacterial exopolysaccharides in phototrophic biofilms and in complex microbial mats. Life (Basel). 2015;5(2):1218–38.

Sanada M, Miyano T, Iwadare S, Williamson JM, Arison BH, Smith JL, et al. Biosynthesis of fluorothreonine and fluoroacetic acid by the thienamycin producer, Streptomyces cattleya. J Antibiot. 1986;39(2):259–65.

Savarese TM, Crabtree GW, Parks RE. 5′-methylthioadenosine phosphorylase—I. Substrate activity of 5′-deoxyadenosine with the enzyme from Sarcoma 180 cells. Biochem Pharmacol. 1981;30(3):189–99.

Schroeder HR, Barnes CJ, Bohinski RC, Mumma RO, Mallette MF. Isolation and identification of 5-methylthioribose from Escherichia coli B. Biochim Biophys Acta. 1972;273(2):254–64.

Schweizer M, Brilisauer K, Triebskorn R, Forchhammer K, Köhler HR. How glyphosate and its associated acidity affect early development in zebrafish (Danio rerio). PeerJ. 2019;7: e7094.

Sekowska A, Ashida H, Danchin A. Revisiting the methionine salvage pathway and its paralogues. Microb Biotechnol. 2019;12(1):77–97.

Sekowska A, Danchin A. The methionine salvage pathway in Bacillus subtilis. BMC Microbiol. 2002;2(1):8.

Sekowska A, Dénervaud V, Ashida H, Michoud K, Haas D, Yokota A, et al. Bacterial variations on the methionine salvage pathway. BMC Microbiol. 2004;4:9.

Sofia HJ, Chen G, Hetzler BG, Reyes-Spindola JF, Miller NE. Radical SAM, a novel protein superfamily linking unresolved steps in familiar biosynthetic pathways with radical mechanisms. Functional characterization using new analysis and information visualization methods. Nucl Acids Res. 2001;29(5):1097–106.

Tallan HH, Cohen PA. Methionine adenosyltransferase: kinetic properties of human and rat liver enzymes. Biochem Med. 1976;16(3): 234–50.

Vendeville A, Winzer K, Heurlier K, Tang CM, Hardie KR. Making 'sense' of metabolism: autoinducer-2, LuxS and pathogenic bacteria. Nat Rev Microbiol. 2005;3(5):383–96.

Wang SC, Frey PA. S-adenosylmethionine as an oxidant: the radical SAM superfamily. Trends Biochem Sci. 2007;32(3):101–10.

White RH. L-Aspartate semialdehyde and a 6-deoxy-5-ketohexose 1-phosphate are the precursors to the aromatic amino acids in Methanocaldococcus jannaschii. Biochemistry. 2004;43(23):7618–27.

White RH, Xu H. Methylglyoxal is an intermediate in the biosynthesis of 6-deoxy-5-ketofructose-1-phosphate: a precursor for aromatic amino acid biosynthesis in Methanocaldococcus jannaschii. Biochemistry. 2006;45(40): 12366–79.

Wray JW, Abeles RH. The methionine salvage pathway in Klebsiella pneumoniae and rat liver. Identification and characterization of two novel dioxygenases. J Biol Chem. 1995;270(7): 3147–53.

Yang SF, Hoffman NE. Ethylene biosynthesis and its regulation in higher plants. Annu Rev Plant Physiol. 1984;35(1):155–89.

Yang Y, Lam V, Adomako M, Simkovsky R, Jakob A, Rockwell NC, et al. Phototaxis in a wild isolate of the cyanobacterium Synechococcus elongatus. Proc Natl Acad Sci USA. 2018; 115(52):E12378–87.

Zappia V, Della Ragione F, Pontoni G, Gragnaniello V, Cartenì-Farina M. Human 5′-deoxy-5′-methylthioadenosine phosphorylase: kinetic studies and catalytic mechanism. Adv Exp Med Biol. 1988;250:165–77.

Zhu X, Li Q, Yin C, Fang X, Xu X. Role of spermidine in overwintering of cyanobacteria. J Bacteriol. 2015;197(14):2325–34.

9.2. Submitted Manuscripts

Publication 5:

The preprint was first posted online on bioRxiv. The manuscript is currently under consideration in the Journal of Biophotonics.

Rammler, Tim; Wackenhut, Frank; Zur Oven-Krockhaus, Sven; Rapp, Johanna; Forchhammer, Karl; Harter, Klaus; Meixner, Alfred J. (2019). Quantum coherence in the photosynthesis apparatus of living cyanobacteria. *bioRxiv*, https://doi.org/10.1101/2019.12.13.875344. © The Authors.

Long-range quantum coherence of the photosystem 2 complexes in living cyanobacteria

Authors: T. Rammler[1,2], F. Wackenhut[1]*, S. zur Oven-Krockhaus[1,2], J. Rapp[3], K. Forchhammer[3], K. Harter[2], A. J. Meixner[1]*.

Affiliations:

[1]Institute of Physical and Theoretical Chemistry, University of Tübingen, Tübingen, Germany

[2]Center for Plant Molecular Biology, University of Tübingen, Tübingen, Germany

[3]Interfaculty Institute of Microbiology and Infection Medicine, University of Tübingen, Tübingen, Germany

*Correspondence to: frank.wackenhut@uni-tuebingen.de, alfred.meixner@uni-tuebingen.de

Abstract

The first step in photosynthesis is an extremely efficient energy transfer mechanism, which is difficult to be explained by classical short-range energy migration (“hopping”) and led to the debate to which extent quantum coherence is involved in the energy transfer between the photosynthetic pigments. Embedding living cyanobacteria between the mirrors of an optical microresonator and using low intensity white light irradiation we observe vacuum Rabi splitting in the transmission and fluorescence spectra as a result of strong light matter coupling of the chlorophyll and the resonator modes. The Rabi-splitting scales with the number of chlorophyll a pigments involved in coherent coupling indicating forming a polaritonic state which is delocalized over the entire cyanobacterial thylakoid system, down to the single photon level. Our data provide evidence that a delocalized polaritonic state is the basis of the extremely high energy transfer efficiency under natural conditions.

Introduction

In photosynthesis, light energy is absorbed and converted into relatively stable chemical products by membrane-integral pigment-protein complexes called photosystems for long-term chemical energy storage.[1] Photosynthetic complexes are optimized to capture photons from solar light and transmit the excitation energy from peripheral pigments to the photosynthetic reaction center with an extremely high efficiency (close to $100\,\%$ [2]). They consist of a collection of pigment molecules, such as chlorophylls and carotenoids, that are arranged by a protein scaffold in a way that near-field dipole coupling is possible.[2] When interacting with light they no longer act as independent excited molecules, but coupling between them results in collective excitations called excitons, whose wave function extends over several chromophore units.[3] [4] Electronic interaction with the local environment tunes individual pigment excitation levels to form an energetic ladder from higher energy at the periphery to lower energy near the reaction center, often described semi-classically as “sequential hopping” [5] of excitation energy. On their way to the reaction center, the excitons loose part of their energy to the vibrational modes of the protein complex that serve as a thermal bath. The transfer efficiency depends on the distance, spectral overlap of the emission and absorption spectrum and relative orientation of the pigment molecules to each other. However, structural analyses of photosynthetic complexes [6] show that none of these factors is optimal for the observed highly efficient energy transfer. Finally, the transfer competes continuously with fluorescence emission and non-radiative deactivation of the excited chlorophylls.

The observation of oscillatory intensity modulations of ultrafast photon echoes from isolated photosynthetic complexes of *Chlorobium* at cryogenic temperatures and under almost physiological conditions has drawn enormous attention and led to the hypothesis that quantum coherence could be a possible explanation for this efficient energy transfer. [7] [3] [8] [9] [10] [11] Recent investigations have revealed that both electronic and vibrational coherences are involved in primary energy transfer in bacterial reaction centers [12] [13]. However, the physiological relevance of photosynthesis-related quantum coherence has rarely been studied in living photosynthetic organisms. Furthermore, excitation in ultrafast time-resolved lasers spectroscopy is pulsed and coherent, while irradiation in nature occurs continuously over the course of minutes to hours by incoherent photons. As a

consequence, the energy transfer in the photosynthetic machinery must operate on the basis of independent single photons. Additionally, it is not clear whether the occurrence of quantum coherence might even be a prerequisite for the function of the photosynthetic machinery and provides a selection advantage in the development of photosynthetic organisms.

To address this open question, we have enclosed living cyanobacteria (*Synechococcus elongates*) in the confined electromagnetic field of an optical microresonator to probe their optical properties *in vivo*. Using low intensity white light irradiation, we show that long-range coherent excitonic coupling between the chlorophyll a pigments of PS2 via the formation of a polaritonic state, delocalized over an entire cyanobacterium, is probably one reason for the very efficient photosynthetic energy transfer not only in cyanobacteria but also related plant chloroplasts.

Results

To study possible long-range quantum coherence effects in the photosynthesis of living organisms at ambient conditions, we embedded cells of *S. elongatus* (strain PCC 7942) in an optical microcavity. In contrast to sulfur bacteria [14 3], *S. elongatus* performs oxygenic photosynthesis that is more related to the photosynthesis of plant chloroplasts and, based on the available data [15], is a particularly well-suited photosynthetic model for the study of quantum physical processes *in vivo* at physiological conditions.

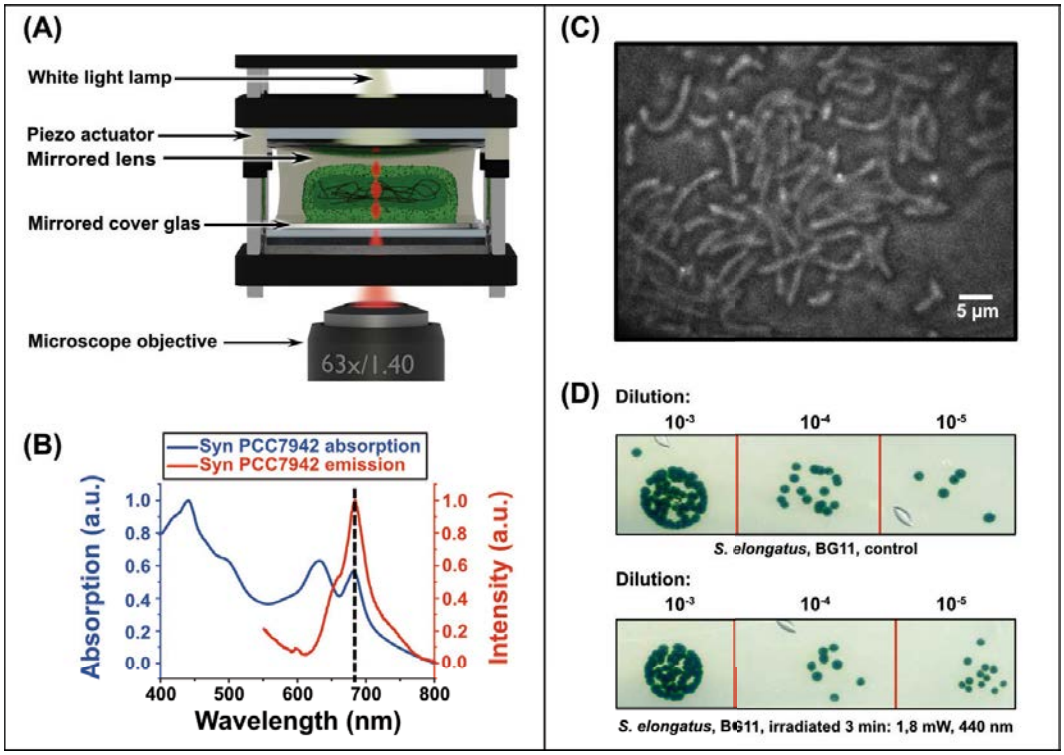

Fig. 1: The spectral properties of the photosynthetic pigments of *S. elongatus* cells and a Fabry-Pérot microresonator. The survival of *S. elongatus* cells is not impaired by the light conditions prevailing in the microcavity. (**A**) Scheme of the Fabry-Pérot microcavity, which consists of two partially transparent mirrors. The distance between the mirrors can be fine-tuned with piezoelectric actuators. Due to constructive and destructive interference, only wavelengths fulfilling the resonance condition of the cavity are transmitted. The bacteria are placed in an agarose matrix inside the cavity. (**B**) Normalized absorption (blue) and fluorescence (red) spectra ($\lambda_{ex} = 440\ nm$) of *S. elongatus* cells located inside the microcavity. The dashed black line indicates the wavelength where the bacteria emit and absorb photons of the same wavelength. (**C**) Light microscopy image of *S. elongatus* cells inside the microcavity. (**D**) Spot assay [16] of *S. elongatus* cells in BG11 medium. Top: Non-irradiated control in a dilution series (1:10), initial concentration: $OD_{750} = 0.5$. Below: Irradiated sample in a dilution series (1:10), initial concentration: $OD_{750} = 0.5$. The bacteria were irradiated with a laser before preparation of a spot assay. The irradiation conditions were comparable to those in the microcavity. The comparable growth rate indicates a negligible impact of the typical irradiation during the experiments.

Our Fabry-Pérot optical microresonator (quality factor, Q = 98) consists of two partially transparent mirrors (Fig. 1A). Their distance can be precisely adjusted with a piezo actuator to control the resonance condition of the microcavity. Compared to previous

works [14], we have chosen silver mirrors with a large layer thickness to achieve a stronger interaction between the microcavity and the cyanobacteria. More details about the experimental set up are given in the supporting information. Transmission spectra were acquired from below via a high numerical aperture (NA) objective lens (NA = 1.4), while the microcavity was irradiated by a continuously emitting white light source from above (Fig. 1A). Additionally, we irradiated the sample with a laser from below to detect strong coupling in the emission spectrum of individual bacteria, which is made possible by the small focal spot size of the high NA objective. As shown in Fig. 1B, the *in vivo* absorption (blue line) shows the typical chlorophyll a maximum at around $680\ nm$ due to a red-shift of protein-bound chlorophyll. [17] The emission spectrum at $440\ nm$ excitation reveals again a maximum at around $680\ nm$ which is assigned to the PS2 complexes and phycobilisome terminal emitters (APC680). [18] [15] The cavity resonance can be tuned across the absorption and emission maximum (see Fig. S1), allowing efficient optical coupling between the cavity modes and the cyanobacteria. Remarkably, the absorption and emission spectra show a significant overlap (Fig. 1B) demonstrating that the cyanobacteria are able to reabsorb their own emitted light. This photophysical feature of *S. elongatus* drastically increases the chance that its photosynthetic pigments can strongly couple to an optical field confined in a microcavity.

The survival rate was assayed to examine the possible impact of the laser irradiation on the cyanobacteria embedded in the microcavity (Fig. 1C). Since only a single bacterium is exposed to the focused laser irradiation inside the cavity at a time, which cannot be isolated after the experiment, we have designed an assay to analyze comparable irradiation conditions by embedding a cyanobacterial culture in a low-melting agarose matrix outside the cavity. The cyanobacteria were then exposed to light conditions ($440\ nm,\ 1.8\ mW,\ 3\ min$) similar to those prevailing in the cavity, while a non-irradiated culture served as a control and the survivability was analyzed by a spot assay (see supporting information for details). No growth difference between the irradiated and non-irradiated sample was observed (Fig 1D), indicating that the light conditions in the microcavity have no discernible impact on the cyanobacterial survivability.

To determine, whether the influence of the microcavity on the cyanobacterial photosynthetic system is detectable *in vivo*, fluorescence lifetimes (FLT) [19] of the photosynthetic pigments in single bacteria were acquired.

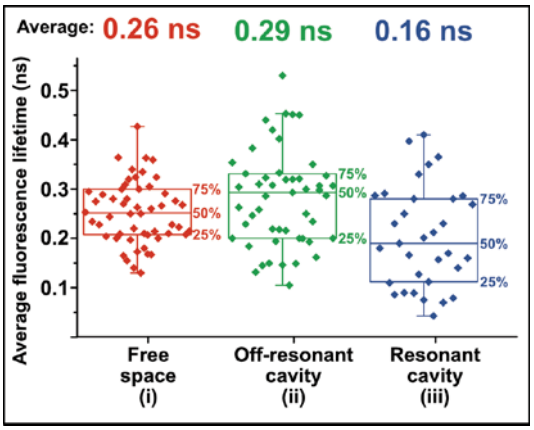

Fig. 2: The fluorescence lifetime (FLT) of *S. elongatus* photosynthetic pigments is influenced *in vivo* by the microcavity. The bacteria were embedded in low-melting agarose and irradiated with short laser pulses ($\lambda_{ex} = 440\,nm$) with a duration of less than $80\,ps$ and a repetition rate of $80\,MHz$. The average intensity-weighted FLTs were recorded in free space ((i), red), inside the off-resonance cavity ((ii), green) or inside the cavity in resonance with the light emission of the cyanobacteria ((iii), blue). A two-tailed t-test confirms a significant difference between the fluorescence lifetimes for the off-resonant (and without) cavity and the resonant cavity, $p = 2.05 \cdot 10^{-5}$, ($p = 3.20 \cdot 10^{-6}$).

The light-harvesting pigments of the photosynthetic complex serve to rapidly and efficiently transfer light energy from the peripheral pigments to the reaction center, therefore, the fluorescence signal of cyanobacteria is weak. Transfer and trapping of the excitation energy in the photosystem leads to a fast non-exponential fluorescence decay, which can be observed from live cyanobacteria with a wide distribution of fluorescence life-time (FLT) components from short ones in the low and mid picosecond range and slow components in the low nanosecond range.[20] The spontaneous emission rate of a chromophore can be increased or decreased by placing it in a microcavity and tuning it in-resonance or off-resonance with the chromophore emission. This is known as Purcell effect [21] [22], leading to shorter or longer FLTs, respectively. The long lived FLT component originates from particularly those photosynthetic pigments, where the excitation energy is

trapped in an emitting state and can therefore be analyzed *in vivo* for three cases: (i) free space (outside of the cavity), (ii) inside the cavity in off-resonance mode and (iii) inside the cavity in resonance mode. Short laser pulses ($\lambda_{ex} = 440\,nm$) with pulse durations of less than $80\,ps$ and a pulse rate of $80\,MHz$ were used. The pigments irradiated in free space (i) reveal a FLT value of $\tau_I = (0.26 \pm 0.006)\,ns$ ((i) in Fig. 2) and a slightly larger value of $\tau_I = (0.29 \pm 0.016)\,ns$ is recorded in the off-resonant microcavity ((ii) in Fig. 2). In contrast, the FLT in the resonant microcavity (iii) decreased to $\tau_I = (0.16 \pm 0.006)\,ns$ and was significantly shorter compared with the data obtained in free space or in the off-resonant cavity. This result is consistent with the Purcell effect [21] of isolated chromophores and demonstrates that the microcavity has a noticeable impact on the photosynthetic processes in single living cyanobacteria.

In general, the interaction of a quantum system with the optical field in a microcavity can be separated in the weak and strong coupling regime. In the weak coupling regime, the individual damping constants of the cavity and the photosynthetic pigments are larger than the coupling constant. In this case, the microcavity only influences the spontaneous emission rate *via* the Purcell effect as observed in the FLT analysis (Fig. 2). However, if the coupling constant exceeds the individual damping constants, the energy of a photon can be coherently cycled back and forth between the oscillating electromagnetic field in the microcavity and the induced polarization formed by a large number of coherent electronically excited chromophores enclosed between the cavity mirrors before it escapes from the cavity; this condition reflects the strong coupling regime [23]. The energy of the photon, which is dispersed in the whole mode volume and shared between the cavity mode and the polarization, is described in quantum electrodynamics as a hybrid light-matter state or polariton. [24] [25] [26] In our case, these so-called polaritonic modes are a coherent superposition of the cavity mode and the electronically excited state of the photosynthetic pigments (chlorophyll a in PS2). As shown in Fig. S2, the back and forth cycling of the photon energy between the electromagnetic field in the microcavity and the polarization in the time domain leads to a splitting in the spectral domain that manifests itself as a double-peaked cavity transmission spectrum with a peak separation referred to as vacuum Rabi splitting, as schematically illustrated in Fig. 3A/B.

To study vacuum Rabi splitting, due to a polaritonic mode in the photosynthetic machinery of a living cyanobacterium and the optical field in the microcavity, we simulated and experimentally investigated the dispersive behavior of the coupled system.

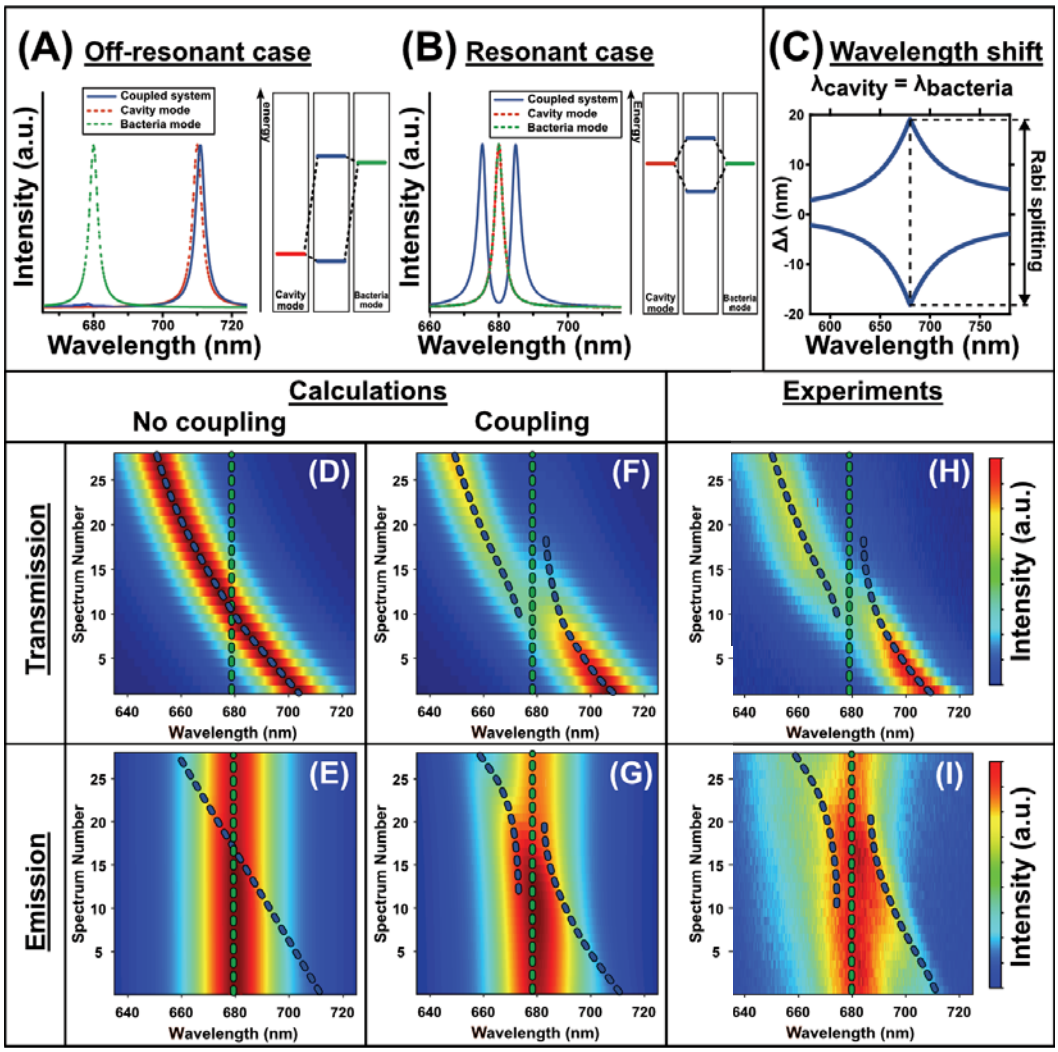

Fig. 3: Strong coupling between a microcavity and the photosynthetic machinery of living cyanobacteria. (**A**) The dashed green and red spectra represent the uncoupled bacteria emission/cavity mode. The blue spectrum illustrates the cavity transmission spectrum for the non-resonant but coupled case and is similar to the uncoupled system. The graph on the right illustrates the corresponding energy level scheme. (**B**) Illustration of the resonant case, where the cavity mode is spectrally overlapping with the

bacteria emission, and two polaritonic modes (blue lines) are clearly visible in the double-peaked cavity transmission spectrum. (**C**) Spectral shift $\Delta\lambda$ of the coupled modes relative to the uncoupled ones. The largest splitting, i.e. vacuum Rabi splitting, is observed when the cavity and bacteria are in resonance. (**D**)/(**E**) Simulated cavity transmission/ bacteria emission spectra without coupling as a function of the decreasing mirror distance (indicated by the spectrum number). The dashed green and blue lines are the spectral position of the uncoupled bacteria emission/cavity resonance, respectively. No anti-crossing can be observed when the cavity mode is tuned across the bacteria emission. (**F**)/(**G**) Simulated cavity transmission/bacteria emission spectra including strong coupling between the cavity mode and the bacteria emission. Strong coupling is visible in (F)/(G) by the anti-crossing dispersion, when the cavity mode is close to the emission of the bacteria. (**H**)/(**I**) Experimental cavity transmission/bacteria emission spectrum. Strong coupling can be observed in **(H)/(I)** by the anti-crossing dispersion and is in perfect agreement with the simulation in (F)/(G).

The dashed lines in Fig. 3A/B illustrate the simulated uncoupled photosystem emission of the cyanobacteria (green) and the cavity mode (red). Fig. 3A illustrates the case when there is no spectral overlap between them. The transmission spectrum of such a coupled, but off-resonant system is similar to that of the uncoupled cavity mode. Conversely, when the cavity mode approaches the spectral position of the chlorophyll a emission, a splitting into two polaritonic modes is visible (Fig. 3B, blue line). Fig. 3C represents the simulated spectral shift $\Delta\lambda$ of the coupled modes relative to the uncoupled modes. The shift caused by strong coupling is largest when the cavity is in resonance with the chlorophyll a emission, leading to a symmetric double-peaked cavity transmission spectrum. The occurrence of such a spectral gap between the two polaritonic modes is called vacuum Rabi splitting. Mathematically, such a coupled system can be modeled by two coupled damped harmonic oscillators, as described in the supporting information or in [27]. First, we want to illustrate in Fig. 3D/E the results of the calculation without coupling ($\kappa = 0\ eV$) between the cavity mode and the chlorophyll a emission. Each line in Fig. 3D represents a cavity transmission spectrum, as indicated by the spectrum number, and its intensity given by the color map. In this simulation, the cavity length gradually increased from top to bottom, leading to a spectral red shift of the cavity resonance. The dashed lines in Fig. 3D/E represent the spectral position of the uncoupled chlorophyll a emission and the cavity mode, respectively. In the absence of strong coupling, no splitting is observed, even when both modes were tuned to the same resonance wavelength; the chlorophyll a

emission was only influenced by the Purcell effect (Fig. 3E). This changes with strong coupling between the cavity mode and the chlorophyll a pigments, with a calculated coupling constant of $\kappa = 0.14\ eV$ in Fig. 3F/G. The calculated cavity transmission spectra in Fig. 3F show a clear anti-crossing behavior when the cavity resonance approaches the spectral position of the chlorophyll a emission at $680\ nm$. In the calculated emission spectra in Fig. 3G, the mode splitting is less obvious because it is obscured by the spectrally broad fluorescence background of chlorophyll a pigments that do not contribute to the polarization. The uncoupled pigments have their electronic transition dipole moments oriented perpendicular to the polarization and constitute about 2/3 of the total number of pigments. By comparing the simulations in Fig. 3D/E with Fig. 3F/G, it is possible to experimentally distinguish between no/weak and strong coupling in the microcavity-cyanobacteria system. Notably, the experimental white light transmission spectra derived from the living cyanobacteria show a clear anti-crossing behavior when the cavity resonance is tuned over the chlorophyll a emission at $680\ nm$. (Fig. 3H). In the emission spectra (Fig. 3I) the splitting is less obvious since it is composed of two types of photons, those that participate in the strong coupling process with the cavity mode and those that escape from the resonator without coupling due to the Purcell effect. The experimental results fit perfectly to the calculated spectra in Fig. 3F/G and prove that strong coupling between the microcavity and the chlorophyll a pigments is achievable in living cyanobacteria.

According to the Jaynes-Cummings model the energy splitting ΔE is given by equation (1) and is proportional to the square root of the number n of fluorophores that coherently couple to the cavity mode with a coupling constant g_0. [23]

$$\Delta E = 2\sqrt{n}\hbar g_o \qquad (1)$$

Therefore, the splitting energy should decrease when the number of fluorophores is reduced. This can indeed be achieved in a living bacterium by photobleaching a fraction of the functional chlorophyll a pigments by increasing the laser intensity by a factor of 100 as compared with the previous experiments.

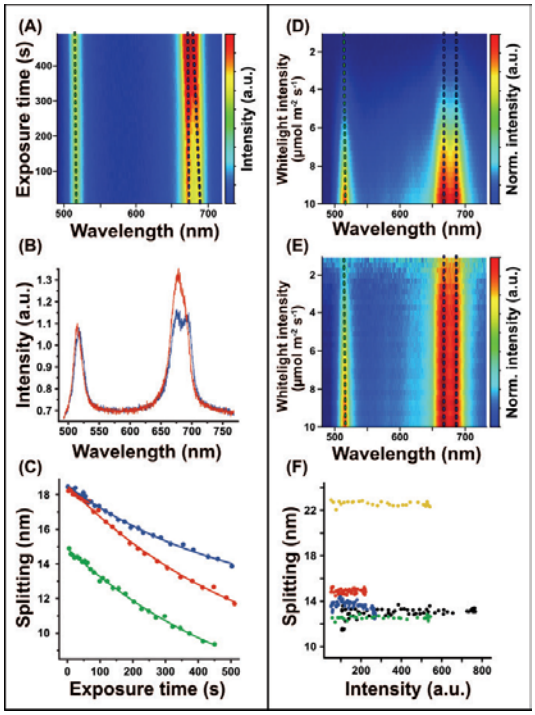

Fig. 4: Reducing the number of pigments in a cyanobacterium by photobleaching reduces vacuum Rabi splitting and shows that pigments all over a bacterium are coherently coupled. (**A**) Cavity transmission spectra with two cavity modes as a function of the exposure time. One mode shows vacuum Rabi splitting (dashed blue line), while the other is not coupled (dashed green line). The splitting energy, and thus the coupling, is reduced by the continuous irradiation and photobleaching the pigments of the bacterium. (**B**) First (blue line, $t = 0\ s$) and last (red line, $t = 500\ s$) spectrum of A. (**C**) Rabi splitting between the two intensity maxima around $680\ nm$ as a function of the exposure time. Three different, individual bacteria (red, green and blue) in the cavity show the decrease of the vacuum Rabi splitting with increasing bleaching of the pigments. (**D**) Cavity transmission spectra with two resonances as a function of the illumination intensity of the white light lamp of $10\ \mu mol\ \mathrm{photons\ s^{-1}\ m^{-2}}$ to $1\ \mu mol\ \mathrm{photons\ s^{-1}\ m^{-2}}$ (corresponding to $28 - 2.8\ mW cm^{-2}$ at $680\ nm$) from bottom to top. The coupling remains constant while the intensity of the white light lamp is reduced. (**E**) Intensity normalized version of (D), where each spectrum is normalized to its maximum intensity, to better visualize the constant splitting. (**F**) Splitting as a function of the white light intensity. At low illumination intensity, five different, individual bacteria in the cavity show that the vacuum Rabi splitting is independent of the light intensity.

As shown in Fig. 4A at the beginning the cavity mode at $\lambda = 680\ nm$ has a spectral dip at the center due to vacuum Rabi splitting and as the photobleaching of the pigment molecules proceeds (Fig. 4A, blue dashed line) the energy splitting between the two

peaks reduces and disappears. In contrast, at the same time for the cavity mode at $\lambda = 546\,nm$ which has no coupling to the chlorophyll a pigments no changes in intensity or spectral position are visible. This is further illustrated in Fig. 4B, where the first (blue line) and the last (red line) spectrum of the spectral series in Fig. 4A are shown.

The number of molecules (n in Eq. 1) decreases exponentially by photobleaching as tested at three different locations in the cavity, resulting in a decreased splitting of the coupled modes, which can be fitted to the square root of an exponential decay (Fig. 4C). These results demonstrate that the extent of the Rabi splitting depends on the number of pigments effectively participating in polaritonic coupling to the optical mode throughout the entire focal volume.

In general, the photosynthetic efficiency would benefit enormously when the coherence between the light harvesting pigments and the cavity is independent of the light intensity. To reveal the light intensity dependence, white-light transmission spectra were acquired with different excitation intensities of $10\,\mu mol\ \mathrm{photons\ s^{-1}\ m^{-2}}$ down to $1\,\mu mol\ \mathrm{photons\ s^{-1}\ m^{-2}}$ (corresponding to $28.0 - 2.8\,mW\,cm^{-2}$ measured at $680\,nm$) in single living cyanobacteria as shown in Fig 4D/E, where the y-axis corresponds to different excitation intensities. The resonance mode at $\lambda = 680\,nm$, which is strongly coupled to chlorophyll a, shows a Rabi splitting which remains constant with decreasing white light irradiation intensity (Fig. 4D). This is even more obvious in the normalized spectra (Fig. 4E), where each spectrum along the y axis is normalized to its maximum intensity. This constant Rabi splitting is observed for different individual cyanobacteria in the sample, as shown in Fig. 4F by plotting the Rabi splitting against the intensity of the cavity mode. As a consequence, since the photons used for white-light illumination are completely incoherent, strong coupling must occur even at very low light intensity; or in other words, one resonant photon is already sufficient to induce a polaritonic state between the microcavity and the chlorophyll a pigments *in vivo*.

Discussion

The emission and transmission spectra presented here demonstrate undoubtedly the existence of an *in vivo* coherent energy exchange between the microcavity and the cyanobacterial photosynthetic light harvesting machinery. Photo-bleaching experiments confirm that the microcavity can couple to about $4.8 \cdot 10^5$ chlorophyll a molecules (calculated from the measured splitting and assuming a chlorophyll a transition dipole moment: $5.39\,D$ @ $n = 1.34$ [28], see supporting information for calculation) at the same time to form a polaritonic state delocalized over the entire thylakoid system of a single cyanobacterium (Fig. 5A). For natural illumination conditions, the semi-classical model of energy "hopping" (Fig. 5B) in the photosynthetic light-harvesting machinery should therefore be expanded to a delocalized wave-like energy transfer (red glow in Fig. 5C). Additionally, the vacuum Rabi splitting is independent of the number of photons, indicating that it works at very low light intensities and for the formation of a polaritonic state one single photon is sufficient. The cell-encompassing delocalization of the polaritonic state guarantees that the photosynthetic reaction centers are optimally supplied with photons and allow growth and survival of the cyanobacteria even in a low-light environment.

The establishment of a long-range polaritonic state requires a complex and dynamic spatial and structural organization of the photosynthetic complexes that compensate or make use of the thermodynamic fluctuations occurring in the natural environment. It can therefore be assumed that the observed cell-encompassing quantum coherence is not merely a byproduct of the evolution of photosynthesis. On the contrary, evolution has rather selected for this process of coherence to optimize photosynthesis to its highest efficiency and makes it very likely that it also occurs in plant chloroplasts, since cyanobacteria are their precursors. As a consequence of our validation of quantum coherence in the photosynthetic machinery of living cyanobacteria at physiological conditions, we believe that the investigation of various other biological processes, which are difficult to be explained by classical thermodynamics, may reveal significant dependencies on quantum electrodynamics effects.[29 2]

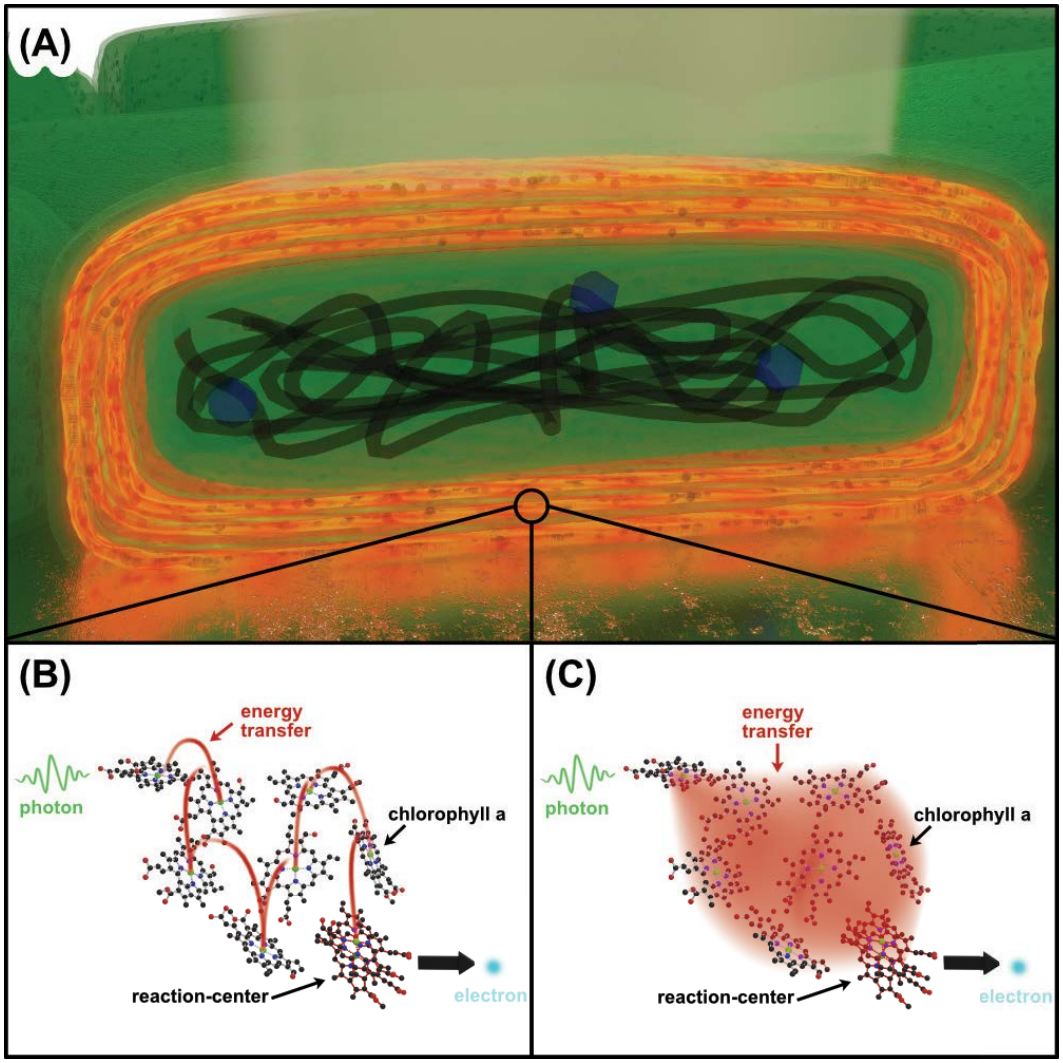

Fig. 5: Models of energy transfer during photosynthesis. (A) Illustration of the energy delocalization over the thylakoid system. (**B**) Classical description: after absorption of a photon (green wavy arrow), the energy transfer from the antenna pigments (chlorophyll a molecules) to the reaction center (chlorophyll a dimer) is described by incoherent energy "hopping" (red energy transfer). (**C**) A collective coherent state between a photon and the antenna pigments generates a coherent energy transfer, being the cause for the very high energy transfer efficiency (close to 100 %).[30]

Methods:

Preparation of cavity mirrors

The mirrors were produced by evaporating a $3\,nm$ thick chromium layer on a glass surface serving as an adhesion layer for the following silver layer, which has a thickness of $30\,nm$ or $60\,nm$ for the lower and upper mirror, respectively. Since silver is bactericidal and very susceptible to damage and oxidation, it was coated with a gold layer ($5\,nm$) and an SiO_2 layer ($20\,nm$).[31] These layer thicknesses result in a microcavity with a quality factor of $Q = 98$. The microcavity was assembled in a custom-built holder with piezo actuators and mounted on a stage scanning confocal microscope for the collection of both white light transmission and fluorescence spectra from the same spatial position.

Light intensity measurements

The light intensity was measured with a Li-Cor Li-189 radiometer from Heinz Walz GmbH (Germany).

Bacterial cultivation conditions

Synechococcus elongatus PCC 7492 cells were cultivated under photoautotrophic conditions with continuous illumination at around $30\,\mu mol\ \mathrm{photons}\ s^{-1}\ m^{-2}$ (Lumilux de Lux, Daylight, Osram) at $28\,°C$. The cultures were grown in $100\,mL$ Erlenmeyer flasks, filled with $40\,mL$ BG11 [32] medium, supplemented with $5\,mM\ NaHCO_3$ and shaken at $120 - 130\,rpm$.

The survivability after laser irradiation analyzed by a spot assay

The *S. elongatus* cultures of both treatments were adjusted to an optical density $OD_{750} = 0.5$, and a dilution series to the power of 10 was made in BG11 medium ($10^0 - 10^{-5}$). $5\,\mu L$ of each dilution was dropped on BG11-agar plates and cultivated at $28\,°C$ [33] under constant light with the intensity of $30\,\mu mol\ \mathrm{photons\ s^{-1}\ m^{-2}}$ for 7 days. All experiments are shown in Fig. 1D. Top: Non-irradiated control in a dilution series (1:10), three replicates. Fig. 1D below: Irradiated sample in a dilution series (1:10), three replicates.

The bacteria were irradiated with a laser ($\lambda_{ex} = 440\ nm$, power: $1.8\ mW$) for three minutes before preparation of a spot assay. Representative results are shown in Fig. 1D.

The spectral properties of *S. elongatus*

To characterize the spectral properties of the photosynthetic pigments, absorption and emission spectra were recorded from $20\ \mu L$ of a cyanobacterial suspension, embedded in a low-melting agarose matrix to prevent cell movement (Fig. 1C). The absorption spectrum shown in Fig. 1B features four distinct bands: the soret band of chlorophyll a at $440\ nm$ [34], the carotenoid band at $500\ nm$ [35], the PBS band at $630\ nm$ [36] and the Q_y band of chlorophyll a at $680\ nm$ [37]. Excitation of the soret band is very efficient, taking additional advantage of the large Stokes shift to separate the laser reflection at the cavity mirrors from the emission signal, which is dominated by the chlorophyll a emission at $680\ nm$. [35]

Acknowledgments:

The authors would like to thank F. de Courcy for English proofreading of the manuscript, M. Kittelberger for initial experiments and M. Harter for the hint of trying quantum biology. Funding: A.J.M., F.W. and K.H. acknowledge support by the VW foundation (project title: A quantum beat for life) and the Deutsche Forschungsgemeinschaft (ME 1600/13-3; HA 2146/23-1; SFB 1101/D02, Z02).

Author contributions:

S.z.O.-K., K.H. and A.J.M. designed the project. T.R. and J.R. performed experiments. T.R. and F.W. analyzed the data and wrote the manuscript with input and proofreading from K.F., K.H., A.J.M., S.z.O.-K. and J.R.

Data Availability

Data are available in the main text or the supplementary materials. Further material is available from the corresponding author upon reasonable request.

Supplementary Materials:

Materials and Methods

Supplementary Text

Figures S1-S2

References 1-7

References:

1. Stirbet, A., Lazár, D., Guo, Y. & Govindjee, G. Photosynthesis: basics, history and modelling. *Ann. Bot.* **126**, 511–537 (2020).

2. Fleming, G. R., Scholes, G. D. & Cheng, Y.-C. Quantum effects in biology. *Procedia Chem.* **3**, 38–57 (2011).

3. Engel, G. S. *et al.* Evidence for wavelike energy transfer through quantum coherence in photosynthetic systems. *Nature* **446**, 782–786 (2007).

4. Strümpfer, J., Şener, M. & Schulten, K. How Quantum Coherence Assists Photosynthetic Light-Harvesting. *J. Phys. Chem. Lett.* **3**, 536–542 (2012).

5. Scholes, G. D. Quantum-Coherent Electronic Energy Transfer: Did Nature Think of It First? *J. Phys. Chem. Lett.* **1**, 2–8 (2010).

6. Vasil'ev, S., Orth, P., Zouni, A., Owens, T. G. & Bruce, D. Excited-state dynamics in photosystem II: Insights from the x-ray crystal structure. *Proc. Natl. Acad. Sci.* **98**, 8602–8607 (2001).

7. Collini, E. Spectroscopic signatures of quantum-coherent energy transfer. *Chem. Soc. Rev.* **42**, 4932 (2013).

8. Collini, E. *et al.* Coherently wired light-harvesting in photosynthetic marine algae at ambient temperature. *Nature* **463**, 644–647 (2010).

9. Cheng, Y.-C. & Fleming, G. R. Dynamics of Light Harvesting in Photosynthesis. *Annu. Rev. Phys. Chem.* **60**, 241–262 (2009).

10. Hildner, R., Brinks, D., Nieder, J. B., Cogdell, R. J. & van Hulst, N. F. Quantum Coherent Energy Transfer over Varying Pathways in Single Light-Harvesting Complexes. *Science* **340**, 1448–1451 (2013).

11. Dahlberg, P. D. *et al.* Communication: Coherences observed *in vivo* in photosynthetic bacteria using two-dimensional electronic spectroscopy. *J. Chem. Phys.*

143, 101101 (2015).

12. Cao, J. *et al.* Quantum biology revisited. *Sci. Adv.* **6**, eaaz4888 (2020).

13. Ma, F., Romero, E., Jones, M. R., Novoderezhkin, V. I. & van Grondelle, R. Both electronic and vibrational coherences are involved in primary electron transfer in bacterial reaction center. *Nat. Commun.* **10**, (2019).

14. Coles, D. *et al.* A Nanophotonic Structure Containing Living Photosynthetic Bacteria. *Small* **13**, 1701777 (2017).

15. Rexroth, S., Nowaczyk, M. M. & Rögner, M. Cyanobacterial Photosynthesis: The Light Reactions. in *Modern Topics in the Phototrophic Prokaryotes: Metabolism, Bioenergetics, and Omics* (ed. Hallenbeck, P. C.) 163–191 (Springer International Publishing, 2017). doi:10.1007/978-3-319-51365-2_5.

16. Doerrich, A. & Wilde, A. Spot Assays for Viability Analysis of Cyanobacteria. *BIO-Protoc.* **5**, (2015).

17. French, C. S., Brown, J. S. & Lawrence, M. C. Four Universal Forms of Chlorophyll *a*. *Plant Physiol.* **49**, 421–429 (1972).

18. Bhatti, A. F., Choubeh, R. R., Kirilovsky, D., Wientjes, E. & van Amerongen, H. State transitions in cyanobacteria studied with picosecond fluorescence at room temperature. *Biochim. Biophys. Acta BBA - Bioenerg.* **1861**, 148255 (2020).

19. Lakowicz, J. R. *Principles of fluorescence spectroscopy*. (Springer, 2006).

20. Byrdin, M., Rimke, I., Schlodder, E., Stehlik, D. & Roelofs, T. A. Decay Kinetics and Quantum Yields of Fluorescence in Photosystem I from Synechococcus elongatus with P700 in the Reduced and Oxidized State: Are the Kinetics of Excited State Decay Trap-Limited or Transfer-Limited? *Biophys. J.* **79**, 992–1007 (2000).

21. Purcell, E. M. Spontaneous Emission Probabilities at Radio Frequencies. in *Confined Electrons and Photons: New Physics and Applications* (eds. Burstein, E. & Weisbuch, C.) 839–839 (Springer US, 1995). doi:10.1007/978-1-4615-1963-8_40.

22. Chizhik, A. I. *et al.* Probing the Radiative Transition of Single Molecules with a Tunable Microresonator. *Nano Lett.* **11**, 1700–1703 (2011).

23. Fox, M. *Quantum optics: an introduction*. (Oxford University Press, 2006).

24. Hutchison, J. A., Schwartz, T., Genet, C., Devaux, E. & Ebbesen, T. W. Modifying Chemical Landscapes by Coupling to Vacuum Fields. *Angew. Chem. Int. Ed.* **51**, 1592–

1596 (2012).

25. Dintinger, J., Klein, S., Bustos, F., Barnes, W. L. & Ebbesen, T. W. Strong coupling between surface plasmon-polaritons and organic molecules in subwavelength hole arrays. *Phys. Rev. B* **71**, (2005).

26. Atlasov, K. A., Karlsson, K. F., Rudra, A., Dwir, B. & Kapon, E. Wavelength and loss splitting in directly coupled photonic-crystal defect microcavities. *Opt. Express* **16**, 16255 (2008).

27. Junginger, A. *et al.* Tunable strong coupling of two adjacent optical λ/2 Fabry-Pérot microresonators. *Opt. Express* **28**, 485 (2020).

28. Knox, R. S. & Spring, B. Q. Dipole Strengths in the Chlorophylls ¶†. *Photochem. Photobiol.* **77**, 497–501 (2003).

29. Marais, A. *et al.* The future of quantum biology. *J. R. Soc. Interface* **15**, 20180640 (2018).

30. van Grondelle, R., Dekker, J. P., Gillbro, T. & Sundstrom, V. Energy transfer and trapping in photosynthesis. *Biochim. Biophys. Acta BBA - Bioenerg.* **1187**, 1–65 (1994).

31. Konrad, A., Metzger, M., Kern, A. M., Brecht, M. & Meixner, A. J. Controlling the dynamics of Förster resonance energy transfer inside a tunable sub-wavelength Fabry–Pérot-resonator. *Nanoscale* **7**, 10204–10209 (2015).

32. Rippka, R., Stanier, R. Y., Deruelles, J., Herdman, M. & Waterbury, J. B. Generic Assignments, Strain Histories and Properties of Pure Cultures of Cyanobacteria. *Microbiology* **111**, 1–61 (1979).

33. Watzer, B. *et al.* The Signal Transduction Protein PII Controls Ammonium, Nitrate and Urea Uptake in Cyanobacteria. *Front. Microbiol.* **10**, (2019).

34. Kondou, Y., Nakazawa, M., Higashi, S., Watanabe, M. & Manabe, K. Equal-quantum Action Spectra Indicate Fluence-rate-selective Action of Multiple Photoreceptors for Photomovement of the Thermophilic Cyanobacterium Synechococcus elongatus¶. *Photochem. Photobiol.* **73**, 90–95 (2007).

35. Kennis, J. T. M. *et al.* Light Harvesting by Chlorophylls and Carotenoids in the Photosystem I Core Complex of *Synechococcus elongatus*: A Fluorescence Upconversion Study. *J. Phys. Chem. B* **105**, 4485–4494 (2001).

36. Lahmi, R. *et al.* Alanine Dehydrogenase Activity Is Required for Adequate

Progression of Phycobilisome Degradation during Nitrogen Starvation in Synechococcus elongatus PCC 7942. *J. Bacteriol.* **188**, 5258–5265 (2006).

37. Damjanović, A., Vaswani, H. M., Fromme, P. & Fleming, G. R. Chlorophyll Excitations in Photosystem I of *Synechococcus elongatus*. *J. Phys. Chem. B* **106**, 10251–10262 (2002).